UNIVERSITY OF CALIFORNIA,
IRVINE

Development of Polydisulfide Polymers for RNA Delivery

DISSERTATION

submitted in partial satisfaction of the requirements
for the degree of

DOCTOR OF PHILOSOPHY

in Chemistry

by

James Collin Hickey

Dissertation Committee:
Professor Zhibin Guan, Chair
Assistant Professor Joseph Patterson
Assistant Professor Seunghyun Sim

2022

DEDICATION

To

Anna

For the endless support, especially in my most troubled times. Without you, none of this would have been possible. Thank you for helping me through this journey.

To

Cassandra (Cass) Yeh and Mikhail (Misha) Gednov

To the countless hours you spent assisting and troubleshooting, my recognition cannot do justice to how much you two have contributed every step of the way in this thesis. I cherished every moment I spent mentoring you and I will always help you whenever you need it.

To

My Family

Your support will never be forgotten. Thank you for helping me every step of the way.

TABLE OF CONTENTS

LIST OF FIGURES

LIST OF TABLES

LIST OF SCHEMES

LIST OF COMMON ABBREVIATIONS

Term 1.0: Messenger ribonucleic acid (mRNA)

Term 1.1: Ribonucleic acid (RNA)

Term 1.2: Clustered regulgarly interspaced short palindromic repeats (CRISPR)

Term 1.3: CRISPR-associated protein (Cas); CRISPR-associated protein 9 (Cas9)

Term 1.4: small guide RNA (sgRNA)

Term 1.5: Ribonucleoprotein (RNP)

Term 1.6: Lipid Nanoparticle (LNP)

Term 1.7: Dynamic light scattering (DLS)

Term 1.8: Cryogenic transmission electron microscopy (cryo-TEM)

Term 1.9: Food and Drug Administration (FDA)

Term 1.10: Lipoic acid (LA)

Term 1.11: Tetraethylene glycol (TEG)

Term 1.12: Ring-opening polymerization (ROP)

Term 1.13: Enhanced green fluorescent protein (EGFP for protein; *egfp* for gene)

Term 1.14: Ovalbumin (OVA for protein)

Term 1.15: Dendronized polypeptide polymer (denpol)

Term 1.16: Gel permeation chromatography (GPC)

Term 1.17: Nuclear magnetic resonance (NMR)

ACKNOWLEDGEMENTS

I have endless gratitude towards Professor Zhibin Guan for all the mentorship and support over the last five years. Zhibin has a boundless enthusiasm for science and the temperance to guide genuine scientific passion into constructive thought. After witnessing so many bright graduate student and postdoctoral fellows mature and excel under his mentorship I understood and appreciate how capable he is at adjusting to the unique personal needs of all his students, myself included. I feel truly fortunate to have achieved my own doctoral degree in such an enriching environment under such an excellent mentor. I also wish to thank the other members of my thesis committee, Professor Joseph Patterson and Professor Seunghyun Sim. Professor Patterson, I always enjoyed our annual meeting discussions and I greatly appreciate all inputs you have provided to help me generate beautiful cryo-TEM nanoparticle images. Professor Sim, I appreciate the time you have dedicated to helping me construct this thesis, and I congratulate you on your beautiful new baby. I hope the future proves happy and healthy for your new family.

I want to personally thank every previous graduate student member of the Guan Lab that I was fortunate to spend years working besides and with. Alex Eldredge, I really appreciate the pep-talks you provided when my experiments first started in the lab, as well as showing me the ropes for all the instruments on campus. You have a boundless enthusiasm for science perhaps only matched by Zhibin and it reflects in the admirable way you conduct your work. Without your aid the CRISPR-Cas9 project would probably be a simple footnote and not the story it is today; working together on that project are some my fondest memories of the lab. Chase Tretbar, I will forever appreciate the positive support you provided throughout our three years in the lab together, along with all the crazy business ideas you came up with. I hope that Olivia and any more newcomers into your family are happy and healthy in the future. I hope to get a picture of you with Olivia on your dream boat in the next couple years. Dongchu Yang, thank you for teaching me a multitude of techniques for both small-molecule and polymer synthesis. I appreciate your candidness and I hope the future is bright for you, no matter where life takes you. Hurik Muradyan, I have never met someone as creative as you, be it in project design or beautiful clay earring sculpting. I hope you and Will have successful careers and happy lives in the Bay Area. James Neal, although we only briefly overlapped in our time together in the Guan lab, I have never met someone as understanding and patient as you. Tyler Albin And Zhiyuan Fan, I hope you two both are extremely successful in the biotech scene; maybe I'll see you two in Boston if you're in for work trips.

To the current members of the Guan group, I want to thank you all for the great experiences we have had together throughout the years together. Jordan, Leslie, and Jayme, I hope the rest of your thesis are as exciting and fulfilling as my own. If you need anything in the future, I'll be there for you. To Serxho, Dipankar, Chenfung, and Kosuke, I hope you all enjoy your time learning in the Guan lab and that your future careers are fruitful.

To Anna and my family, thank you for the constant support you have provided me throughout this experience. You've always been supportive, even when I call during unconventional hours. I will forever be grateful for all you've done.

VITA

JAMES COLLIN HICKEY

EDUCATION:

University of California, Irvine; Irvine, CA, 92617.
Medicinal Chemistry and Pharmacology Gateway Program: 2017
Ph.D Candidate in Chemistry: 2018-2022
Advisor: Prof. Zhibin Guan

St. Mary's College of Maryland; St. Mary's City, MD 20686. B.A. in Biochemistry, 2015.
Capstone Advisor: Prof. Andrew Koch

PUBLICATIONS:

1. Dong-Chu Yang, Alexander C. Eldredge**, James C. Hickey**, Hurik Muradyan, and Zhibin Guan; "Multivalent Peptide-functionalized Bioreducible Polymers for Cellular Delivery of Various RNAs." Biomacromolecules, 2020, 21, 4, 1613–1624.
2. Zhiyuan Fan, Jan, Sharon, **James C. Hickey**, D. Huw Davies, Jiin Felgner, Philip L. Felgner, and Zhibin Guan; "Multifunctional dendronized polypeptides for controlled adjuvanticity." Biomacromolecules, 2021, 22, 12, 5074–5086.
3. **James C. Hickey**, Paul J. Hurst, Joseph P. Patterson, and Zhibin Guan; "Facile Synthesis of Multifunctional Bioreducible Polymers For mRNA Delivery." *Manuscript submitted*
4. **James C. Hickey**,[±] Alexander C. Eldredge,[±] Lingyi Tang, Paul J. Hurst, Qin Yang, Joseph P. Patterson, and Zhibin Guan; "Dendronized Polypeptide Polymers for CRISPR-Cas9 Gene Editing *In Vitro* and mRNA Delivery *In Vivo*." *Manuscript in preparation*

AWARDS AND RECOGNITIONS:

2011-2015 Propeller Club of Baltimore Scholarship
2016-2017 Postbaccalaureate Cancer Research Training Award
2019 Vertex Scholar Award
2022 Graduate Dissertation Fellowship Award

POSTERS AND PRESENTATIONS:

1. Hickey, J.C., Eitan, E., Mattson, M.P. *Method Development for High Throughput Detection of Extracellular Vesicle Transfer between cells.* National Institute on Aging Internship Conference. 251 Bayview Blvd, Baltimore, MD 21224, USA. 2014
2. Hickey, J.C., Seith, D., Frey, T., Guan. Z. *Bioinspired Materials and their applications.* UCI Chemical Biology Club Presentation Session. Ring Rd, Irvine, CA 92697. 2018
3. Hickey, J.C. *Dendronized Polypeptide polymers as nanocarriers of RNA-mediated CRISPR-Cas9 gene editing.* UCI Chemistry Student Colloquium Research Presentation Session. Ring Rd, Irvine, CA 92697. 2019
4. Hickey, J.C., Castro, J., Tretbar, C., Fan, S., Selmani, S., Guan. Z. *Dynamic Materials and Biomaterials.* UCI Recruitment Virtual Poster Presentation Session. Ring Rd, Irvine, CA 92697. 2021
5. Hickey, J.C., Castro, J., Tretbar, C., Fan, S., Selmani, S., Guan. Z. *Dynamic Materials and Biomaterials Synthesis.* UCI Recruitment Virtual Poster Presentation Session. Ring Rd, Irvine, CA 92697. 2022

RESEARCH EXPERIENCE:

1. **Summer Internship Program, National Institute on Aging**: 2014
   High throughput methods of extracellular vesicle/exosome detection were explored using fluorescent cell membrane dyes and microplate readers. Cellular transfections with plasmids and siRNA-expressing vectors were also performed to manipulate generated exosome populations.

2. **St. Mary's College of Maryland**: 2015
   Investigated the synthesis of symmetrical and asymmetrical diaryliodonium salts and reductive elimination of aryl(thienyl)iodoniumsalts to viologen-related compounds and polythiophene species.

3. **Sphingolipid and Phospholipid Signaling, National Cancer Institute.** 2015-2016
   Performed immunohistochemistry experiments on Ceramide phosphoethanolamine synthase (CPES) Drosophila melanogaster mutants, with heavy emphasis on confocal and fluorescent microscopy. Tissue-specific gene expression, qPCR, plasma membrane, and lipid raft isolation, and western blot analysis of target species was also performed.

4. **Functional Biomaterials Group, University of California, Irvine.** 2017-2022
   Utilizing dendritic cationic polymers to deliver RNA-polymer nanoparticles to immortalized cell lines. Combined RNA delivery of Cas9 mRNA and target sgRNA via cationic dendronized polymer vectors leads to remarkable gene editing *in vitro*. *In vivo* RNA-polymer nanoparticle tracking demonstrates outstanding RNA delivery and expression within immune cells.
   Development and synthesis of novel polydisulfide polymeric vectors for RNA complexation, RNA-polymer nanoparticle formation, and therapeutic RNA delivery *in vitro*. Cationic-mediated and non-cationic RNA complexation methods are currently being explored the generate next-generation polymeric vectors for therapeutic RNA delivery.

MENTORSHIP AND OUTREACH:

UCI Chemistry Outreach Program: 2017-2018

Reach Out Teach Out (ROTO) Member and Committee Financial Representative: 2018-2020

- High School Mentees Received Engle Award at Orange County Science and Engineering Fair in 2019
- High School Mentees Progressed to First Round Qualifications of National Samsung Solve Competition in 2020

Prison Education Program (PEP): 2018-2019

Mentorship Over Two UCI Allergan Undergraduate Research Program Recipients: 2021

TEACHING EXPERIENCE:

Laboratory Teaching Assistant, St. Mary's College of Maryland. 2013-2015
Courses: CHEM311L: Organic Chemistry I Lab and CHEM312L: Organic Chemistry II Lab
Laboratory Teaching Assistant, University of California, Irvine. 2017-2022

Courses: PHRMSCI 90: Speaking Science, CHEM1LC/1LD: General Chemistry Lab, CHEM1A: General Chemistry Lecture, CHEM51LC: Organic Chemistry Lab

ABSTRACT OF THE DISSERTATION

Development of Polydisulfide Polymers for RNA Delivery

by

James Collin Hickey

Doctor of Philosophy in Chemistry

University of California, Irvine, 2022

Professor Zhibin Guan, Chair

As a result of the COVID-19 pandemic, mRNA-based therapeutics have rapidly changed from being the "therapeutics of the future" to tangible FDA-approved medicines available for people of all ages and medical backgrounds. One advance that allowed these therapies to be so effective are lipid nanoparticle-based delivery vehicles. However, despite the tremendous advances in lipid nanoparticle technologies, there are some inherent disadvantages in using lipid nanoparticles in therapeutic designs. To circumvent these limitations, new biodegradable and biocompatible mRNA delivery vehicles are being pursued as tools that can accommodate roles where lipid nanoparticles prove insufficient, particularly in the field of RNA therapeutics and gene therapy.

Chapter 1 of this thesis provides an extensive introduction on the background of gene therapy, RNA-based therapeutics, and current mRNA therapy delivery vehicles/ approaches along with relevant limitations. CRISPR-Cas9 gene editing will also be briefly explored, along with the different viral and synthetic vectors that are currently being explored for relevant CRISPR-Cas therapies. Chapter 2 explores a novel approach of generating multifunctional polydisulfide polymers using a post-polymerization

using two model mRNAs. Chapter 3 explores using multifunctional dendronized linear polymers to generate polymeric-RNA nanoparticles containing Cas9-encoding mRNA and gene-targeting sgRNA. CRISPR-Cas9 gene editing using these polymeric nanoparticles is discussed, and relevant nanoparticle *in vivo* distribution is examined. Chapter 4 discusses exploration into a facile cryopolymerization methodology to generate anionic and cationic polydisulfides for the purpose of mRNA delivery. With the works explored in Chapters 2 and 4, two new synthetic methodologies are outlined that greatly expand the use of lipoic acid-derived polydisulfides for mRNA delivery. From these new methodologies and the CRISPR-Cas9 gene editing obtained from the thiol-reducible polymers in chapter 3, the works described within this thesis should expand the utility of polydisulfide as biodegradable polymers for next-generation RNA delivery applications.

Chapter 1: Gene Editing and RNA Delivery: Methods and Progress

1.1 Genetic Disorders, Gene Therapy, and RNA Therapy Background

According to the canonical central dogma of molecular biology, cellular information is classically transferred from deoxyribonucleic acid (DNA) templates in genomes to intermediate messenger ribonucleic acid (mRNA) constructs and finally to highly specific polypeptide/ protein sequences that facilitate most known cellular functions.[1] Under normal circumstances, a given DNA template and mRNA intermediate encodes and generates a protein optimized for a specialized function in healthy organisms. However in instances where a gene-coding DNA template is mutated, the resulting translation product can be altered, creating an abnormal protein.[2-3] DNA mutations can be harmless (silent mutation), drastic with the subsequent protein having varying degrees of functionality (missense mutation), or completely destructive, stopping the protein from ever being generated (nonsense mutation).[4-7]

When a person has altered DNA that produces an abnormally functioning or non-functional protein, they are classified as having a genetic disorder.[8] The frequency for this simplified definition is difficult to quantify for the total human population, but estimates for all genetic disorders (including other mutation types) predict 3.5-3.9% of the global population to be affected.[9] However, with increasing access to DNA sequencing and ever-more sophisticated technologies/ techniques correlating DNA mutations to diseases with previously unknown causes (idiopathic diseases), the estimated number of individuals living with genetic disorders is continuously increasing.[10]

In many cases, treatment of individuals with severe genetic disorders is limited to hospice care, with only a few notable small molecule drugs known to alter disease-related proteins to their proper functional state.[11-12] However, several therapeutics have been developed in the past decade to alter cellular machinery at the DNA and ribonucleic acid (RNA) levels. The therapeutic technique of introducing DNA or editing the DNA of cells to alter cell functions is colloquially referred to as gene therapy.[13-14] Developments in gene therapy enable control of specific genes, affecting subsequent RNA and protein levels, and allowing for previously untreatable genetic disorder targets to be targeted with high specificity.[15] Further exploration into gene therapy can provide treatments for diseases that were previously non-targetable by small-molecule drugs.

While the field of gene therapy is expanding, there are generally two broad classes of treatments: DNA-based gene insertions and gene editing.[16] DNA-based insertions require the delivery of desired DNA sequences into the nucleus of target cells.[17] This delivery is commonly performed using physiochemical methods,[18-19] synthetic nanoparticles containing DNA cargo,[20-21] or by viral vectors containing desired nucleic acid cargo (detailed further in Section 1.5).[22] Gene therapy treatments utilizing gene editing to alter DNA sequences requires highly specific proteins.[23] Notable gene editing proteins include Zinc Finger Nucleases, Transcription Activator-like Effector Nucleases (TALENs), and most importantly Clustered Regulatory Interspaced Short Palindromic Repeats (CRISPR) associated proteins (Cas proteins). These proteins bind to genomic DNA with varying degrees of specificity and cleave the DNA backbone at desired sites (detailed further in Section 1.3).[24] Induced DNA cleavage results in DNA mutations, with the potential to fundamentally correct the DNA and disease state.

Unlike gene therapies, RNA therapeutics can be used to temporarily modulate protein expression in genetic disorder patients (and those without genetic disorders) using a variety of different RNA molecules. Due to the transient nature of RNAs in cells, administered RNA therapeutics will lead to a temporary pharmacological effect, which can be controllably dosed unlike the DNA-altering events in gene therapies. RNA therapeutics encompass a large variety of RNA species, with RNA-based drugs ranging from 10's to 10,000 of nucleotides (nt) in size and different species possessing unique functions as medicines.[25-27] One of the smaller RNA therapeutics, antisense oligonucleotides (ASOs), are single-stranded 15-30 nt RNAs (or DNAs) that interfere/prevent the expression of target mRNA species, effectively lowering the expression of the proteins the target mRNA encodes (See Figure 1.1).[28] Impressively, these drugs have been clinically available for a few decades. The first FDA-approved ASO drug, Fomivirisen (developed by Isis Pharmaceuticals/Ionis Pharmaceuticals and approved in 1998), was administered via intraocular injection without the need for a carrier/delivery vehicle, due to the ability of ASOs to passively traffic across cellular membranes and tissues.[29] As of this writing, there are seven FDA-approved ASO therapies, and it remains a rapidly-developing market for genetic disorder treatments with no known small-molecule treatments.[30-31]

Double-stranded small-interfering RNAs (siRNAs) are slightly larger than ASOs, generally ranging from 20-25 nt in length (along with corresponding sense strand; 40-50 nt in total) and operate in a manner different from ASOs, but ultimately result in the knockdown/reduced translation of targeted mRNAs.[32] As of this writing there are four FDA-approved siRNA therapies, including givosiran, a siRNA therapy for the treatment of

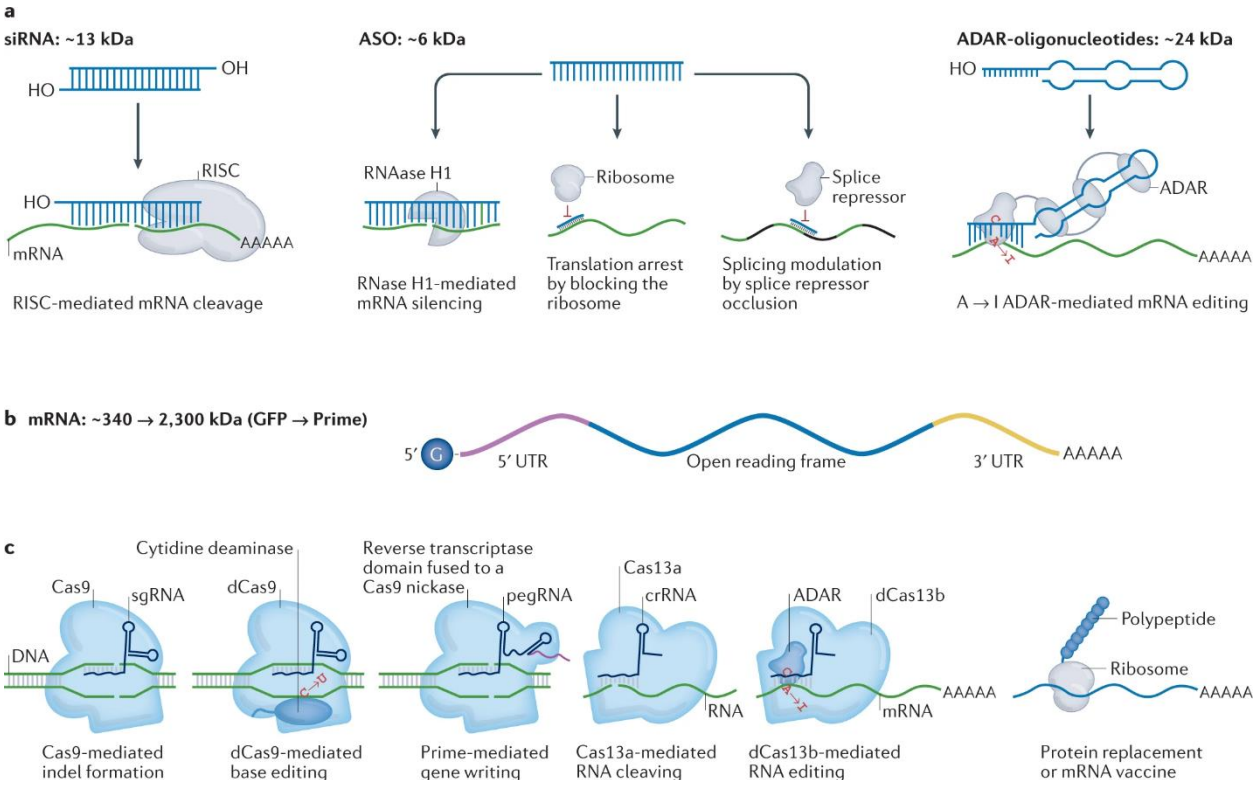

Figure 1.1 Overview of different therapeutic RNAs, CRISPR-Cas gene editing tools, and mechanisms. **A**) mechanisms of siRNA, ASO, and double-stranded RNA-specific adenosine deaminase (ADAR-oligonucleotides; not detailed in this work) therapeutics. **B**) schematic of model (GFP) mRNA including relevant regions within mRNA. **C**) Various Cas-containing RNPs capable of gene editing (detailed further in Section 1.3) and mechanism of mRNA being translated for therapeutics protein replacement/vaccine applications. Reprinted from ref.[27]

primary hyperoxaluria type 1 which previously had no known treatment or cure.[33] With the resounding success of givosiran, accelerated development of siRNA drugs for other genetic disorders will surely follow. Givosiran's success is partially accredited to its chemically-modified siRNA, circumventing the need for a delivery vehicle. Newer siRNA chemistries may assist in translating more RNA therapies to unique disease states.[34]

The largest RNA therapeutics are single-stranded mRNA molecules, typically ranging from 300-10,000 nt and functioning as template molecules for the generation of desired proteins.[35] Treating patients with specific mRNAs can temporarily add desired protein(s) to patients with protein/-enzyme deficiencies, bypassing the limitations of a person's

flawed protein-coding gene. mRNAs are also effective vaccine agents capable of encoding pathogen-specific antigens, such as the immunogenic spike protein found on the COVID-19 virus.[36-37] Lastly, Cas mRNA can be delivered to target cells along with a targeting RNA species to accomplish CRISPR-Cas gene editing (detailed further in Section 1.3).[38]

1.2 mRNA Therapeutic Landscape and Challenges

The mRNA therapeutic landscape is rapidly evolving, but most developments are utilizing mRNA for three major applications: vaccine development, protein replacement therapies, and CRISPR-Cas gene editing (See Figure 1.2).[36]

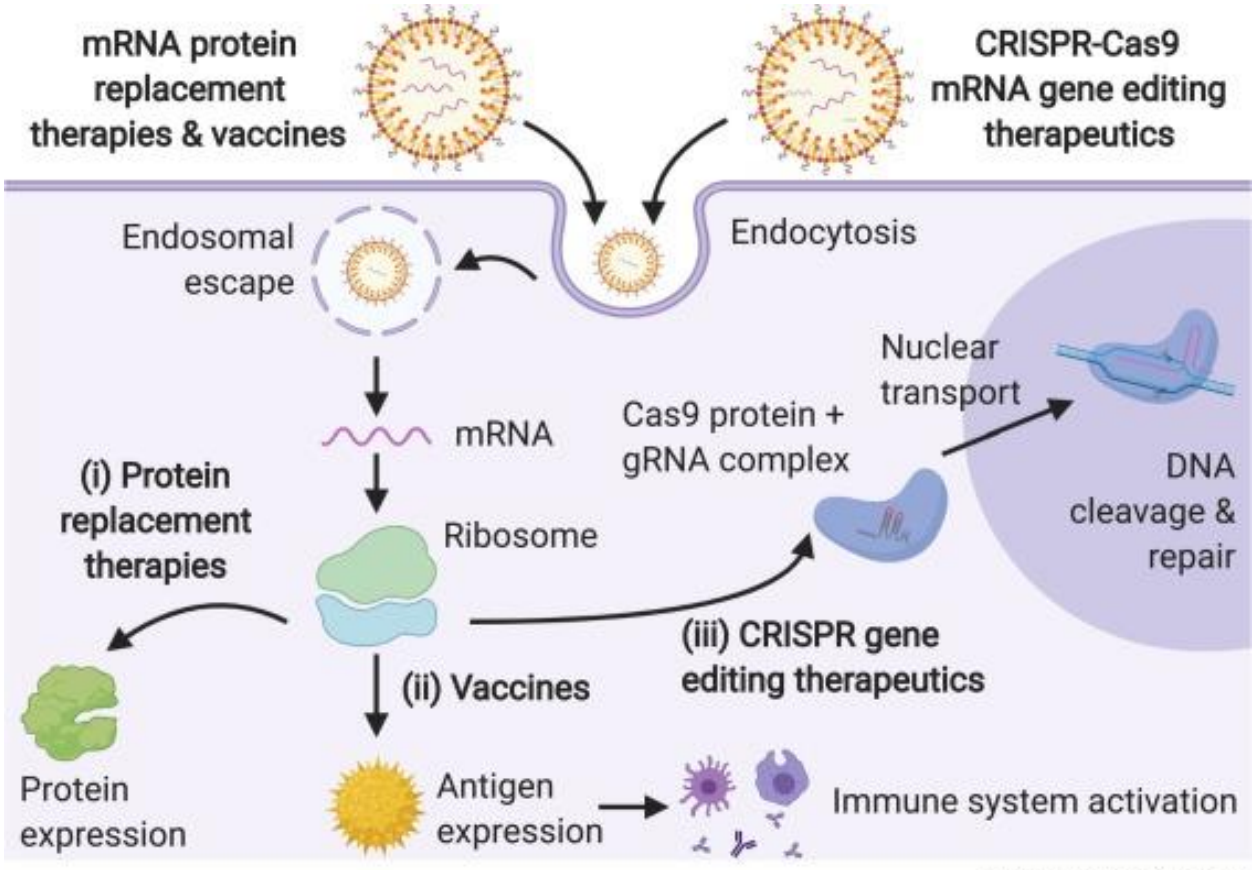

Figure 1.2 Applications of mRNA-based therapeutics. Exogenously-delivered mRNA can be utilized for protein replacement therapies or vaccine antigen expression. Delivery of Cas9-encoding mRNA and sgRNA/gRNA can also be used for CRISPR gene editing applications. Reprinted from ref.[36]

The COVID-19 pandemic led to the rapid development of numerous next-generation vaccines, including two mRNA-based vaccines, SPIKEVAX™ and COMINARTY™, generated by Moderna and Pfizer/BioNTech, respectively. Both of these first-in-class mRNA vaccines encode the COVID-19-specific spike protein that the immune system metabolizes for immune responses against the live COVID-19 virus.[39] Prior to the events of the pandemic, numerous complications that hindered mRNA applications existed, notably limitations in mRNA stability and a lack of delivery vehicles to shield mRNA from degradation prior to delivery in target cells.[40-41]

To aid mRNA stability, Moderna incorporated N1-methylpseudouridine (m1Ψ) nucleobases in place of conventional uridine nucleobases to prevent undesirable immune responses occurring from internal cellular RNA receptors, alter mRNA secondary structure, and generally increase overall target protein production from the mRNA.[42-43] Both Moderna and Pfizer/BioNTech incorporate additional elements on their mRNA strands, including 5'- caps, optimized 5'-untranslated regions, 3'-polyadenosine tails, along with other specific codon optimized sequences to ensure high translation efficiency.[42, 44] Exclusion of these elements results in undesired immune responses in recipient cells along with poor overall protein production. While initially developed for vaccine applications, these mRNA modifications will also be important for the development of mRNAs for protein replacement therapies to ensure that maximal protein production can be obtained from delivered mRNA.

The lack of effective delivery vehicles also stymied mRNA therapeutic translation prior to the COVID pandemic. Despite the stability improvements from the aforementioned mRNA modifications, mRNA is still highly susceptible to degradation in biological

fluids/tissues.[45] Encapsulation of mRNA within a delivery vehicle prevents enzymes such as RNase and other exonucleases from accessing the mRNA phosphodiester backbone and prematurely degrading the mRNA therapeutic before reaching target tissues.[46-47] The development of Moderna's and Pfizer/BioNTech's proprietary lipid nanoparticle constructs (detailed further in Section 1.4) resulted in novel mRNA-lipid formulation strategies with high encapsulation efficiency and mRNA stability.

Leveraging both of these new design elements, numerous other prophylactic vaccines are currently in development using mRNA-based therapeutics, targeting numerous previously neglected viral pathogens including the Epstein-Barr virus (EBV), while also aiming to improve pre-existing influenza vaccines.[48-49] More exciting however are the new approaches taken to generate "therapeutic vaccines" or vaccines administered to persons actively fighting a given disease.[50] These new vaccine designs target persons with latent viral infections, such as human immunodeficiency virus HIV or cytomegalovirus (CMV), to prevent future viral breakouts in patients and other side effects associated with viral infections. Another avenue for these "therapeutic vaccines" are single-protein cancer vaccines and personalized cancer vaccines, where each patient's administered mRNA vaccine sequence is specific to enriched proteins in the individual's cancer.[50] With the promising T cell activation profile obtained from previous mRNA vaccine designs, designing optimal immune responses from these personalized cancer mRNA vaccines appears highly feasible.

Other new developments in mRNA therapies are protein-replacement therapies. As of this writing, Moderna is currently pursuing mRNA replacement therapies for numerous genetic disorders, including *PAH*-induced Phenylketonuria and Ornithine transcarbamylase

deficiency, amongst many others.[27]

Another increasingly popular application of mRNA therapies is CRISPR-Cas gene editing; by incorporating an mRNA transcript that encodes a specific Cas protein (most commonly Cas9), a nucleic acid-editing protein can be produced in the cytosol of target cells.[51] When combined with relevant small guide RNA sequences (either pre-existing in the cell or also delivered exogenously), the mRNA-encoded Cas protein is produced and, specifically for Cas9 protein, migrates to a specific DNA sequence in the nucleus to conduct precise gene editing.[52] An advantage of this methodology is the transient nature of the Cas9 mRNA, producing numerous copies of Cas9 protein in a short timeframe to conduct gene editing. Subsequently, the Cas9 mRNA degrades and no further protein is produced. This shortened expression and gene editing timeframe may reduce off-target effects.[38]

Despite major advances in these mRNA applications, the field of mRNA therapeutics is not without challenges. The most formidable challenge thus far remains targeted cellular delivery, particularly for protein replacement therapy and CRISPR-Cas applications.[53] As of this writing, FDA-approved mRNA therapeutics have been focused on generating responses from immune cells (COVID-19 vaccines), which is the desired therapeutic profile for vaccine delivery. Precision targeting to extrahepatic tissues without undesired immune cell responses remains an unsolved challenge for both protein replacement therapies and CRISPR-Cas applications (detailed further in Section 1.4).[54]

1.3 CRISPR-Cas Gene Editing Background, Therapeutics, and Challenges

Clustered regularly interspaced short palindromic repeats (CRISPRs) are a naturally occurring bacterial defense mechanism in prokaryotes, adapted to identify

foreign pathogenic DNA/RNA sequences (originating from viruses) present within the cell.[52] As a defense against these viruses freely using their host's machinery to replicate, prokaryotes utilize genomic CRISPR array elements to generate specific RNA sequences unique to the pathogen.[55] These small, highly-specific RNAs (crispr RNAs; crRNAs) can hybridize to DNA/RNA sequences from the pathogen genome and act as a form of sequence-specific identification. These small RNAs then associate with a desired CRISPR-associated protein (Cas protein) to form a complete ribonucleoprotein (RNP) complex that is capable of binding to the pathogenic DNA/RNA sequence and cleaving the phosphodiester backbone, deactivating the pathogenic DNA/RNA sequence.

While many Cas proteins and engineered derivatives exist, each possessing unique nuclease activities, the most utilized Cas protein is Cas9. For typical CRISPR-Cas9 gene editing applications, Cas9 protein is assembled with a small guide RNA (sgRNA), which contains both a genomic targeting sequence and sequences to enable proper Cas9 functionality (trans-activating crispr RNA; tracrRNA), to form complete RNPs.[56] This Cas9 RNP translocates to the genome, hybridizes to the specific target DNA sequence, and generates a double-strand DNA break, cleaving both DNA strands in the genome (See Figure 1.3).

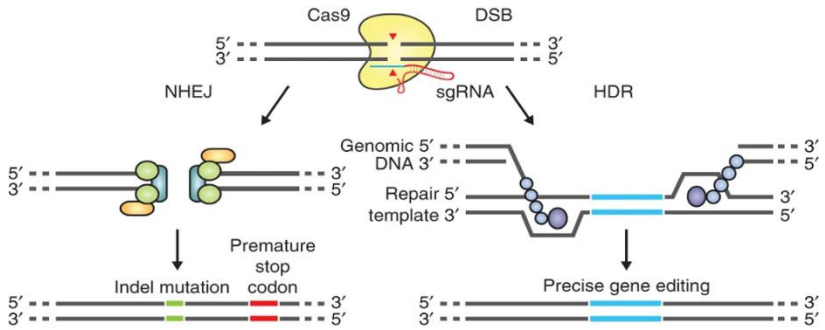

Figure 1.3 CRISPR-Cas9 gene editing mechanism. CRISPR-Cas9 generates double-stranded DNA breaks that undergo NHEJ- or HDR-based repair. Reprinted from ref.[56]

The resulting double-stranded DNA breakage can be mended by two different DNA repair mechanisms: non-homologous end joining (NHEJ) and homology-directed repair (HDR).[57-58] For NHEJ events, the blunt ends of the cleaved DNA are identified as "incomplete" by genomic repair mechanisms, and random insertions of nucleotides at the cleavage site are made before strand re-ligation, resulting in various mutations in the target sequence. Alternatively, NHEJ can result in deleted nucleotides at the cleavage site generated, rejoining the blunt ends with fewer nucleotides than before. Ultimately, NHEJ typically leads to missense and nonsense mutations, resulting in a mistranslated, non-functional protein or premature stop codons that prevent full transcription of the target protein, effectively removing the target protein from the affected genome. Notably, NHEJ ligation of blunt ends without additional insertions or deletions can rejoin the DNA strands, but blunt end ligation would regenerate the original sequence, making this sequence susceptible to cleavage by the RNP complex again.

The NHEJ mechanism is extremely effective at eliminating undesired protein expression in target cells, but it generally lacks the ability to mutate a given DNA sequence to a corrected "healthy" sequence. HDR, the other predominant DNA repair mechanism after Cas9 cleavage, allows for precise genome editing. By including an exogenous DNA template with the correct DNA sequence, genomic repair mechanisms can use the external DNA template as a reference for DNA repair following DNA cleavage. However, this method does require the exogenous delivery of a correct DNA template into the nucleus of the cell, which generates additional complexity when designing appropriate delivery systems.[59]

As of this writing, no CRISPR-Cas therapies have obtained FDA approval, but two notable clinical trials are in progress using CRISPR-Cas9 genomic editing strategies.

CTX001, a collaborative clinical trial managed by both Vertex and CRISPR Therapeutics, is an *ex vivo* CRISPR-Cas9 gene therapy targeting the *BCL11A* enhancer region responsible for repressing γ-globin expression in adults with transfusion-dependent β-thalassemia and sickle cell disease.[60] In these diseased patients there is a mutation in the hemoglobin subunit beta (HBB) gene that results in deformed hemoglobin proteins. This eventually leads to erythrocyte deformation, anemia, and painfully enlarged spleens in affected patients.[61] In this therapy, patients have their hematopoietic stem cells and progenitor cells removed and treated with CRISPR-Cas9 *ex vivo* to enable γ-globin (fetal hemoglobin; functional hemoglobin) expression. After expanding these cells in culture and confirming gene editing, the hematopoietic stem cells are re-injected back into patients. A majority of treated patients reported alleviated symptoms, and improved clinical markers were observed up to one-year post-transfusion. Interestingly, this therapeutic does not target the defective *HBB* gene, but increases expression of γ-globin to alleviate the negative effects of the defective HBB expression. Further developments are sure to follow this highly promising treatment approach.

Another clinical trial, NTLA-2001, managed by Intellia Therapeutics and Regeneron Pharmaceuticals, involves the simultaneous codelivery of Cas9 mRNA and sgRNA within a lipid nanoparticle (LNP) to patient hepatocytes, editing a hereditary misfolding variant of transthyretin (*TTR*) gene (See Figure 1.4).[62] For patients with defective *TTR*, amyloidosis eventually occurs in the liver and heart, resulting in cardiomyopathy, polyneuropathy, and other liver complications if left untreated. Amazingly, after a single dose treatment of these LNPs, patients observed >90% reduction in serum TTR protein 28 days post-injection.

Evaluating patients at longer timepoints will determine if more chronic disease symptoms are alleviated using this therapy.

While these two clinical trials and other preclinical advances using CRISPR-Cas technologies are extremely promising, some issues are still present in CRISPR Cas9 therapies, notably off-target effects.[63] Advances in Cas protein evolution and sgRNA design are partially alleviating off-target concerns, preventing non-specific sequences in target genomes from being accidentally cleaved, but further genomic studies are needed to confirm the improved benefits of these design modifications.[64] Unfortunately, similar to the RNA therapeutics mentioned earlier, delivery of CRISPR-Cas9 components to specific tissues/cells remains one of the most difficult barriers for these remarkable gene editing tools.

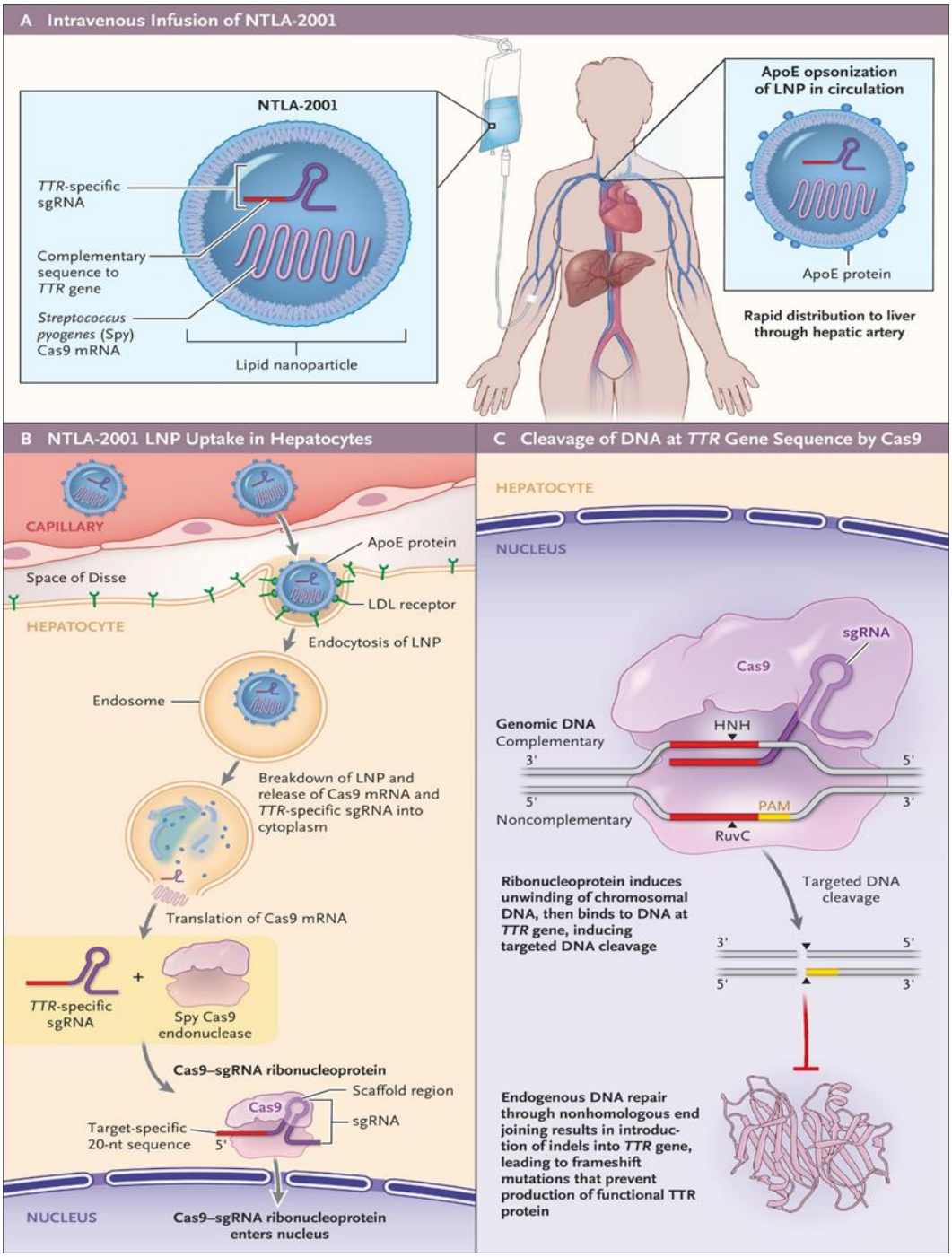

Figure 1.4 Overview of NTLA-2001 *in vivo* gene editing clinical trial. **A**) Structure and administration route of NTLA-2001 LNP containing Cas9 mRNA and *TTR*-specific sgRNA. **B**) Diagram depicting hepatocyte uptake and LNP decomplexation to generate Cas9 RNPs *in situ* (within patients). **C**) Cas9 RNP-induces cleavage of *TTR* in patients, preventing further generation of TTR proteins. Reprinted from ref.[62]

There are three different methods of expressing CRISPR-Cas9 using exogenously supplied components to target cells. By delivering a CRISPR-Cas9-encoding plasmid (usually 7-10 kilobases [kb]), all CRISPR-Cas9 RNP components can be generated *in situ* to perform gene editing. By codelivering Cas9 mRNA (~4,500 nt) along with a relevant sgRNA, Cas9 protein is generated *in situ*, and supplied sgRNA combines with Cas9 protein to from RNPs. Lastly, pre-formulated Cas9-sgRNA RNPs (~200 kDa each) can be administered to cells directly.[65] Unfortunately, all these CRISPR-Cas9 cargoes are large and, particularly for plasmids and mRNA, highly negatively charged. These large sizes and unfavorable charge properties drastically limit passive cell membrane permeability. Moreover, when exposed to biological fluids, degradation of CRISPR-Cas9 cargoes can occur quickly through exposure to native DNases, RNases, or proteases. To overcome these hurdles for *in vitro* and *in vivo* delivery, CRISPR-Cas9 machinery needs to be encapsulated within a construct/delivery vehicle to facilitate transport in biological fluids and across the cell membrane.

The recent utilization of Cas9 mRNA and sgRNA in NTLA-2001 emphasizes the strong potential of delivery constructs, particularly synthetic delivery vehicles, as carriers for CRISPR-Cas9 machinery. NTLA-2001's Cas9 mRNA formulation exhibits excellent encapsulation of large Cas9 mRNA (>90% efficiency) within a synthetic LNP vehicle and enables efficient release of mRNA cargo upon entry into the cytosol.[62] Moreover, unlike CTX001, NTLA-2001 is the first *in vivo* gene editing therapy, editing cells within a person without a need for invasive surgery. This tremendous accomplishment in targeted lipid nanoparticle delivery sets an excellent precedent for future *in vivo* CRISPR-Cas therapies.

1.4 Lipid Nanoparticles: Mechanistic Design, Profound Success, and Limitations

The first FDA-approved small-interfering RNA (siRNA) therapy, Patirisan (developed by Alnylam Pharmaceuticals and approved in 2018), is administered using a lipid nanoparticle platform that facilitates siRNA cargo transport in biological fluids, trafficking across the cell membrane, and successful delivery of siRNA cargo into the cytosol of cells.[66] This exciting siRNA approval somewhat overshadowed another equally exciting aspect of this therapy: the first FDA approval of a heterogeneous lipid nanoparticle containing numerous components, notably an ionizable lipid species.

Modern LNP formulations are multifunctional and contain numerous components (See Figure 1.5), including helper lipids to increase LNP monolayer stability,[67] cholesterol to enhance core stability,[68] PEGylated lipid to prevent aggregation,[69] optional targeting ligands, and mRNA at the nanoparticle core.[36] However, the largest component in these

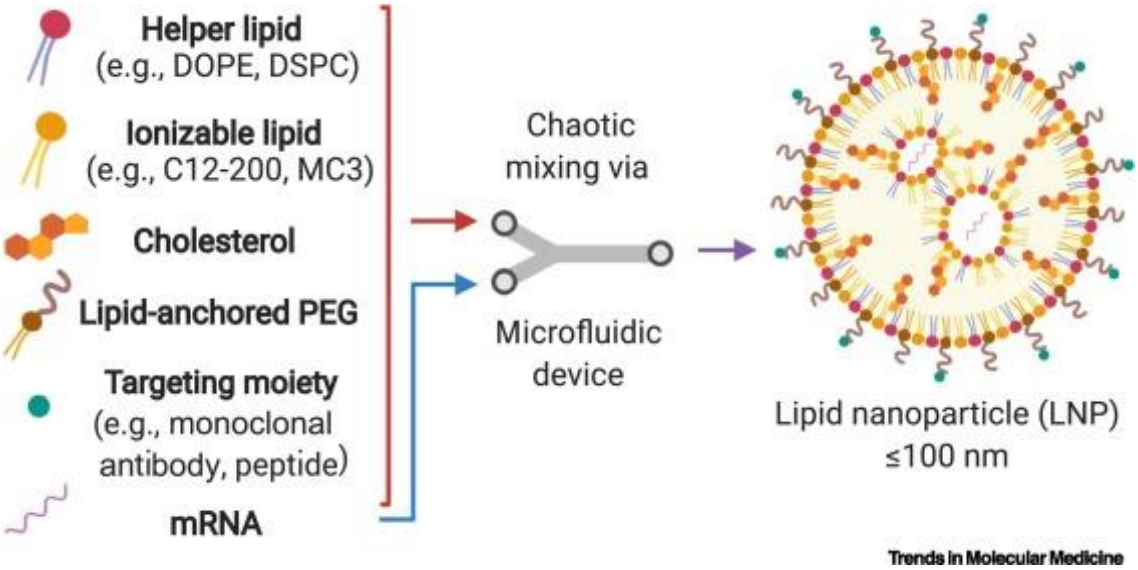

Figure 1.5 Formulation approach to generate mRNA-encapsulated LNPs. Chaotic mixing of hydrophobic components (within red bracket; containing organic solvent) and aqueous-buffered mRNA results in heterogenous mRNA-containing LNPs. Reprinted from ref.[36]

LNP designs is the most important: the ionizable lipid species, usually ranging from 40-50 mol%.[70-71] These ionizable lipids, typically containing tertiary amines, are designed to have a conjugate acid p*K*a within the range of 5 to 7. During formulation, a buffered mRNA solution (pH 4-5) is mixed with the cocktail of desired lipids from a separate mixture (generally aqueous with 10-20% organic solvent or completely organic) in a microfluidic chamber, ensuring precise, controlled mixing of these two components. Due to the low pH of the mRNA solution, the ionizable lipid species is protonated upon mixing and associates with the phosphates on the mRNA through electrostatic interactions, forming micelles/reverse micelles with mRNA at the core. Later buffer exchange steps bring LNPs to physiological pH and result in more lipid species condensing to form a monolayer around the micelles, ultimately generating LNPs with neutral ionizable lipid species in the outermost layer.[36]

This successful formulation strategy has been repeated for both FDA-approved mRNA drugs and for one siRNA drug therapy. However, the exact ionizable lipid species differs for each of these therapies (See Figure 1.6). As stated previously, lipids containing tertiary amines are the most common and commercially adopted form of ionizable lipids. As of this

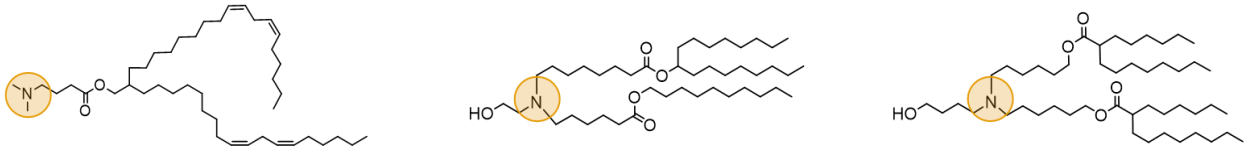

Dlin-MC3-DMA
p*K*a 6.44

ONPATTRO™
(Alnylam, 2018)

SM-102
p*K*a 6.75

SPIKEVAX™
(Moderna, 2022)

ALC-0315
p*K*a 6.09

COMIRNATY™
(Pfizer-BioNTech, 2021)

Figure 1.6 Ionizable lipids used in current FDA-approved LNPs. Yellow circles highlight ionizable amines that make these lipids pH-responsive (conjugate acid p*K*a values for amines listed below structures).

writing, no other chemical motifs for mRNA association, condensation, and ionization are being explored at the clinical level.

These ionizable lipid species also possess a secondary function: assisting in endosomal escape upon LNP internalization by target cells.[72] After LNP administration *in vitro/vivo*, these nanoparticles are internalized by cells through an endocytic pathway, during which the nanoparticles are subject to increasingly acidic environments (endosomes or lysosomes). In these acidic environments, the ionizable lipid species within the LNP becomes protonated, generating a cationic charge that favors closer interactions with the negatively-charged inner leaflet of the endosome/lysosome membrane (See Figure 1.7).[73] After enough ionizable lipids become protonated, the lipids of the LNP

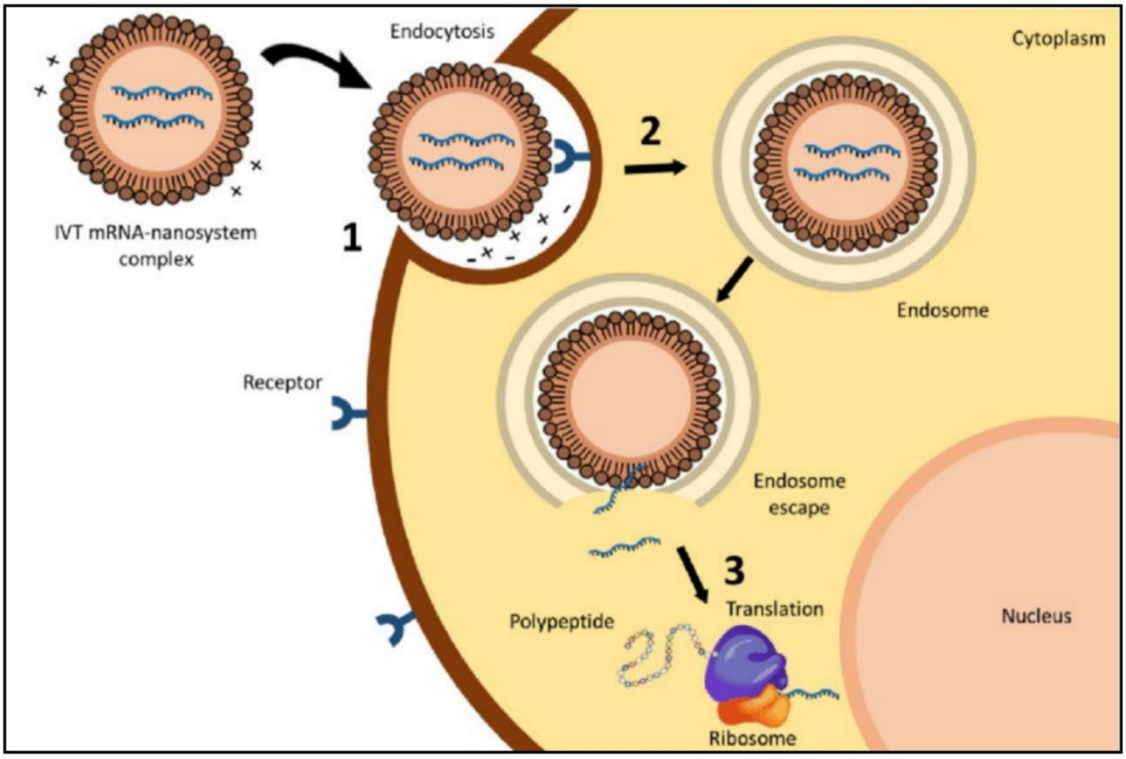

Figure 1.7 LNP endocytosis and endosomal escape mechanism. mRNA-containing LNPs are internalized by cells through endocytosis and perform endosomal escape by fusing with endosome lipid membranes after endosomal acidification. Resulting LNP fusion releases mRNA cargo into cells. Reprinted from ref.[73]

destabilize the inner leaflet of the endosomal/lysosomal membrane, enabling fusion of the LNP to the endosomal membrane and releasing mRNA cargo into the cytosol of the target cell.

The remarkable success of LNP delivery vehicles for RNA therapy is a turning point for new therapeutic development, but there are still limitations to the platform. LNP colloidal stability over long periods of time remains a challenge, despite PEGylation.[74] Additional small-molecule additives and alternative storage conditions, notably lyophilization, and currently being explored to increase the long-term stability of these LNP systems. Another potential problem with current LNP systems arises from the non-biodegradability (and tissue accumulation) of current ionizable lipid species.[75] Upon endosomal membrane fusion with LNPs, the ionizable lipid species is physically incorporated into host membranes and remains if no pathways exist to degrade the ionizable lipid into smaller soluble metabolites. While the issue of nonbiodegradable ionizable lipid toxicity is not problematic for vaccines, predominantly because the overall dosage is low, this can cause undesired toxicity in applications where repeated dosing is required, like in protein replacement therapies. To tackle this issue, researchers are attempting to incorporate bioreducible motifs, like disulfide linkages, within the ionizable lipid/lipidoid species so that tertiary amino groups can be metabolized after incorporation into the cell membranes.[76] Numerous lipid-like materials are also being investigated as alternatives to non-biodegradable ionizable lipid species.[77-78]

Targeted delivery remains the greatest limitation on the development of new LNP-based RNA therapies. While both SPIKEVAX™ and COMINARTY™ achieve delivery to antigen-presenting cells of the immune system, ONPATTRO™ remains the only FDA-

approved organ-specific LNP therapy, delivering siRNA cargo specifically to the liver.[66] While other therapies in clinical development are capitalizing on the tendency of LNPs to target hepatic tissues, delivery of RNA to extrahepatic tissues remains a significant obstacle. The incorporation of cell-targeting ligands is an exciting new approach to making LNPs tissue- and cell-specific, but the identification of viable ligands is a continuously evolving field. Fortunately, LNPs are highly modular systems, and the incorporation of unique cell-targeting ligands into lipids can usually be achieved through facile bioconjugation techniques.[79]

In an approach not following the targeting ligands paradigm, Siegwart and coworkers used different cationic lipid species during the complexation of mRNA-loaded LNPs to control organ-specific expression.[80] This selective organ targeting (SORT) system so far has predominantly shown success in targeting the lungs, spleen, and livers of treated mice using model mRNAs (See Figure 1.8). Further expansion of the SORT system demonstrated >10% gene editing in all the lungs and livers of targeted animals when administering LNPs complexed with SORT lipids, Cas9 mRNA, and sgRNA. More derivations of this system are expected, mixing various combinations of ionizable lipid species, SORTing lipids, and various other ligand-conjugated lipids to obtain a more expanded scope of organ-specificity.

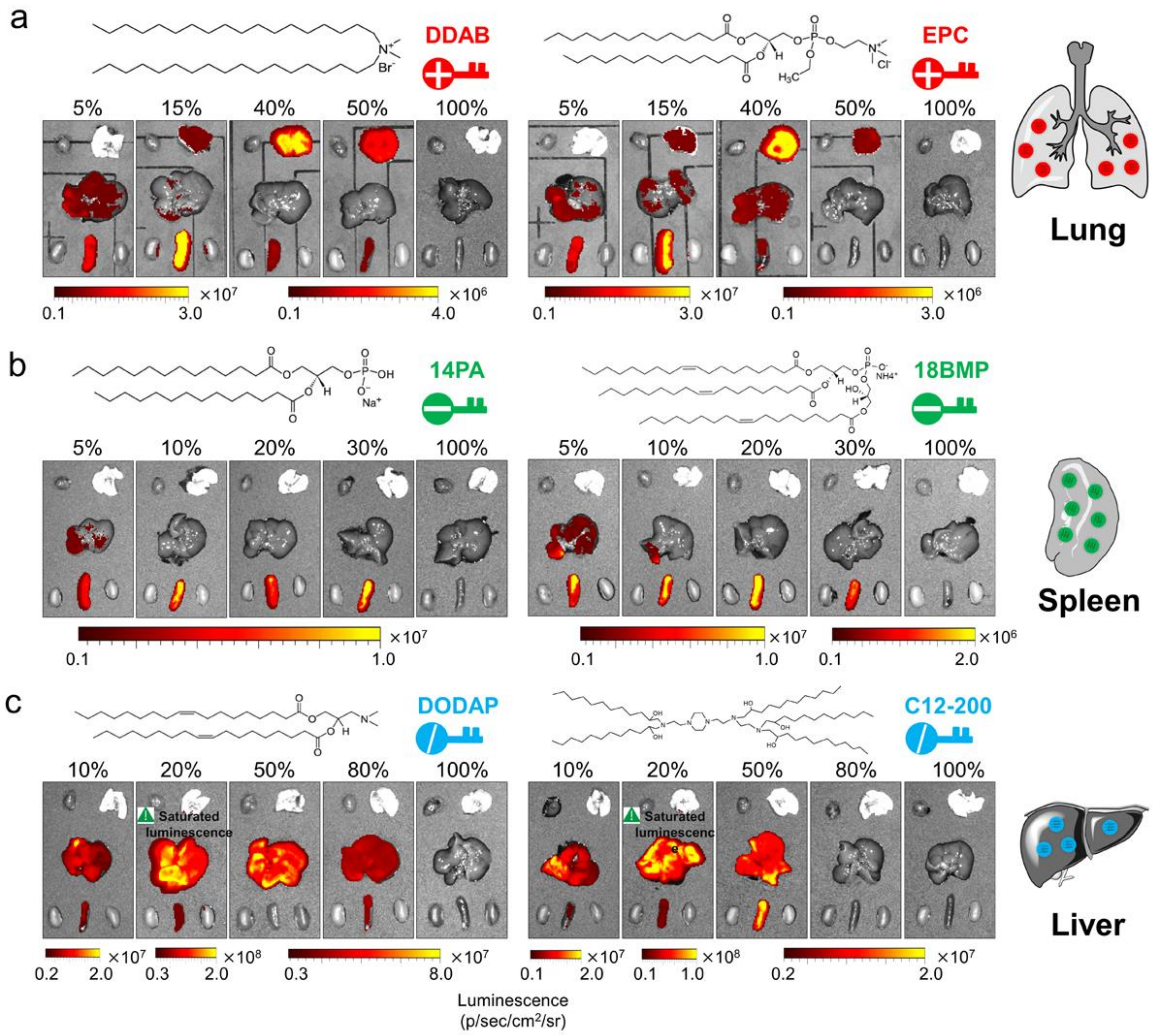

Figure 1.8 Organ-specific SORT LNPs for targeted RNA delivery. Specific ratios of unique cationic lipids can be used in LNPs to obtain organ-specific mRNA delivery to lungs, spleens, and livers of mice. Reprinted from ref.[80]

Further developments in the field of targeted therapy designs are rapidly progressing, and major breakthroughs in targeted therapies will likely follow as novel cell-targeting ligands, cationic lipids, and ionizable lipids are discovered.

1.5 Viral Vectors as CRISPR-Cas Therapeutic Delivery Vehicles

Throughout eons of continuous evolution and competition with eukaryotic organisms, Nature has generated pathogenic tissue-specific nucleic acid delivery vehicles,

also known as viruses. The objective of a virus is fundamentally simple: targeting specific cells in a host, hijacking the host's cellular machinery to replicate more viral genomes and capsid proteins, and generating more virus particles to infect more cells. While straightforward in strategy, different viruses target different cell types, possess varied viral genome nucleic acid composition (DNA or RNA), and have differing mechanisms for viral genome replication in the host cell.[81-82] While these aspects of viral pathology are important in combating disease, they are now equally important in the design of next-generation RNA therapy and gene therapy delivery vehicles.

Cell-specific targeting capability is a quintessential trait of viruses; infecting the correct cells is needed to ensure propagation and transmission to new hosts. By capitalizing on viral cell-specificity, viral cargo can be altered to include therapeutically relevant DNA. One of the most rapidly developing viral vectors for targeted gene therapy are adeno-associated viruses (AAVs). AAVs are extremely small (20nm) replication-defective single-stranded DNA viruses that actively infect a variety of human cells but are not known to cause any specific disease. AAV's ability to infect different types of human cells (tropism) is a by-product of their unique serotyping, or the unique receptor-binding proteins displayed on the AAV capsid.[83-84] For example, AAV serotype 2 (AAV2) displays a natural tropism towards skeletal muscle cells, neurons, and other cells while AAV serotype 8 (AAV8) possesses excellent tropism towards liver hepatocytes and pancreatic cells. Researchers and clinicians can easily engineer AAVs to possess further enhanced tropism and cater specific gene therapies to these target tissues. The first *in vivo* FDA-approved gene therapy, Luxturna (developed by Spark Therapeutics), used an AAV2-serotyped virus

to treat retinal cells in patients with Leber congenital amaurosis.[85] As of this writing, only two AAV vectors have been FDA-approved, but many more are in drug pipelines.[86]

However, there are two potential pitfalls of using AAVs for gene therapy: low genomic cargo size and potential immunogenicity. Despite AAVs possessing ssDNA genomes, the size limit for AAV cargo is 4.8 kb, which is much smaller than many desired gene editing plasmids, particularly those encoding CRISPR-Cas9 machinery.[87] While this remains problematic for specific gene therapy designs, truncated CRISPR-Cas designs could be generated to overcome AAV size limitations. As for immunogenicity, AAVs do not generally create a cytotoxic response, but they do generate neutralizing antibodies upon repeat exposure.[88] Despite these issues, more AAV vectors are being researched and translated, making them extremely promising vectors for future genetic disorder treatments.

Lentiviruses are another highly developed viral vector class already utilized for gene therapies. These vectors, which are engineered from retroviruses (such as HIV), contain RNA genomic cargo but also possess copies of reverse transcriptase and restriction enzymes to insert a given gene into the target cell genome.[89] Two FDA-approved lentiviral gene therapies exist, Skysona and Zynteglo (both developed by Bluebird Bio), that insert corrected genes for ABCD1 and HBB, respectively.[90-91] Both of these lentiviral therapies rely on *ex vivo* cell treatment, which somewhat limits the scope of genetic disorders that can be targeted/treated. However, the success of these trials will certainly increase the likelihood of future trials for individuals with hematopoietic stem cell-based genetic diseases. Interestingly, no CRISPR-Cas lentiviral clinical trials are currently underway,

although CRISPR-Cas technologies are fully compatible with lentiviral vectors. Finally, despite the exciting success of these viruses *ex vivo*, the immunogenicity and lack of cell specificity remain major challenges for these viral vectors as *in vivo* gene editing vehicles.[89]

Two other viral vectors with preclinical promise in gene therapy are modified herpes simplex viral vectors and modified polioviruses. Herpes simplex viruses and polioviruses are both capable of infecting neuronal cells, which are of great interest to many genetic disease models. Herpes simplex viruses also have larger genomic size limits (~125-300 kbp) than AAVs, making them amenable to containing CRISPR-Cas9-encoding DNA elements.[92] Polioviruses also have a larger genomic capacity (~7 kbp) than AAVs, making them more favorable for containing CRISPR-Cas9 DNA elements. Unfortunately, neither polioviruses nor herpesviruses have yet been utilized in gene therapy clinical trials.

1.6 Biodegradable Cationic Polymer Designs for RNA-Based CRISPR-Cas9 Gene Editing

As stated previously, ionizable cationic lipids are favored in modern synthetic nanoparticle RNA delivery designs because they complex with RNA species through electrostatic interactions. Similar cationic motifs were already implemented in polymeric nucleic acid delivery vehicles, predating the use of modern cationic lipid designs. Polyethyleneimine (PEI) was one of the first studied cationic polymer systems for DNA and RNA delivery.[93] PEI complexes to phosphate groups present on nucleic acids via amines that are protonated at physiological pH. However, PEI contains additional amines that are not protonated at physiological pH due to the inductive effect of adjacent protonated

ammonium groups. This effect is beneficial for the cellular delivery of PEI-RNA nanoparticles, as these neutral amines become protonated at endosomal/lysosomal pH (pH 5-7), destabilizing the endosome/lysosome through the proton sponge effect.[94-95] These two properties, having cationic motifs for RNA complexation and ionizable groups for endosomal escape, have become essential in other cationic polymer designs for RNA delivery.

Unfortunately there is a major disadvantage to PEI: cytotoxicity in recipient cells due to poor PEI biodegradability in the cytosol.[96] Unlike cationic lipid nanoparticles that fuse directly with their target cell membranes, cationic polyplexes undergo endosomal escape to release polyplexes into the cytosol of target cells (See Figure 1.9).[97] Cationic polyplexes remain intact within the cytosol after endosomal escape and RNA cargo must

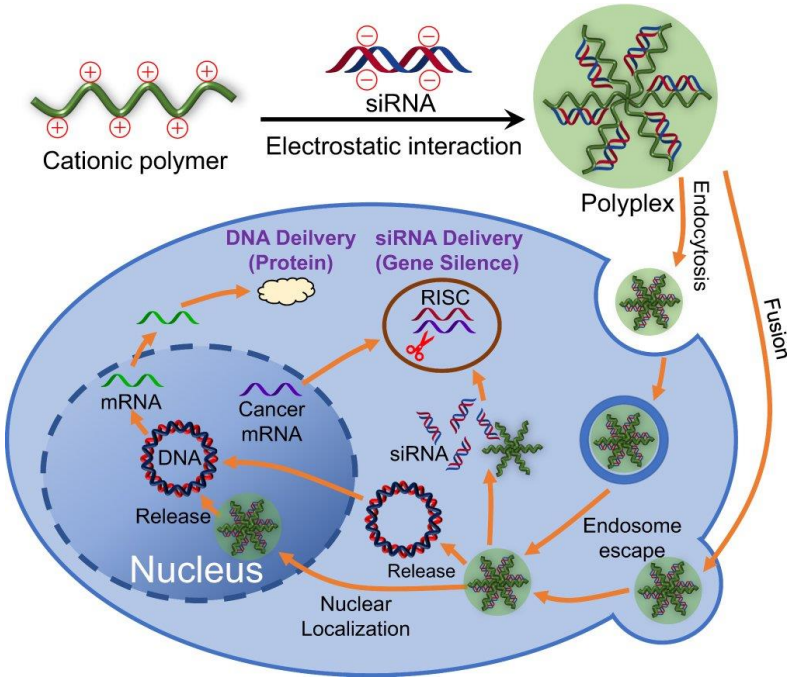

Figure 1.9 Polymer-RNA polyplex endocytosis and endosomal escape mechanism. Cationic polyplexes with RNA entering cells through endocytosis or fusion persist within cellular cytosol. Additional polyplex decomplexation is needed to fully release RNA cargo. Reprinted from ref.[97]

undergo additional decomplexation to enact their intended biological effect. PEI successfully fulfills this requirement, but the decomplexed PEI remaining in the cytosol after RNA release is non-biodegradable, ultimately resulting in accumulation and cytotoxicity. To alleviate this, researchers have pursued synthetic methodologies to include biodegradable linkages, like disulfide motifs or ketal motifs, into the PEI backbone so that smaller, less toxic polymer segments can be generated.[98] While successful at reducing cytotoxicity, the basic subunits of PEI remain non-biodegradable, which may still result in accumulation if cells are subject to repeated doses.

To alleviate cytotoxicity issues of arising from biodegradability, numerous polymer constructs have been developed containing fundamentally biocompatible monomer units or biodegradable linkages between repeat units. Three exemplary biodegradable polymer systems useful for RNA and CRISPR-Cas delivery are poly-β-amino esters (PBAE), cationic dendrimers, and charge-altering releasable transporters (CARTs).

PBAE polymers are usually synthesized through the step-growth polymerization between an amino- monomer and a diacrylate monomer (via aza-Michael addition).[99] PBAE polymers are highly biodegradable due to the presence of ester bonds between each repeat unit, which can hydrolyze in the cytosol over time. This biodegradability can be augmented by introducing disulfide groups into monomer feedstocks without compromising RNA delivery capabilities.[100] However, the advantages of this system are truly seen by its large monomer scope and various potential architectures. By screening numerous amine-containing monomers, the polymer pK_a can be optimized to the endosomal/lysosomal pH range, and the hydrophobicity can additionally be modified from the diacrylate monomer selected.[101] Furthermore, by using various tri- and tetra-acrylate monomers, PBAEs with

various degrees of crosslinking can easily be synthesized.[102] These different polymer architectures have been successful in RNA delivery experiments and further expand the applicability of this system.

PBAEs that are highly successful as mRNA and CRISPR-Cas9 gene editing vehicles can be readily generated through monomer derivatizations. Recent works have expanded the usual two-component PBAE synthesis to include three-component PBAEs.[101] By incorporating different hydrophilic and hydrophobic amine-containing groups, Green and coworkers were able to generate PBAEs that can deliver plasmid DNA, siRNA, and mRNA with varying delivery efficacies depending on the polymer composition.[101] Moreover, polymer pK_a values, nanoparticle uptake efficiency, and endosomal escape efficiency were also quantified for each polymer /nucleic acid cargo combination. These vectors were capable of *in vivo* mRNA delivery to the lungs, spleen, and livers of treated mice (See Figure 1.10). A similar study by Green and coworkers utilized branched PBAE polymers to complex and deliver CRISPR-Cas9-encoding plasmid DNA to perform gene editing *in vitro*.[103] Lastly, a carboxylated derivative of these branched PBAE polymers successfully complexed Cas9 RNPs to perform gene editing in a tumor model but has not yet been applied towards nucleic acid delivery.[104] With proven *in vi*vo applications and excellent chemical-tunability, future PBAE derivatives show great promise as mRNA/ CRISPR-Cas9 gene editing delivery vehicles.

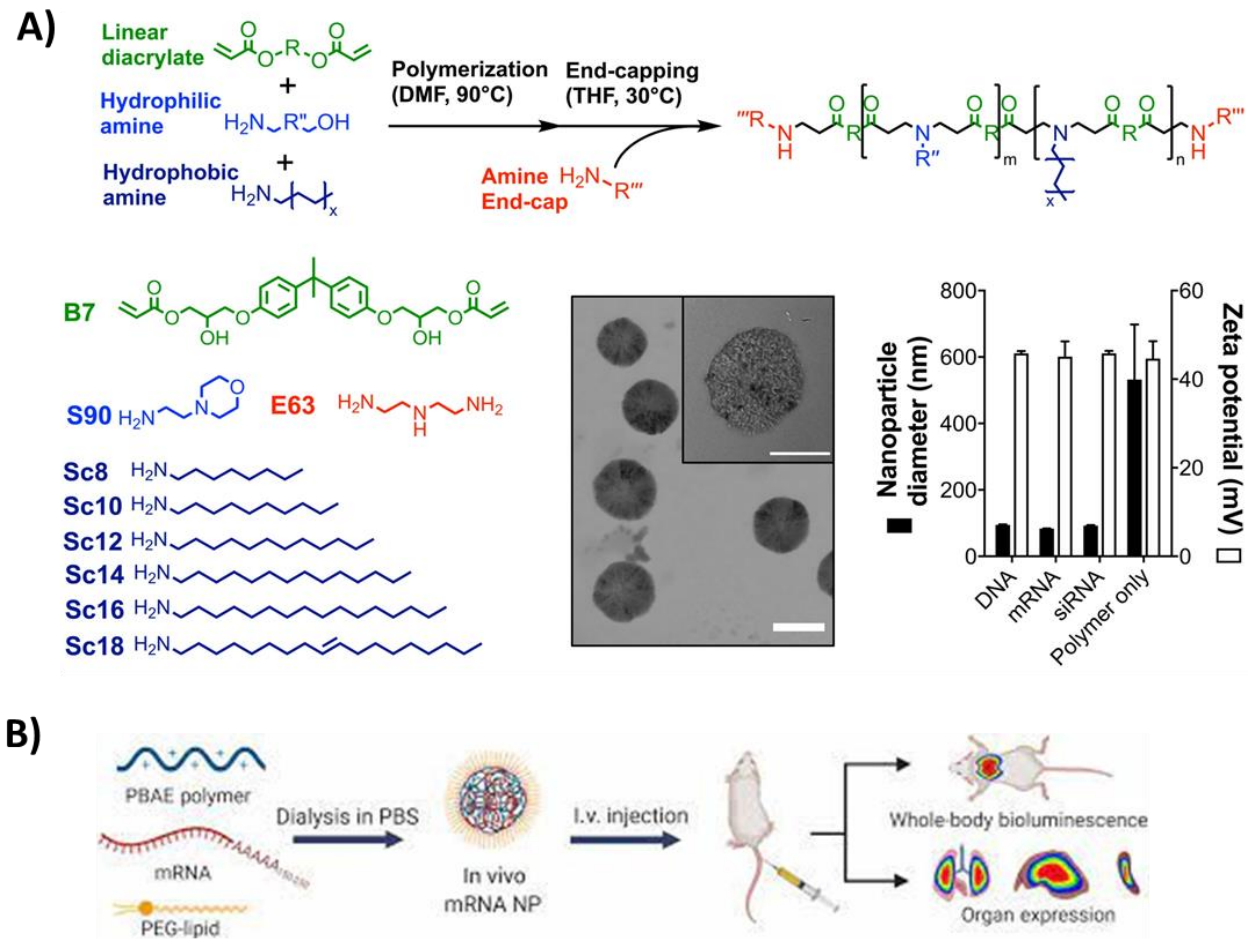

Figure 1.10 PBAE polymers for the delivery of DNA and RNAs *in vivo*. PBAE polymers are complexed with siRNA or mRNA to generate polycationic polymeric nanoparticles delivering RNA to lungs, livers, and spleens *in vivo*. Reprinted from ref.[101]

Polyamidoamine (PAMAM) dendrimers are another class of polymers containing numerous amines for RNA complexation. Unlike linear or branched PEI, PAMAM dendrimers are well-defined hyperbranched polymers generated from a symmetrical core.[105] Classical PAMAM dendrimers have been utilized for siRNA delivery applications,[106] but the diversity of this system has enabled other dendrimer systems to be synthesized for RNA delivery applications.[107]

Percec and coworkers have shown success in synthesizing amphiphilic Janus-type dendrimers, which generated 100-350 nm nanoparticles after formulation with mRNA.[108]

These dendrimer-RNA polyplexes provided mRNA expression in the livers and spleens after *in vivo* administration. Anderson and coworkers utilized a well-defined amino-alcohol dendron to assemble mRNA-polymer nanoparticles; resulting polyplexes generated excellent desired immune response profiles towards RNA viruses and intracellular pathogens in *in vivo* challenge studies (See Figure 1.11).[109] Although only one dendron species was synthesized, this simple approach towards dendron synthesis and nanoparticle formulation approach can readily be derivatized in future mRNA applications. In a third example, Seigwart and coworkers were also able to synthesize dendrimer-based lipid nanoparticles capable of complexing with three different nucleic acid species simultaneously (sgRNA, Cas9 mRNA, and ssDNA) to form <200 nm nanoparticles as measured by dynamic light scattering (DLS).[110] *In vivo* Injection of these nanoparticles resulted in >20% HDR-mediated gene editing within a tumor model. With new developments in dendrimer chemistries and formulation techniques, the future of

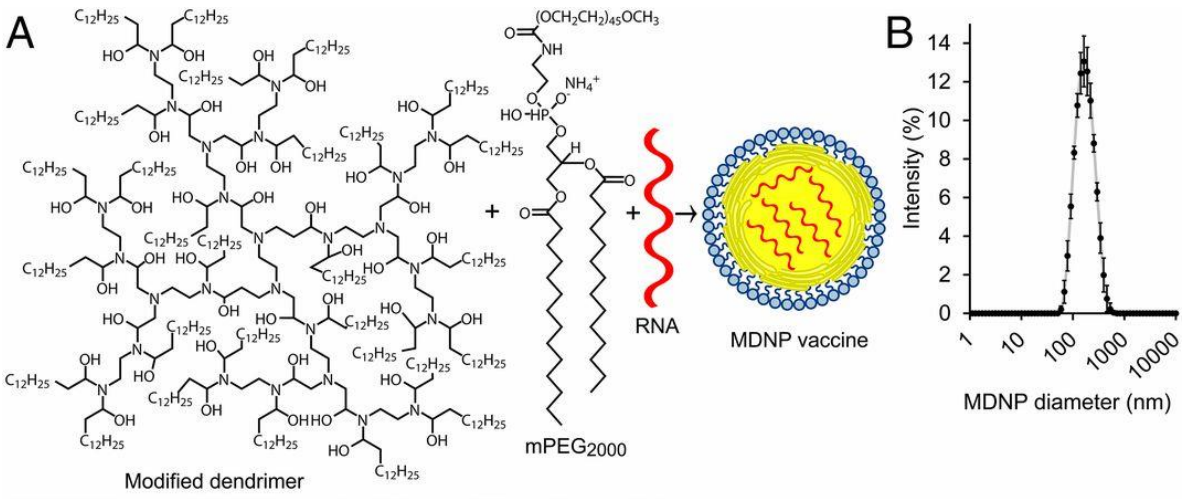

Figure 1.11 Amino-alcohol dendrimer for mRNA vaccine applications. **A**) Small molecule amino-alcohol dendrimer can complex with mRNA (and PEG) to generate nanoparticles. **B**) Amino-alcohol dendrimer complexed with mRNA generates well-defined nanoparticles by DLS. Reprinted from ref.[109]

dendrimer applications in mRNA delivery and gene editing remains promising.

Waymouth and coworkers (along with Grinstaff et al.) have pioneered the synthesis of charge-altering oligo(carbonate-b-α-amino ester) polymers (CARTs) through a simple organic ring-opening polymerization (OROP) methodology (See Figure 1.12).[111-112] Resulting polymers have polycarbonate and α-amino ester block segments that govern polymer hydrophobicity and cationic charge capability, respectively. A small library of these polymers was shown to be effective at complexing with model mRNA species, and resulting nanoparticles demonstrated uptake by antigen-presenting cells, making them excellent candidates for future mRNA vaccine vectors. Further derivatization of this vector platform added α-amino ester monomers and amino-acid derived lactones for a more

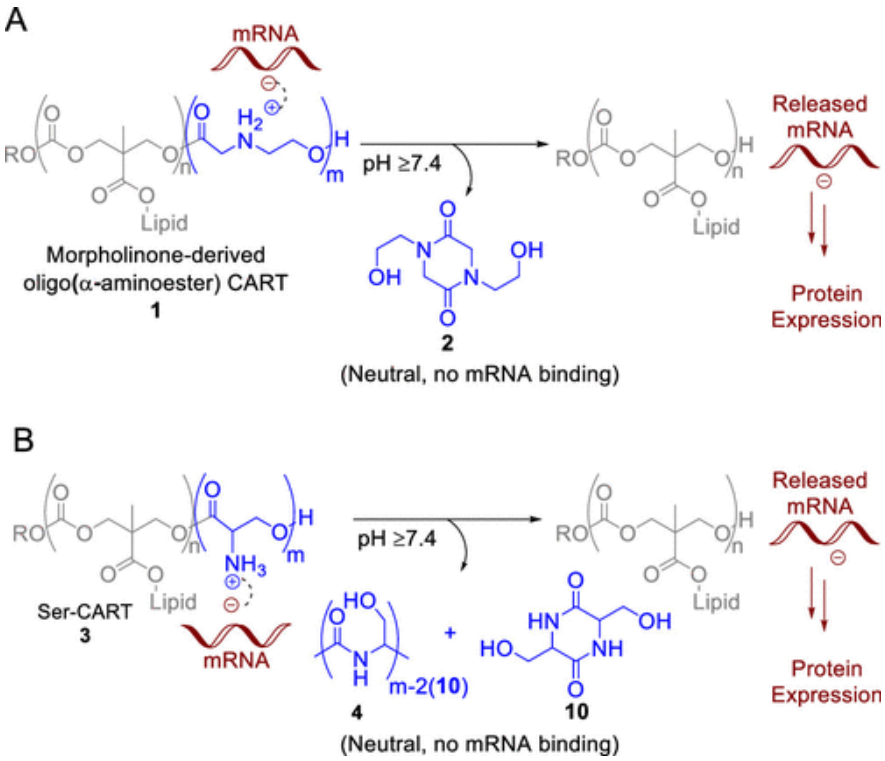

Figure 1.12 CART polymer designs for bio-compatible mRNA delivery and depolymerization. CARTs generated from: **A**) α-aminoester -containing monomers or **B**) amino-acid-derived lactone monomers can complex with mRNA, delivery mRNA to cells, and depolymerize rapidly to release mRNA cargo. Reprinted from ref.[112]

compatible facile OROP methodology.[113] These vectors possess rapid biodegradability (<60 minutes until fully depolymerized) resulting from their various ester and carbonate motifs and readily degrade to form cyclic monomers upon cytosolic entry to release mRNA cargo. This polymer platform has also been used to achieve CRISPR-Cas9 gene editing *in vitro*, using nanoparticles generated from CART polymers, Cas9 mRNA, and a 2'-acetylated "cloaked" sgRNA.[114] While excellent gene editing was obtained, interestingly, the nanoparticles generated were not fully characterized, but future CART derivatives of this design will be promising CRISPR-Cas9 gene editing tools.

1.7 Polydisulfide Polymers: Synthetic Approaches and RNA Delivery Applications

Among the most exciting polymers to be generated within the past few decades are polydisulfides, particularly those generated from α-lipoic acid (LA). LA is a naturally-occurring 1,2-dithiolane with a pendant carboxylic acid motif. LA is an essential cofactor for certain enzymes but is generally found in the human body as a covalent adduct to proteins instead of in the soluble small molecule form.[115] Generally, a LA-protein adduct is generated through an amide bond of lysine residue to LA's carboxylate group, suggesting LA-amide conjugates are already biocompatible. As a potential monomer for polymerizations, the 1,2-dithiolane of LA is estimated to possess a ring strain of 4-6 kcal/mol, suggesting ROP is feasible under specific conditions.[116] Similar calculations for the carboxylate form of LA were found to possess an ROP enthalpy of -2.7 kcal/mol in aqueous media[117]; a methylated LA derivative was also calculated to have an ROP of -4.8 kcal/mol in THF.[118] These enthalpies suggest that LA ROP should be synthetically feasible

in both organic and aqueous solvents and recent works explored how this can be leveraged to make new biodegradable polymeric materials.

One of the first LA-derived polydisulfides used in a biological context was conducted by Chroboczek and coworkers, performing an alkaline anionic ROP of a quaternary ammonium-containing LA derivative and using the resulting polymer for DNA delivery.[119] Unfortunately, the resulting polymers were not extensively characterized. It was not until 2013 when Matile and coworkers generated a robust anionic ROP protocol where cationic polydisulfides could be fully characterized by size exclusion chromatography.[120] These polydisulfides, which were synthesized from LA derivatives containing guanidium pendant groups, were polymerized in a pH 7 buffer with or without a thiolate initiator and demonstrated excellent depolymerization capability (See Figure 1.13). Matile and

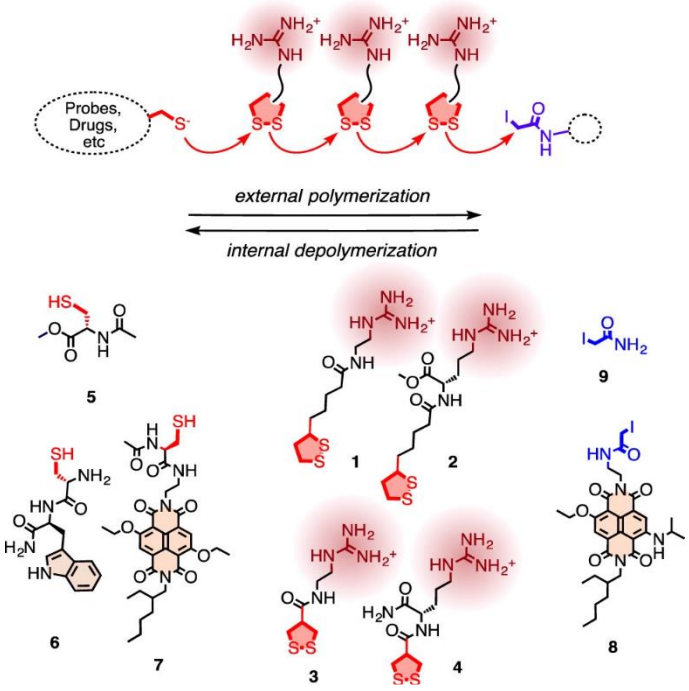

Figure 1.13 Aqueous-phase cationic polydisulfide synthesis and depolymerization. Guanidium-containing lipoic acid monomers (1-4) can generate polydisulfides using initiator-driven (5-7) ROP along with relevant terminators (8-9) in aqueous conditions. Reprinted from ref.[120]

coworkers explored using these polydisulfides for biological applications, determining that polydisulfides containing amphiphilic monomers (still containing guanidinium groups) or high molecular weight (MW) affect cellular localization and polymer depolymerization kinetics.[121] More specifically, cationic polydisulfides containing aromatic functionalities localized to and became trapped within endosomes, whereas strictly cationic polymers translocated directly across the cell membrane and sometimes to the nucleus. A similar trend was observed for these polymers when applied for protein delivery; streptavidin complexation with purely cationic polydisulfides resulted in direct cell membrane translocation instead of uptake into endosomal compartments.[122]

Other research groups have also utilized this polymerization approach to generate cationic polydisulfides for different biological delivery applications. Ping and coworkers copolymerized a diamino-LA monomer along with established guanidium-containing monomers to generate an ionizable motif for endosomal escape.[123] This polymer successfully complexed with CRISPR-Cas9 plasmid DNA, Cas9 mRNA with sgRNA, or with Cas9 RNPs to generate cationic polymeric nanoparticles. One vector, DET-CPD-12 (See Figure 1.14), demonstrated 16.5% gene editing in the livers of mice after treatment with DET-CPD-12-CRISPR-Cas9 DNA plasmid nanoparticles. While the polymers generated through this synthetic methodology did not differ in molecular weight (all M_n <20 kDa; compared to monomers used by the Matile group), they also demonstrated excellent depolymerization capabilities. The liver-specific expression profile for this system is extremely promising for future gene therapy and RNA delivery applications.

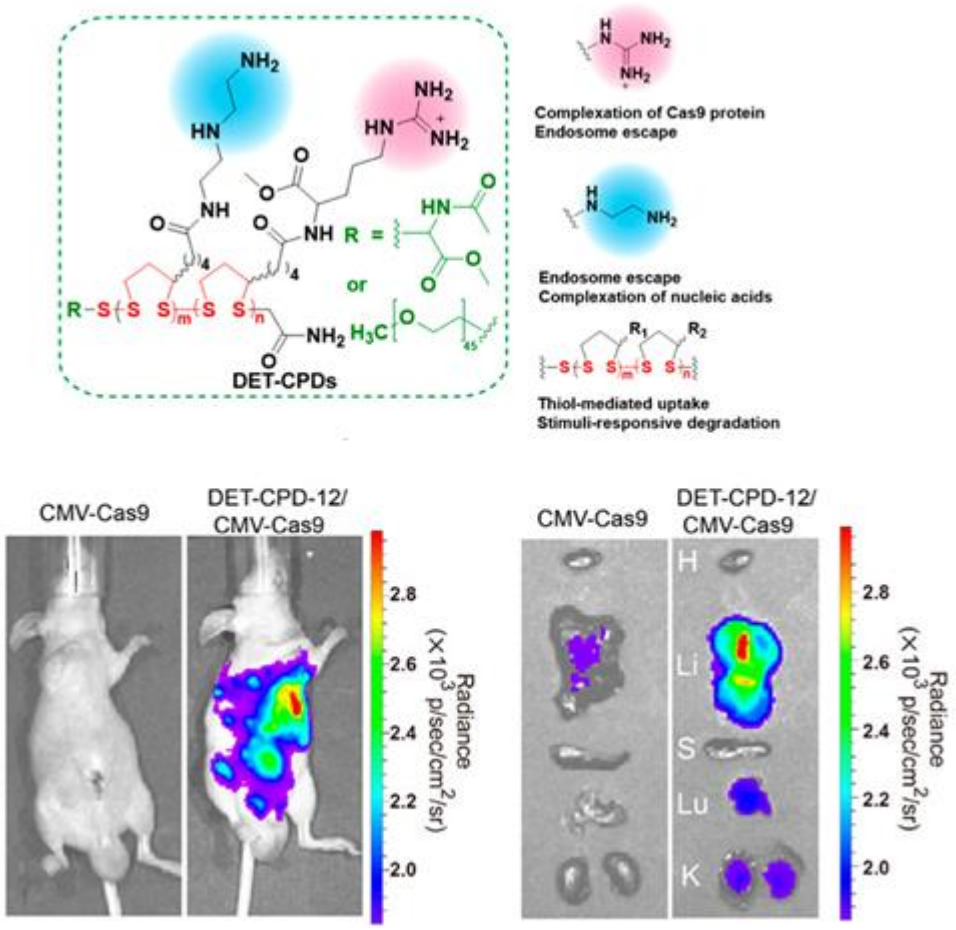

Figure 1.14 Cationic and ionizable polydisulfide utilized for *in vivo* CRISPR-Cas9 gene editing. Bioreducible cationic polydisulfide DET-CPD was successfully complexed with CRISPR-Cas9-encoding plasmids and resulting nanoparticles deliver to livers of treated mice. Reprinted from ref.[123]

Another aqueous-phase LA polymerization technique was developed 2020 by Lu and coworkers, utilizing a freezing-based "cryopolymerization" technique to generate protein-polydisulfide conjugates (See Figure 1.15).[117] Capitalizing on the ability of LA-based monomers to polymerize within the ice lattice of aqueous solutions, Lu and coworkers generated cationic polydisulfide-polymer conjugates will excellent cell-penetrating capability. Further studies by Lu and coworkers determined that more hydrophobic LA derivatives can generate protein-polydisulfide conjugates through a room temperature aggregation-induced polymerization technique.[124] The efficacy of this

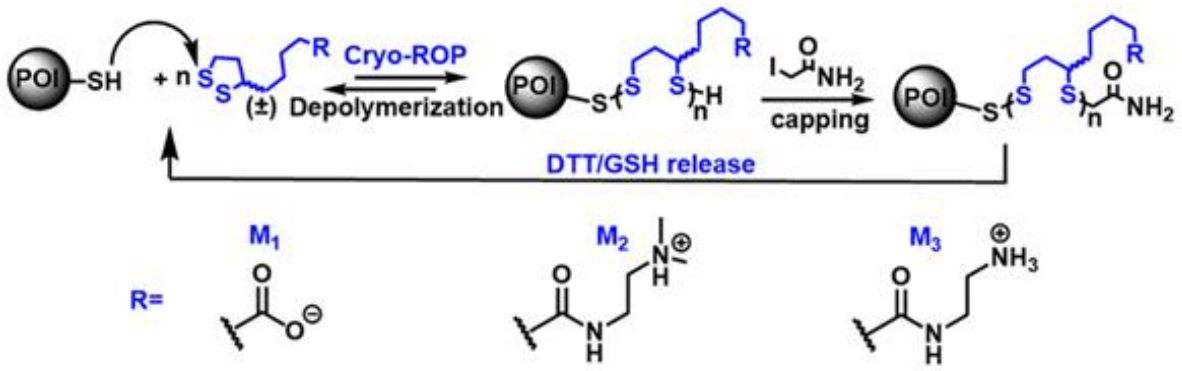

Figure 1.15 Aqueous cryopolymerization approach to generate polydisulfide polymers. Proteins of interest (POI) were frozen with three lipoic acid-derived monomers to generate protein-polydisulfide conjugates that can be depolymerized with additional thiols (DTT/GSH). Reprinted from ref.[117]

technique depends heavily on the monomer equilibrium concentration in aqueous solutions.

Polymers generated from organic-phase LA ROP protocols have yet to be applied towards biological applications. However, Moore and coworkers developed a facile anionic ROP protocol in THF, generating polydisulfides using a methylated LA derivative (See Figure 1.16).[118] Interestingly, the architecture and molecular weight of LA-derived

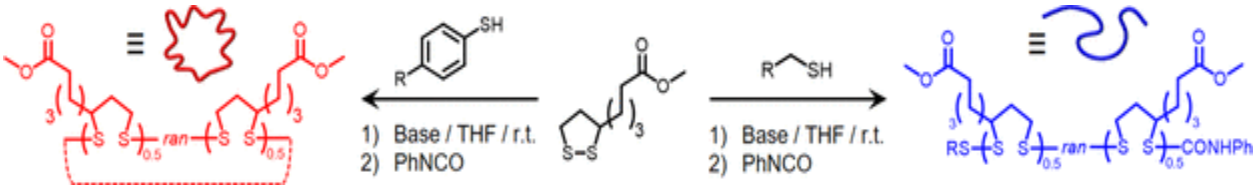

Figure 1.16 Organic-phase anionic ROP methodology to generate polydisulfides with different architectures. ROP of a methyl-ester-containing LA derivative with alkyl thiols or aromatic thiols results in linear or cyclic polydisulfides, respectively. Reprinted from ref.[118]

polydisulfides could be controlled based on the type of thiolate initiator and quantity of thiolate initiator, respectively. This ROP protocol has been successfully used with three other monomers, but resulting polymers were not applied towards any biological or material end. Despite this, the ease of this polymerization methodology makes this

synthesis approach very attractive for generating biologically-relevant new LA-based polydisulfides.

1.8 Previous Guan Lab Polymer Designs for mRNA Delivery

Published works from Guan and coworkers have focused on the design of bioreducible polymers for the purpose of siRNA and mRNA delivery. The types of polymer architectures generated for this purpose are vast, ranging from bolaamphiphiles to dendronized polymers.[125-126] Specifically for mRNA delivery, two dendronized polymer systems have shown excellent *in vitro* delivery profiles. One such dendronized polymer system uses a disulfide-reducible linear backbone with lysine dendrons and two specific amino acids, histidine and tryptophan, as terminal dendron functionalities (See Figure 1.17). On these dendronized polypeptide polymers (denpols), the imidazole motif on histidine functions as an ionizable group to promote endosomal escape upon nanoparticle uptake, and tryptophan provides an aromatic motif that can potentially increase binding to nucleobases through pi-pi stacking.[127] In addition to these two functionalities, cationic amines present on the dendrons facilitate RNA complexation (through electrostatic interactions with nucleic acid phosphate groups), and the disulfide motifs present within the polymer backbone enable thiol-mediated depolymerization upon polyplex entry into the cell cytosol. Together, these functionalities facilitate excellent RNA-polymer complexation, endosomal escape, and biodegradability in recipient cells.

Denpol constructs designed for mRNA delivery included an additional tetraethylene glycol (TEG) motif functionalized on the polymer backbone to prevent nanoparticle

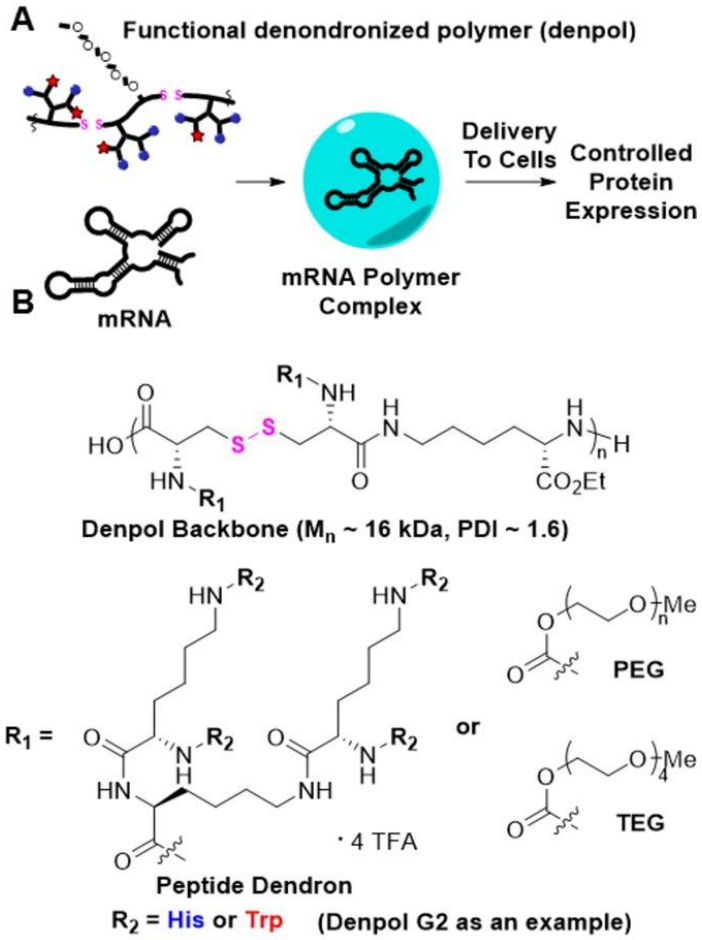

Figure 1.17 Dendronized polypeptides polymers for mRNA delivery. **A**) Multifunctional dendronized polypeptide polymers (denpols) can be complexed with mRNA to form nanoparticles capable of *in vitro* mRNA delivery. **B**) Expanded chemical structure of denpol backbone, dendrons, and potential TEG/PEG functionalizations. Reprinted from ref.[125]

aggregation. mRNA delivery using these dendronized polymers was successful, particularly when dendronized to second generations and dendrons were functionalized at a ratio of two histidines for every one tryptophan motif (G2 2:1). Fifty percent TEGylation of the polymer backbone also resulted in excellent nanoparticle stability in buffered saline at physiological pH. This excellent nanoparticle stability profile, coupled with robust mRNA delivery capability, makes these dendronized polymers excellent polymer tools for future RNA delivery applications.

Another mRNA delivery vehicle developed by Guan and coworkers utilized a similar polymer backbone design with similar lysine dendrons, but the backbone and dendrons were functionalized with hydrophobic alkyl chains, hydrophilic TEG, or linear peptides (See Figure 1.18).[128] For this series of dendronized polymers, a multifunctional peptide containing lysines, histidines, and tryptophan residues were conjugated to the end of dendrons, providing cationic charge, ionizable motifs for endosomal escape, and hydrophobicity all within a simplified peptide. When complexed with firefly luciferase

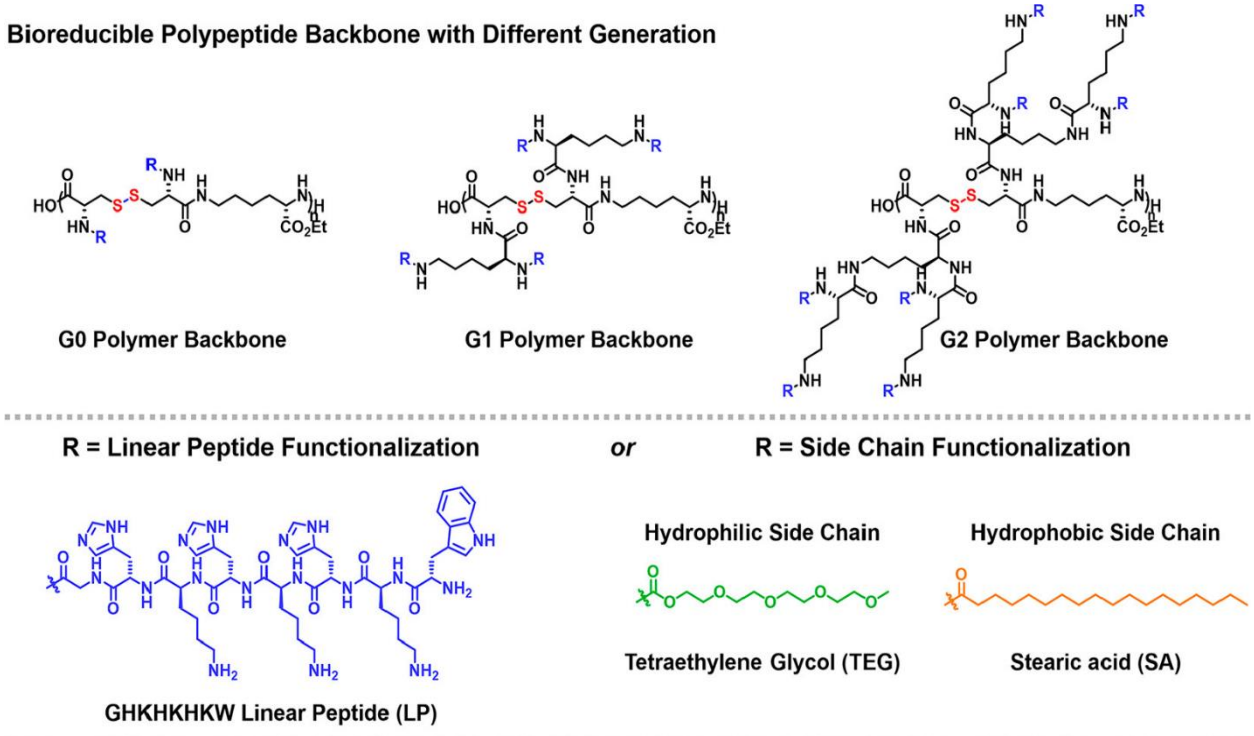

Figure 1.18 Multivalent peptide-functionalized bioreducible polymers for mRNA delivery. Various dendronized polypeptide polymer backbones (G0, G1, and G2) were functionalized with multifunctional linear peptides, TEG, and SA functionalizations. Resulting polymers demonstrated success at binding and delivering various RNA cargoes *in vitro*. Reprinted from ref.[127]

(Fluc) mRNA, polymer-mRNA nanoparticles with diameters between 100-250 nm were obtained, as determined by DLS measurements. Administration of these polymer-mRNA nanoparticles to NIH-3T3 cells, HEK 293 cells, and BHK cells all resulted in excellent RNA delivery. Depending on the ratio of hydrophobic, hydrophilic, and linear peptide substituents, different RNA species (siRNA, mRNA, CRISPR-Cas9 mRNA and sgRNA) could be efficiently delivered to cells. More specifically, RNA-mediated CRISPR-Cas9 gene editing (from simultaneous complexation of Cas9 mRNA and sgRNA) was most effective using polymeric nanoparticles containing 20% hydrophobic stearic acid-functionalized polymers. High cellular transfection efficiency and mRNA expression were also observed when two other reporter mRNAs (sizes ranging from ~1000 nt to ~10,000 nt) were tested *in vitro*. Due to the high modality of this system, further exploration into different peptide sequences should yield more RNA delivery vehicles.

1.9 Summary

Within the last decade, remarkable progress has been made in the synthesis and applications of RNA therapies and gene therapies, with new drug candidates continuously being added to development pipelines. However, a lack of safe, efficient, and target-specific delivery vehicles for RNA and gene editing therapies remains one of the greatest challenges to the implementation of new life-changing therapeutics. For RNA therapeutics, the FDA approval of three excellent LNP-based RNA delivery vehicles has propelled lipids to the center-stage for the development of RNA-based drugs. While lipids still possess tremendous potential, they have fundamental limitations and specific delivery

characteristics compared to other nucleic acid complexation vehicles. Expanded development of other delivery vehicles remains a priority for applications where LNPs prove unsuccessful or inefficient. Polymer-based vehicles remain one of the most promising alternatives to LNPs, with biodegradable polymers being very attractive for therapies that require repeated dosing. Novel chemical functionalities, polymerization methodologies, and formulation techniques are certain to make polymeric delivery vehicles an essential tool in the development of next-generation RNA therapies and gene editing technologies.

1.10 References

(1) Crick, F., Central dogma of molecular biology. *Nature* **1970,** *227* (5258), 561-563.
(2) Witkin, E. M., Ultraviolet-induced mutation and DNA repair. *Annual Review of Microbiology* **1969,** *23*, 487-514.
(3) Hanawalt, P. C.; Cooper, P. K.; Ganesan, A. K.; Smith, C. A., DNA Repair in Bacteria and Mammalian Cells. *Annual Review of Biochemistry* **1979,** *48* (1), 783-836.
(4) Miles, C.; Meuth, M., DNA sequence determination of γ-radiation-induced mutations of the hamster aprt locus. *Mutation Research Letters* **1989,** *227* (2), 97-102.
(5) Witkin, E. M., Radiation-Induced Mutations and Their Repair. *Science* **1966,** *152* (3727), 1345-1353.
(6) Freese, E., Molecular Mechanisms of Mutations. In *Chemical Mutagens: Principles and Methods for Their Detection Volume 1*, Hollaender, A., Ed. Springer US: Boston, MA, 1971; pp 1-56.
(7) Streisinger, G.; Okada, Y.; Emrich, J.; Newton, J.; Tsugita, A.; Terzaghi, E.; Inouye, M., Frameshift mutations and the genetic code. This paper is dedicated to Professor Theodosius Dobzhansky on the occasion of his 66th birthday. *Cold Spring Harbor Symposium on Quantitative Biology* **1966,** *31*, 77-84.
(8) Claussnitzer, M.; Cho, J. H.; Collins, R.; Cox, N. J.; Dermitzakis, E. T.; Hurles, M. E.; Kathiresan, S.; Kenny, E. E.; Lindgren, C. M.; MacArthur, D. G.; North, K. N.; Plon, S. E.; Rehm, H. L.; Risch, N.; Rotimi, C. N.; Shendure, J.; Soranzo, N.; McCarthy, M. I., A brief history of human disease genetics. *Nature* **2020,** *577* (7789), 179-189.
(9) Nguengang Wakap, S.; Lambert, D. M.; Olry, A.; Rodwell, C.; Gueydan, C.; Lanneau, V.; Murphy, D.; Le Cam, Y.; Rath, A., Estimating cumulative point prevalence of rare diseases: analysis of the Orphanet database. *European Journal of Human Genetics* **2020,** *28* (2), 165-173.

(10) 100,000 Genomes Pilot on Rare-Disease Diagnosis in Health Care — Preliminary Report. *New England Journal of Medicine* **2021,** *385* (20), 1868-1880.
(11) Convertino, M.; Das, J.; Dokholyan, N. V., Pharmacological Chaperones: Design and Development of New Therapeutic Strategies for the Treatment of Conformational Diseases. *ACS Chemical Biology* **2016,** *11* (6), 1471-1489.
(12) Fiedorczuk, K.; Chen, J., Mechanism of CFTR correction by type I folding correctors. *Cell* **2022,** *185* (1), 158-168.e111.
(13) Friedmann, T., Progress Toward Human Gene Therapy. *Science* **1989,** *244* (4910), 1275-1281.
(14) Anderson, W. F., Prospects for Human Gene Therapy. *Science* **1984,** *226* (4673), 401-409.
(15) Dunbar, C. E.; High, K. A.; Joung, J. K.; Kohn, D. B.; Ozawa, K.; Sadelain, M., Gene therapy comes of age. *Science* **2018,** *359* (6372), eaan4672.
(16) Porteus, M. H., A New Class of Medicines through DNA Editing. *New England Journal of Medicine* **2019,** *380* (10), 947-959.
(17) Gonçalves, G. A. R.; Paiva, R. M. A., Gene therapy: advances, challenges and perspectives. *Einstein (Sao Paulo)* **2017,** *15* (3), 369-375.
(18) Young, J. L.; Dean, D. A., Electroporation-mediated gene delivery. *Advanced Genetics* **2015,** *89*, 49-88.
(19) Wells, D. J., Gene Therapy Progress and Prospects: Electroporation and other physical methods. *Gene Therapy* **2004,** *11* (18), 1363-1369.
(20) Vijayanathan, V.; Thomas, T.; Thomas, T. J., DNA Nanoparticles and Development of DNA Delivery Vehicles for Gene Therapy. *Biochemistry* **2002,** *41* (48), 14085-14094.
(21) Durymanov, M.; Reineke, J., Non-viral Delivery of Nucleic Acids: Insight Into Mechanisms of Overcoming Intracellular Barriers. *Front Pharmacol* **2018,** *9*, 971.
(22) Robbins, P. D.; Ghivizzani, S. C., Viral vectors for gene therapy. *Pharmacology & Therapeutics* **1998,** *80* (1), 35-47.
(23) Gaj, T.; Sirk, S. J.; Shui, S. L.; Liu, J., Genome-Editing Technologies: Principles and Applications. *Cold Spring Harb Perspect Biol* **2016,** *8* (12).
(24) Li, H.; Yang, Y.; Hong, W.; Huang, M.; Wu, M.; Zhao, X., Applications of genome editing technology in the targeted therapy of human diseases: mechanisms, advances and prospects. *Signal Transduction and Targeted Therapy* **2020,** *5* (1), 1.
(25) Kaczmarek, J. C.; Kowalski, P. S.; Anderson, D. G., Advances in the delivery of RNA therapeutics: from concept to clinical reality. *Genome Medicine* **2017,** *9* (1), 60.
(26) Kim, Y.-K., RNA therapy: rich history, various applications and unlimited future prospects. *Experimental & Molecular Medicine* **2022,** *54* (4), 455-465.
(27) Paunovska, K.; Loughrey, D.; Dahlman, J. E., Drug delivery systems for RNA therapeutics. *Nature Reviews Genetics* **2022,** *23* (5), 265-280.
(28) Roberts, T. C.; Langer, R.; Wood, M. J. A., Advances in oligonucleotide drug delivery. *Nature Reviews Drug Discovery* **2020,** *19* (10), 673-694.
(29) Vitravene, A randomized controlled clinical trial of intravitreous fomivirsen for treatment of newly diagnosed peripheral cytomegalovirus retinitis in patients with AIDS. *American Journal of Ophthalmology* **2002,** *133* (4), 467-474.
(30) Rüger, J.; Ioannou, S.; Castanotto, D.; Stein, C. A., Oligonucleotides to the (Gene) Rescue: FDA Approvals 2017–2019. *Trends in Pharmacological Sciences* **2020,** *41* (1), 27-41.

(31) Stein, C. A.; Castanotto, D., FDA-Approved Oligonucleotide Therapies in 2017. *Molecular Therapy* **2017,** *25* (5), 1069-1075.
(32) Hu, B.; Zhong, L.; Weng, Y.; Peng, L.; Huang, Y.; Zhao, Y.; Liang, X.-J., Therapeutic siRNA: state of the art. *Signal Transduction and Targeted Therapy* **2020,** *5* (1), 101.
(33) Zogg, H.; Singh, R., Current Advances in RNA Therapeutics for Human Diseases. *Int J Mol Sci* **2022,** *23* (5).
(34) Brown, C. R.; Gupta, S.; Qin, J.; Racie, T.; He, G.; Lentini, S.; Malone, R.; Yu, M.; Matsuda, S.; Shulga-Morskaya, S.; Nair, A. V.; Theile, C. S.; Schmidt, K.; Shahraz, A.; Goel, V.; Parmar, R. G.; Zlatev, I.; Schlegel, M. K.; Nair, J. K.; Jayaraman, M.; Manoharan, M.; Brown, D.; Maier, M. A.; Jadhav, V., Investigating the pharmacodynamic durability of GalNAc–siRNA conjugates. *Nucleic Acids Research* **2020,** *48* (21), 11827-11844.
(35) Qin, S.; Tang, X.; Chen, Y.; Chen, K.; Fan, N.; Xiao, W.; Zheng, Q.; Li, G.; Teng, Y.; Wu, M.; Song, X., mRNA-based therapeutics: powerful and versatile tools to combat diseases. *Signal Transduction and Targeted Therapy* **2022,** *7* (1), 166.
(36) Swingle, K. L.; Hamilton, A. G.; Mitchell, M. J., Lipid Nanoparticle-Mediated Delivery of mRNA Therapeutics and Vaccines. *Trends in Molecular Medicine* **2021,** *27* (6), 616-617.
(37) Pardi, N.; Hogan, M. J.; Porter, F. W.; Weissman, D., mRNA vaccines — a new era in vaccinology. *Nature Reviews Drug Discovery* **2018,** *17* (4), 261-279.
(38) Oude Blenke, E.; Evers, M. J. W.; Mastrobattista, E.; van der Oost, J., CRISPR-Cas9 gene editing: Delivery aspects and therapeutic potential. *Journal of Controlled Release* **2016,** *244*, 139-148.
(39) Bettini, E.; Locci, M., SARS-CoV-2 mRNA Vaccines: Immunological Mechanism and Beyond. *Vaccines (Basel)* **2021,** *9* (2).
(40) Liu, A.; Wang, X., The Pivotal Role of Chemical Modifications in mRNA Therapeutics. *Front Cell Dev Biol* **2022,** *10*, 901510.
(41) Current Status of Messenger RNA Delivery Systems. *Nucleic Acid Therapeutics* **2018,** *28* (3), 158-165.
(42) Nance, K. D.; Meier, J. L., Modifications in an Emergency: The Role of N1-Methylpseudouridine in COVID-19 Vaccines. *ACS Central Science* **2021,** *7* (5), 748-756.
(43) Andries, O.; Mc Cafferty, S.; De Smedt, S. C.; Weiss, R.; Sanders, N. N.; Kitada, T., N(1)-methylpseudouridine-incorporated mRNA outperforms pseudouridine-incorporated mRNA by providing enhanced protein expression and reduced immunogenicity in mammalian cell lines and mice. *Journal of Controlled Release* **2015,** *217*, 337-344.
(44) Kim, S. C.; Sekhon, S. S.; Shin, W. R.; Ahn, G.; Cho, B. K.; Ahn, J. Y.; Kim, Y. H., Modifications of mRNA vaccine structural elements for improving mRNA stability and translation efficiency. *Mol Cell Toxicol* **2022,** *18* (1), 1-8.
(45) Zhang, H.; Rombouts, K.; Raes, L.; Xiong, R.; De Smedt, S. C.; Braeckmans, K.; Remaut, K., Fluorescence-Based Quantification of Messenger RNA and Plasmid DNA Decay Kinetics in Extracellular Biological Fluids and Cell Extracts. *Advanced Biosystems* **2020,** *4* (5), 2000057.
(46) Houseley, J.; Tollervey, D., The Many Pathways of RNA Degradation. *Cell* **2009,** *136* (4), 763-776.

(47) Ramachandran, S.; Satapathy, S. R.; Dutta, T., Delivery Strategies for mRNA Vaccines. *Pharmaceutical Medicine* **2022,** *36* (1), 11-20.
(48) Rozman, M.; Korać, P.; Jambrosic, K.; Židovec Lepej, S., Progress in Prophylactic and Therapeutic EBV Vaccine Development Based on Molecular Characteristics of EBV Target Antigens. *Pathogens* **2022,** *11* (8), 864.
(49) Deviatkin, A. A.; Simonov, R. A.; Trutneva, K. A.; Maznina, A. A.; Khavina, E. M.; Volchkov, P. Y., Universal Flu mRNA Vaccine: Promises, Prospects, and Problems. *Vaccines (Basel)* **2022,** *10* (5), 709.
(50) Abbasi, J., First mRNA HIV Vaccine Clinical Trial Launches. *Journal of the American Medical Association* **2022,** *327* (10), 909-909.
(51) Pickar-Oliver, A.; Gersbach, C. A., The next generation of CRISPR–Cas technologies and applications. *Nature Reviews Molecular Cell Biology* **2019,** *20* (8), 490-507.
(52) Doudna, J. A.; Charpentier, E., The new frontier of genome engineering with CRISPR-Cas9. *Science* **2014,** *346* (6213), 1258096.
(53) Meyer, R. A.; Neshat, S. Y.; Green, J. J.; Santos, J. L.; Tuesca, A. D., Targeting strategies for mRNA delivery. *Materials Today Advances* **2022,** *14*, 100240.
(54) Nakamura, T.; Sato, Y.; Yamada, Y.; Abd Elwakil, M. M.; Kimura, S.; Younis, M. A.; Harashima, H., Extrahepatic targeting of lipid nanoparticles in vivo with intracellular targeting for future nanomedicines. *Advanced Drug Delivery Reviews* **2022,** *188*, 114417.
(55) Jinek, M.; Chylinski, K.; Fonfara, I.; Hauer, M.; Doudna, J. A.; Charpentier, E., A Programmable Dual-RNA-Guided DNA Endonuclease in Adaptive Bacterial Immunity. *Science* **2012,** *337* (6096), 816-821.
(56) Ran, F. A.; Hsu, P. D.; Wright, J.; Agarwala, V.; Scott, D. A.; Zhang, F., Genome engineering using the CRISPR-Cas9 system. *Nature Protocols* **2013,** *8* (11), 2281-2308.
(57) Chang, H. H. Y.; Pannunzio, N. R.; Adachi, N.; Lieber, M. R., Non-homologous DNA end joining and alternative pathways to double-strand break repair. *Nature Reviews Molecular Cell Biology* **2017,** *18* (8), 495-506.
(58) Jasin, M.; Rothstein, R., Repair of strand breaks by homologous recombination. *Cold Spring Harb Perspect Biol* **2013,** *5* (11), a012740.
(59) Lin, S.; Staahl, B. T.; Alla, R. K.; Doudna, J. A., Enhanced homology-directed human genome engineering by controlled timing of CRISPR/Cas9 delivery. *Elife* **2014,** *3*, e04766.
(60) Frangoul, H.; Altshuler, D.; Cappellini, M. D.; Chen, Y.-S.; Domm, J.; Eustace, B. K.; Foell, J.; de la Fuente, J.; Grupp, S.; Handgretinger, R.; Ho, T. W.; Kattamis, A.; Kernytsky, A.; Lekstrom-Himes, J.; Li, A. M.; Locatelli, F.; Mapara, M. Y.; de Montalembert, M.; Rondelli, D.; Sharma, A.; Sheth, S.; Soni, S.; Steinberg, M. H.; Wall, D.; Yen, A.; Corbacioglu, S., CRISPR-Cas9 Gene Editing for Sickle Cell Disease and β-Thalassemia. *New England Journal of Medicine* **2020,** *384* (3), 252-260.
(61) Cao, A.; Galanello, R., Beta-thalassemia. *Genetics in Medicine* **2010,** *12* (2), 61-76.
(62) Gillmore, J. D.; Gane, E.; Taubel, J.; Kao, J.; Fontana, M.; Maitland, M. L.; Seitzer, J.; O'Connell, D.; Walsh, K. R.; Wood, K.; Phillips, J.; Xu, Y.; Amaral, A.; Boyd, A. P.; Cehelsky, J. E.; McKee, M. D.; Schiermeier, A.; Harari, O.; Murphy, A.; Kyratsous, C. A.; Zambrowicz, B.; Soltys, R.; Gutstein, D. E.; Leonard, J.; Sepp-Lorenzino, L.; Lebwohl,

D., CRISPR-Cas9 In Vivo Gene Editing for Transthyretin Amyloidosis. *New England Journal of Medicine* **2021,** *385* (6), 493-502.
(63) Zhang, X.-H.; Tee, L. Y.; Wang, X.-G.; Huang, Q.-S.; Yang, S.-H., Off-target Effects in CRISPR/Cas9-mediated Genome Engineering. *Molecular Therapy - Nucleic Acids* **2015,** *4*, e264.
(64) Manghwar, H.; Li, B.; Ding, X.; Hussain, A.; Lindsey, K.; Zhang, X.; Jin, S., CRISPR/Cas Systems in Genome Editing: Methodologies and Tools for sgRNA Design, Off-Target Evaluation, and Strategies to Mitigate Off-Target Effects. *Advanced Science* **2020,** *7* (6), 1902312.
(65) Yip, B. H., Recent Advances in CRISPR/Cas9 Delivery Strategies. *Biomolecules* **2020,** *10* (6).
(66) Adams, D.; Gonzalez-Duarte, A.; O'Riordan, W. D.; Yang, C.-C.; Ueda, M.; Kristen, A. V.; Tournev, I.; Schmidt, H. H.; Coelho, T.; Berk, J. L.; Lin, K.-P.; Vita, G.; Attarian, S.; Planté-Bordeneuve, V.; Mezei, M. M.; Campistol, J. M.; Buades, J.; Brannagan, T. H.; Kim, B. J.; Oh, J.; Parman, Y.; Sekijima, Y.; Hawkins, P. N.; Solomon, S. D.; Polydefkis, M.; Dyck, P. J.; Gandhi, P. J.; Goyal, S.; Chen, J.; Strahs, A. L.; Nochur, S. V.; Sweetser, M. T.; Garg, P. P.; Vaishnaw, A. K.; Gollob, J. A.; Suhr, O. B., Patisiran, an RNAi Therapeutic, for Hereditary Transthyretin Amyloidosis. *New England Journal of Medicine* **2018,** *379* (1), 11-21.
(67) Cheng, X.; Lee, R. J., The role of helper lipids in lipid nanoparticles (LNPs) designed for oligonucleotide delivery. *Advanced Drug Delivery Reviews* **2016,** *99* (Pt A), 129-137.
(68) Paunovska, K.; Gil, C. J.; Lokugamage, M. P.; Sago, C. D.; Sato, M.; Lando, G. N.; Gamboa Castro, M.; Bryksin, A. V.; Dahlman, J. E., Analyzing 2000 in Vivo Drug Delivery Data Points Reveals Cholesterol Structure Impacts Nanoparticle Delivery. *ACS Nano* **2018,** *12* (8), 8341-8349.
(69) Suk, J. S.; Xu, Q.; Kim, N.; Hanes, J.; Ensign, L. M., PEGylation as a strategy for improving nanoparticle-based drug and gene delivery. *Advanced Drug Delivery Reviews* **2016,** *99* (Pt A), 28-51.
(70) Schoenmaker, L.; Witzigmann, D.; Kulkarni, J. A.; Verbeke, R.; Kersten, G.; Jiskoot, W.; Crommelin, D. J. A., mRNA-lipid nanoparticle COVID-19 vaccines: Structure and stability. *International Journal of Pharmaceutics* **2021,** *601*, 120586.
(71) Hassett, K. J.; Benenato, K. E.; Jacquinet, E.; Lee, A.; Woods, A.; Yuzhakov, O.; Himansu, S.; Deterling, J.; Geilich, B. M.; Ketova, T.; Mihai, C.; Lynn, A.; McFadyen, I.; Moore, M. J.; Senn, J. J.; Stanton, M. G.; Almarsson, Ö.; Ciaramella, G.; Brito, L. A., Optimization of Lipid Nanoparticles for Intramuscular Administration of mRNA Vaccines. *Molecular Therapy - Nucleic Acids* **2019,** *15*, 1-11.
(72) Schlich, M.; Palomba, R.; Costabile, G.; Mizrahy, S.; Pannuzzo, M.; Peer, D.; Decuzzi, P., Cytosolic delivery of nucleic acids: The case of ionizable lipid nanoparticles. *Bioengineering & Translational Medicine* **2021,** *6* (2), e10213.
(73) Aldosari, B. N.; Alfagih, I. M.; Almurshedi, A. S., Lipid Nanoparticles as Delivery Systems for RNA-Based Vaccines. *Pharmaceutics* **2021,** *13* (2), 206.
(74) Uddin, M. N.; Roni, M. A., Challenges of Storage and Stability of mRNA-Based COVID-19 Vaccines. *Vaccines (Basel)* **2021,** *9* (9).
(75) Hu, B.; Li, B.; Li, K.; Liu, Y.; Li, C.; Zheng, L.; Zhang, M.; Yang, T.; Guo, S.; Dong, X.; Zhang, T.; Liu, Q.; Hussain, A.; Weng, Y.; Peng, L.; Zhao, Y.; Liang, X.-J.; Huang, Y.,

Thermostable ionizable lipid-like nanoparticle (iLAND) for RNAi treatment of hyperlipidemia. *Science Advances* **2022,** *8* (7), eabm1418.
(76) Qiu, M.; Glass, Z.; Chen, J.; Haas, M.; Jin, X.; Zhao, X.; Rui, X.; Ye, Z.; Li, Y.; Zhang, F.; Xu, Q., Lipid nanoparticle-mediated codelivery of Cas9 mRNA and single-guide RNA achieves liver-specific in vivo genome editing of Angptl3 *Proceedings of the National Academy of Sciences* **2021,** *118* (10), e2020401118.
(77) Zhang, X.; Zhao, W.; Nguyen, G. N.; Zhang, C.; Zeng, C.; Yan, J.; Du, S.; Hou, X.; Li, W.; Jiang, J.; Deng, B.; McComb, D. W.; Dorkin, R.; Shah, A.; Barrera, L.; Gregoire, F.; Singh, M.; Chen, D.; Sabatino, D. E.; Dong, Y., Functionalized lipid-like nanoparticles for in vivo mRNA delivery and base editing. *Science Advances* **2020,** *6* (34), eabc2315.
(78) Hou, X.; Zaks, T.; Langer, R.; Dong, Y., Lipid nanoparticles for mRNA delivery. *Nature Reviews Materials* **2021,** *6* (12), 1078-1094.
(79) Kularatne, R. N.; Crist, R. M., The Future of Tissue-Targeted Lipid Nanoparticle-Mediated Nucleic Acid Delivery. *Pharmaceuticals (Basel)* **2022,** *15* (7).
(80) Cheng, Q.; Wei, T.; Farbiak, L.; Johnson, L. T.; Dilliard, S. A.; Siegwart, D. J., Selective organ targeting (SORT) nanoparticles for tissue-specific mRNA delivery and CRISPR–Cas gene editing. *Nature Nanotechnology* **2020,** *15* (4), 313-320.
(81) Rampersad, S.; Tennant, P., Chapter 3 - Replication and Expression Strategies of Viruses. In *Viruses*, Tennant, P.; Fermin, G.; Foster, J. E., Eds. Academic Press: 2018; pp 55-82.
(82) Maginnis, M. S., Virus-Receptor Interactions: The Key to Cellular Invasion. *J Mol Biol* **2018,** *430* (17), 2590-2611.
(83) Wang, D.; Tai, P. W. L.; Gao, G., Adeno-associated virus vector as a platform for gene therapy delivery. *Nature Reviews Drug Discovery* **2019,** *18* (5), 358-378.
(84) Naso, M. F.; Tomkowicz, B.; Perry, W. L., 3rd; Strohl, W. R., Adeno-Associated Virus (AAV) as a Vector for Gene Therapy. *BioDrugs* **2017,** *31* (4), 317-334.
(85) Russell, S.; Bennett, J.; Wellman, J. A.; Chung, D. C.; Yu, Z. F.; Tillman, A.; Wittes, J.; Pappas, J.; Elci, O.; McCague, S.; Cross, D.; Marshall, K. A.; Walshire, J.; Kehoe, T. L.; Reichert, H.; Davis, M.; Raffini, L.; George, L. A.; Hudson, F. P.; Dingfield, L.; Zhu, X.; Haller, J. A.; Sohn, E. H.; Mahajan, V. B.; Pfeifer, W.; Weckmann, M.; Johnson, C.; Gewaily, D.; Drack, A.; Stone, E.; Wachtel, K.; Simonelli, F.; Leroy, B. P.; Wright, J. F.; High, K. A.; Maguire, A. M., Efficacy and safety of voretigene neparvovec (AAV2-hRPE65v2) in patients with RPE65-mediated inherited retinal dystrophy: a randomised, controlled, open-label, phase 3 trial. *Lancet* **2017,** *390* (10097), 849-860.
(86) Mendell, J. R.; Al-Zaidy, S. A.; Rodino-Klapac, L. R.; Goodspeed, K.; Gray, S. J.; Kay, C. N.; Boye, S. L.; Boye, S. E.; George, L. A.; Salabarria, S.; Corti, M.; Byrne, B. J.; Tremblay, J. P., Current Clinical Applications of In Vivo Gene Therapy with AAVs. *Molecular Therapy* **2021,** *29* (2), 464-488.
(87) Wang, D.; Zhang, F.; Gao, G., CRISPR-Based Therapeutic Genome Editing: Strategies and In Vivo Delivery by AAV Vectors. *Cell* **2020,** *181* (1), 136-150.
(88) Rapti, K.; Louis-Jeune, V.; Kohlbrenner, E.; Ishikawa, K.; Ladage, D.; Zolotukhin, S.; Hajjar, R. J.; Weber, T., Neutralizing Antibodies Against AAV Serotypes 1, 2, 6, and 9 in Sera of Commonly Used Animal Models. *Molecular Therapy* **2012,** *20* (1), 73-83.
(89) Durand, S.; Cimarelli, A., The inside out of lentiviral vectors. *Viruses* **2011,** *3* (2), 132-159.

(90) Keam, S. J., Elivaldogene Autotemcel: First Approval. *Molecular Diagnosis & Therapy* **2021,** *25* (6), 803-809.
(91) Harrison, C., First gene therapy for [beta]-thalassemia approved. *Nature Biotechnology* **2019,** *37*, 1102+.
(92) Glorioso, J. C.; DeLuca, N. A.; Fink, D. J., Development and application of herpes simplex virus vectors for human gene therapy. *Annu Rev Microbiol* **1995,** *49*, 675-710.
(93) van den Berg, A. I. S.; Yun, C.-O.; Schiffelers, R. M.; Hennink, W. E., Polymeric delivery systems for nucleic acid therapeutics: Approaching the clinic. *Journal of Controlled Release* **2021,** *331*, 121-141.
(94) Behr, J.-P., The proton sponge: a trick to enter cells the viruses did not exploit. *CHIMIA International Journal for Chemistry* **1997,** *51* (1-2), 34-36.
(95) Bus, T.; Traeger, A.; Schubert, U. S., The great escape: how cationic polyplexes overcome the endosomal barrier. *Journal of Materials Chemistry B* **2018,** *6* (43), 6904-6918.
(96) Kafil, V.; Omidi, Y., Cytotoxic impacts of linear and branched polyethylenimine nanostructures in a431 cells. *Bioimpacts* **2011,** *1* (1), 23-30.
(97) Chen, C. K.; Huang, P. K.; Law, W. C., Biodegradable Polymers for Gene-Delivery Applications. *Int J Nanomedicine* **2020,** *15*, 2131-2150.
(98) Cho, C.-S., Design and Development of Degradable Polyethylenimines for Delivery of DNA and Small Interfering RNA: An Updated Review. *ISRN Materials Science* **2012,** *2012*, 798247.
(99) Lynn, D. M.; Langer, R., Degradable Poly(β-amino esters): Synthesis, Characterization, and Self-Assembly with Plasmid DNA. *Journal of the American Chemical Society* **2000,** *122* (44), 10761-10768.
(100) Lin, C.; Lammens, T. M.; Zhong, Z. Y.; Gu, H.; Lok, M. C.; Jiang, X.; Hennink, W. E.; Feijen, J.; Engbersen, J. F., Disulfide-containing poly(beta-amino ester)s for gene delivery. *Journal of Controlled Release* **2006,** *116* (2), e79-81.
(101) Rui, Y.; Wilson, D. R.; Tzeng, S. Y.; Yamagata, H. M.; Sudhakar, D.; Conge, M.; Berlinicke, C. A.; Zack, D. J.; Tuesca, A.; Green, J. J., High-throughput and high-content bioassay enables tuning of polyester nanoparticles for cellular uptake, endosomal escape, and systemic in vivo delivery of mRNA. *Science Advances* **2022,** *8* (1), eabk2855.
(102) Zhou, D.; Cutlar, L.; Gao, Y.; Wang, W.; O'Keeffe-Ahern, J.; McMahon, S.; Duarte, B.; Larcher, F.; Rodriguez, B. J.; Greiser, U.; Wang, W., The transition from linear to highly branched poly(β-amino ester)s: Branching matters for gene delivery. *Science Advances* **2016,** *2* (6), e1600102.
(103) Rui, Y.; Varanasi, M.; Mendes, S.; Yamagata, H. M.; Wilson, D. R.; Green, J. J., Poly(Beta-Amino Ester) Nanoparticles Enable Nonviral Delivery of CRISPR-Cas9 Plasmids for Gene Knockout and Gene Deletion. *Molecular Therapy - Nucleic Acids* **2020,** *20*, 661-672.
(104) Rui, Y.; Wilson, D. R.; Choi, J.; Varanasi, M.; Sanders, K.; Karlsson, J.; Lim, M.; Green, J. J., Carboxylated branched poly(β-amino ester) nanoparticles enable robust cytosolic protein delivery and CRISPR-Cas9 gene editing. *Science Advances* **2019,** *5* (12), eaay3255.

(105) Maiti, P. K.; Çağın, T.; Wang, G.; Goddard, W. A., Structure of PAMAM Dendrimers: Generations 1 through 11. *Macromolecules* **2004,** *37* (16), 6236-6254.
(106) Zhou, J.; Wu, J.; Hafdi, N.; Behr, J. P.; Erbacher, P.; Peng, L., PAMAM dendrimers for efficient siRNA delivery and potent gene silencing. *Chemical Communications* **2006,** (22), 2362-2364.
(107) Palmerston Mendes, L.; Pan, J.; Torchilin, V. P., Dendrimers as Nanocarriers for Nucleic Acid and Drug Delivery in Cancer Therapy. *Molecules* **2017,** *22* (9), 1401.
(108) Zhang, D.; Atochina-Vasserman, E. N.; Maurya, D. S.; Huang, N.; Xiao, Q.; Ona, N.; Liu, M.; Shahnawaz, H.; Ni, H.; Kim, K.; Billingsley, M. M.; Pochan, D. J.; Mitchell, M. J.; Weissman, D.; Percec, V., One-Component Multifunctional Sequence-Defined Ionizable Amphiphilic Janus Dendrimer Delivery Systems for mRNA. *Journal of the American Chemical Society* **2021,** *143* (31), 12315-12327.
(109) Chahal, J. S.; Khan, O. F.; Cooper, C. L.; McPartlan, J. S.; Tsosie, J. K.; Tilley, L. D.; Sidik, S. M.; Lourido, S.; Langer, R.; Bavari, S.; Ploegh, H. L.; Anderson, D. G., Dendrimer-RNA nanoparticles generate protective immunity against lethal Ebola, H1N1 influenza, and Toxoplasma gondii challenges with a single dose. *Proceedings of the National Academy of Sciences* **2016,** *113* (29), E4133-E4142.
(110) Farbiak, L.; Cheng, Q.; Wei, T.; Álvarez-Benedicto, E.; Johnson, L. T.; Lee, S.; Siegwart, D. J., All-In-One Dendrimer-Based Lipid Nanoparticles Enable Precise HDR-Mediated Gene Editing In Vivo. *Advanced Materials* **2021,** *33* (30), 2006619.
(111) Prata, C. A. H.; Zhao, Y.; Barthelemy, P.; Li, Y.; Luo, D.; McIntosh, T. J.; Lee, S. J.; Grinstaff, M. W., Charge-Reversal Amphiphiles for Gene Delivery. *Journal of the American Chemical Society* **2004,** *126* (39), 12196-12197.
(112) McKinlay, C. J.; Vargas, J. R.; Blake, T. R.; Hardy, J. W.; Kanada, M.; Contag, C. H.; Wender, P. A.; Waymouth, R. M., Charge-altering releasable transporters (CARTs) for the delivery and release of mRNA in living animals. *Proceedings of the National Academy of Sciences* **2017,** *114* (4), E448-E456.
(113) Benner, N. L.; McClellan, R. L.; Turlington, C. R.; Haabeth, O. A. W.; Waymouth, R. M.; Wender, P. A., Oligo(serine ester) Charge-Altering Releasable Transporters: Organocatalytic Ring-Opening Polymerization and their Use for in Vitro and in Vivo mRNA Delivery. *Journal of the American Chemical Society* **2019,** *141* (21), 8416-8421.
(114) Habibian, M.; McKinlay, C.; Blake, T. R.; Kietrys, A. M.; Waymouth, R. M.; Wender, P. A.; Kool, E. T., Reversible RNA acylation for control of CRISPR–Cas9 gene editing. *Chemical Science* **2020,** *11* (4), 1011-1016.
(115) Zhao, X.; Miller, J. R.; Jiang, Y.; Marletta, M. A.; Cronan, J. E., Assembly of the Covalent Linkage between Lipoic Acid and Its Cognate Enzymes. *Chemistry & Biology* **2003,** *10* (12), 1293-1302.
(116) Schmidt, U.; Grafen, P.; Goedde, H. W., Chemistry and Biochemistry of α-Lipoic Acid. *Angewandte Chemie International Edition in English* **1965,** *4* (10), 846-856.
(117) Lu, J.; Wang, H.; Tian, Z.; Hou, Y.; Lu, H., Cryopolymerization of 1,2-Dithiolanes for the Facile and Reversible Grafting-from Synthesis of Protein–Polydisulfide Conjugates. *Journal of the American Chemical Society* **2020,** *142* (3), 1217-1221.
(118) Liu, Y.; Jia, Y.; Wu, Q.; Moore, J. S., Architecture-Controlled Ring-Opening Polymerization for Dynamic Covalent Poly(disulfide)s. *Journal of the American Chemical Society* **2019,** *141* (43), 17075-17080.

(119) Balakirev, M.; Schoehn, G.; Chroboczek, J., Lipoic acid-derived amphiphiles for redox-controlled DNA delivery. *Chemistry & Biology* **2000,** *7* (10), 813-819.
(120) Bang, E.-K.; Gasparini, G.; Molinard, G.; Roux, A.; Sakai, N.; Matile, S., Substrate-Initiated Synthesis of Cell-Penetrating Poly(disulfide)s. *Journal of the American Chemical Society* **2013,** *135* (6), 2088-2091.
(121) Gasparini, G.; Bang, E.-K.; Molinard, G.; Tulumello, D. V.; Ward, S.; Kelley, S. O.; Roux, A.; Sakai, N.; Matile, S., Cellular Uptake of Substrate-Initiated Cell-Penetrating Poly(disulfide)s. *Journal of the American Chemical Society* **2014,** *136* (16), 6069-6074.
(122) Gasparini, G.; Matile, S., Protein delivery with cell-penetrating poly(disulfide)s. *Chemical Communications* **2015,** *51* (96), 17160-17162.
(123) Guo, J.; Wan, T.; Li, B.; Pan, Q.; Xin, H.; Qiu, Y.; Ping, Y., Rational Design of Poly(disulfide)s as a Universal Platform for Delivery of CRISPR-Cas9 Machineries toward Therapeutic Genome Editing. *ACS Central Science* **2021,** *7* (6), 990-1000.
(124) Lu, J.; Xu, Z.; Fu, H.; Lin, Y.; Wang, H.; Lu, H., Room-Temperature Grafting from Synthesis of Protein–Polydisulfide Conjugates via Aggregation-Induced Polymerization. *Journal of the American Chemical Society* **2022,** *144* (34), 15709-15717.
(125) Zeng, H.; Johnson, M. E.; Oldenhuis, N. J.; Tiambeng, T. N.; Guan, Z., Structure-Based Design of Dendritic Peptide Bolaamphiphiles for siRNA Delivery. *ACS Central Science* **2015,** *1* (6), 303-312.
(126) Oldenhuis, N. J.; Eldredge, A. C.; Burts, A. O.; Ryu, K. A.; Chung, J.; Johnson, M. E.; Guan, Z., Biodegradable Dendronized Polymers for Efficient mRNA Delivery. *ChemistrySelect* **2016,** *1* (15), 4413-4417.
(127) Pecsi, I.; Leveles, I.; Harmat, V.; Vertessy, B. G.; Toth, J., Aromatic stacking between nucleobase and enzyme promotes phosphate ester hydrolysis in dUTPase. *Nucleic Acids Research* **2010,** *38* (20), 7179-7186.
(128) Yang, D.-C.; Eldredge, A. C.; Hickey, J. C.; Muradyan, H.; Guan, Z., Multivalent Peptide-Functionalized Bioreducible Polymers for Cellular Delivery of Various RNAs. *Biomacromolecules* **2020,** *21* (4), 1613-1624.

Chapter 2: Facile Synthesis of Multifunctional Bioreducible Polymers For mRNA Delivery

2.1 Introduction

The utilization of polymers from readily derivatized bio-derived monomers is an excellent strategy for RNA therapeutic delivery due to the rapid polymer biodegradability and compatible metabolism of the bio-derived monomers.[1-2] Polydisulfides from lipoic acid (LA) remain a promising class of RNA delivery vehicles due to their favorable bioreducibility and highly biocompatible LA monomers.[3-4] As previously stated, aqueous-phase ring-opening polymerization (ROP) methodologies have become popular for the generation of cationic polydisulfides from cationic LA derivative monomers. However, this ROP methodology limits the scope of functional groups included within these polymers; the inclusion of hydrophobic derivatives or hydrophobic ionizable motifs is not favorable due to solubility factors.

Incorporation of hydrophobic groups, notably alkyl functionalities, has not been attempted for biologically-focused LA-based polydisulfides. Moreover, combining cationic, ionizable, and hydrophobic motifs has demonstrated success in siRNA, mRNA,[5] and RNA-mediated CRISPR-Cas9 (Cas9 mRNA and sgRNA formulated together) gene editing applications[6] with other polymeric systems. Exploration into synthetic methodologies that could include all three of these functionalities, preferably with the capacity to include others in future designs, would greatly expand the potential of polysulfide polymers as RNA delivery vectors.

The incorporation of multiple chemical motifs onto the same polymer backbone has

been previously reported using a post-polymerization functionalization strategy. Theato and coworkers demonstrated the viability of this system by polymerizing pentafluorophenyl acrylate monomers, then subjecting the poly(active ester)polymer to an extensive 24-hour post-polymerization reaction at elevated temperatures.[7] With >95% conversion after 24 hours of aminolysis, the poly(active ester)polymers were shown to have excellent reactivity towards primary and secondary amines,[7] but require catalysts for alcohols.[8] Similar derivations of this work have functionalized polymers with motifs for drug/protein conjugation,[9-10] but not for mRNA delivery applications.

We proceeded to utilize a similar post-polymerization functionalization approach to generate biocompatible multifunctional polydisulfides, first by synthesizing an active ester-containing polydisulfide (poly(AE)disulfide), then performing aminolysis to attach multiple specific functionalities (See Scheme 2.1) to the polymer. Despite the promise of this design,

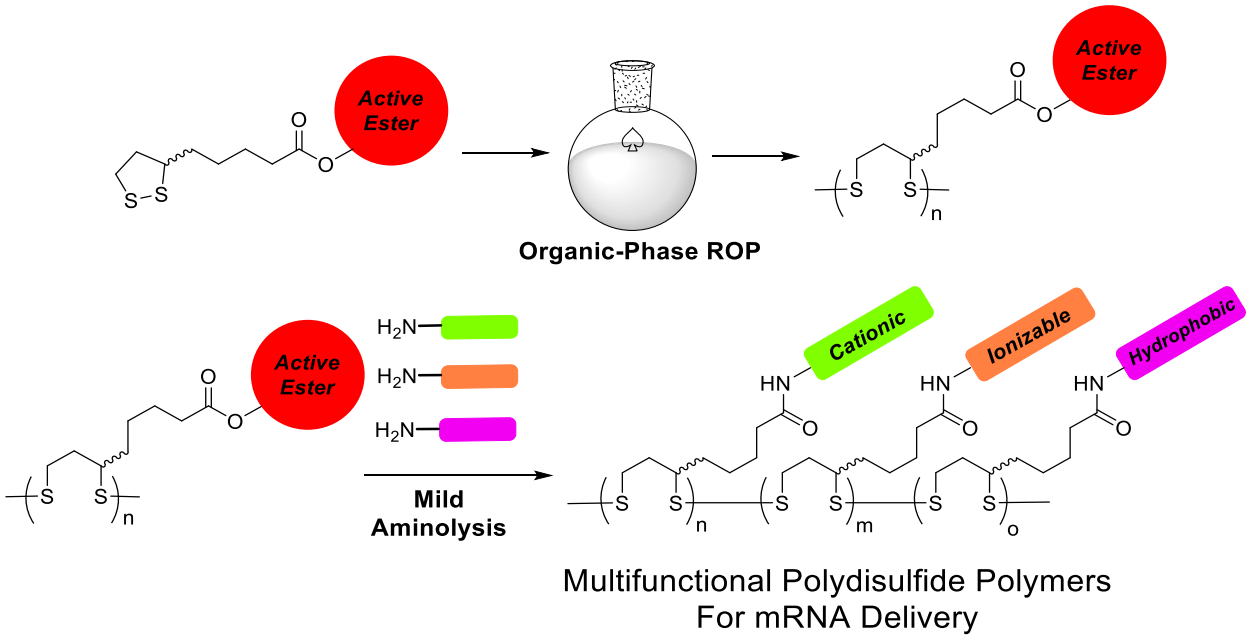

Scheme 2.1 Overview of two-step post-polymerization functionalization to generate multifunctional polydisulfides.

the synthesis of active ester-containing polymers from biocompatible monomers is relatively unexplored, particularly for polymers generated from anionic ROP reactions. To investigate if such polymers were capable of being generated, five different active ester-containing LA derivatives were synthesized (**M1**-**M5;** See Small Molecule Characterization Data) and polymerized using an organic-phase polymerization protocol developed by Moore and coworkers (See Scheme 2.2).[11] Subsequent poly(AE)disulfides were fully characterized by proton nuclear magnetic resonance (^{1}H NMR) and gel-permeation chromatography (GPC).

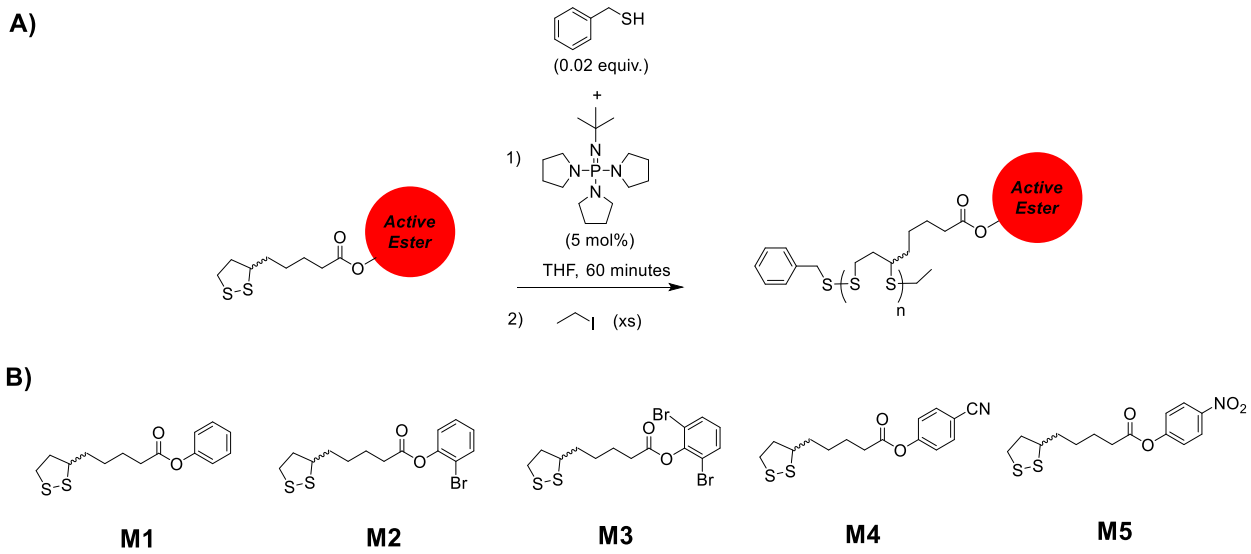

Scheme 2.2 Anionic ROP approach to generate poly(active ester)disulfides. **A**) Organic-phase ROP scheme for active-ester-containing LA derivatives. **B**) Different active-ester-containing LA derivatives used in this study (**M1**-**M5**).

^{1}H NMR small molecule aminolysis trials on active ester-containing LA monomers demonstrated that many primary amine-containing substrates were compatible with this system. This was leveraged to generate multifunctional polydisulfides with cationic groups, ionizable groups, and hydrophobic groups (See Scheme 2.3). A conventional tertiary amine (C1) was selected to provide additional cationic charge to the polymer system; a

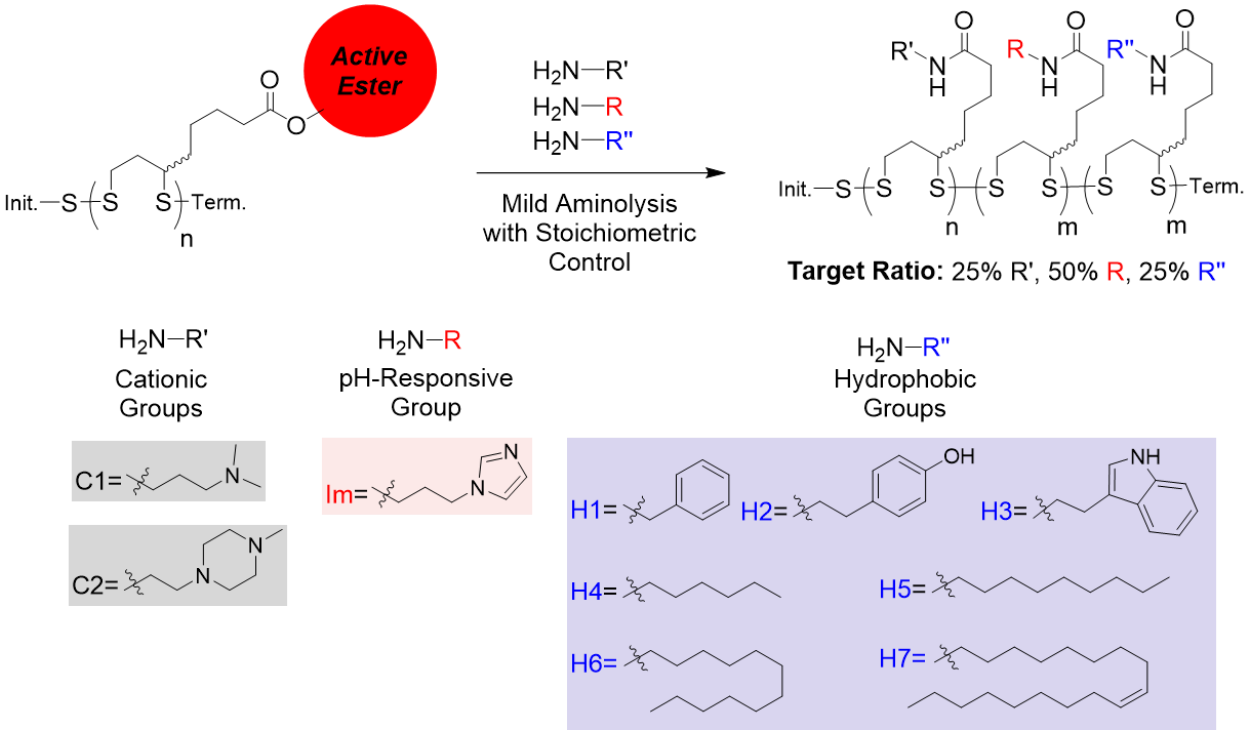

Scheme 2.3 Post-polymerization aminolysis approach to generating multifunctional polydisulfides. A combination of cationic (C1-C2), pH-responsive (Im), and hydrophobic motifs (H1-H7) were utilized in the multifunctional polydisulfides herein.

piperazine-containing amine (C2) was also chosen as a more hydrophilic non-ionizable cationic species. 3-aminopropylimidazole was used as the ionizable motif, with the imidazole (estimated conjugate acid pK_a of 7) facilitating endosomal escape in all polymer combinations through the proton sponge effect.[12] For hydrophobic functionalities, three different functional group types were examined: aromatic motifs, saturated alkyl motifs, and oleyl motifs. Benzyl (H1), tyrosine (H2), and tryptophan (H3) groups were selected as these functionalities mimic the aromatic groups present on numerous cell-penetrating peptides and additional pi-pi stacking between nucleobases and aromatic functional groups could affect RNA binding capability.[13-14] Hexyl (H4), nonyl (H5), and dodecyl (H6) groups were also incorporated into these polymers, as these short alkyl chains mimic the short alkyl peptides (Val, Leu, Iso) on cell-penetrating peptides;[15-16] alkyl functionalization is also

known to improve nanoparticle stability.[17] Lastly, oleyl (H7) functionality was also utilized to similarly stabilize nanoparticles.[18]

Herein, a library of fifteen different multifunctional polymer combinations was generated and confirmed through ^{1}H NMR spectroscopy. Multifunctional polymers were formulated with enhanced green fluorescent protein (EGFP) mRNA to generate polymer-mRNA polyplexes/nanoparticles that were characterized by DLS and cryogenic transmission electron microscopy (cryo-TEM). Polymer-EGFP mRNA nanoparticles were also evaluated *in vitro* for delivery efficacy. Successful polymer vectors were also formulated with ovalbumin (OVA) mRNA-polymer nanoparticles and tested *in vitro*.

2.2 Results and Discussion

The anionic ROP of **M1**-**M5** using a 50:1 ratio of monomer to thiol initiator yielded polymers for **M1**, **M2**, and **M3** in decent yield. These isolated polymers were confirmed by GPC, with poly(**M1**)-, poly(**M2**)-, and poly(**M3**)disulfides all possessing *M*n greater than 18 kDa (See Figure 2.1A; See Table 2.1). Using **M2** as a model monomer, varying initiator ratios were also successfully utilized to generate polymers of different *M*n (Figure 2.1B; Table 2.2). The largest Mn polymer obtained in this study was generated at a 100:1 ratio of monomer to thiol initiator, yielding a poly(**M2**)disulfide polymer of 37 kDa at 36% yield. These poly(AE)disulfide polymers were also confirmed by ^{1}H NMR, with key diagnostic peaks indicating polymers no longer possess signals from the ring-closed 1,2-dithiolane of LA monomers (See Figure 2.1C; See Figures S2.1-S2.3). Notably, both **M4** and **M5** monomers generated no significant polymeric material.

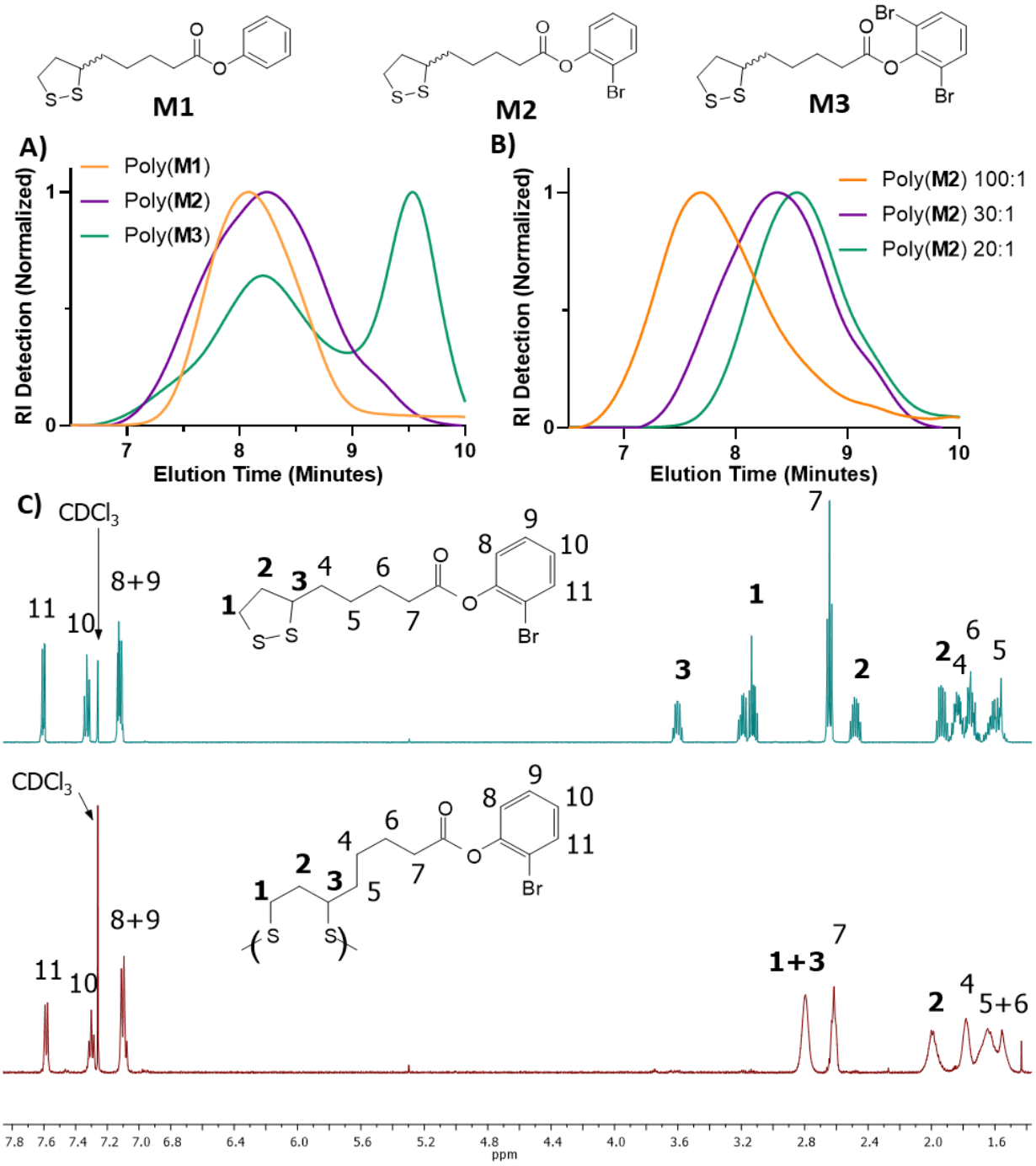

Figure 2.1 Organic-phase ROP of active-ester-containing LA derivatives yields poly(AE)disulfides. **A**) Overlaid GPC traces of poly(**M1**)-, poly(**M2**)-, and poly(**M3**)-disulfides polymerized at a ratio of 50:1 monomer to initiator. **B**) Overlaid GPC traces of poly(**M2**)disulfides polymerized at various monomer to initiator ratios. **C**) ^{1}H NMR (in $CDCl_3$) overlay of **M2** and poly(**M2**)disulfide; diagnostic peaks indicated ring-opening are bolded.

Table 2.1. Summary of polymerization screening conditions, including samples found in Figure 2.1A.

Monomer	Monomer: Initiator Ratio	*M*n (kDa)	*D*	Yield
M1	50:1	19.1	1.7	40%
M2	50:1	13.4	2.4	35%
M3[a]	50:1	22.0	1.7	33%
M4[b]	50:1	3.89	1.9	2.1%
M5[b]	50:1	N/A	N/A	0%

[a] Smaller oligomers not included in GPC analysis. [b] GPC and ^{1}H NMR data not included.

Table 2.2 Summary of polymerization conditions found in Figure 2.1B.

Monomer	Monomer: Initiator Ratio	*M*n (kDa)	*D*	Yield
M2	100:1	37.0	2.1	36%
M2	30:1	9.71	2.3	32%
M2	20:1	7.12	1.8	34%

With polymerization established, post-polymerization functionalization reactions were explored. Model small molecule aminolysis reactions were performed on **M1**, **M2**, and **M3** monomers using primary amine substrates and monitored via ^{1}H NMR. Aminolysis of **M1** does not functionalize under stoichiometric amine conditions. Even with three equivalents of primary amine, only ~75% conversion is obtained after 1 hour of incubation with 500 mM **M1** in acetonitrile (See Figure S2.4). Fortunately, aminolysis can be obtained under stoichiometric conditions when reacting **M2** at or **M3** at 500 mM in *d*6-DMSO (See Figure S2.5-2.6). While both **M2** and **M3** monomers are excellent candidates for post-polymerization functionalization, **M3** requires elevated temperatures (313 K/40 ˚C) to solubilize the monomer in *d*6-DMSO during the aminolysis reaction, whereas **M2** can solubilize and undergo aminolysis in *d*6-DMSO at room temperature (298 K/25 ˚C). Knowing this, **M2** was used in an expanded aminolysis screen and various feedstock

primary amino-containing compounds were tested to confirm reactivity and optimal conditions via ^{1}H NMR (See Figures 2.7-2.14; See Table 2.1). Expanding on this even further, aminolysis conversion using a model primary amine was also investigated under different concentrations (63 mM, 125 mM, 250 mM) using ^{1}H NMR. For these other three concentrations, 70-90% conversion was obtained after 30 minutes while >95% conversion was obtained after 60 minutes, confirming that this aminolysis methodology is viable even with low monomer concentrations (See Figures 2.15-2.16).

While excellent aminolysis conversion is obtained using a variety of primary amine substrates, there are limits in viable nucleophiles for this system. Aminolysis using fluorinated amine-containing compounds was also attempted with **M2**. However, even in the presence of catalysts poor conversion was observed after 24 hours (See Figure 2.17). Similarly, alcoholysis of **M2** was attempted using an excess of primary alcohol, with poor conversion also observed after 24 hours (See Figures 2.18). These results confirm previous literature observations, suggesting that primary amines and secondary amines (not tested here) are model nucleophiles for poly(active ester)polymer post-polymerization functionalizations without additional catalysts.[7]

With excellent polymerization and aminolysis conditions obtained for **M2**, poly(**M2**)disulfide was selected as the model polymer for post-polymerization functionalization derivatization. The purity of poly(**M2**)disulfide after precipitation purification also reinforced this decision; poly(**M3**)disulfide is coprecipitated with low molecular weight oligomers during purification (See Figure 2.1A). Poly(**M2**)disulfide can be readily functionalized without additional purification steps. After post-polymerization

functionalization, sixteen different multifunctional polydisulfides were generated from poly(**M2**)disulfide and characterized by ^{1}H NMR to confirm motif incorporation ratios (See Figures S2.19-S2.34).

With a library of different multifunctional polymers, optimal formulation conditions with a model mRNA were explored. Due to the poor solubility of these multifunctional polymers in aqueous conditions, all multifunctional polymers were solubilized in DMSO prior to bulk mixing complexation with aqueous mRNA solutions. Using 100% Im-functionalized polymer as a model polydisulfide for RNA complexation, 100% Im was formulated with EGFP mRNA in PBS (pH 7.4); subsequent gel electrophoresis (GE) of polymer-mRNA formulations determined that no mRNA complexation was obtained at pH 7.4, presumably because there are no cationic groups to electrostatically complex with phosphates of the mRNA (See Figure 2.2A). Formulation of 100% Im polymer with EGFP mRNA at pH 6.0 resulted in complexation at a 1:1 ratio of cationic imidazolium groups to phosphate groups ("N/P Ratio"; See Figure 2.2B), confirming that imidazolium groups can complex with phosphate groups at lower pH conditions.

To determine if cationic amines can alter mRNA complexation behavior the cationic ammonium group C1 was added to an Im-containing polymer (C1-Im; 20% C1+ 80% Im). Formulation of C1-Im with mRNA resulted in successful complexation at cationic nitrogen/ammonium to phosphate ratios (N/P ratio) of 2.5 and above in PBS (pH 7.4; See Figure 2.2C), indicating cationic amines complex with mRNA at physiological pH. Additionally, when C1-Im polymer was formulated with EGFP mRNA at identical N/P ratios (from Figure 2.2D) in pH 6.0 buffer, complete polymer-mRNA complexation occurred at

lower N/P ratios, indicating both amines and imidazolium ions complex with phosphate groups of the mRNA. Understanding that future formulations will undergo buffer switching from low pH buffer to PBS (pH 7.4) prior to administration to cells, cationic amine-

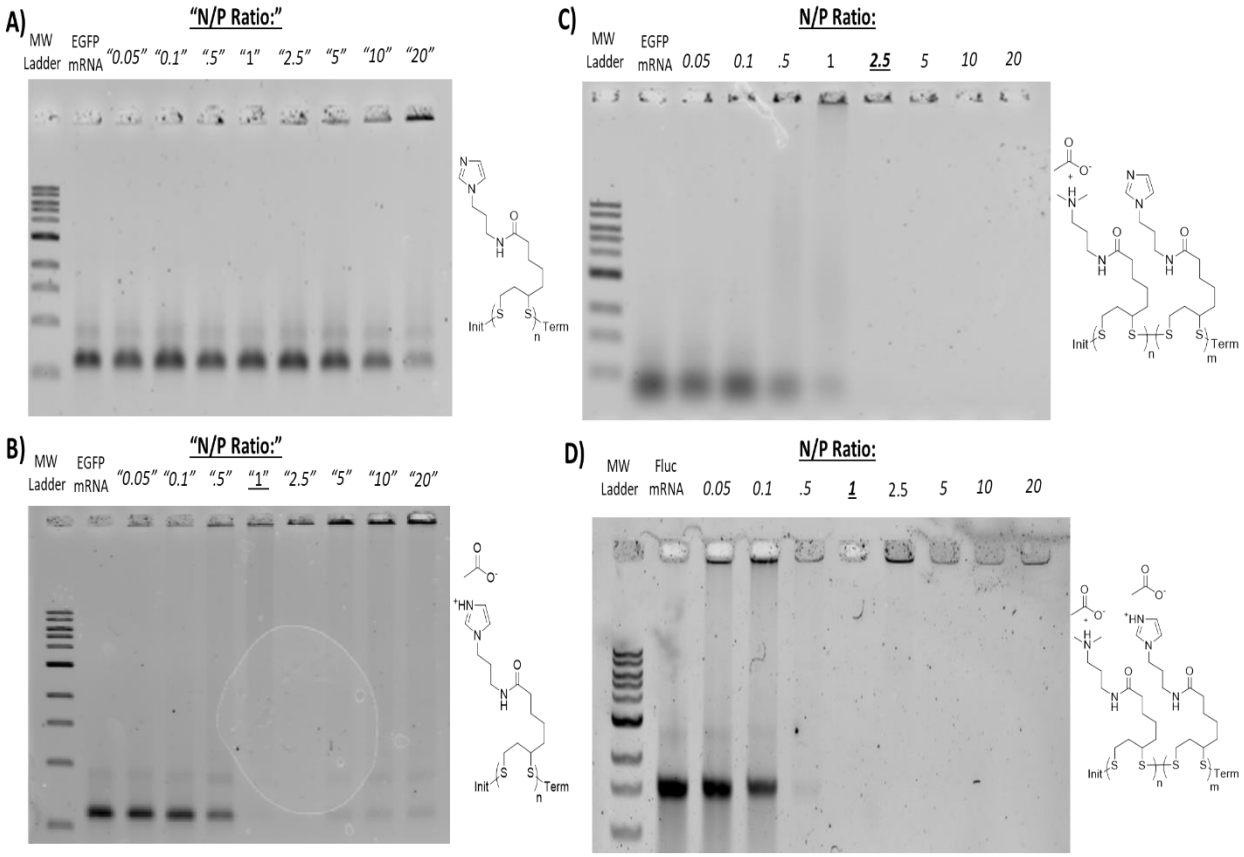

Figure 2.2 Multifunctional polymer-mRNA complexation via gel electrophoresis. "N/P Ratio" was calculated from number of imidazole groups to phosphate groups of mRNA and N/P Ratio was calculated from number of imidazole groups to phosphate groups of mRNA. Ratios where mRNA is fully complexed are bolded and underlined. **A**) Complexation of 100% Im polymer with EGFP mRNA in PBS buffer (pH 7.4). **B**) Complexation of 100% Im polymer with EGFP mRNA in pH 6.0 buffer. **C**) Complexation of C1-Im polymer with EGFP mRNA in PBS buffer (pH 7.4). **D**) Complexation of C1-Im polymer with Fluc mRNA in pH 6.0 buffer.

containing groups (C1 or C2) were incorporated in all multifunctional polymer designs as enhanced RNA-complexing groups at all relevant pH ranges.

Expanding these formulation principles to other multifunctional polydisulfides, complexation of polymers with EGFP mRNA was further optimized to generate well-

defined nanoparticles. At pH 4.0, all multifunctional polydisulfides generated nanoparticles with diameters <200 nm according to DLS measurements (See Figure 2.3A; See Table S2.3); nanoparticles were also confirmed by cryo-TEM (See Figure 2.3B; See Figure S2.35). Nanoparticle stability studies of some non-loaded nanoparticles (without mRNA) and mRNA-polymer polyplexes were measured upon pH switching from 4.0 to 7.4; time-dependent aggregation of polyplexes is observed for both non-loaded and mRNA-

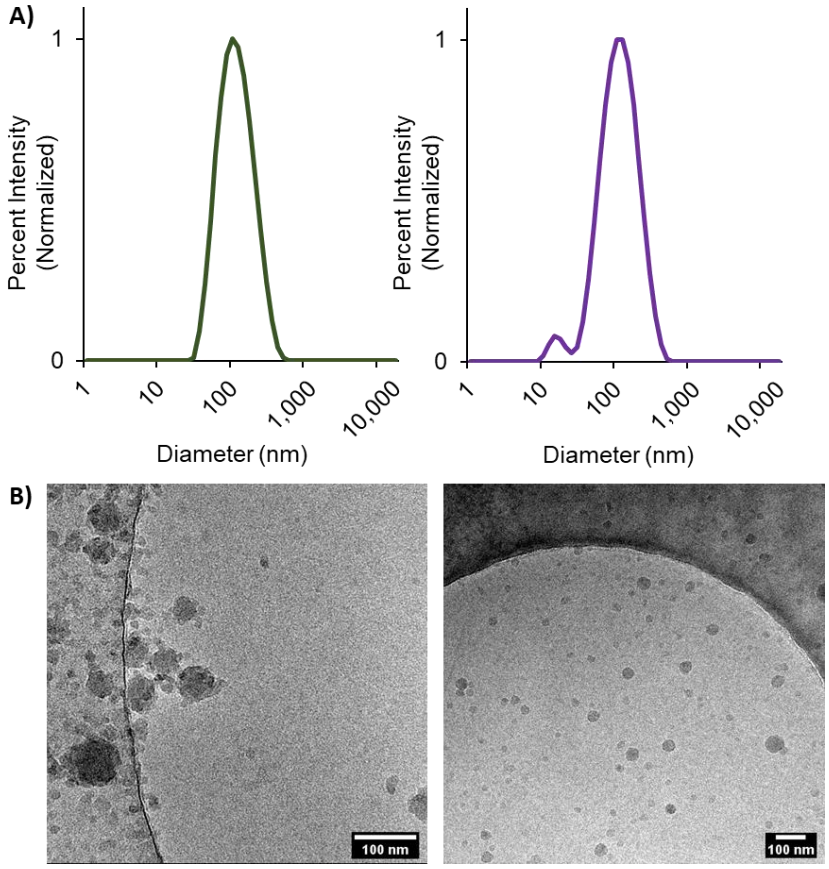

Figure 2.3 Representative Multifunctional polydisulfide-EGFP mRNA Nanoparticles characterized by DLS and Cryo-TEM. **A**) DLS size distributions for C1-Im-H1 (left) and C1-Im-H4 (right) coformulated with EGFP mRNA at an N/P ratio of 5. **B)** Cryo-TEM images for C1-Im-H1 (left) and C1-Im-H4 (right) coformulated with EGFP mRNA at an N/P ratio of 5. Scale bar represents 100 nm.

complexed nanoparticles (See Table S2.4-2.5; See Figures S2.36-2.37).

A small number of these multifunctional polymer-EGFP mRNA nanoparticles were then treated with glutathione (GSH; a thiol present in cellular cytosol) to determine if decomplexation of mRNA-polymer polyplexes by exogenous thiols could be modeled *ex vivo*. Of the model decomplexation conditions sampled, no depolymerization/decomplexation is observed without GSH or with GSH at pH 4.5 (the pH of lysosomes) for any polymers (See Figure S2.38) However, for certain polymers depolymerization was observed at pH 7.4 (physiological/cytosol pH). Interestingly, polymers containing C2 cationic functionality are seen to have more consistent depolymerization/decomplexation, suggesting that the hydrophilicity of the C2 motif may assist in polyplex decomplexation. *Ex vivo* polyplex decomplexation does not fully replicate the complex reducing environment of the cytosol, so *in vitro* validation was still desired to assess mRNA delivery efficacy.

To validate these multifunctional polymers as delivery vehicles for mRNA, nanoparticle cell uptake was investigated. Cy5-labeled EGFP mRNA-polymer polyplexes were administered to HeLa and DC2.4 cells and treated cells were analyzed after six hours of nanoparticle incubation. Within this brief period, >90% of all treated HeLa and DC2.4 cells internalized nanoparticles, according to flow cytometry measurements (See Figures S2.39). Longer incubation of these cells with Cy5-labeled EGFP mRNA-polymer polyplexes resulted in EGFP expression for numerous multifunctional polymer species, notably C2-Im-H1 and C2-Im-H4 (See Figure 2.4; See Figure S2.40). For general EGFP expression trends, multifunctional polymeric nanoparticles containing C2 cationic amines resulted in better EGFP mRNA expression than C1-containing counterparts. Interestingly, multifunctional polymers with certain hydrophobic functionalities (H1, H4, and H5) are capable of EGFP

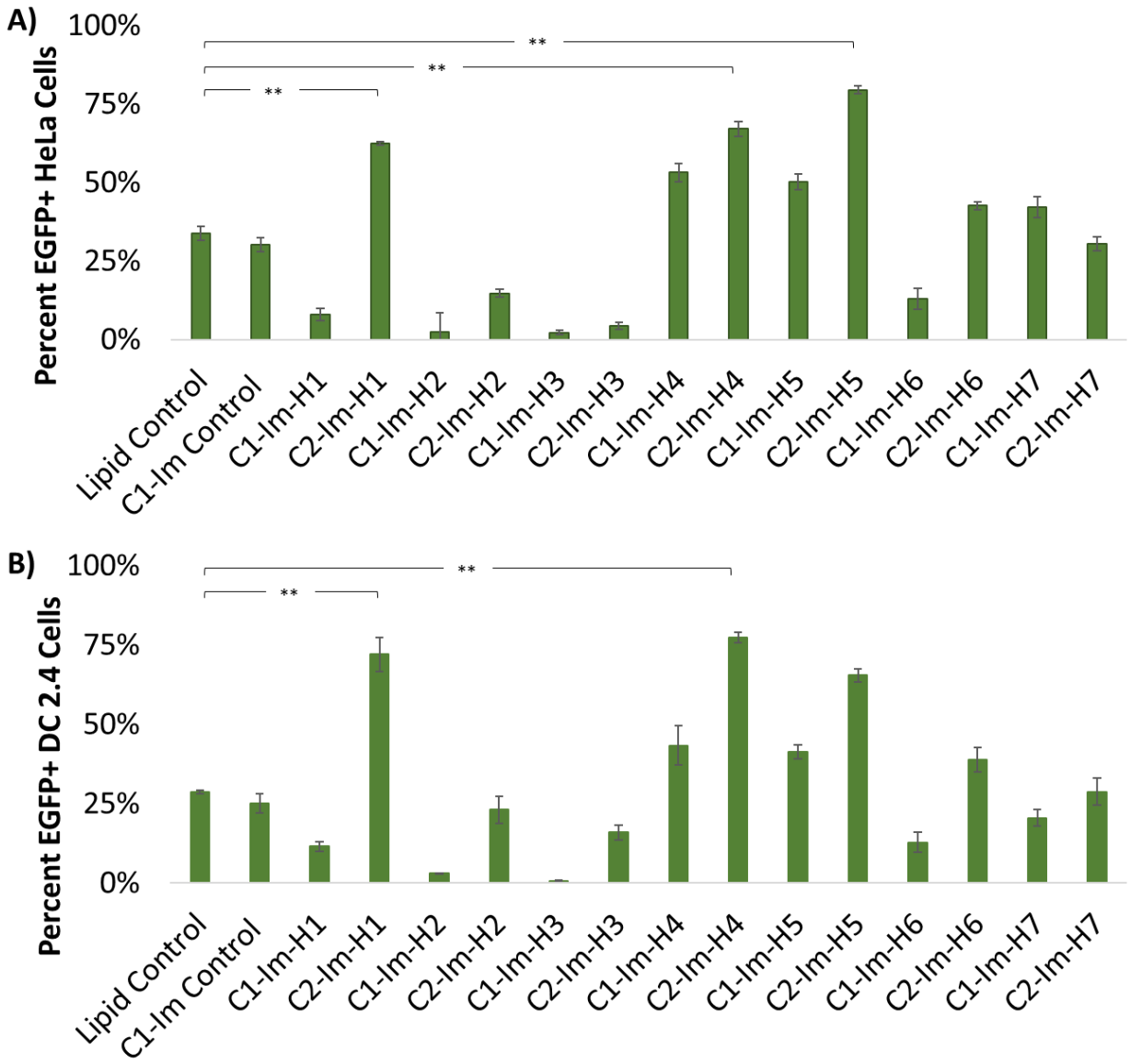

Figure 2.4 Number of cells expressing EGFP after treatment with multifunctional polymer-mRNA nanoparticles containing Cy5-labeled mRNA. Number of EGFP+ **A**) HeLa cells and **B**) DC2.4 cells. EGFP+ cells determined by flow cytometry 48 hours after nanoparticle administration. All nanoparticles formualated at an N/P ratio of 5 and 150 ng of mRNA was administered per 5K cells. Lipofectamine MessengerMAX was used as a lipid control. ** indicates $p<0.005$. n=3 for all sample treatments.

mRNA delivery, however other hydrophobic functionalities (H2, H3, H7, H8) are unable to deliver EGFP mRNA effectively.

Overall EGFP delivery efficacy also corresponds to Cy5-labelled EGFP mRNA presence after 48 hours. Flow cytometry indicates that cells not expressing EGFP retain

Cy5+ character after 48 hours of nanoparticle incubation (See Figure S2.41); these cells also exhibit nominal cytotoxicity after 6 hours and 48 hours (See Figures S2.42-2.43), suggesting poor EGFP expression is not due to toxicity. Confocal microscopy was used to investigate these poorly-expressing multifunctional polymers further; after 12 hours of incubation with Cy5+ EGFP mRNA-polymer nanoparticles, DC2.4 cells demonstrated EGFP expression in well-performing vectors, indicating these nanoparticles have escaped the endosome and began releasing mRNA cargo (See Figure 2.5).

However, for poorly performing multifunctional polymer vectors no EGFP

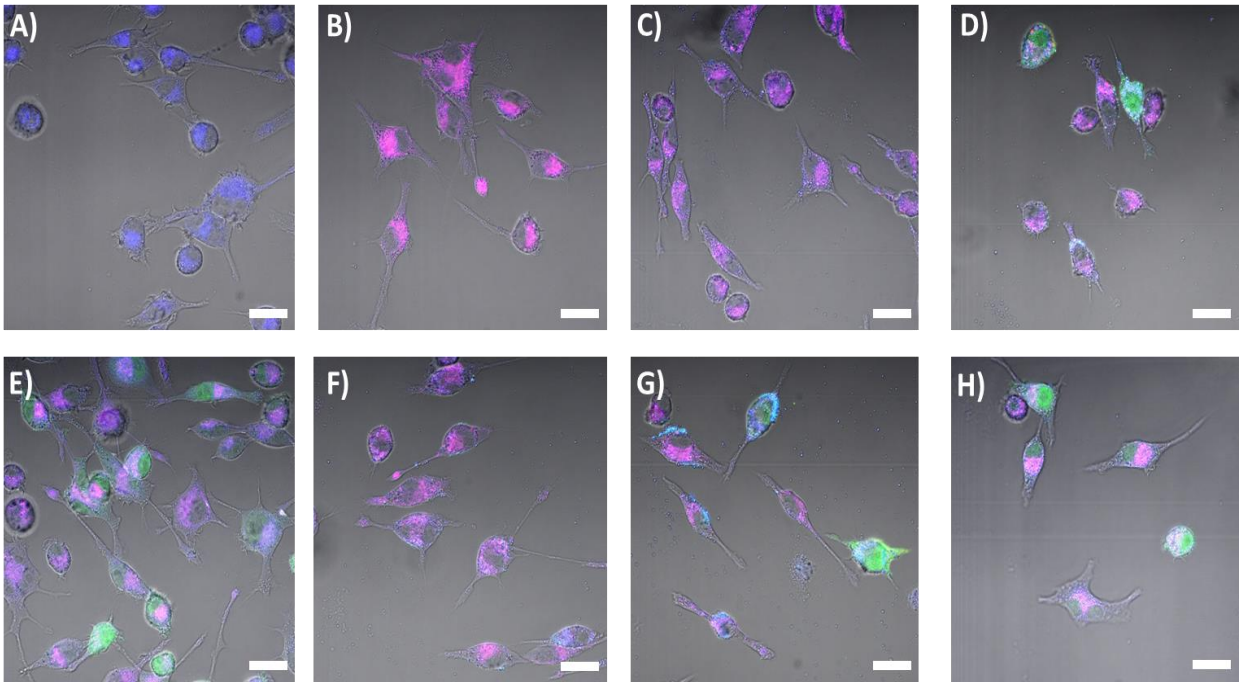

Figure 2.5 Confocal fluorescence microscopy images of DC2.4 cells after 12 hours of Cy5-labeled EGFP mRNA-polymer nanoparticle treatment. Colors indicate lysosomal staining (blue), Cy5-labeled EGFP mRNA (red), and EGFP expression (green). **A)** Lysotracker Blue control (no treatment), **B)** Nanoparticles with Cy5-labeled EGFP mRNA and C1-Im-H2 polymer, **C)** Nanoparticles with Cy5-labeled EGFP mRNA and C1-Im-H1 polymer, **D)** Nanoparticles with Cy5-labeled EGFP mRNA and C1-Im-H4 polymer, **E)** Cy5-labeled EGFP mRNA Lipofectamine control, **F)** Nanoparticles with Cy5-labeled EGFP mRNA and C2-Im-H2 polymer, **G)** Nanoparticles with Cy5-labeled EGFP mRNA and C2-Im-H1 polymer, **H)** Nanoparticles with Cy5-labeled EGFP mRNA and C2-Im-H4 polymer. Scale bar represents 20 μm for all images.

expression was observed and Cy5+ puncta can be seen that are not localized to lysosomes (as visualized by lysosomal staining; See Figure 2.6). Treatment of DC2.4 cells with poorly performing vectors and chloroquine supplementation (a small ionizable molecule) to force endosomal escape of nanoparticles resulted in a negligible increase in overall EGFP+ cells, suggesting EGFP expression in poorly-performing vectors is not limited by endosomal escape efficiency (See Figure S2.44). From this result, we suggest that specific hydrophobic-functionalized mRNA-polymer polyplexes, particularly those containing H2. H3, H7, and H8 species, are not efficiently decomplexed upon cytosol entry, preventing mRNA release and expression.

With excellent EGFP mRNA delivery results obtained for different multifunctional polymers, four multifunctional polymers (C1-Im-H1, C1-Im-H5, C2-Im-H1, and C2-Im-H4) were complexed with OVA mRNA (encoding immunogenic ovalbumin protein) to test a

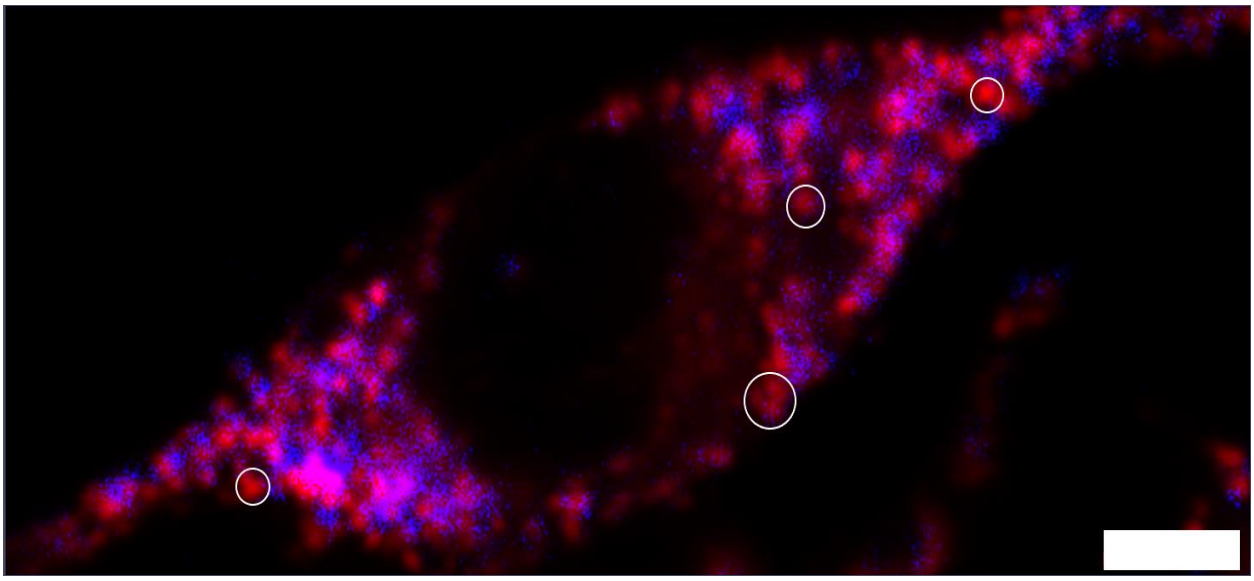

Figure 2.6 Expanded confocal fluorescence microscopy image of a DC2.4 cell after 12 hours of Cy5-labeled EGFP mRNA-C2-Im-H2 polymeric nanoparticle treatment. Colors visualize lysosomal staining (blue) and Cy5-labeled EGFP mRNA (red). Selected regions with no overlap of lysosomal staining and Cy5-containing nanoparticles are encompassed within white circles. Scale bar represents 5 μm.

model mRNA-encoding vaccine antigen. After OVA mRNA-polymer nanoparticle generation was confirmed with one multifunctional polymer by DLS (See Figure S2.45; See Table S2.6), nanoparticles from four multifunctional polydisulfides were administered to DC2.4 cells. Successful nanoparticle delivery should result in ovalbumin expression within DC2.4 cells, leading to ovalbumin proteolytic breakdown and the resulting immunogenic peptides being complexed to major histocompatibility complex I (MHC-I) on the surface of these cells (See Figure 2.7A). By using propidium iodide (PI)-conjugated antibody specific to the OVA peptide fragment (SIINFEKL) complexed on MHC-I, we can label and sort cells that have presented these OVA peptide fragments to generate further immune responses.[19] For nanoparticles complexed with C2-Im-H1 and C2-Im-H4 multifunctional polymers, >30% of DC2.4 cells treated with these polymeric nanoparticles were positive for OVA peptide-MHC-I complexed assemblies (See Figure 2.7B), indicating that these multifunctional polymers can provide immune responses for mRNA-encoded antigens.

Knowing that these multifunctional polymers can deliver two different types of mRNAs *in vitro*, we decided to explore additional modifications to promote nanoparticle stability upon pH change and in biological fluids. Unfortunately, aggregation behavior was observed for these mRNA-polymer polyplexes upon switching from pH 4.0 to 7.4. To combat aggregation in similar nanoparticle designs, insertion of polyethylene glycol (PEG) into the polymer backbone is commonly utilized to sterically inhibit hydrophobic intermolecular interactions between polyplexes.[20]

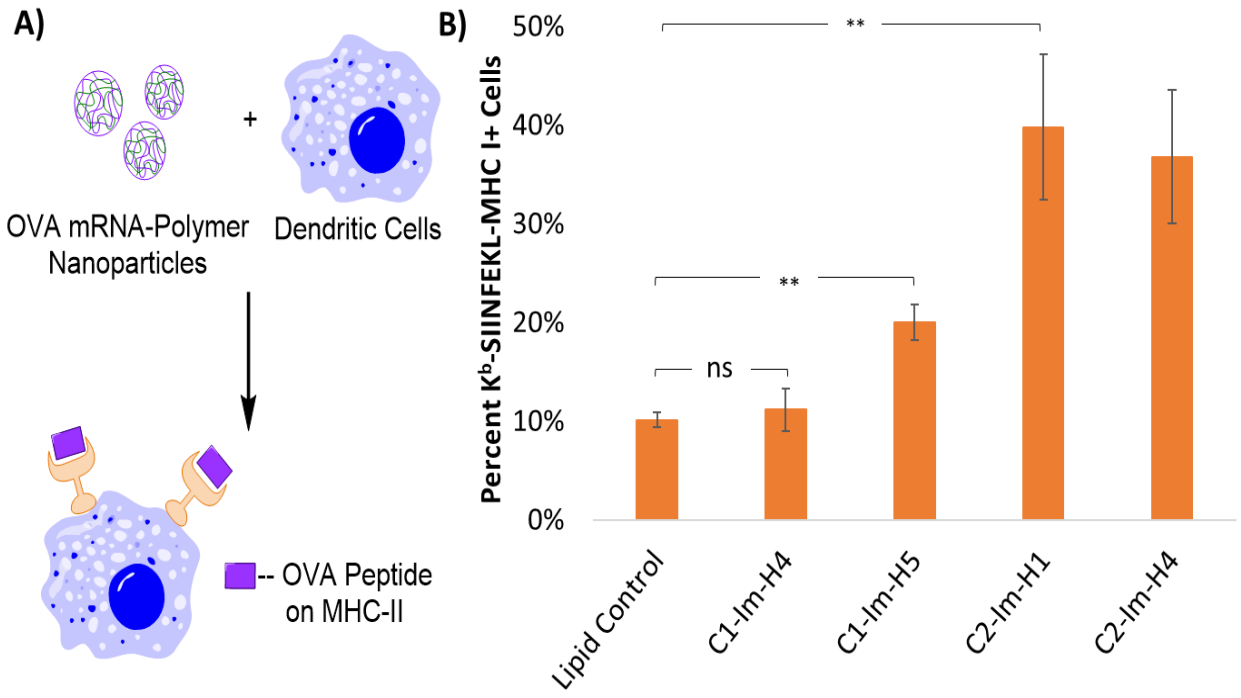

Figure 2.7 Delivery of multifunctional polydisulfide-OVA mRNA nanoparticles to dendritic cells. **A)** Cellular delivery of OVA mRNA-containing nanoparticles results in antigen fragment presentation on dendritic cells. **B)** Percent K^b- SIINFEKL-MHC-I+ DC2.4 cells 24 hours after treatment of OVA mRNA-polymer nanoparticles. Lipofectamine MessengerMAX used as lipid control. ** indicates $p<0.005$; ns indicates not statistically significant. n=3 for all sample treatments.

Following this PEGylation strategy, we synthesized a LA derivative containing PEG 2K (see Supplementary Spectra) and copolymerized it with **M2** at an estimated 7% incorporation based on stoichiometric monomer ratios. The resulting PEGylated-poly(**M2**)disulfide (See Figure S2.46) was isolated, characterized, and functionalized in a similar manner to other multifunctional polymers (See Figures S2.46-2.50). When these polymers were complexed with EGFP mRNA at pH 4.0, polyplexes were generated and showed excellent stability when resuspended in PBS (pH 7.4) for at least two hours (See Figure 2.8). With this stability profile and previous *in vitro* mRNA delivery capability, these vectors are extremely promising tools for systemic nanoparticle delivery and potential vaccine mRNA administration.

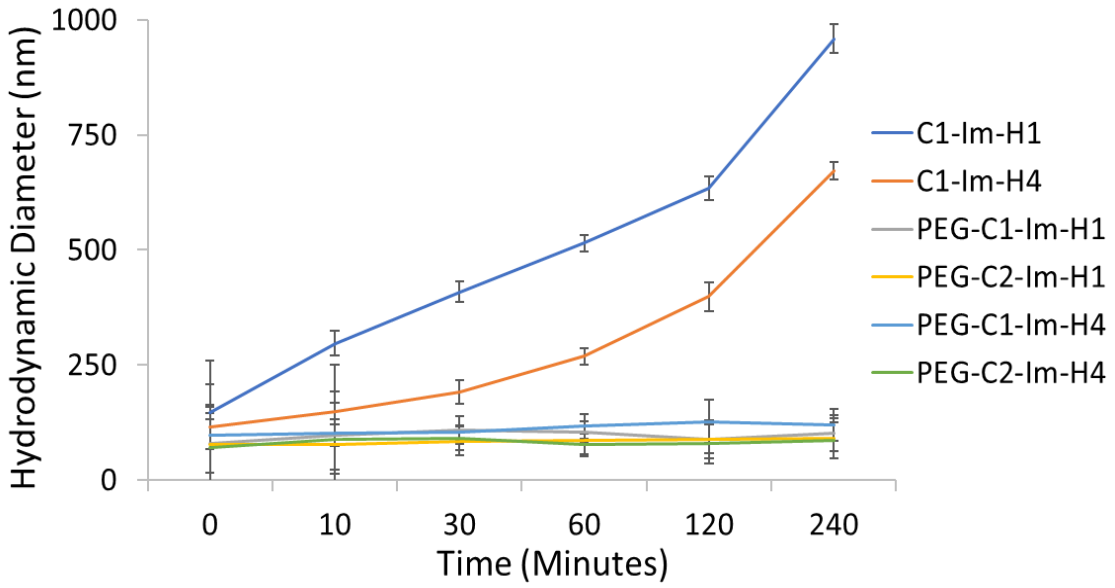

Figure 2.8 Stability of PEGylated and non-PEGylated multifunctional polymer-EGFP mRNA nanoparticles. Nanoparticle size measured by DLS after switching from pH 4.0 buffer to PBS (pH 7.4).

2.3 Conclusions

Within this project we validated a new synthetic methodology to generate poly(active ester)disulfide polymers from biocompatible lipoic acid-derived monomers using an established organic-phase ROP methodology. Subsequent post-polymerization functionalization of these polymers was achieved through a facile and stoichiometrically-controlled aminolysis reaction to include functional groups not previously viable from other LA-based polymerization methodologies. A multifunctional polydisulfide polymer library was generated using this post-polymerization approach, in which each polymer was functionalized with various cationic, ionizable, and hydrophobic motifs. These multifunctional polymers formed nanoparticles with both EGFP mRNA and OVA mRNA, successfully delivering these mRNAs *in vitro*. While some hydrophobic functionalities

affected polyplex decomplexation in cells, short alkyl chain and benzyl functionalizations prove to be rapidly biodegradable in this polydisulfide system. Future functionalizations with different cationic and ionizable groups can readily be investigated within this platform to determine effects on mRNA delivery. PEGylation is also feasible in this platform, making systemic *in vivo* mRNA delivery using these polyplexes extremely promising. Altogether, this synthetic strategy should make future novel multifunctional polydisulfide synthesis, including exotic ligands and targeting motifs, synthetically viable and applicable in new mRNA therapy developments.

2.4 References

(1) Chen, C. K.; Huang, P. K.; Law, W. C., Biodegradable Polymers for Gene-Delivery Applications. *International Journal of Nanomedicine* **2020,** *15*, 2131-2150.

(2) Huang, P.; Deng, H.; Zhou, Y.; Chen, X., The roles of polymers in mRNA delivery. *Matter* **2022,** *5* (6), 1670-1699.

(3) Bang, E.-K.; Gasparini, G.; Molinard, G.; Roux, A.; Sakai, N.; Matile, S., Substrate-Initiated Synthesis of Cell-Penetrating Poly(disulfide)s. *Journal of the American Chemical Society* **2013,** *135* (6), 2088-2091.

(4) Zhang, R.; Nie, T.; Fang, Y.; Huang, H.; Wu, J., Poly(disulfide)s: From Synthesis to Drug Delivery. *Biomacromolecules* **2022,** *23* (1), 1-19.

(5) Rui, Y.; Wilson, D. R.; Tzeng, S. Y.; Yamagata, H. M.; Sudhakar, D.; Conge, M.; Berlinicke, C. A.; Zack, D. J.; Tuesca, A.; Green, J. J., High-throughput and high-content bioassay enables tuning of polyester nanoparticles for cellular uptake, endosomal escape, and systemic in vivo delivery of mRNA. *Science Advances* **2022,** *8* (1), eabk2855.

(6) Kim, H. J.; Ogura, S.; Otabe, T.; Kamegawa, R.; Sato, M.; Kataoka, K.; Miyata, K., Fine-Tuning of Hydrophobicity in Amphiphilic Polyaspartamide Derivatives for Rapid and Transient Expression of Messenger RNA Directed Toward Genome Engineering in Brain. *ACS Central Science* **2019,** *5* (11), 1866-1875.

(7) Eberhardt, M.; Mruk, R.; Zentel, R.; Théato, P., Synthesis of pentafluorophenyl(meth)acrylate polymers: New precursor polymers for the synthesis of multifunctional materials. *European Polymer Journal* **2005,** *41* (7), 1569-1575.

(8) Das, A.; Theato, P., Multifaceted Synthetic Route to Functional Polyacrylates by Transesterification of Poly(pentafluorophenyl acrylates). *Macromolecules* **2015,** *48* (24), 8695-8707.
(9) Son, H.; Ku, J.; Kim, Y.; Li, S.; Char, K., Amine-Reactive Poly(pentafluorophenyl acrylate) Brush Platforms for Cleaner Protein Purification. *Biomacromolecules* **2018,** *19* (3), 951-961.
(10) McRae, S.; Chen, X.; Kratz, K.; Samanta, D.; Henchey, E.; Schneider, S.; Emrick, T., Pentafluorophenyl Ester-Functionalized Phosphorylcholine Polymers: Preparation of Linear, Two-Arm, and Grafted Polymer–Protein Conjugates. *Biomacromolecules* **2012,** *13* (7), 2099-2109.
(11) Liu, Y.; Jia, Y.; Wu, Q.; Moore, J. S., Architecture-Controlled Ring-Opening Polymerization for Dynamic Covalent Poly(disulfide)s. *Journal of the American Chemical Society* **2019,** *141* (43), 17075-17080.
(12) Behr, J.-P., The proton sponge: a trick to enter cells the viruses did not exploit. *CHIMIA International Journal for Chemistry* **1997,** *51* (1-2), 34-36.
(13) Kalafatovic, D.; Giralt, E., Cell-Penetrating Peptides: Design Strategies beyond Primary Structure and Amphipathicity. *Molecules* **2017,** *22* (11), 1929.
(14) Warren, G. M.; Meir, A.; Wang, J.; Patel, D. J.; Greene, E. C.; Shuman, S., Structure–activity relationships at a nucleobase-stacking tryptophan required for chemomechanical coupling in the DNA resecting motor-nuclease AdnAB. *Nucleic Acids Research* **2021,** *50* (2), 952-961.
(15) Min, S. H.; Lee, D. C.; Lim, M. J.; Park, H. S.; Kim, D. M.; Cho, C. W.; Yoon, D. Y.; Yeom, Y. I., A composite gene delivery system consisting of polyethylenimine and an amphipathic peptide KALA. *Journal of Gene Medicine* **2006,** *8* (12), 1425-1434.
(16) Summerton, J. E., Endo-Porter: a novel reagent for safe, effective delivery of substances into cells. *Annals of the New York Academy of Science* **2005,** *1058*, 62-75.
(17) Venancio, J. C. C.; Nascimento, R. S. V.; Pérez-Gramatges, A., Colloidal stability and dynamic adsorption behavior of nanofluids containing alkyl-modified silica nanoparticles and anionic surfactant. *Journal of Molecular Liquids* **2020,** *308*, 113079.
(18) Mourdikoudis, S.; Liz-Marzán, L. M., Oleylamine in Nanoparticle Synthesis. *Chemistry of Materials* **2013,** *25* (9), 1465-1476.
(19) Dersh, D.; Yewdell, J. W.; Wei, J., A SIINFEKL-Based System to Measure MHC Class I Antigen Presentation Efficiency and Kinetics. *Methods in Molecular Biology* **2019,** *1988*, 109-122.
(20) Suk, J. S.; Xu, Q.; Kim, N.; Hanes, J.; Ensign, L. M., PEGylation as a strategy for improving nanoparticle-based drug and gene delivery. *Advanced Drug Delivery Reviews* **2016,** *99* (Pt A), 28-51.

2.5 Experimental Protocols

Instruments: Nuclear Magnetic Resonance (NMR) spectra were recorded on 500 MHz Bruker spectrometers at 25 °C with chemical shifts reported in ppm and coupling constants in Hertz (Hz). ^{1}H NMR chemical shifts were referenced to either $CDCl_3$ or DMSO-*d*6. Number average molecular weight (*Mn*), weight average molecular weight (M_w), and Dispersity (*D*) were determined via Gel Permeation Chromatography (GPC). All GPC experiments were performed on an Agilent 1100 SEC system using a PLGel 5 μm MIXED-C 300 x 7.5mm column from Agilent Technologies (PN PL1110-6500) and polymer molecular weight was determined with respect to polystyrene standards purchased from Sigma-Aldrich. THF was used as the eluent at a flow rate of 1mL/min and at a column temperature of 35 °C. EGFP mRNA-polymer nanoparticle sized were measured at 633 nm using a Zetasizer Nano ZS dynamic light scattering instrument (Malvern Instruments, Malvern, UK) at 25 ˚C with detection angle of 173°. Confocal fluorescence microscopy images were obtained using a Zeiss LSM 780 (Carl Zeiss AG, Oberkochen, Germany) and image analysis performed in ZEN software. All flow cytometry was performed on a NovoCyte flow cytometer (ACEA Biosciences, San Diego) using NovoExpress Software. Student's T-Test was used for all statistical analysis. All EGFP mRNA-polymer nanoparticles were visualized using a JEOL 2100F TEM utilizing a Schottky type field emission gun operating at 200 keV. All pH measurements were measured using an Accumet Basic AB15 pH probe. Multifunctional polymer-mRNA nanoparticle depolymerization/ decomplexation assays were performed using agarose gel electrophoresis and imaged on a Typhoon 9410 system (GE). Decomplexation of gels was quantified using ImageJ.

Materials: All commercially available chemicals were used without further purification unless otherwise noted and all reactions performed using HPLC grade solvents.

Reagents: All reagents described within have purity denoted as percent purity (%). D,L-α-Lipoic acid (LA; 99.3%) was purchased from Chem-Impex (USA, IL). Phenol (99.0%), 2-Bromophenol (98%), 2,6-Dibromophenol (99%), 4-Nitrophenol (99%), PEG 2K (CAS# 9004-74-4), Iodoethane (98%) and Phosphazene P1-t-Bu-tris(tetramethylene) base (CAS#161118-67-8; >97.0%) were all purchased from Sigma-Aldrich. 4-Cyanophenol (99.0%) was purchased from Frontier Specialty Chemicals (USA, UT). 1-(3-Aminopropyl)imidazole (>97.0%) and Hexylamine (99.0%) were purchased from TCI America. 2-(Dimethylamino)ethylamine (>98.0%), 3-Dimethylaminopropylamine (99.0%), acetic anhydride (99%), Nonylamine (98%), Dodecylamine (98%), and Oleylamine (CAS#112-90-3; 70%) were purchased from Sigma-Aldrich. Tryptamine (97%) was purchased from Acros Organics, and Tyramine (97%) was purchased from Frontier Scientific. Benzylamine (>98%), N,N′-Dicyclohexylcarbodiimide (99%), and 4-Dimethylaminopyridine (99%) were purchased from Alfa Aesar, and 2-(4-Methylpiperazin-1-yl)ethanamine (99.7%) was purchased from ChemScene (CAS# 934-98-5). Dimethylaminoethanol (>99%), Trifluoroethylamine (99.5%), 2,2,3,3,3-pentafluoropropylamine (>98%), and L-glutathione (reduced, >98%) were also purchased directly from Sigma-Aldrich.

mRNAs and Tissue Culturing: Cy5-labeled EGFP mRNA (Catalog #L-7701), EGFP mRNA (Catalog #L-7201), OVA mRNA (Catalog #L-7610), and Fluc mRNA (L-7602) were all purchased directly from TriLink BioTechnologies. Dulbecco's modified Eagle's medium (DMEM), fetal bovine serum (FBS), Trypsin-EDTA solution (0.05%), and OptiMEM were

purchased from Invitrogen (Carlsbad, CA). Lipofectamine MessengerMAX was purchased from Invitrogen (Carlsbad, CA) and used as a positive control in phosphate-buffered saline (PBS) buffer. All buffers were generated using DEPC-Treated Water (ThermoFisher Scientific, CA) unless provided from manufacturer. HeLa cells were generously provided from Professor James Nowick (Department of Chemistry, UC Irvine, CA). DC2.4 dendritic cells were generously provided by Professor Jennifer Prescher (Department of Chemistry, UC Irvine, CA).

General Active Ester Monomer Synthesis Procedure: D,L-α-Lipoic acid [5.00 grams; 24.2 mmol; 1 equiv.] was dissolved in 350 mLs of dry, 4 °C -prechilled acetonitrile (ACN) containing 1.05 equivalents of corresponding phenol [25.5 mmol] and 5 mol% 4-dimethylaminopyridine (DMAP) [1.21 mmol; 148 mgs] and stirred under inert gas until fully dissolved. 1.05 equivalents of N,N′-dicyclohexylcarbodiimide (DCC) [5.25 grams; 25.5 mmol] was dissolved in a 30 mLs of dry, 4 °C -prechilled ACN and added dropwise to the stirring solution of LA and phenol. The reaction mixture was gradually warmed to 25 °C and stirred for 8 hrs. After 8 hours the reaction mixture was filtered, stored at -20 °C for 12 hours, and filtered again. Afterwards the reaction mixture was reduced *in vacuo*, resuspended in dichloromethane (DCM), washed with 1M HCl (3X 250 mL washes), followed by Brine (3X 250 mL washes), then dried with $MgSO_4$ and filtered. The organic layer was reduced *in vacuo* and loaded on silica for flash chromatography; columns were run with Hexane:DCM gradient.

N-Acetyl C2 Synthesis Procedure: 1-(2-Aminoethyl)-4-methylpiperazine (1 equiv.; 2.10 mmol) was added to a dried round-bottom flask along with 10 mLs of dried DCM and

2.0 equiv. of dry N,N-diisopropylethylamine (DIPEA; 4.2 mmol). After stirring for five minutes 0.75 equiv. of acetic anhydride (1.58 mmol) was diluted in 5 mLs of dry DCM and added dropwise to the solution containing 1-(2-aminoethyl)-4-methylpiperazine. After stirring for 15 minutes at 25 °C the solution was reduced *in vacuo* and loaded on silica for flash chromatography using a DCM: basified methanol (90% DCM: 9% MeOH: 1% NH_4OH) gradient. N-Acetyl C2 product eluted in 90% basified methanol.

Ring-Opening Polymerization Procedure (for M1-M5) and Polymer Characterizations: Polymerization procedures were adapted from previous works.[1] Active ester-bearing lipoic acid monomer (1.07 mmol) was added to a clean 1-dram vial with a magnetic stir bar and 280 μL of anhydrous tetrahydrofuran (THF). After evacuating the dram vial and flushing with inert gas 3X, the solution was set to stir for at least 5 minutes. In a separate vial benzyl mercaptan (BnSH; 21.4 μmol) and 5mol% phosphazene P1-t-Bu-tris(tetramethylene) base (53.5 μmol) were mixed in 25 μL of anhydrous THF and added to the stirring monomer solution via syringe (3.5M monomer final concentration). The reaction was stirred for 60 minutes at 25 °C, while also vortexing the reaction mixture every 15 minutes. After 60 minutes an excess of iodoethane was added to the reaction mixture and stirred for another 20 minutes. After completion the reaction mixture was precipitated into 4 °C -prechilled 50:50 v/v ACN:methanol (MeOH) and centrifuged. Precipitated polymer was resuspended in 300 μL of anhydrous DCM and precipitated in 4 °C -prechilled 50:50 v/v ACN:MeOH two more times to yield white polymer precipitate. For GPC analysis, samples were prepared to a concentration of 10 mgs/mL and filtered before analysis. ^1H NMR analysis was conducted in $CDCl_3$.

Scaled M2 Polymerization Procedure: Active ester-bearing lipoic acid monomer (750 mgs, 2.08 mmol) was added to a clean 1-dram vial with a magnetic stir bar and 545 µL of anhydrous THF. After evacuating the dram vial and flushing with inert gas 3X, the solution was set to stir for at least 5 minutes. In a separate vial benzyl mercaptan (BnSH; 20.8 µmol) and 5 mol% phosphazene P1-t-Bu-tris(tetramethylene) base (104 µmol) were mixed in 50 µL of anhydrous THF and added to the stirring monomer solution via syringe (3.5M monomer final concentration). The reaction was stirred for 60 minutes at 25 °C, while also vortexing the reaction mixture every 15 minutes. After 60 minutes an excess of iodoethane was added to the reaction mixture and stirred for another 20 minutes. After completion the reaction mixture was precipitated into 4 °C -prechilled 50:50 v/v ACN:MeOH and centrifuged. Precipitated polymer was resuspended in 300 µL of anhydrous DCM and precipitated in 4 °C -prechilled 50:50 v/v ACN:MeOH two more times to yield white polymer precipitate. For GPC analysis, samples were prepared to a concentration of 10 mgs/mL and filtered before analysis. After analysis Poly(**M2**) was resuspended in THF and aliquoted into vials for subsequent reactions.

Small-Molecule Model Studies for Aminolysis Procedure and ^{1}H NMR Studies: In a 1-dram vial active ester monomer is added (250 µmol) along with 1.1 equivalents of anhydrous DIPEA (275 µmol), 500 µL of DMSO-*d*6 (500 mM monomer), and a magnetic stir bar. This mixture is vortexed until thoroughly dissolved and after 5 minutes of stirring 1 equivalent of desired amine (250 µmol) is added and the mixture and vortex again. The aminolysis reaction mixture was stirred at 30 °C and analyzed via ^{1}H NMR at various timepoints.

Post-Polymerization Functionalization Procedure and ^{1}H NMR Measurement of Multifunctional Polydisulfide Polymers: In a 0.5-dram vial containing 10 mgs of Poly(M2) (27.8 μmol, 1 equiv.) 1.5 equivalents of anhydrous DIPEA (41.7 μmol) was added along with 35 μL of 50:50 (v/v) dioxane: dimethylformamide (DMF) solution and vortexed until fully dissolved. In a separate microfuge tube 0.25 equivalents of cationic feedstock (6.95 μmol), 0.5 equivalents of pH-responsive feedstock (20.9 μmol), and 0.25 equivalents of hydrophobic feedstock (6.95 μmol) were premixed with 35 μL of 50:50 (v/v) dioxane: DMF solution and vortexed until homogenized. Afterwards the feedstock solution was added to the polymer solution and dram vial containing the reaction mixture was vortexed thoroughly and incubated at a designated temperature for 60 minutes (with additional periodic vortexing). After 60 minutes 1 mL of -20 °C-prechilled methyl tert-butyl ether (MTBE) was added to the reaction mixture and vortexed to yield a white polymer precipitate. This precipitate was washed with -20 °C MTBE twice before resuspension in 75 μL -20 °C acetic acid and a final precipitation in another 1 mL of -20 °C MTBE, followed by another two washes with -20 °C MTBE. The resulting white polymer solid was reduced *in vacuo***,** dissolved in DMSO-*d*6 to a concentration of 5 mg/mL, and analyzed via ^{1}H NMR.

Nanoparticle Formulation Procedure, DLS Measurements of mRNA-Polymer Nanoparticles, and Gel Electrophoresis Assays: EGFP and OVA mRNA were diluted to a concentration of 50 ng/ μL in 10 mM sodium acetate (NaOAc) buffer (pH 4) prior to use. For cell culture experiments, 150ng of mRNA was administered per well and for dynamic light scattering (DLS) measurements 2 μg of EGFP mRNA was used for nanoparticle characterization. For cryo-TEM experiments 150ng of mRNA was used for the analysis of each sample (protocol continued in next section). After the desired amount of mRNA was

pipetted into a clear microfuge tube, the mRNA solution as heated to 50 °C prior to use. In parallel the 5 mg/ mL solution of multifunctional polymer in DMSO was also heated to 50 °C and thoroughly mixed via vortexing. For all experiments in this work a nitrogen-to-phosphate (N/P) ratio of 5:1 was used for polymer-RNA complexation (N quantity was determined from the average number of cationic residues per repeat unit of polymer). The desired amount of heated polymer solution was mixed with the corresponding mRNA solution under continuous pipetting and vortexing for 30 seconds.

For DLS experiments, the resulting EGFP mRNA-polymer nanoparticles were resuspended in 600 μL of 10 mM NaOAc buffer (pH 4), placed in a clean cuvette, briefly mixed, and incubated at 25 °C for 10 minutes before measurement. DLS measurements were taken measured at 633 nm using Zetasizer Nano ZS dynamic light scattering instrument (Malvern Instruments, Malvern, UK) at 25 ˚C with detection angle of 173 ˚. A minimum of three measurements were taken for each sample and the mean Z-average values were reported. OVA mRNA-containing polymeric nanoparticles were measured using the same protocol.

For gel electrophoresis assays, EGFP mRNA-polymer nanoparticles were formulated as described above and brought to desired pH using PBS (pH 7.4) or sodium acetate buffer (pH 4.0). Additional DMSO (50% final volume) and glutathione (10 mM final concentration) were added to the buffered nanoparticle solutions and resulting decomplexation solutions were incubated at 37 ˚C for 12 hours before analysis. 1kb DNA ladder was purchased from NEB (Catalog # N3232S) and used as the molecular weight ladder subsequent relevant gel electrophoresis assays.

Cryo-TEM Nanoparticle Preparation: Cryo-TEM samples were prepared from resuspended or extracted solutions onto Quantifoil R2/2 (Electron Microscopy Sciences) grids that were layered with graphene oxide following an established procedure.[2] Vitrification was carried out by an automatic plunge freezer ME GP2 (Leica Microsystems) with 3 μL of sample. Grid preparation was performed at 95% humidity. After loading the sample, grids were let to sit for 15 minutes before being blotted for 3 seconds prior to plunging into liquid propane. Cryo-TEM samples were then placed on a Gatan cryo-TEM holder and imaged on a JEOL 2100F TEM using a Schottky type field emission gun operating at 200 keV. Images were recorded using SerialEM low dose imaging mode with a Gatan OneView CMOS camera at 4k × 4k resolution.

General Procedure for *In Vitro* Delivery of EGFP mRNA-Polymer Nanoparticles and Chloroquine-Treatment Protocols: HeLa and DC2.4 transfections were performed in triplicate within cell culture-treated clear-bottom 96-well plates (Corning). After passaging, cells were seeded at a density of 10,000 cells/ 96 well and incubated for 24 hours prior to treatment. The Cy5-labeled EGFP mRNA-polymer nanoparticles were formulated as mentioned previously (with 150ng of mRNA was administered per well), resuspended in 30 μL of PBS, and gently mixed via pipette in PBS for 30 seconds before administering to cells. After an additional 50 μL of OptiMEM was added to each treated well, cells were incubated for 6 hours before media was exchanged with DMEM containing 10% FBS. After 6 hours or 48 hours of incubation media was removed, cells were trypsinized, and transferred to non-binding V-bottom 96 well microplate plates (Greiner) for flow cytometry analysis. To determine cytotoxicity propidium iodide (PI) was added to sample wells at a final concentration of 2.5 μg/ mL and incubated for at least five minutes prior to

flow cytometry analysis. Nanoparticle uptake (Cy5 fluorescence), EGFP expression, and cytotoxicity (PI fluorescence) were determined using a NovoCyte flow cytometer. For lipid control samples, Cy5-EGFP mRNA (150 ng of mRNA per well; 50 ng/ μL in pH 7.4 PBS) was complexed with Lipofectamine MessengerMAX in PBS under continuous mixing before administering to cells.

For chloroquine-related experiments, EGFP mRNA was formulated with polymers using the methodology above, with the addition of chloroquine diphosphate (CAS# 50-63-5; Sigma-Aldrich) to a final concentration of 25 μM in each well during the initial 6-hour nanoparticle treatment period and the next subsequent 18 hours.

General Procedure for Confocal Fluorescence Microscopy Study: DC2.4 cells were seeded at a density of 30,000 cells/ well within a poly-lysine-treated 8-well chamber slide (Lab-Tek, Rochester, NY) and incubated for 24 hours prior to transfection. Cy5-labeled EGFP mRNA nanoparticles were formulated using the aforementioned protocol and incubated for 12 hours. Afterwards cells were stained with LysoTracker® Blue (150 nM final concentration; for lysosome staining) and incubated at 37 °C for 15 minutes. After two washes with FluoroBrite™ DMEM (ThermoFisher, USA) cells were replaced with fresh FluoroBrite™ DMEM and analyzed via confocal fluorescence microscopy. Confocal images were acquired using a Zeiss LSM 780 inverted laser scanning confocal microscope; a 40X oil objective was used for endosomal escape imaging experiments.

General Procedure for *In Vitro* Delivery of OVA mRNA-Polymer Nanoparticles: DC2.4 transfections were performed in triplicate within cell culture-treated clear-bottom 96-well plates (Corning). After passaging, cells were seeded at a density of 15,000 cells/

well and incubated for 24 hours prior to treatment. The OVA mRNA-polymer nanoparticles were formulated as mentioned previously (with 150ng of mRNA was administered per well), resuspended in 30 µL of PBS, and gently mixed via pipette in PBS for 30 seconds before administering to cells. After an additional 50 µL of OptiMEM was added to each treated well cells were incubated for 5 hours before media was exchanged with DMEM containing 10% FBS. After 24 hours of incubation the media was removed and cells were incubated in 20 µL 0.05% ethylenediaminetetraacetic acid (EDTA) solution at 37 °C for 20 minutes to dislodge cells. Dislodged cells were resuspended in another 80 µL of PBS (pH 7.4), transferred to a non-binding V-bottom 96 well microplate plate, and PE-tagged anti-mouse H-2Kb bound to SIINFEKL antibody was added to each well (BioLegend; Catalog # 141603; 2.5 µg/ µL final concentration). After gentle shaking for 5 minutes samples were analyzed using a NovoCyte flow cytometer. For lipid control samples, OVA mRNA (150 ng of mRNA per well; 50 ng/ µL in pH 7.4 PBS) was complexed with Lipofectamine MessengerMAX in PBS under continuous mixing before administering to cells.

LA(PEG 2K) Synthesis and Copolymerization Procedure: To synthesize LA(PEG 2K) monomer, D,L-α-Lipoic acid [2.00 grams; 9.68 mmol; 1 equiv.] was dissolved in 200 mLs of dry, 4 °C -prechilled ACN containing 1.05 equivalents of corresponding PEG 2K [20.34 grams; 10.16 mmol] and 5 mol% DMAP [0.48 mmol; 59 mgs] and stirred under inert gas until fully dissolved. 1.05 equivalents of DCC [2.10 grams; 10.16 mmol] was dissolved in a 15 mLs of dry, 4 °C -prechilled ACN and added dropwise to the stirring solution of LA and PEG 2K. The reaction mixture was gradually warmed to 25 °C and stirred for 8 hrs. After 8 hours the reaction mixture was filtered, stored at -20 °C for 12 hours, and filtered again. Afterwards the reaction mixture was reduced in vacuo, resuspended in DCM, washed

with 1M HCl (3X 250 mL washes), followed by Brine (3X 250mL washes), then dried with MgSO4 and filtered. The organic layer was reduced in vacuo and loaded on silica for flash chromatography; column was run with DCM:MeOH gradient.

For copolymerization of LA(PEG 2K) and **M2**, LA(PEG 2K) (0.1 equiv., 0.139 mmol, 306 mgs) monomer was placed into a clean 1-dram vial with a magnetic stir bar and dissolved in 85 μL of anhydrous ACN. Afterwards **M2** (0.93 mmol) was added along with 195 of anhydrous THF and vortexed until all components were dissolved. After evacuating the dram vial and flushing with inert gas 3X, the solution was set to stir for at least 5 minutes. In a separate vial benzyl mercaptan (BnSH; 21.4 μmol) and 5 mol% Phosphazene P1-t-Bu-tris(tetramethylene) base (53.5 μmol) were mixed in 25 μL of anhydrous THF and added to the stirring monomer solution via syringe. The reaction was set to stir for 60 minutes at 25 °C, while also vortexing the reaction mixture every 15 minutes. After 60 minutes an excess of iodoethane was added to the reaction mixture and stirred for another 20 minutes. After completion the reaction mixture was precipitated into 4 °C -prechilled 40:40:20 v/v/ ACN:MeOH:Et_2O and centrifuged. Precipitated polymer was resuspended in 300 μL of anhydrous DCM and precipitated in 4 °C -prechilled 40:40:20 v/v/ ACN:MeOH:Et_2O two more times to yield white polymer precipitate (132 mgs isolated). For GPC analysis, samples were prepared to a concentration of 10 mgs/mL and filtered before analysis. ^1H NMR analysis was conducted in $CDCl_3$; NMR analysis determined the ratio of **M2**:LA(PEG 2K) incorporation to be 93:7.

Post-polymerization functionalization of poly(M2+PEG 2K)disulfide was accomplished using the same aminolysis procedures stated above.

DLS Nanoparticle Aggregation Procedure and Results: To test nanoparticle aggregation for multifunctional polymers with and without PEG, nanoparticles were formulated using the established protocol for other nanoparticle formulations analyzed by DLS. After formulation in NaOAc (pH 4) nanoparticles were resuspended in 50 μL of DI water, followed by 450 μL of PBS (pH 7.4). After mixing via pipette the nanoparticle solution was transferred to clean cuvettes and analyzed via DLS at various timepoints using aforementioned DLS parameters.

2.6 References for Experimental Protocol

(1) Liu, Y.; Jia, Y.; Wu, Q.; Moore, J. S., Architecture-Controlled Ring-Opening Polymerization for Dynamic Covalent Poly(disulfide)s. *Journal of the American Chemical Society* **2019,** *141* (43), 17075-17080.

(2) Patterson, J. P.; Sanchez, A. M.; Petzetakis, N.; Smart, T. P.; Epps, T. H., 3rd; Portman, I.; Wilson, N. R.; O'Reilly, R. K., A simple approach to characterizing block copolymer assemblies: graphene oxide supports for high contrast multi-technique imaging. *Soft Matter* **2012,** *8* (12), 3322-3328.

2.7 Supplementary Figures

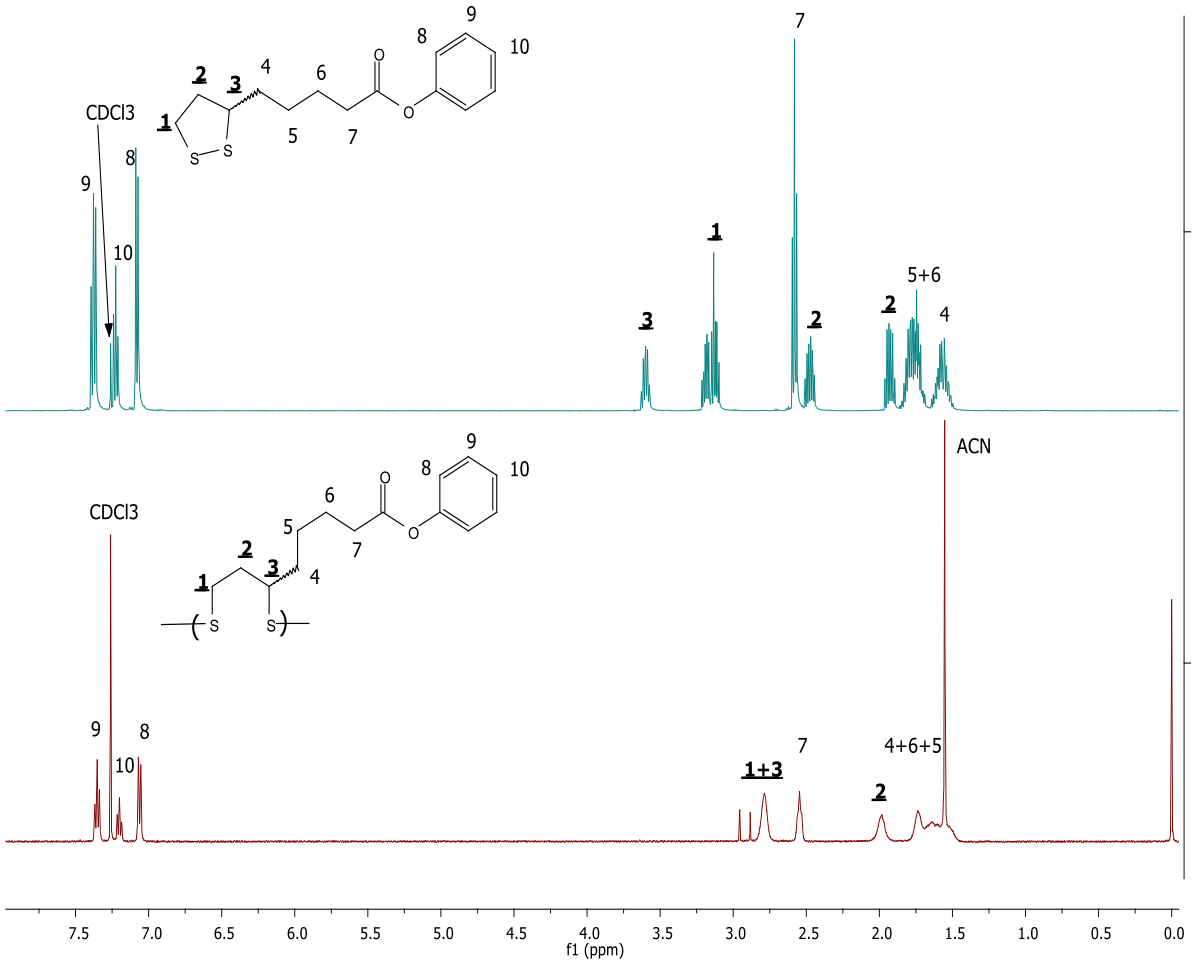

Figure S2.1 ^{1}H NMR overlay of **M1** and poly(**M1**). Diagnostic polymerization peaks are bolded and underlined.

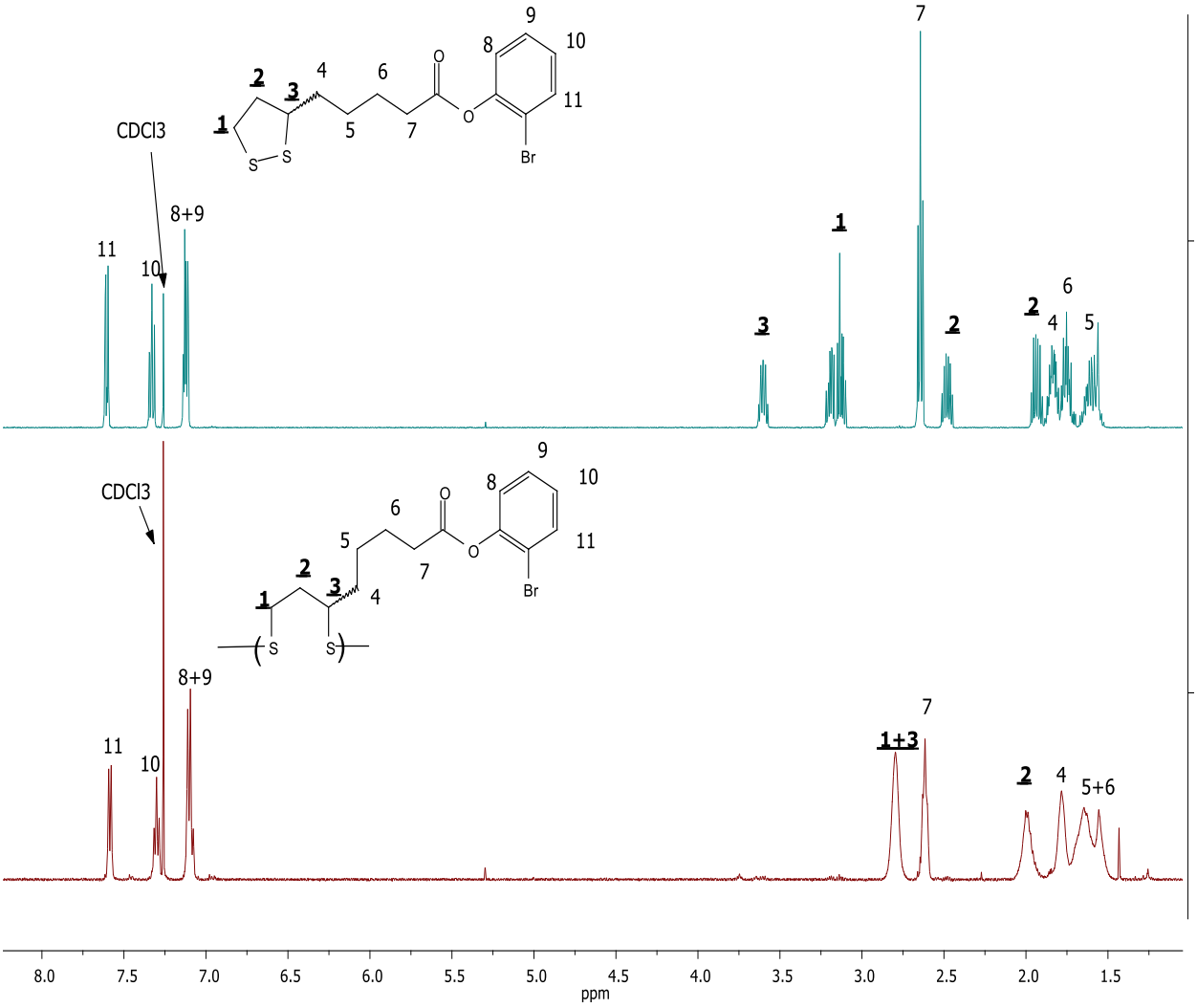

Figure S2.2 ^{1}H NMR overlay of **M2** and poly(**M2**). Diagnostic polymerization peaks are bolded and underlined.

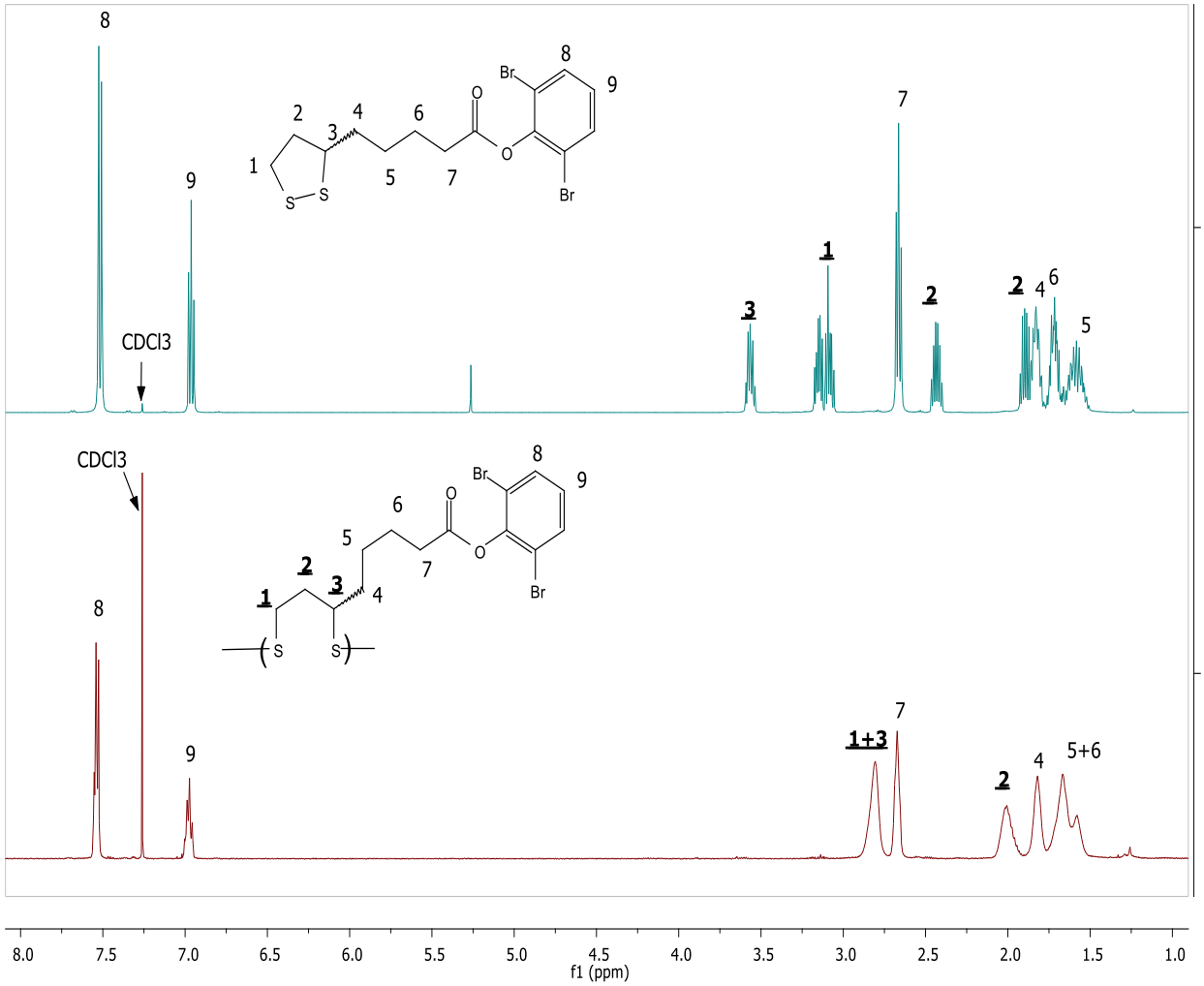

Figure S2.3 ^{1}H NMR overlay of **M3** and poly(**M3**). Diagnostic polymerization peaks are bolded and underlined.

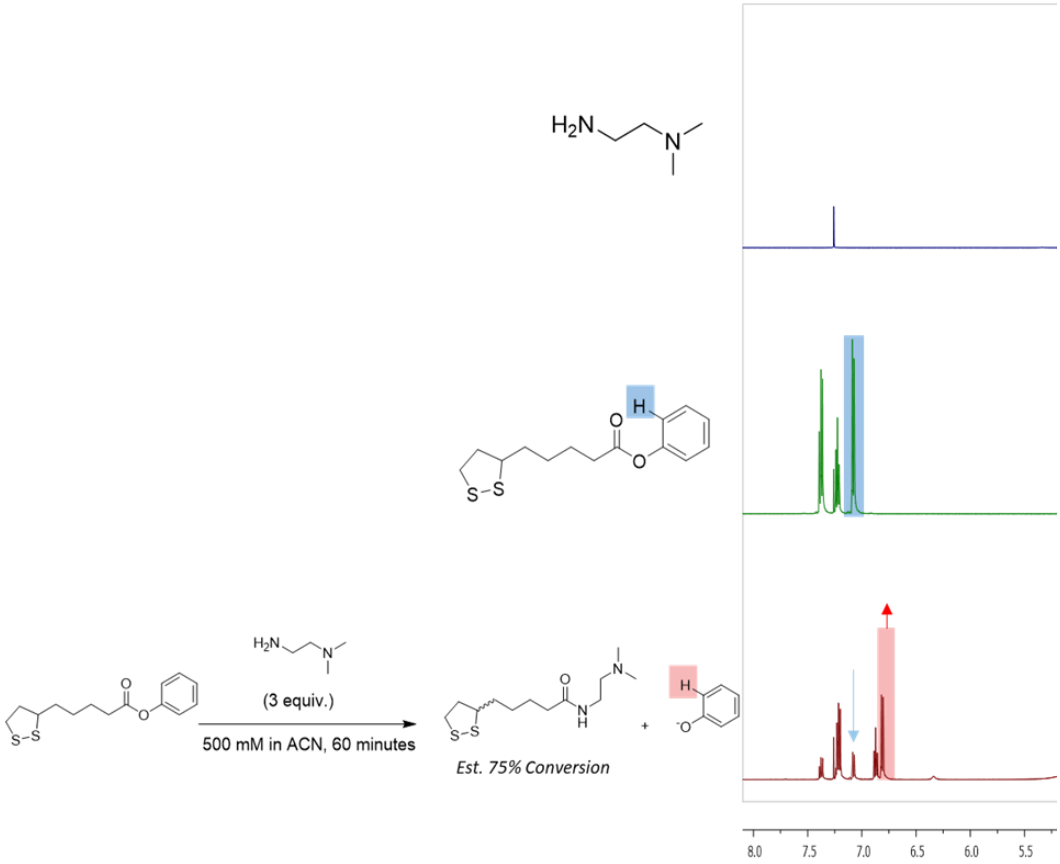

Figure S2.4 ^{1}H NMR overlay (only aromatic signals shown) of attempted aminolysis reaction using **M1** and 2-(dimethylamino)ethylamine. Blue boxes/ arrows highlight diagnostic peaks from monomer starting material and red boxes/ arrows highlight diagnostic peaks for aminolysis product. Aminolysis was conducted in 500 mM ACN before reducing the reaction mixture *in vacuo* and ^{1}H NMR analysis in $CDCl_3$. Product conversion (est. 75%) was determined via relative peak integrations. **M1** demonstrates lower reactivity compared to **M2**, even with larger equivalents of amine feedstocks.

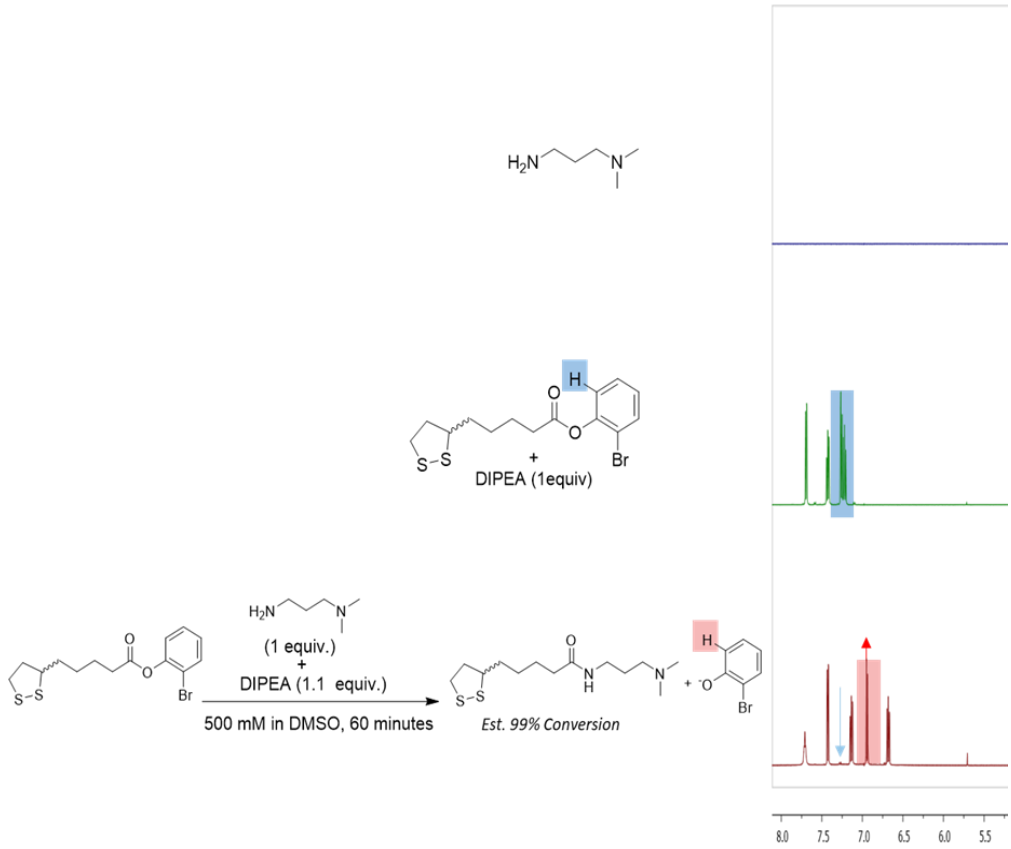

Figure S2.5 ^{1}H NMR overlay (only aromatic signals shown) of aminolysis reaction using **M2** and 3-dimethylaminopropylamine at 500 mM monomer concentration after 60 minutes in DMSO-*d*6. Blue boxes/ arrows highlight diagnostic peaks from monomer starting material and red boxes/ arrows highlight diagnostic peaks for aminolysis product. Product conversion was determined via relative peak integrations.

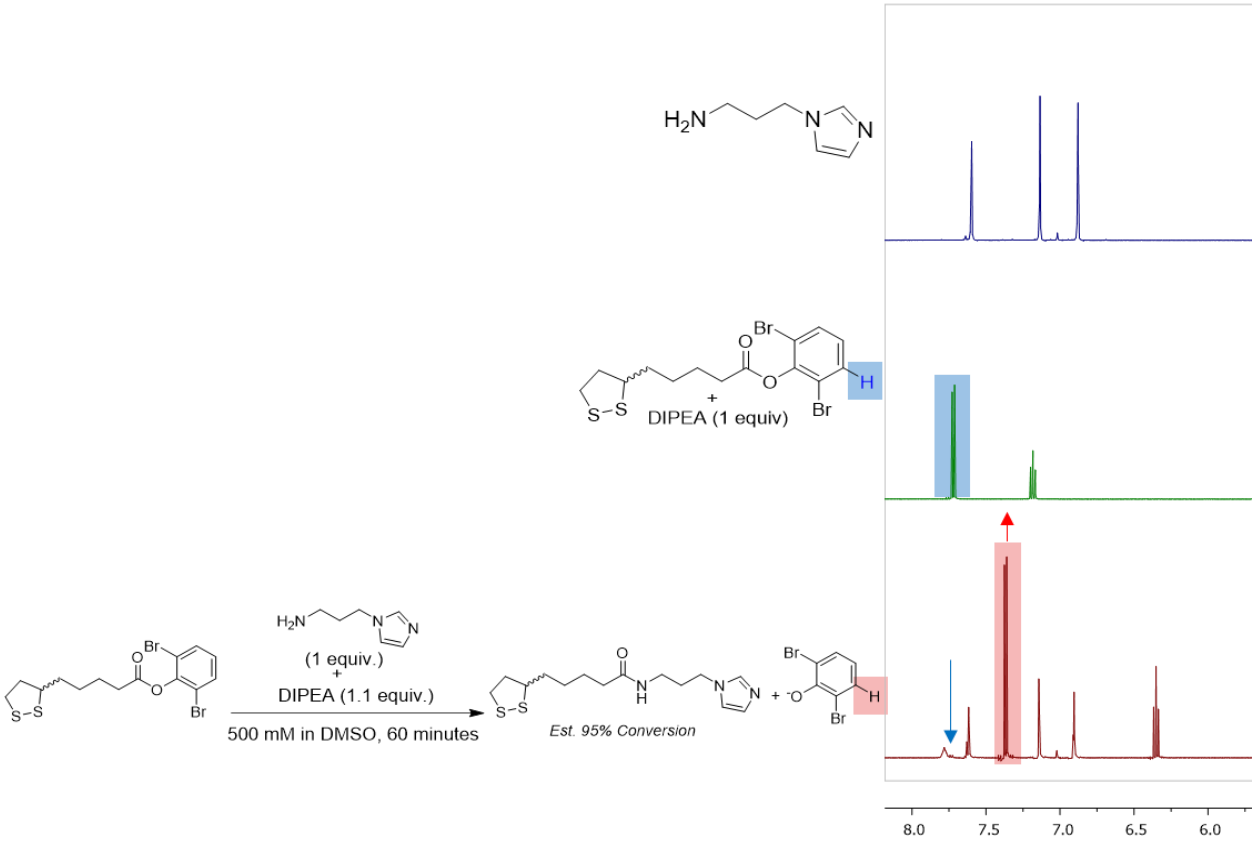

Figure S2.6 ^{1}H NMR overlay (only aromatic signals shown) of aminolysis reaction using **M3** and 1-(3-aminopropyl)imidazole at 500 mM monomer concentration after 60 minutes in DMSO-*d*6. Blue boxes/ arrows highlight diagnostic peaks from monomer starting material and red boxes/ arrows highlight diagnostic peaks for aminolysis product. Product conversion was determined via relative peak integrations.

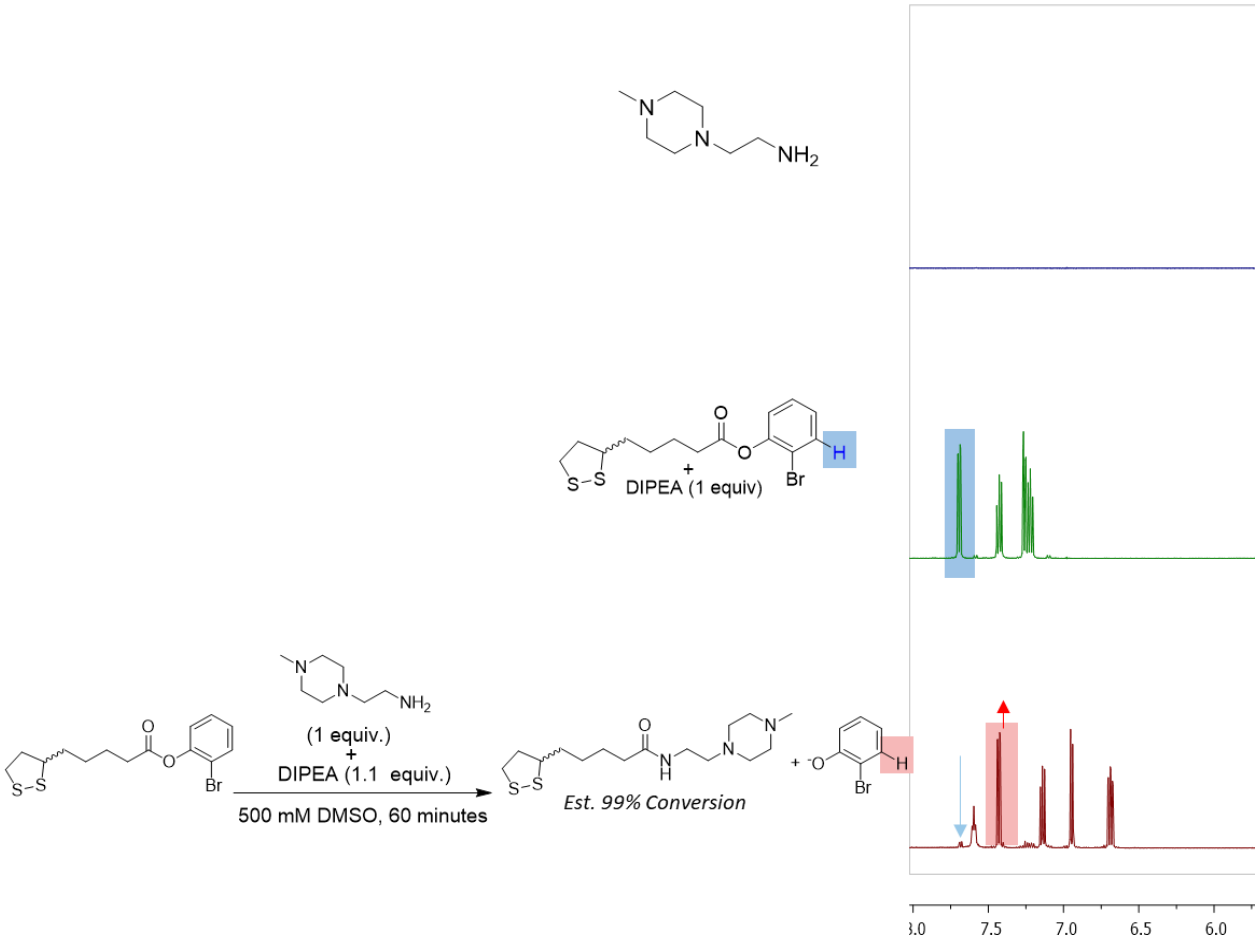

Figure S2.7 ^{1}H NMR overlay (only aromatic signals shown) of aminolysis reaction using **M2** and 1-(2-aminoethyl)-4-methylpiperazine at 500 mM monomer concentration after 60 minutes in DMSO-*d*6. Blue boxes/ arrows highlight diagnostic peaks from monomer starting material and red boxes/ arrows highlight diagnostic peaks for aminolysis product. Product conversion was determined via relative peak integrations.

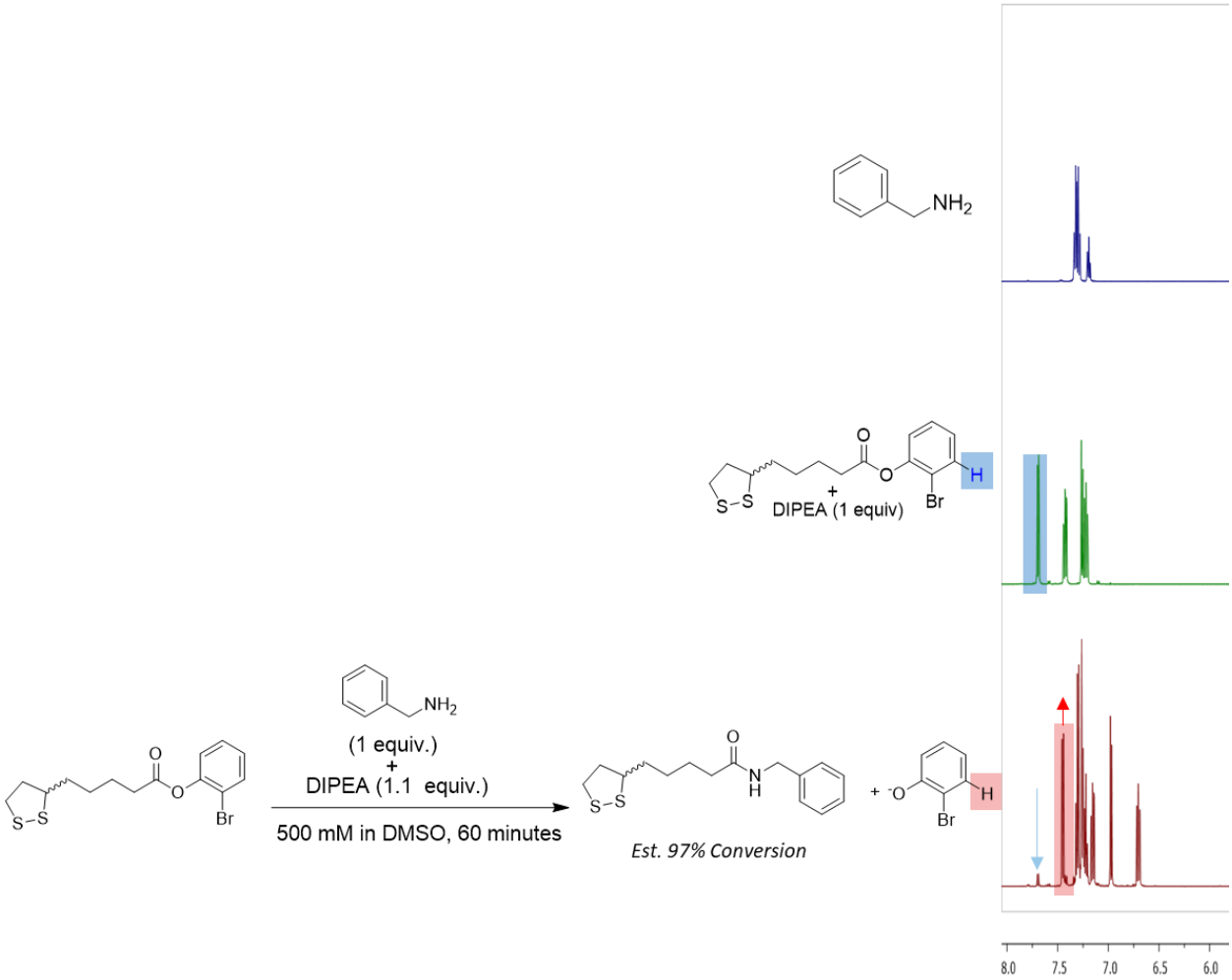

Figure S2.8 ^{1}H NMR overlay (only aromatic signals shown) of aminolysis reaction using **M2** and benzylamine at 500 mM monomer concentration after 60 minutes in DMSO-*d*6. Blue boxes/ arrows highlight diagnostic peaks from monomer starting material and red boxes/ arrows highlight diagnostic peaks for aminolysis product. Product conversion was determined via relative peak integrations.

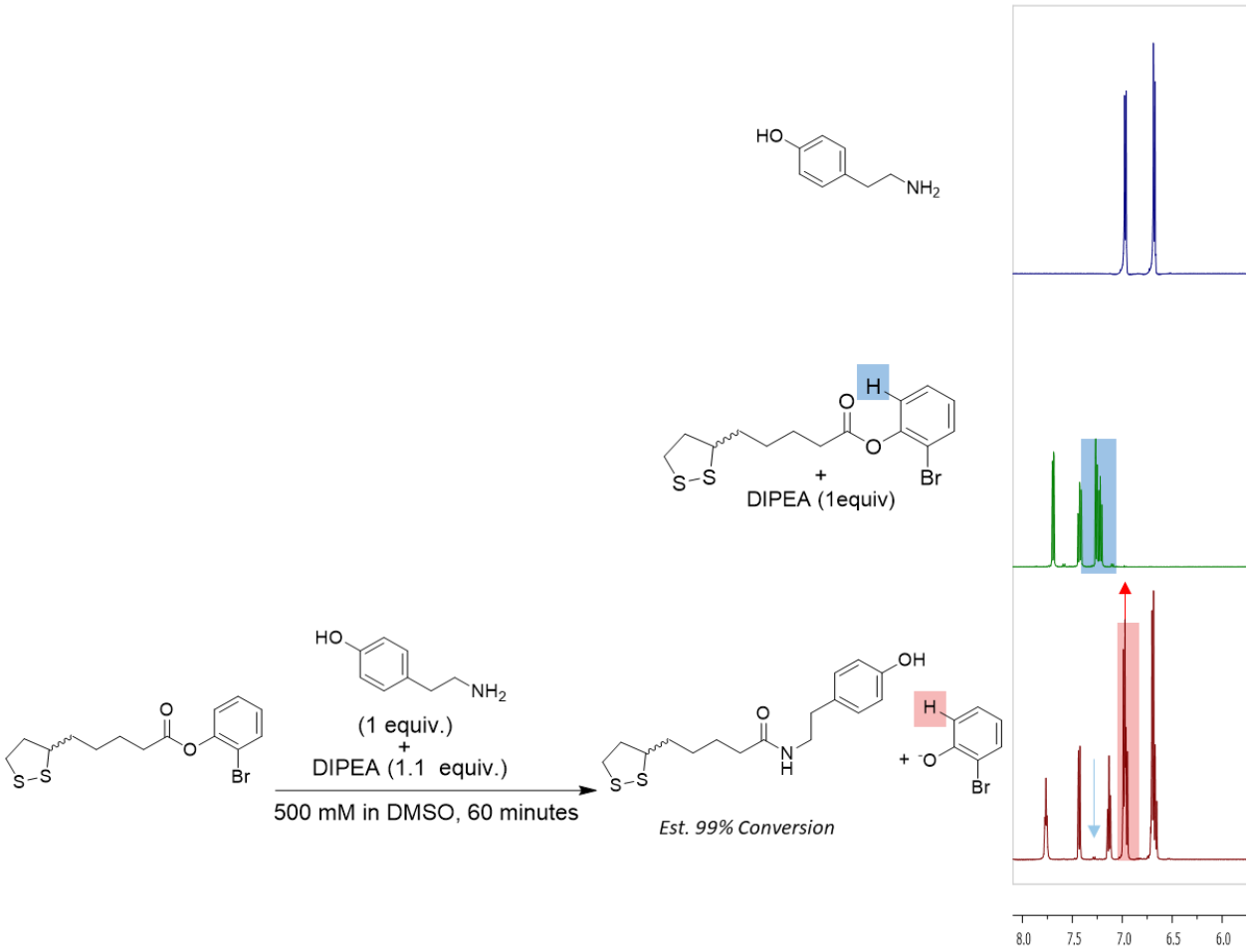

Figure S2.9 ^{1}H NMR overlay (only aromatic signals shown) of aminolysis reaction using **M2** and tyramine at 500 mM monomer concentration after 60 minutes in DMSO-*d*6. Blue boxes/ arrows highlight diagnostic peaks from monomer starting material and red boxes/ arrows highlight diagnostic peaks for aminolysis product. Product conversion was determined via relative peak integrations.

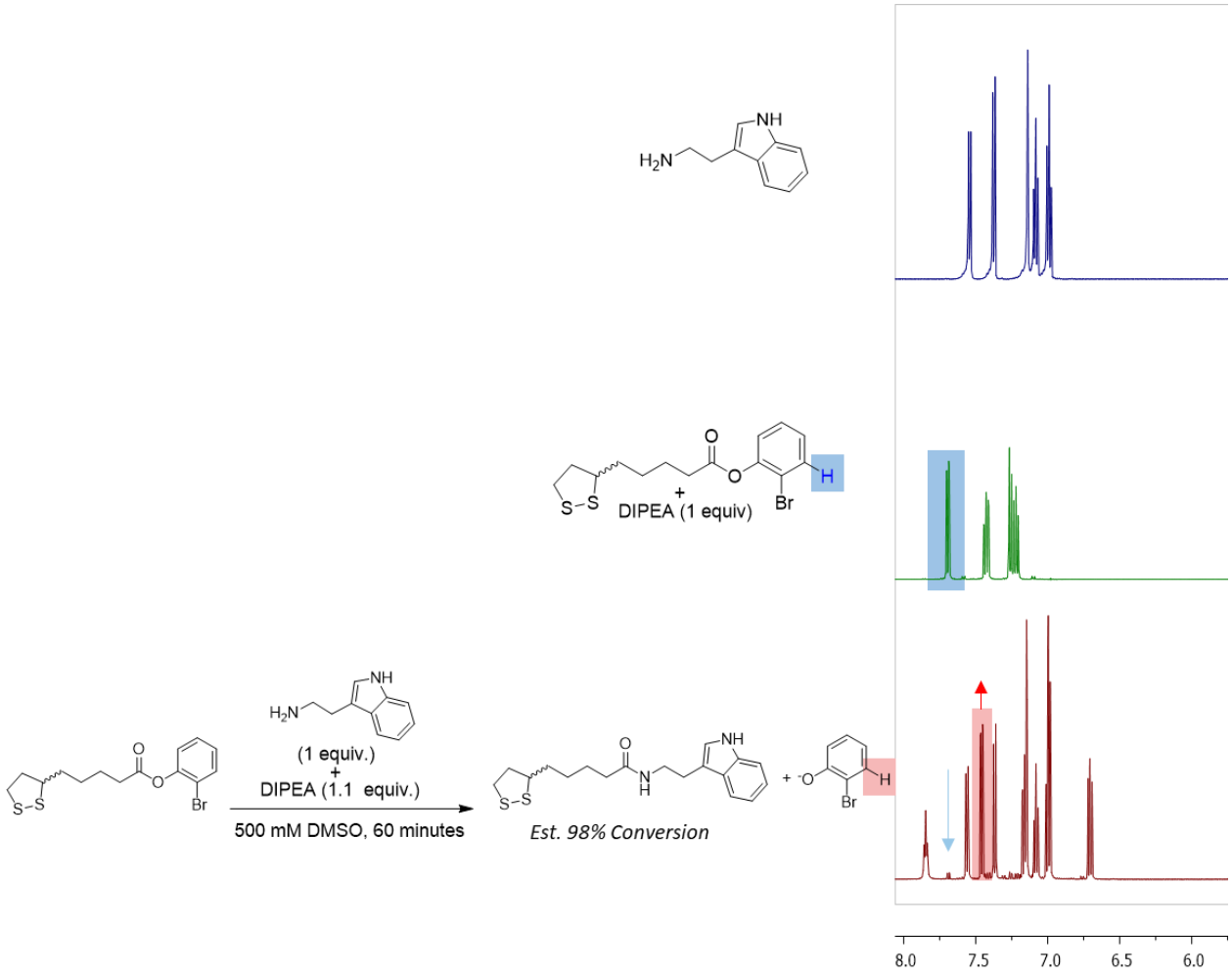

Figure S2.10 ^{1}H NMR overlay (only aromatic signals shown) of aminolysis reaction using **M2** and tryptamine at 500 mM monomer concentration after 60 minutes in DMSO-*d6*. Blue boxes/ arrows highlight diagnostic peaks from monomer starting material and red boxes/ arrows highlight diagnostic peaks for aminolysis product. Product conversion was determined via relative peak integrations.

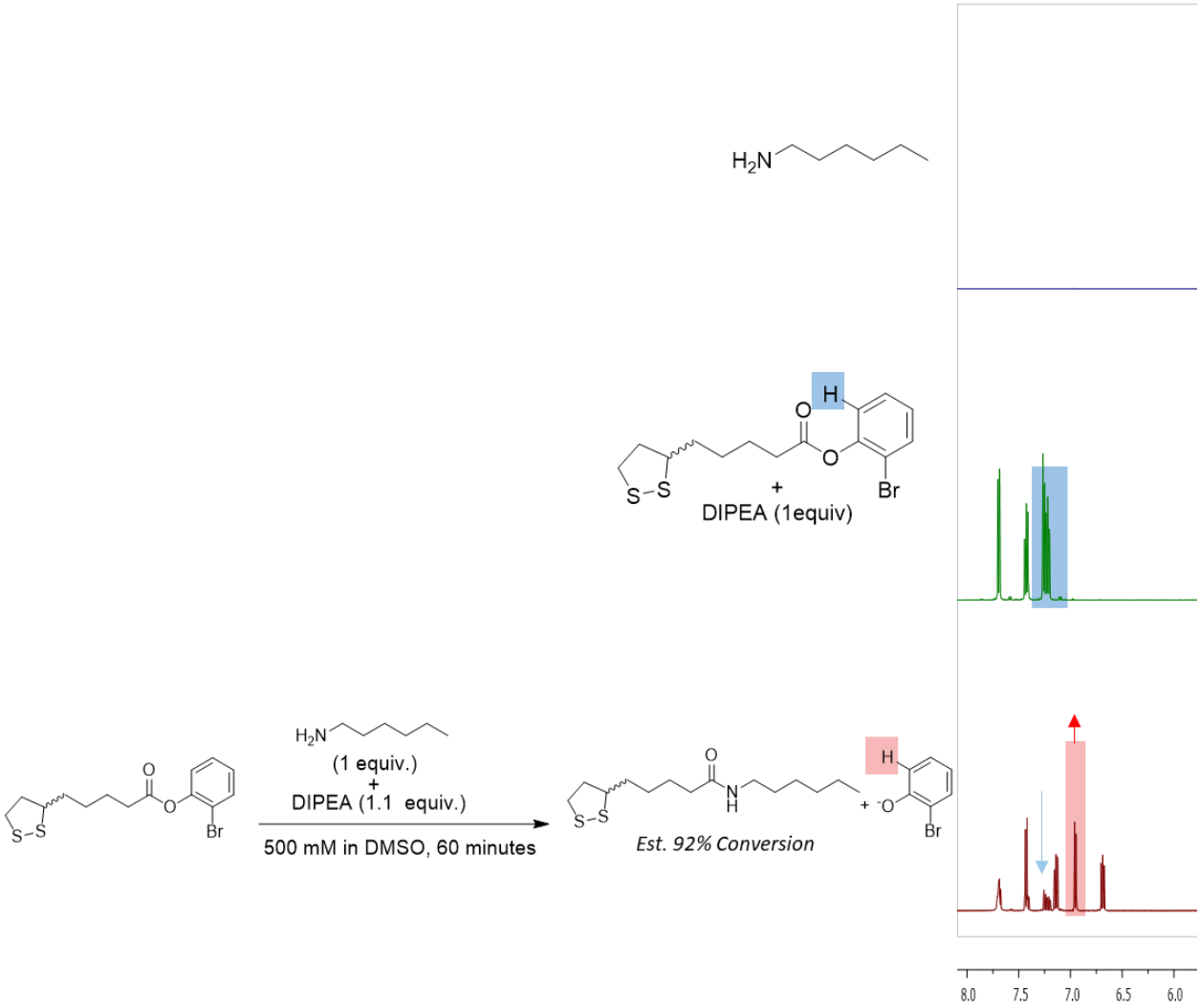

Figure S2.11 ^{1}H NMR overlay (only aromatic signals shown) of aminolysis reaction using **M2** and hexylamine at 500 mM monomer concentration after 60 minutes in DMSO-*d*6. Blue boxes/ arrows highlight diagnostic peaks from monomer starting material and red boxes/ arrows highlight diagnostic peaks for aminolysis product. Product conversion was determined via relative peak integrations.

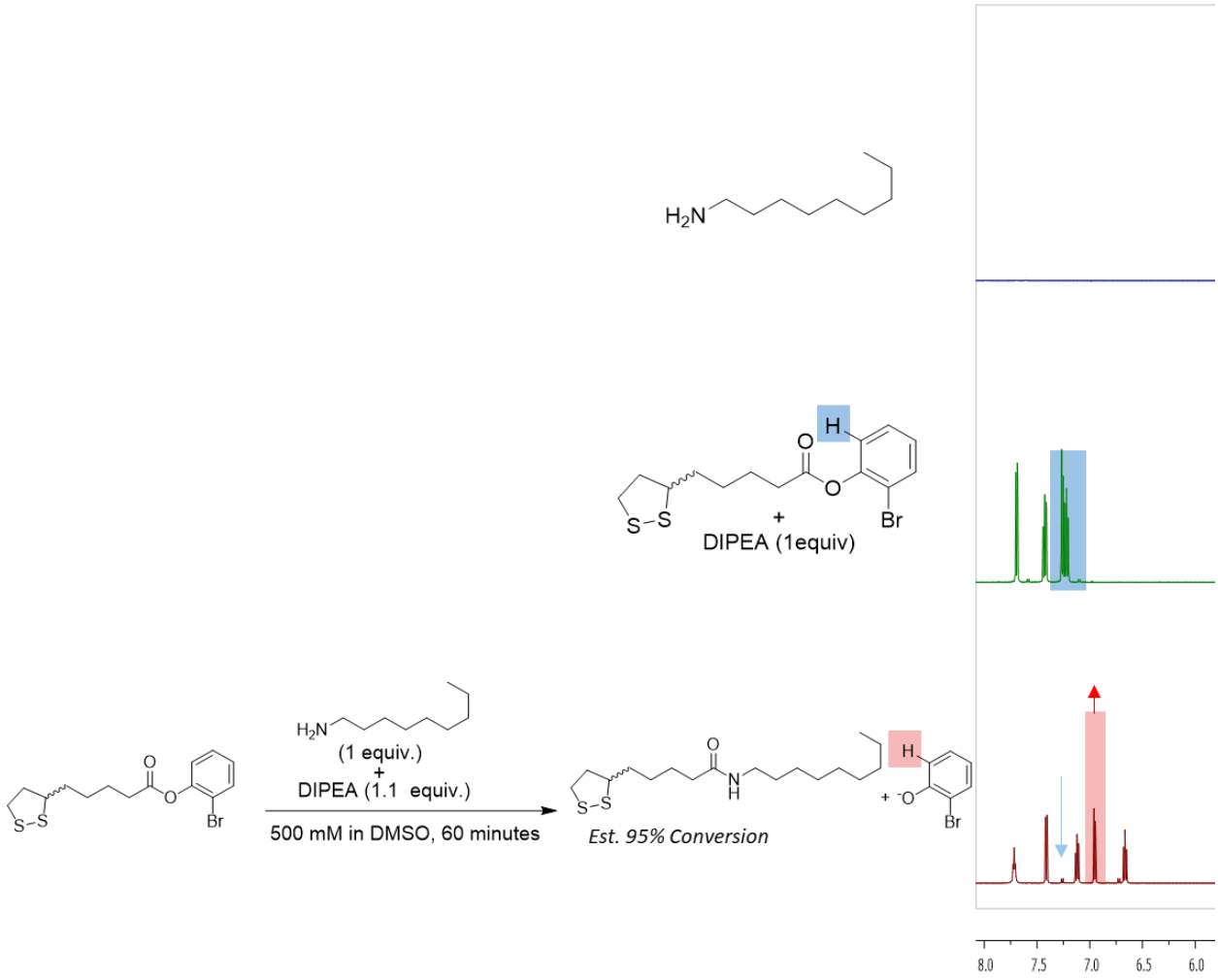

Figure S2.12 ^{1}H NMR overlay (only aromatic signals shown) of aminolysis reaction using **M2** and nonylamine at 500 mM monomer concentration after 60 minutes in DMSO-*d*6. Blue boxes/ arrows highlight diagnostic peaks from monomer starting material and red boxes/ arrows highlight diagnostic peaks for aminolysis product. Product conversion was determined via relative peak integrations.

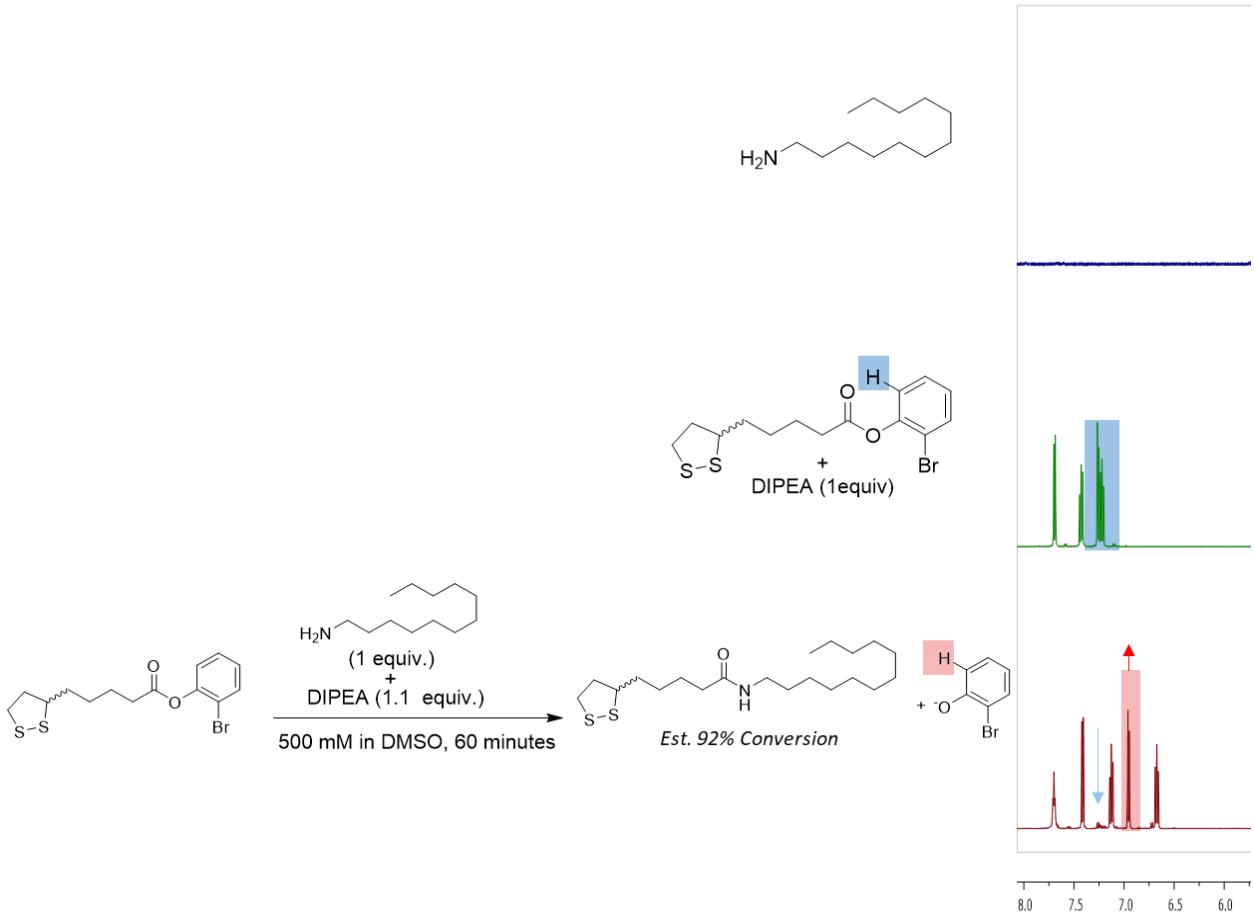

Figure S2.13 ^{1}H NMR overlay (only aromatic signals shown) of aminolysis reaction using **M2** and dodecylamine at 500 mM monomer concentration after 60 minutes in DMSO-*d*6. Blue boxes/ arrows highlight diagnostic peaks from monomer starting material and red boxes/ arrows highlight diagnostic peaks for aminolysis product. Product conversion was determined via relative peak integrations.

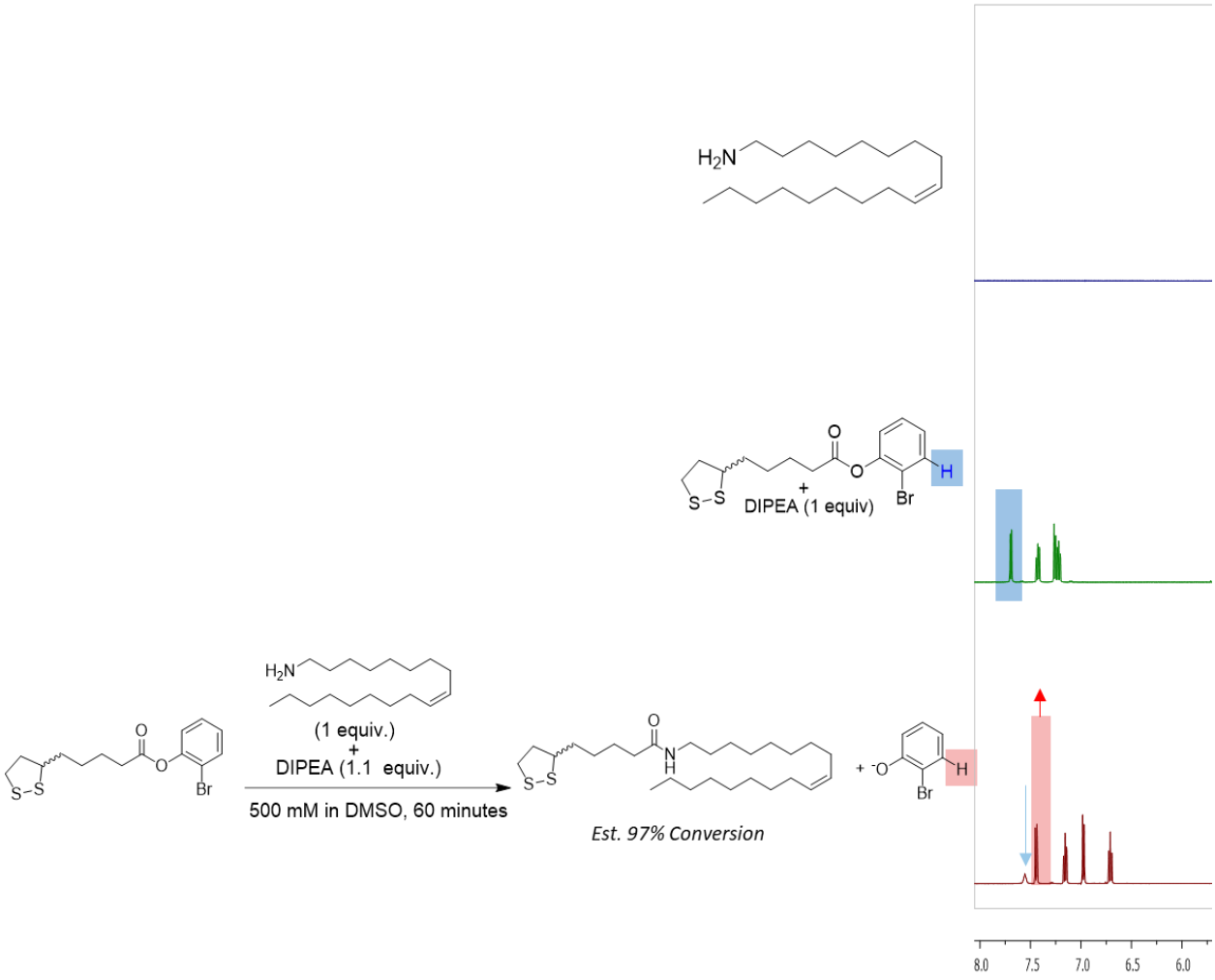

Figure S2.14 ^{1}H NMR overlay (only aromatic signals shown) of aminolysis reaction using **M2** and oleylamine at 500 mM monomer concentration after 60 minutes in DMSO-*d*6. Blue boxes/ arrows highlight diagnostic peaks from monomer starting material and red boxes/ arrows highlight diagnostic peaks for aminolysis product. Product conversion was determined via relative peak integrations.

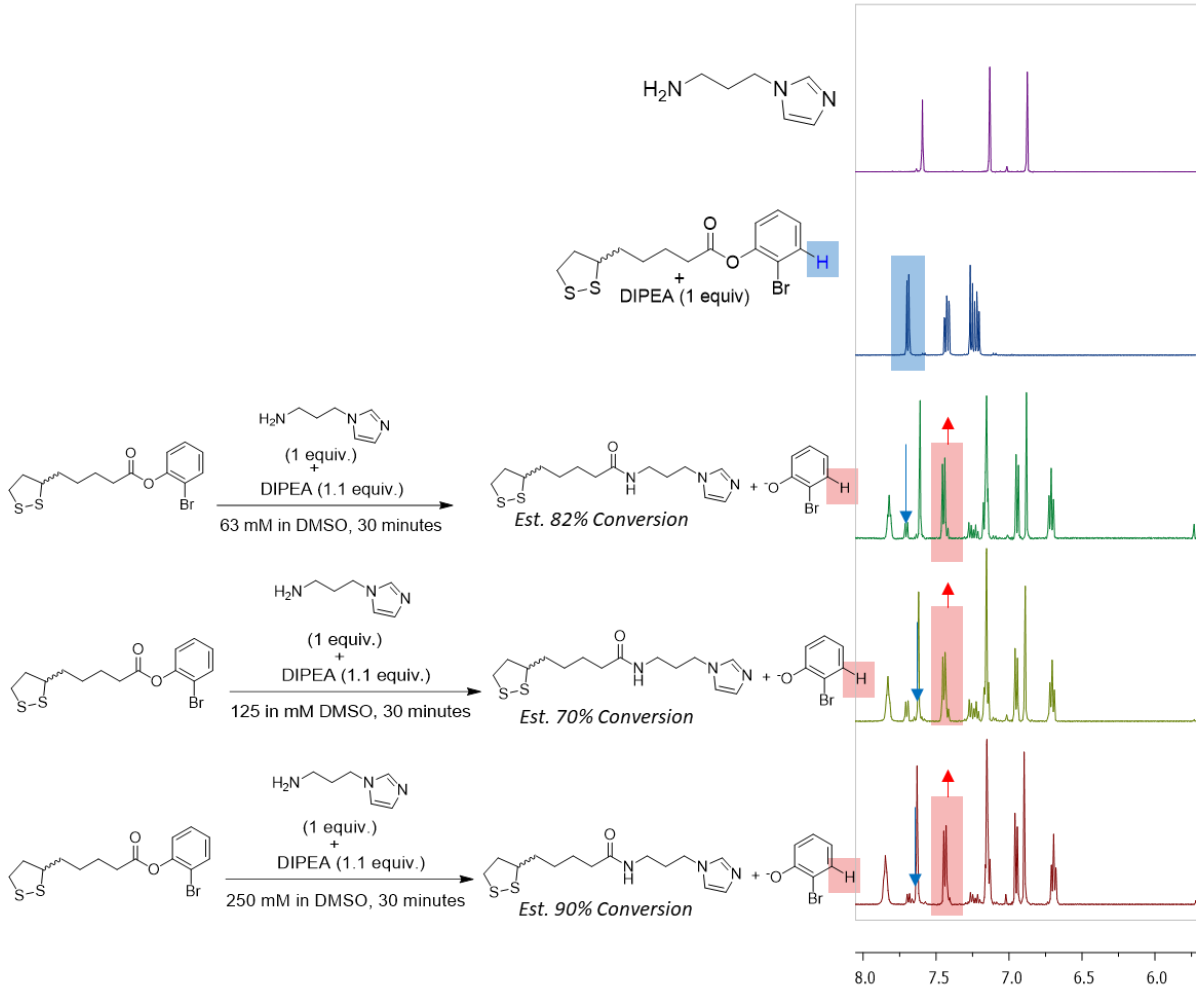

Figure S2.15 ^{1}H NMR overlay (only aromatic signals shown) of aminolysis reaction using **M2** and 1-(3-aminopropyl)imidazole at different monomer concentrations (63 mM, 125 mM, and 250 mM) after 30 minutes in DMSO-*d*6. Blue boxes/ arrows highlight diagnostic peaks from monomer starting material and red boxes/ arrows highlight diagnostic peaks for aminolysis product. Product conversion was determined via relative peak integrations.

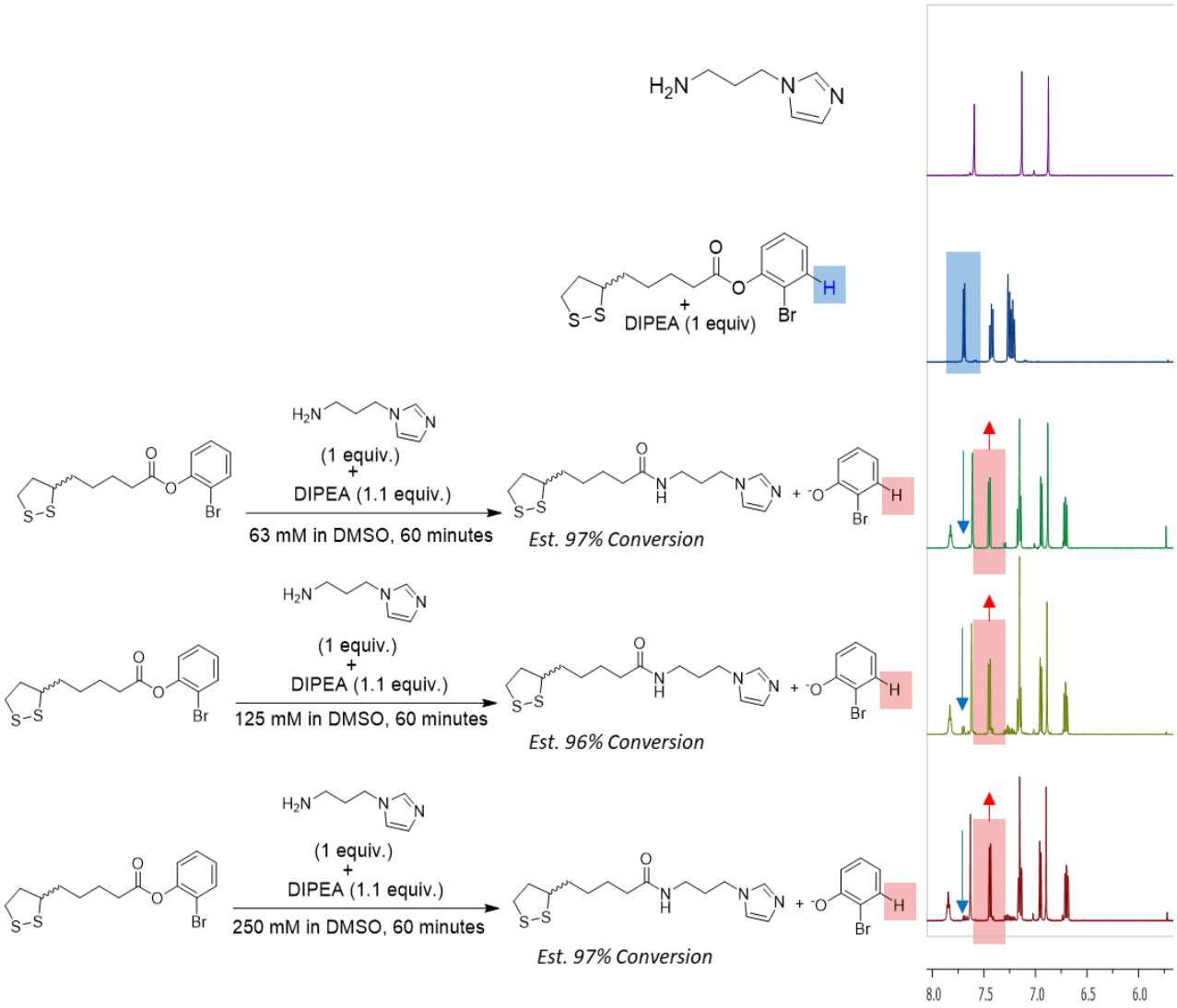

Figure S2.16 ^{1}H NMR overlay (only aromatic signals shown) of aminolysis reaction using **M2** and 1-(3-aminopropyl)imidazole at different monomer concentrations (63 mM, 125 mM, and 250 mM) after 60 minutes in DMSO-*d*6. Blue boxes/ arrows highlight diagnostic peaks from monomer starting material and red boxes/ arrows highlight diagnostic peaks for aminolysis product. Product conversion was determined via relative peak integrations.

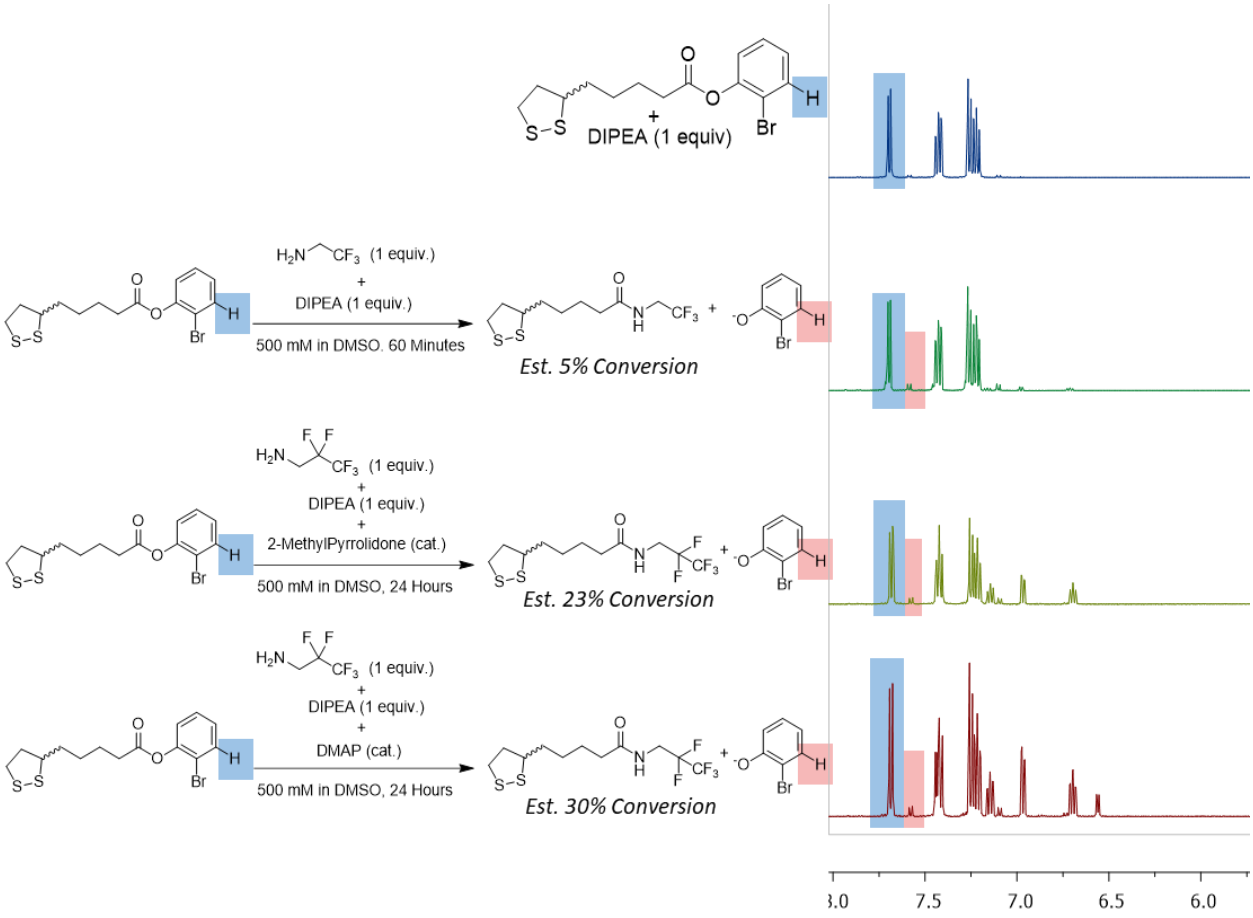

Figure S2.17 ^{1}H NMR overlay (only aromatic signals shown) of aminolysis reactions using **M2** and two fluorinated amino-containing compounds: trifluoroethylamine, and 2,2,3,3,3-pentafluoropropylamine. All reactions performed in DMSO-*d*6 and analyzed at 1 hour or 24 hours. Blue boxes highlight diagnostic peaks from monomer starting material and red boxes highlight diagnostic peaks for aminolysis product. Product conversion was determined via relative peak integrations.

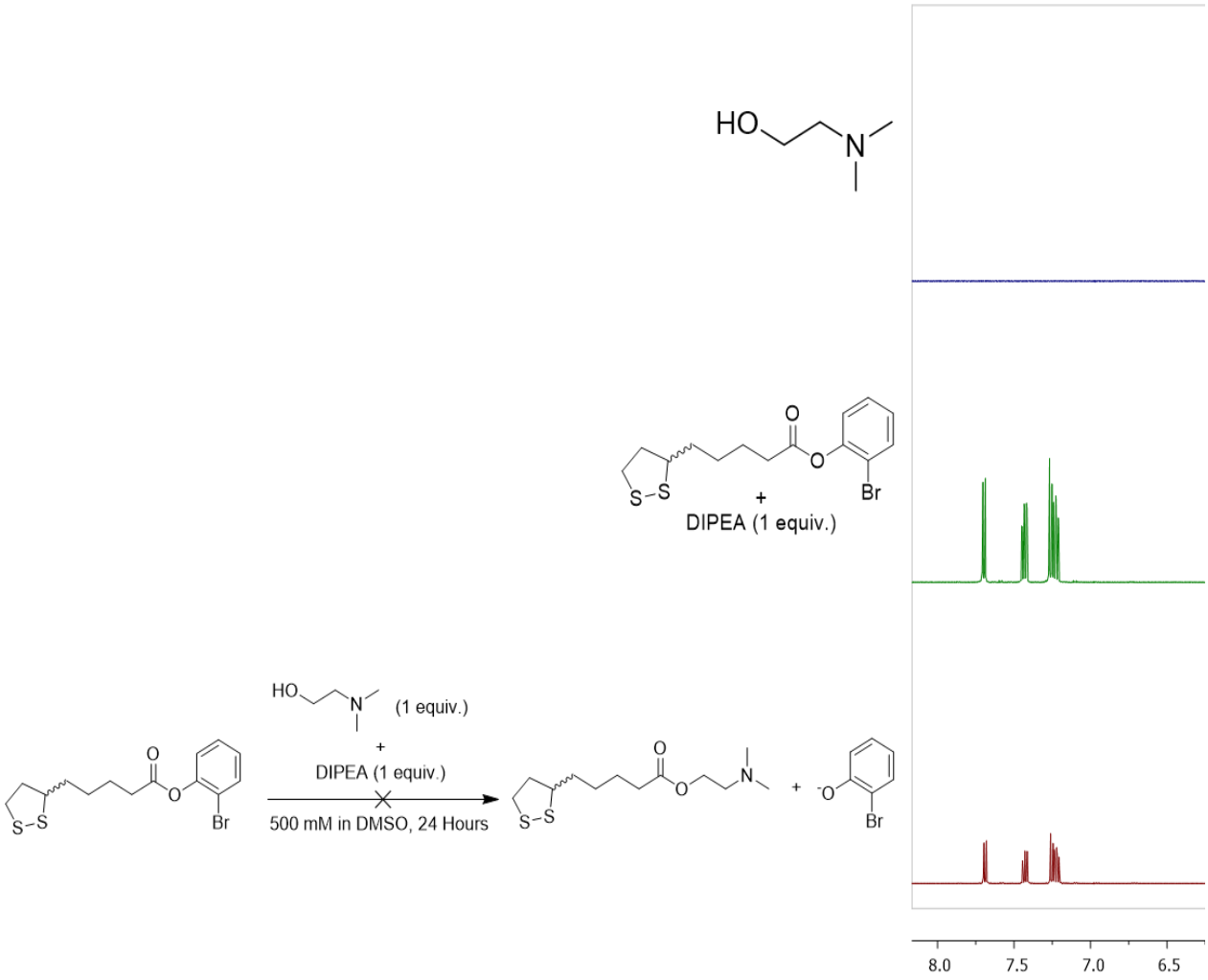

Figure S2.18 ^{1}H NMR overlay (only aromatic signals shown) of alcoholysis reaction using **M2** and 2-(N,N-dimethylamino)ethanol. Alcoholysis was performed in DMSO-*d*6 and analyzed at 24 hours. No product conversion observed.

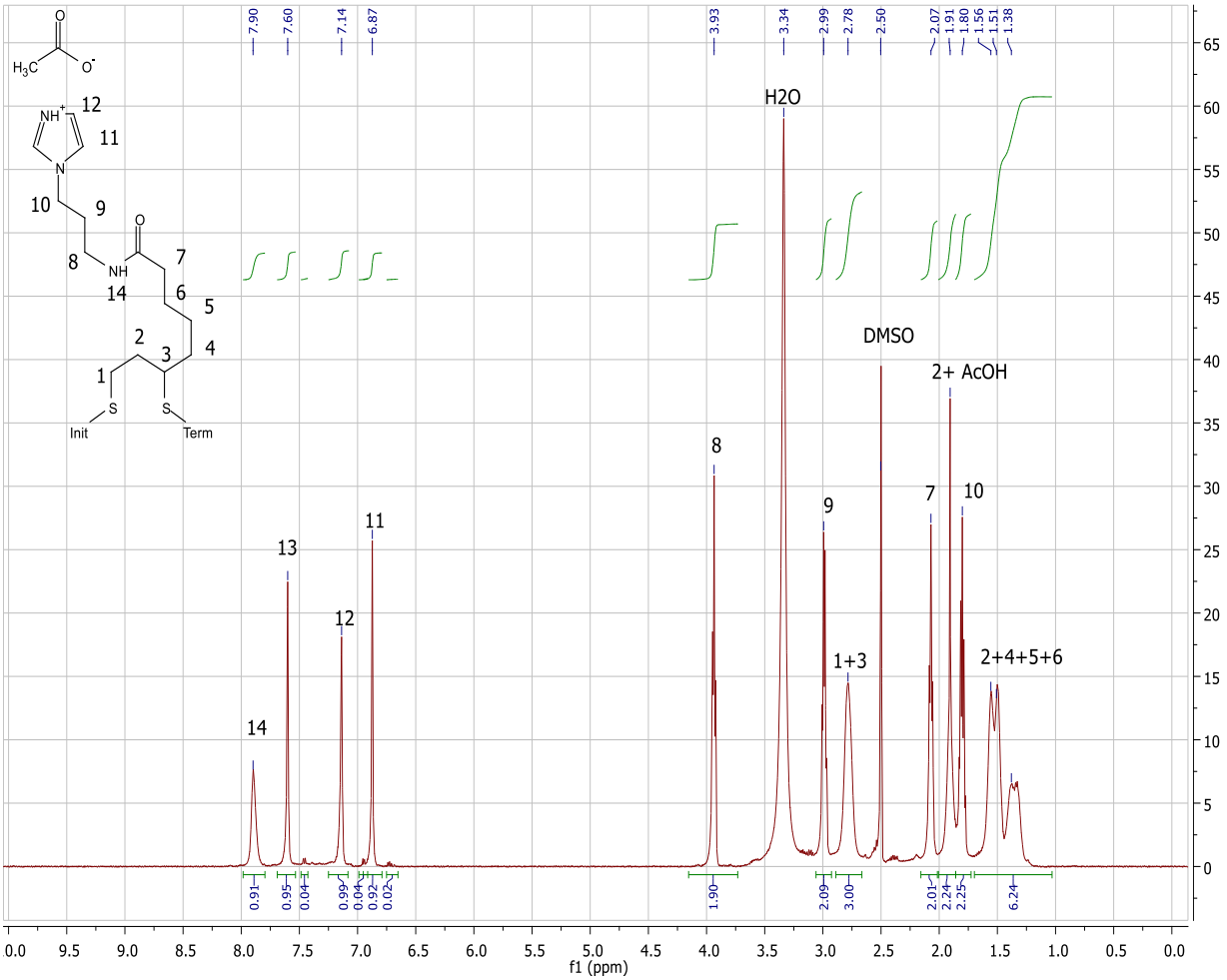

Figure S2.19 ^{1}H NMR of 100% Im multifunctional polymer in DMSO-*d*6 obtained from post-polymerization functionalization.

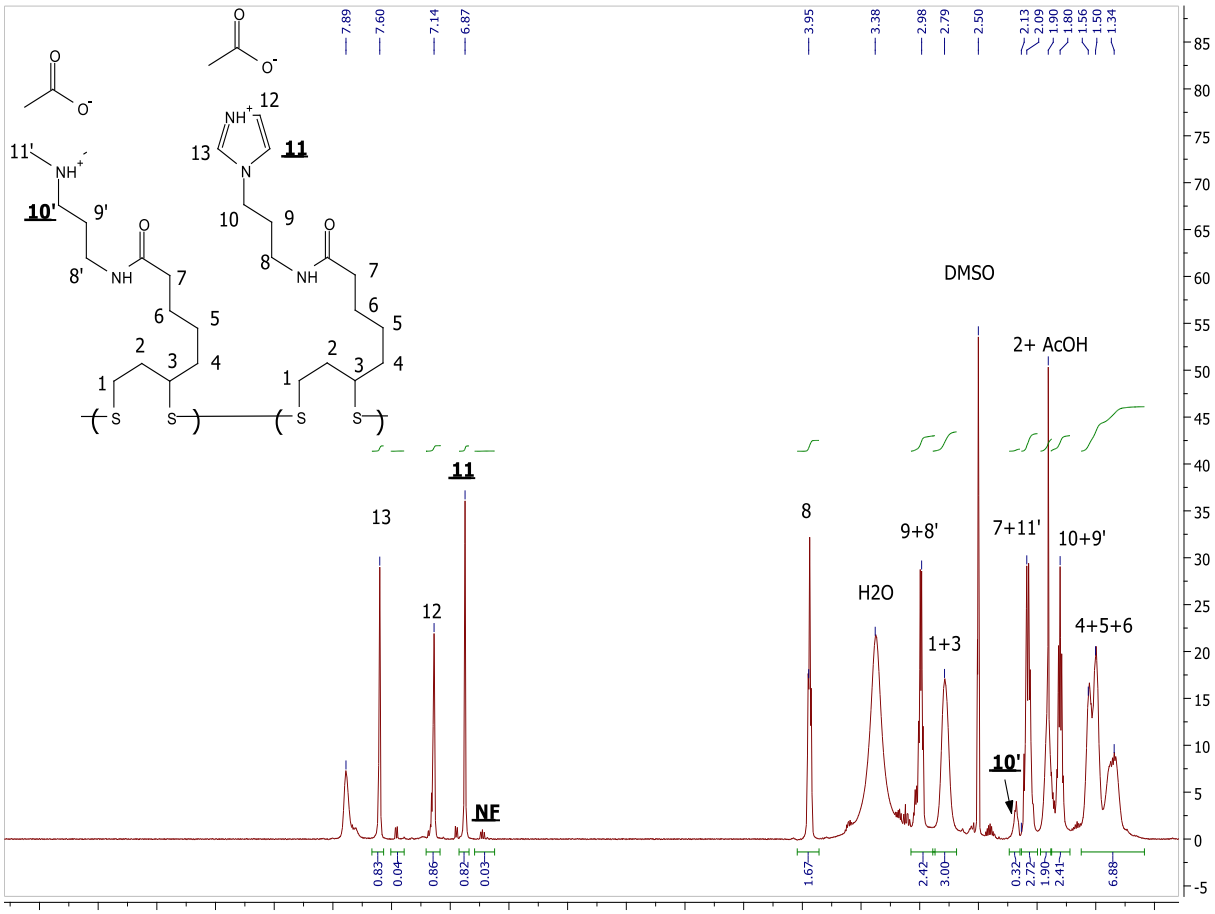

Figure S2.20 ^{1}H NMR of C1-Im multifunctional polymer in DMSO-*d*6 obtained from post-polymerization functionalization. Diagnostic peaks (and non-functionalized [NF] polymer peak) used to determine incorporated functional groups ratios are bolded and underlined.

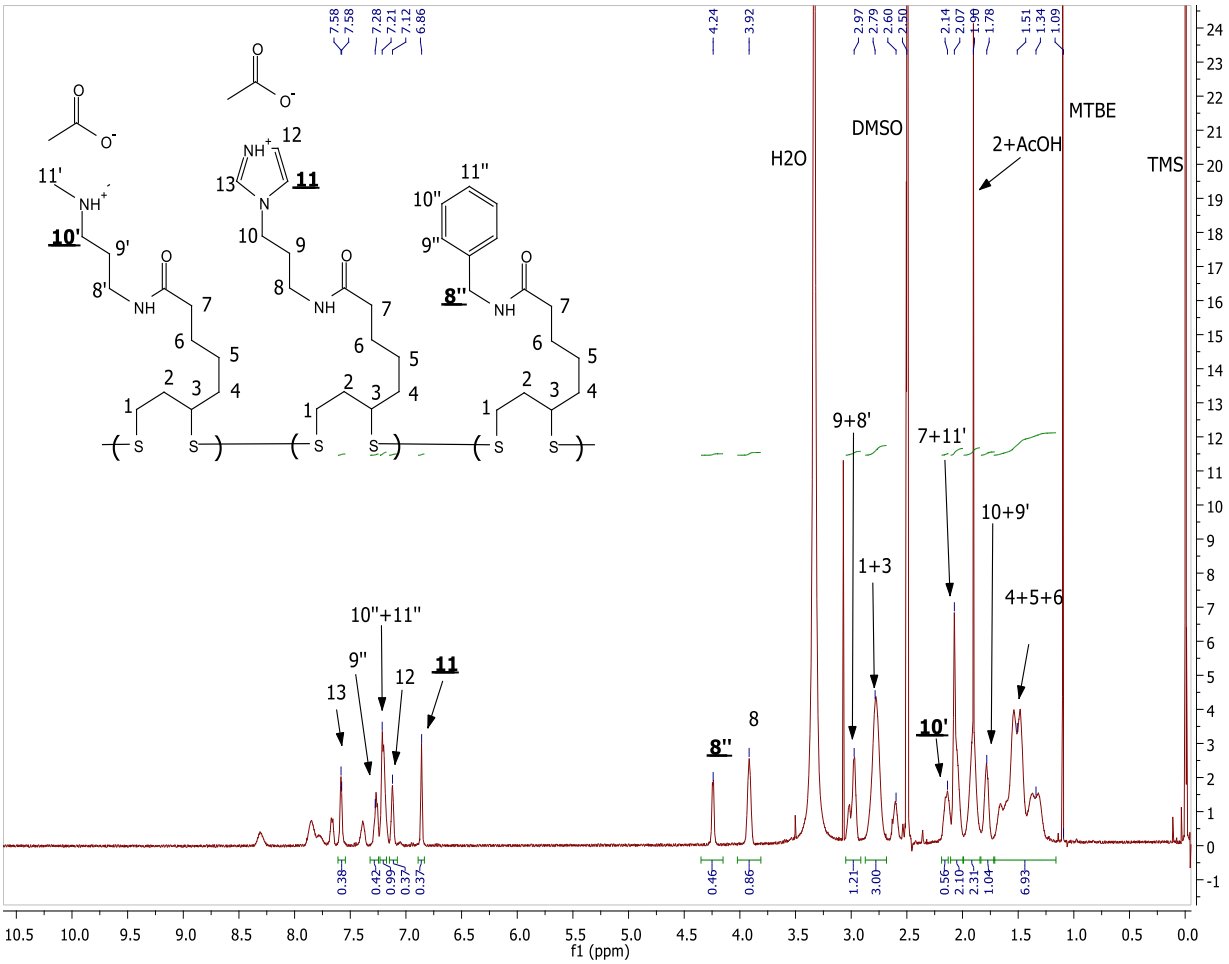

Figure S2.21 ^{1}H NMR of C1-Im-H1 multifunctional polymer in DMSO-*d*6 obtained from post-polymerization functionalization. Diagnostic peaks used to determine incorporated functional groups ratios are bolded and underlined.

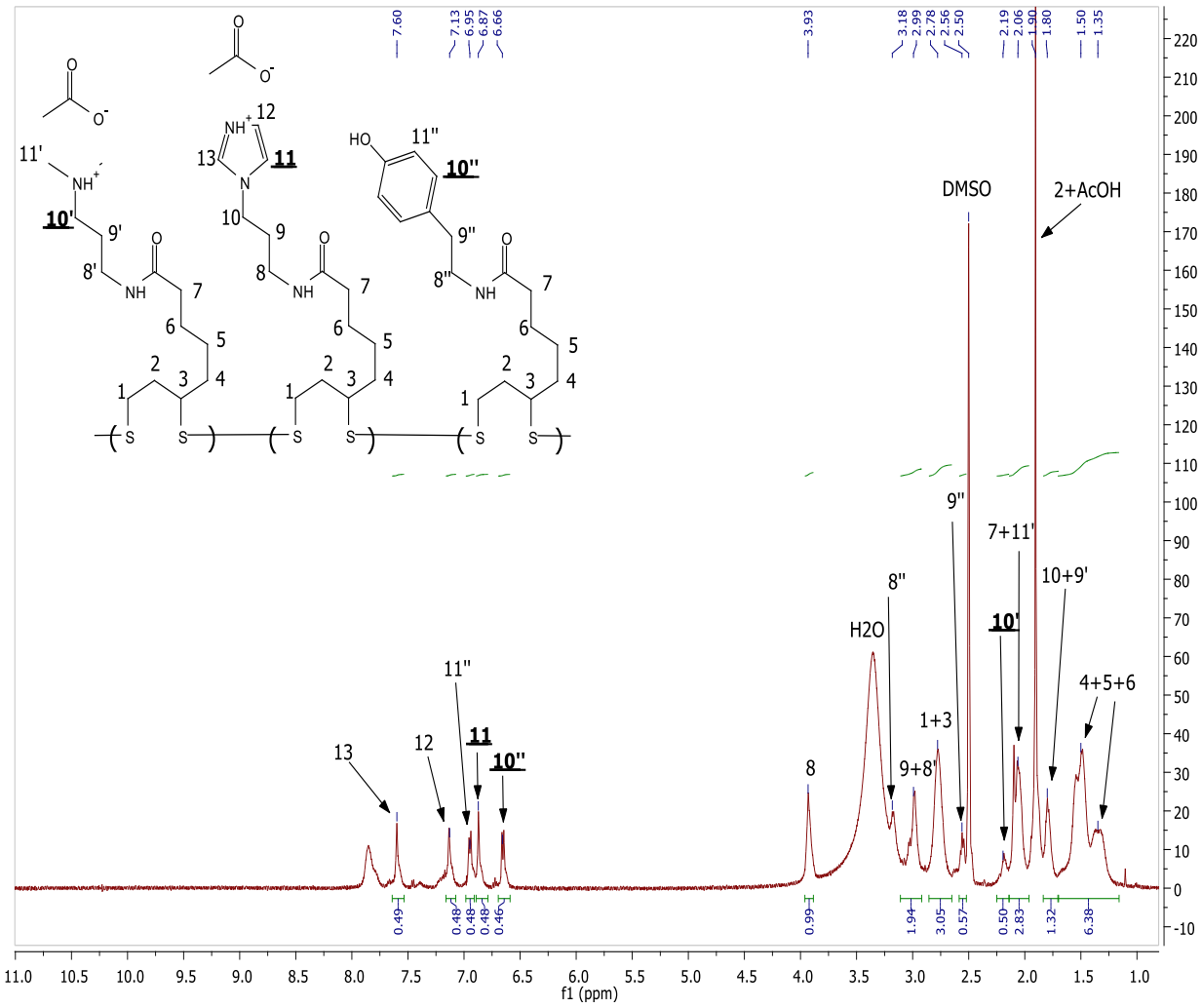

Figure S2.22 ^{1}H NMR of C1-Im-H2 multifunctional polymer in DMSO-*d*6 obtained from post-polymerization functionalization. Diagnostic peaks used to determine incorporated functional groups ratios are bolded and underlined.

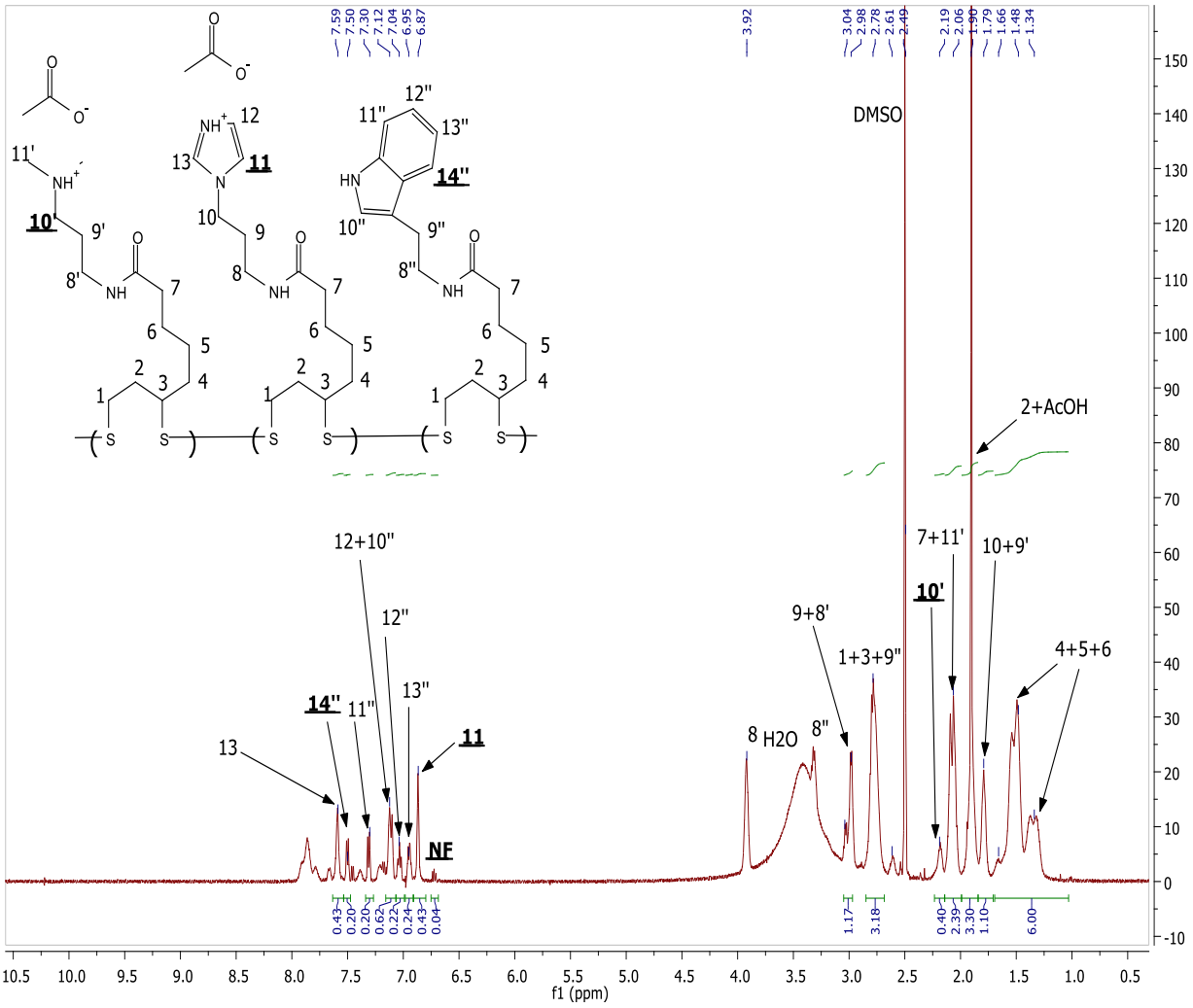

Figure S2.23 ^{1}H NMR of C1-Im-H3 multifunctional polymer in DMSO-*d*6 obtained from post-polymerization functionalization. Diagnostic peaks used to determine incorporated functional groups ratios are bolded and underlined.

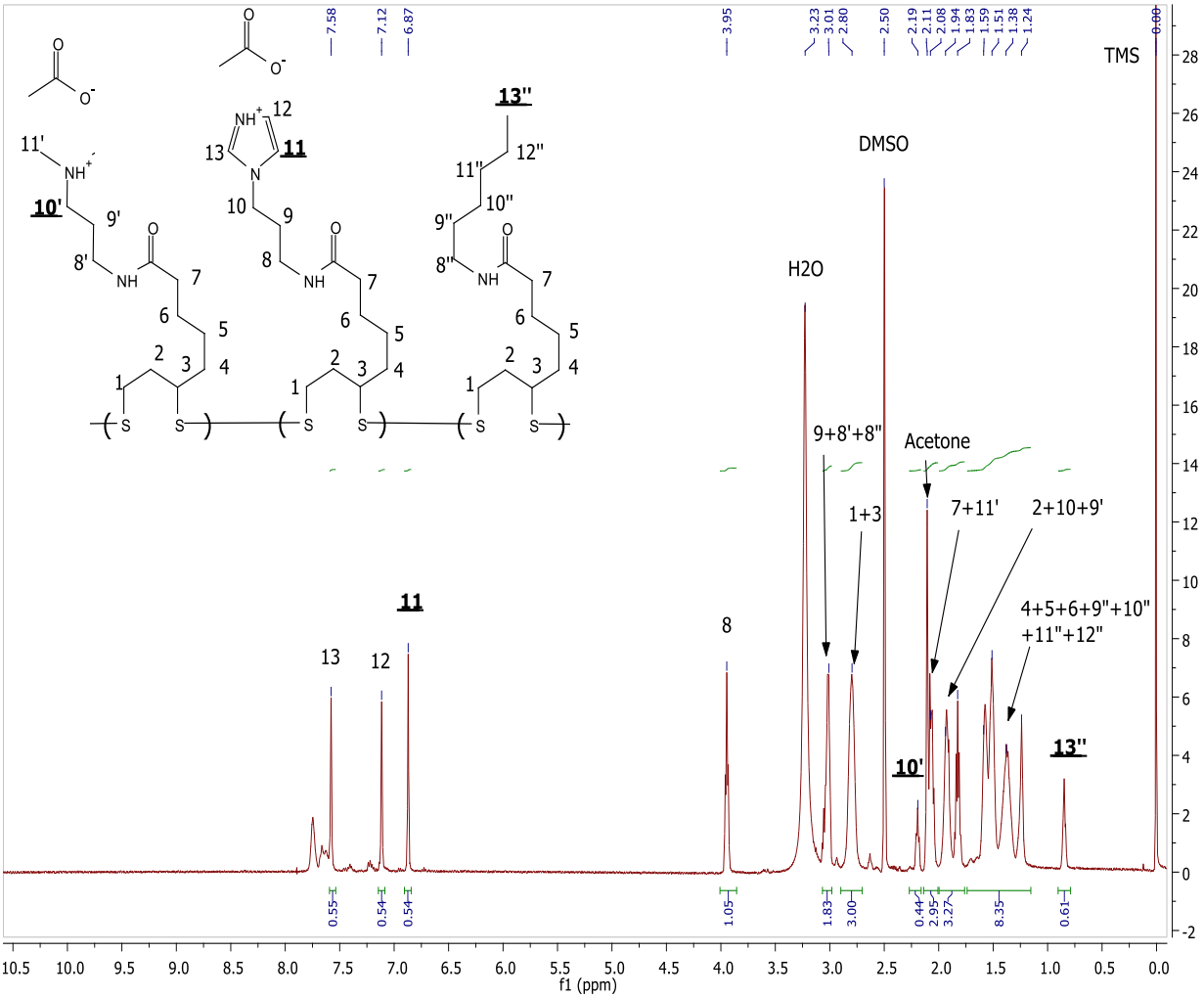

Figure S2.24 ^{1}H NMR of C1-Im-H4 multifunctional polymer in DMSO-*d*6 obtained from post-polymerization functionalization. Diagnostic peaks used to determine incorporated functional groups ratios are bolded and underlined.

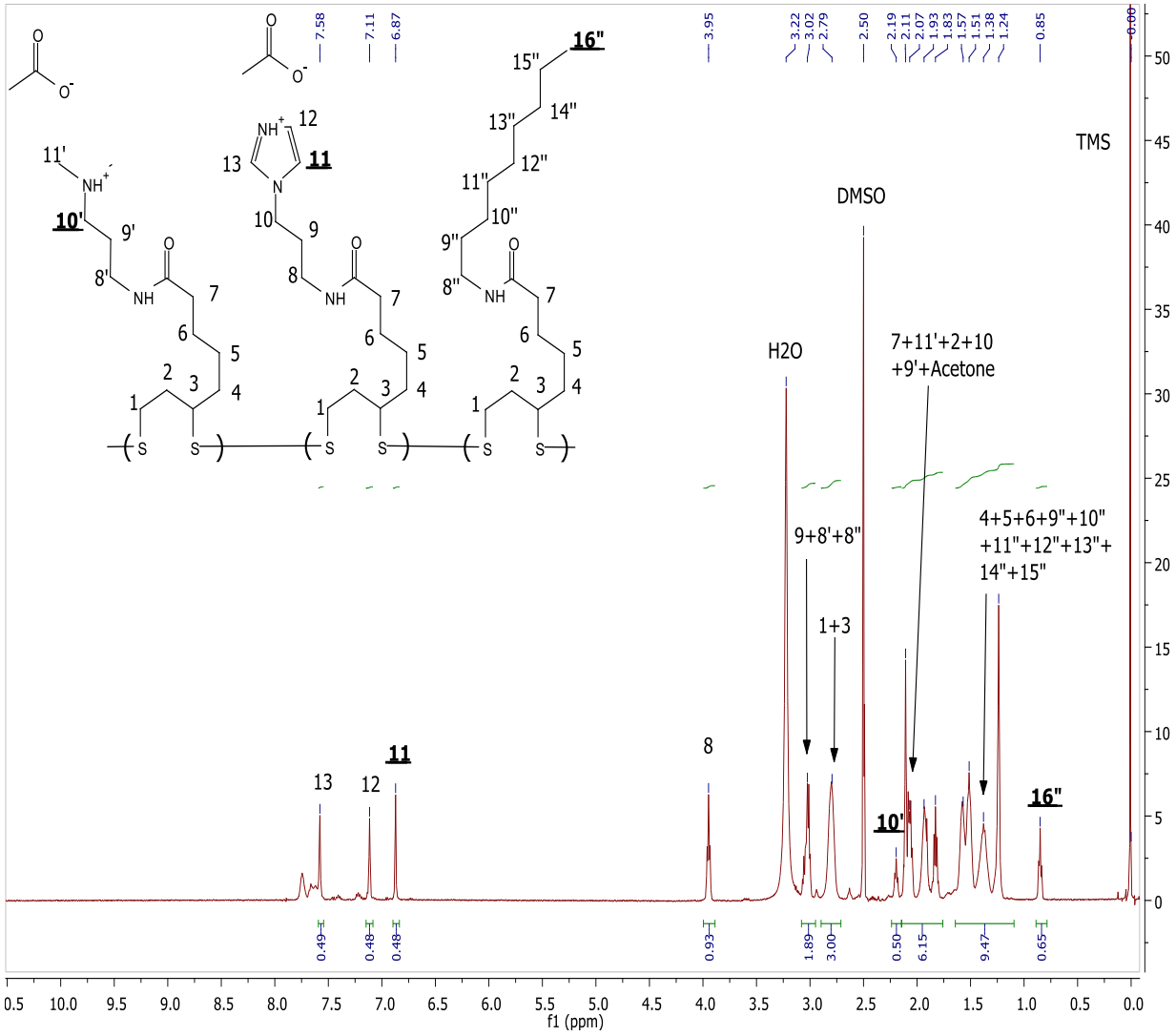

Figure S2.25 ^{1}H NMR of C1-Im-H5 multifunctional polymer in DMSO-*d*6 obtained from post-polymerization functionalization. Diagnostic peaks used to determine incorporated functional groups ratios are bolded and underlined.

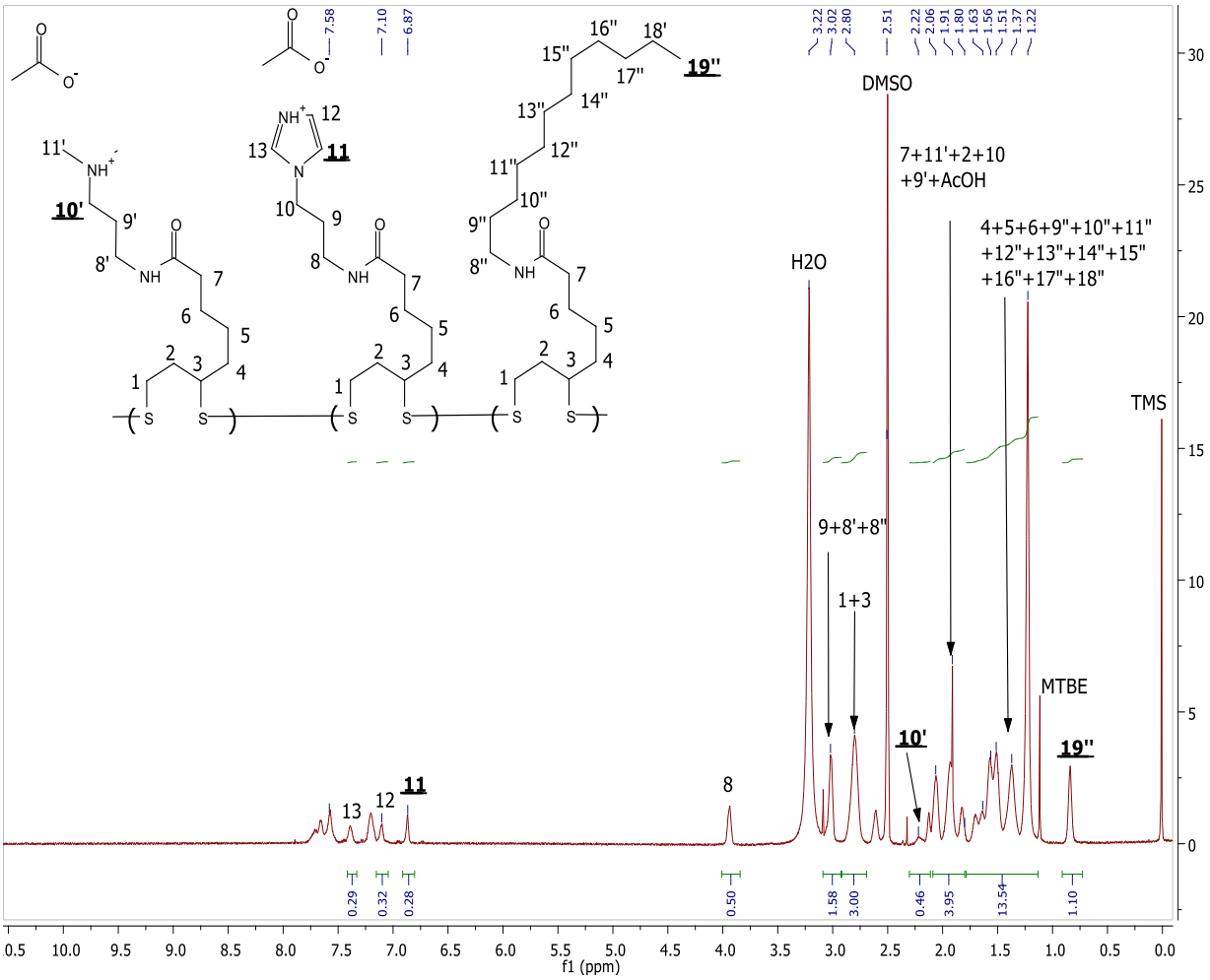

Figure S2.26 ^{1}H NMR of C1-Im-H6 multifunctional polymer in DMSO-*d*6 obtained from post-polymerization functionalization. Diagnostic peaks used to determine incorporated functional groups ratios are bolded and underlined.

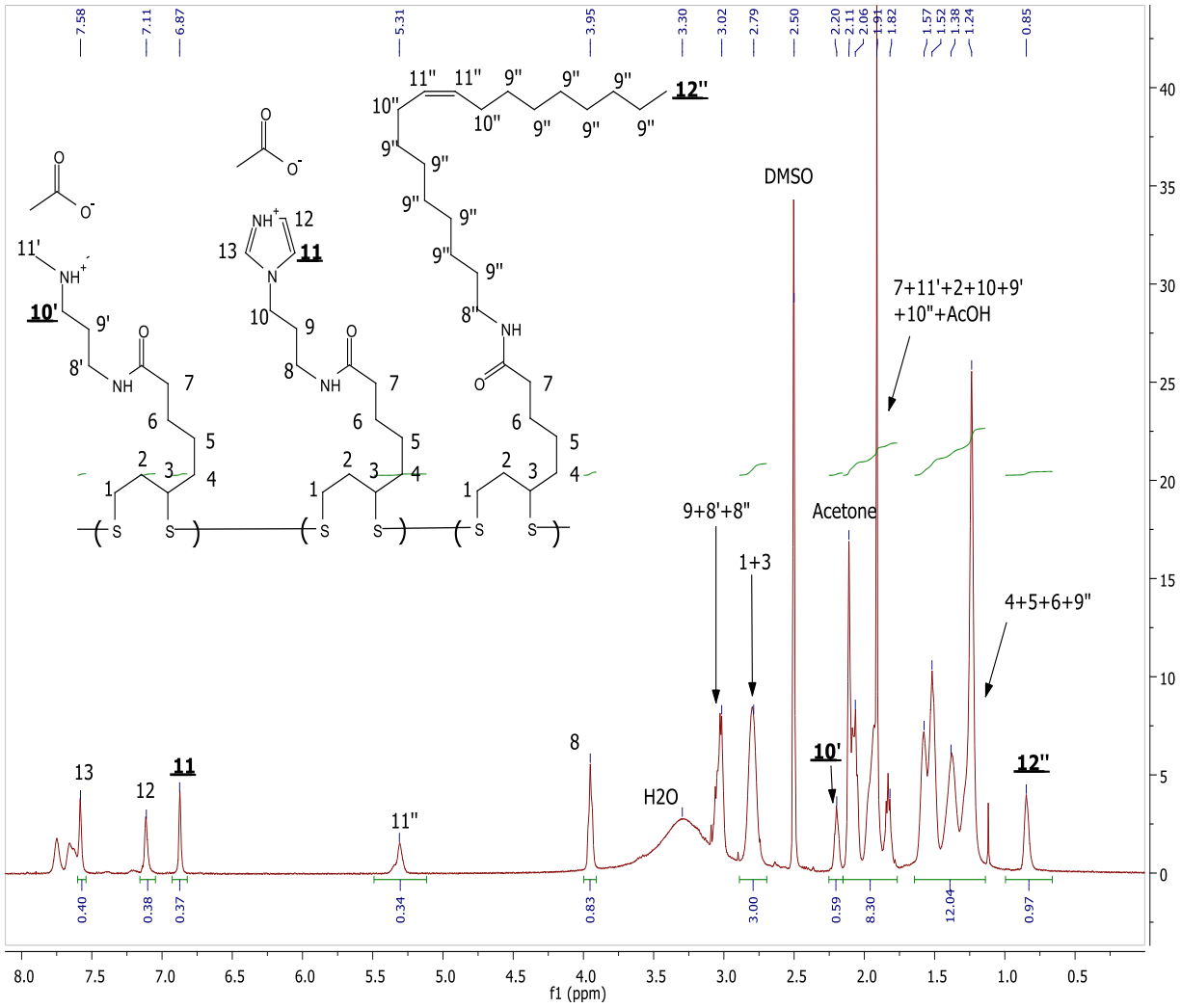

Figure S2.27 ^{1}H NMR of C1-Im-H7 multifunctional polymer in DMSO-*d*6 obtained from post-polymerization functionalization. Diagnostic peaks used to determine incorporated functional groups ratios are bolded and underlined.

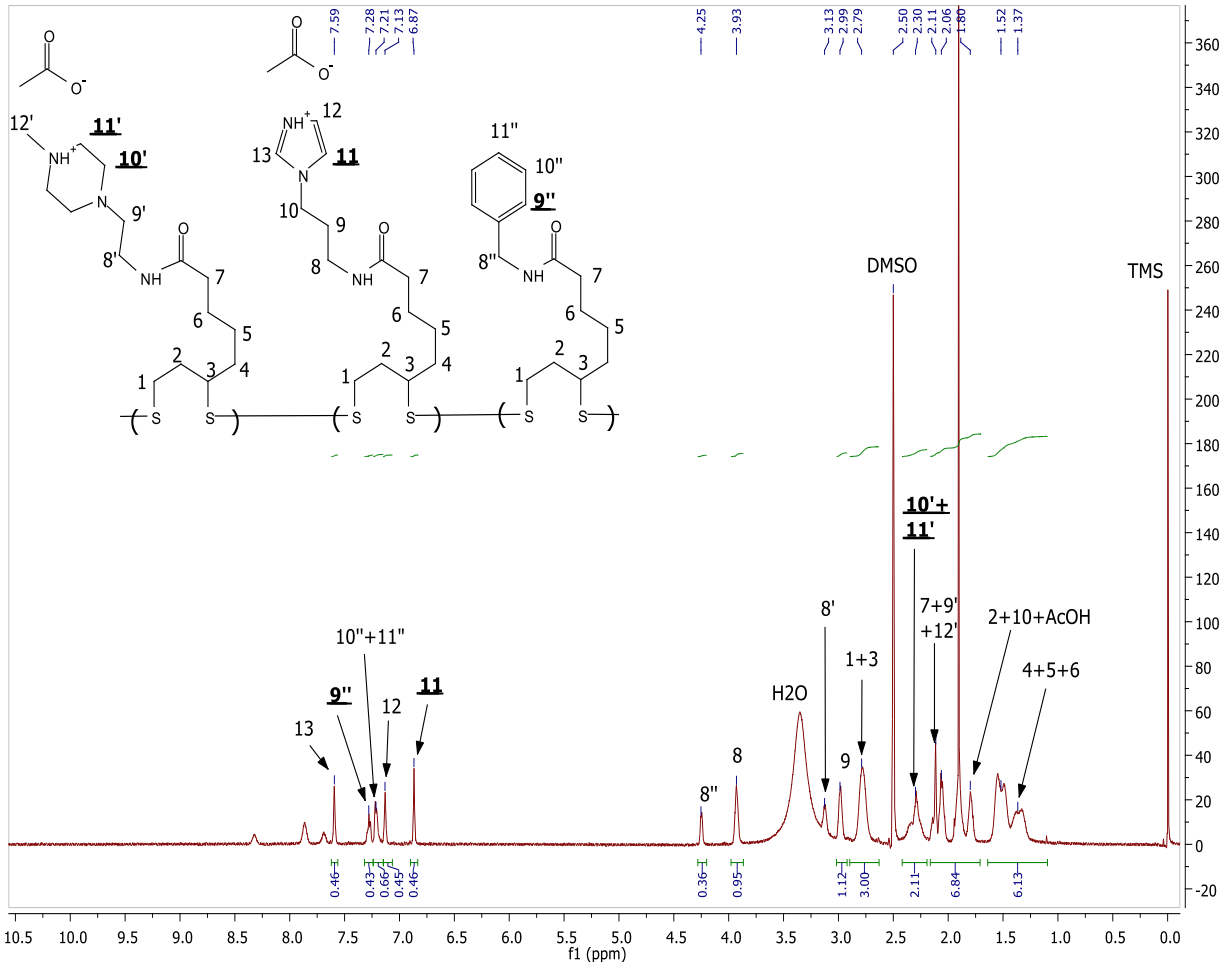

Figure S2.28 ^{1}H NMR of C2-Im-H1 multifunctional polymer in DMSO-*d*6 obtained from post-polymerization functionalization. Diagnostic peaks used to determine incorporated functional groups ratios are bolded and underlined.

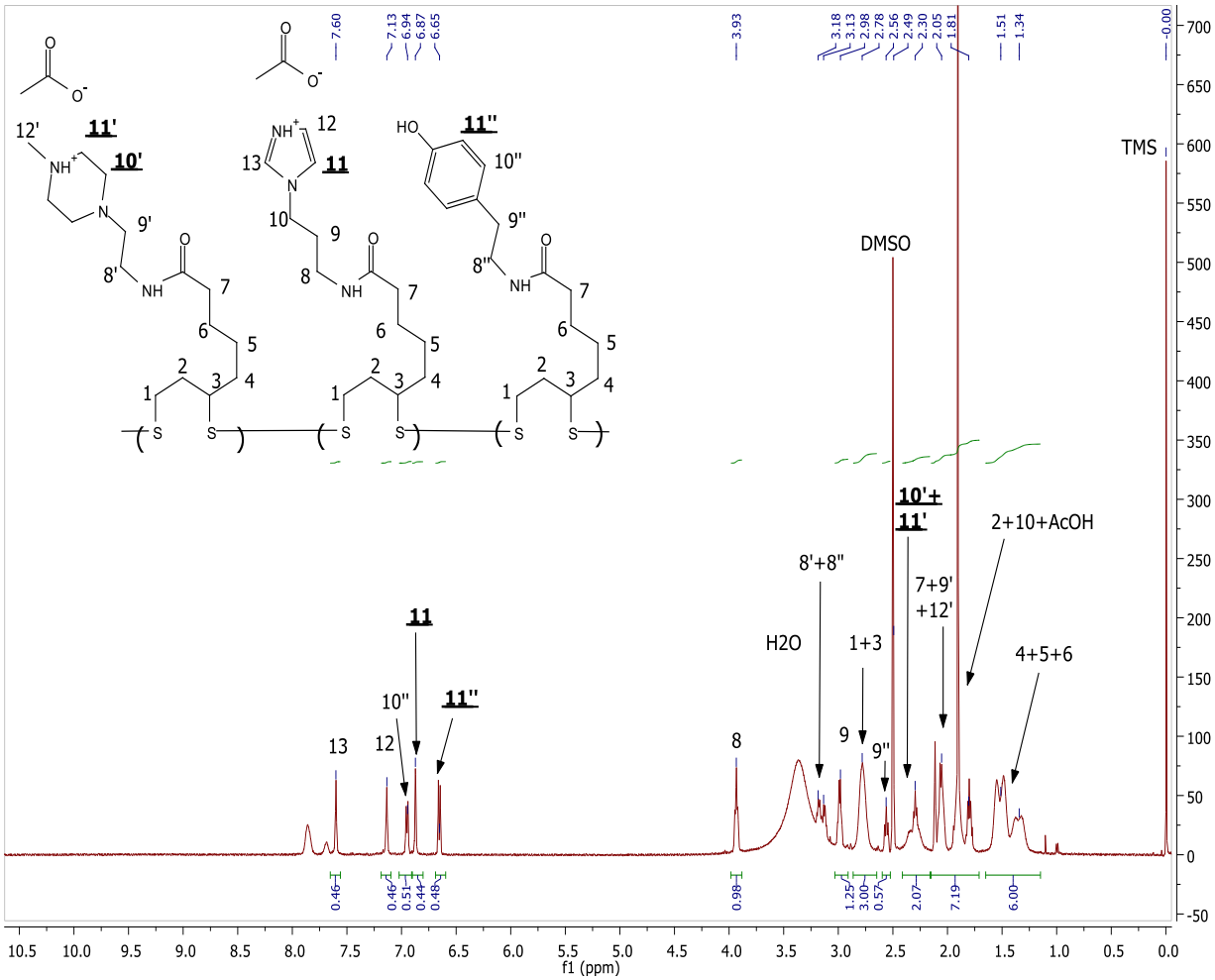

Figure S2.29 ^{1}H NMR of C2-Im-H2 multifunctional polymer in DMSO-*d6* obtained from post-polymerization functionalization. Diagnostic peaks used to determine incorporated functional groups ratios are bolded and underlined.

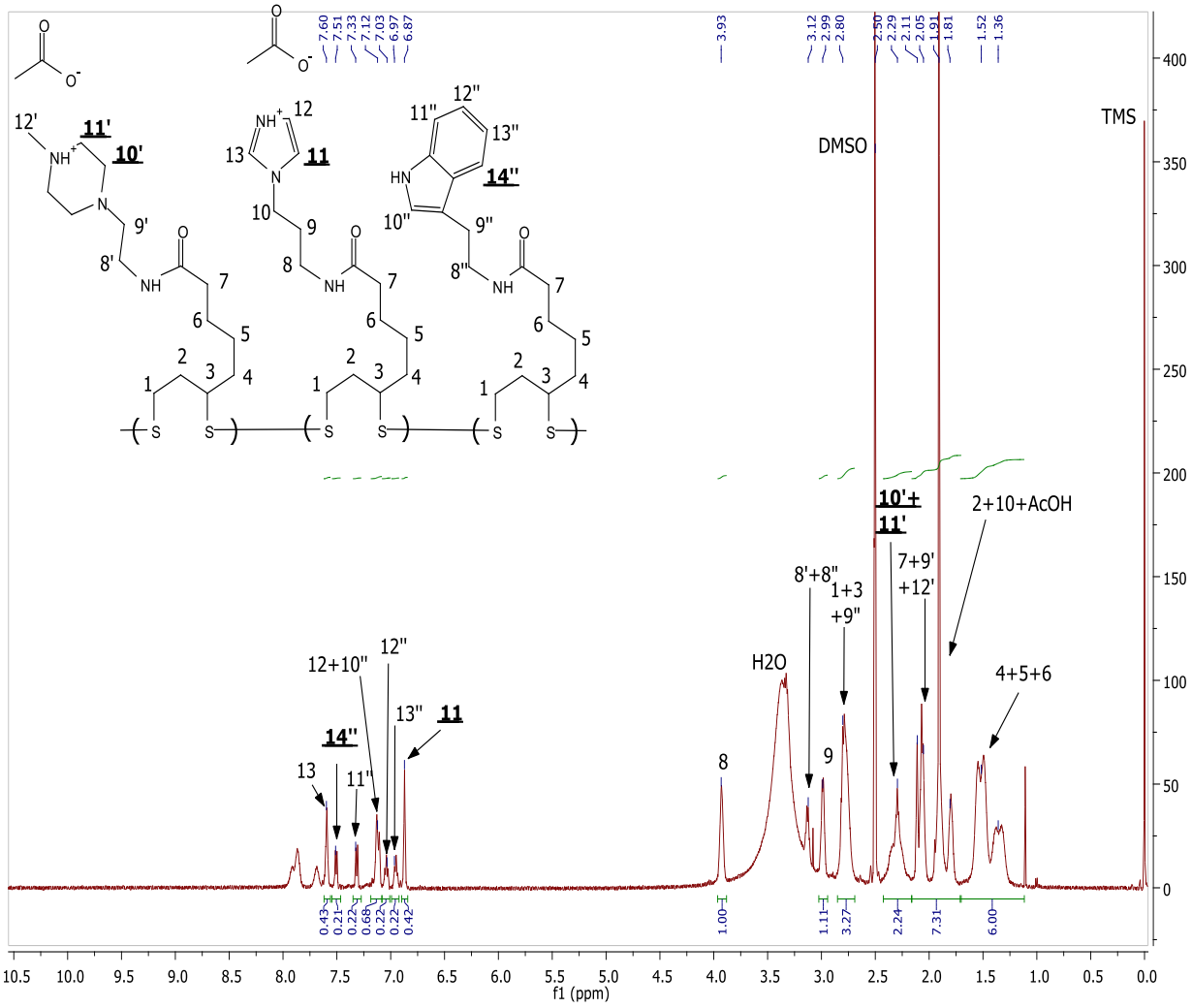

Figure S2.30 ^{1}H NMR of C2-Im-H3 multifunctional polymer in DMSO-*d*6 obtained from post-polymerization functionalization. Diagnostic peaks used to determine incorporated functional groups ratios are bolded and underlined.

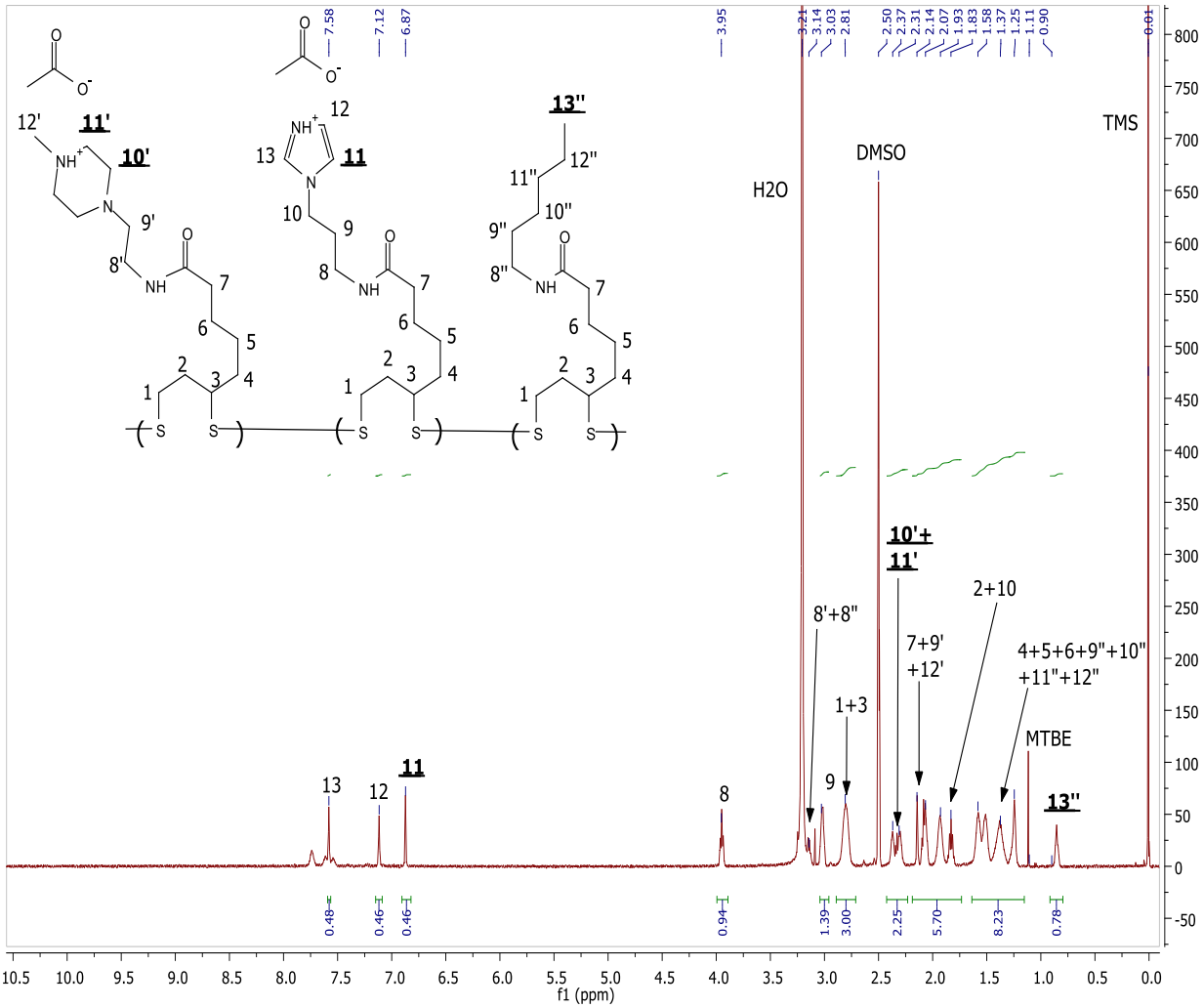

Figure S2.31 ^{1}H NMR of C2-Im-H4 multifunctional polymer in DMSO-*d*6 obtained from post-polymerization functionalization. Diagnostic peaks used to determine incorporated functional groups ratios are bolded and underlined.

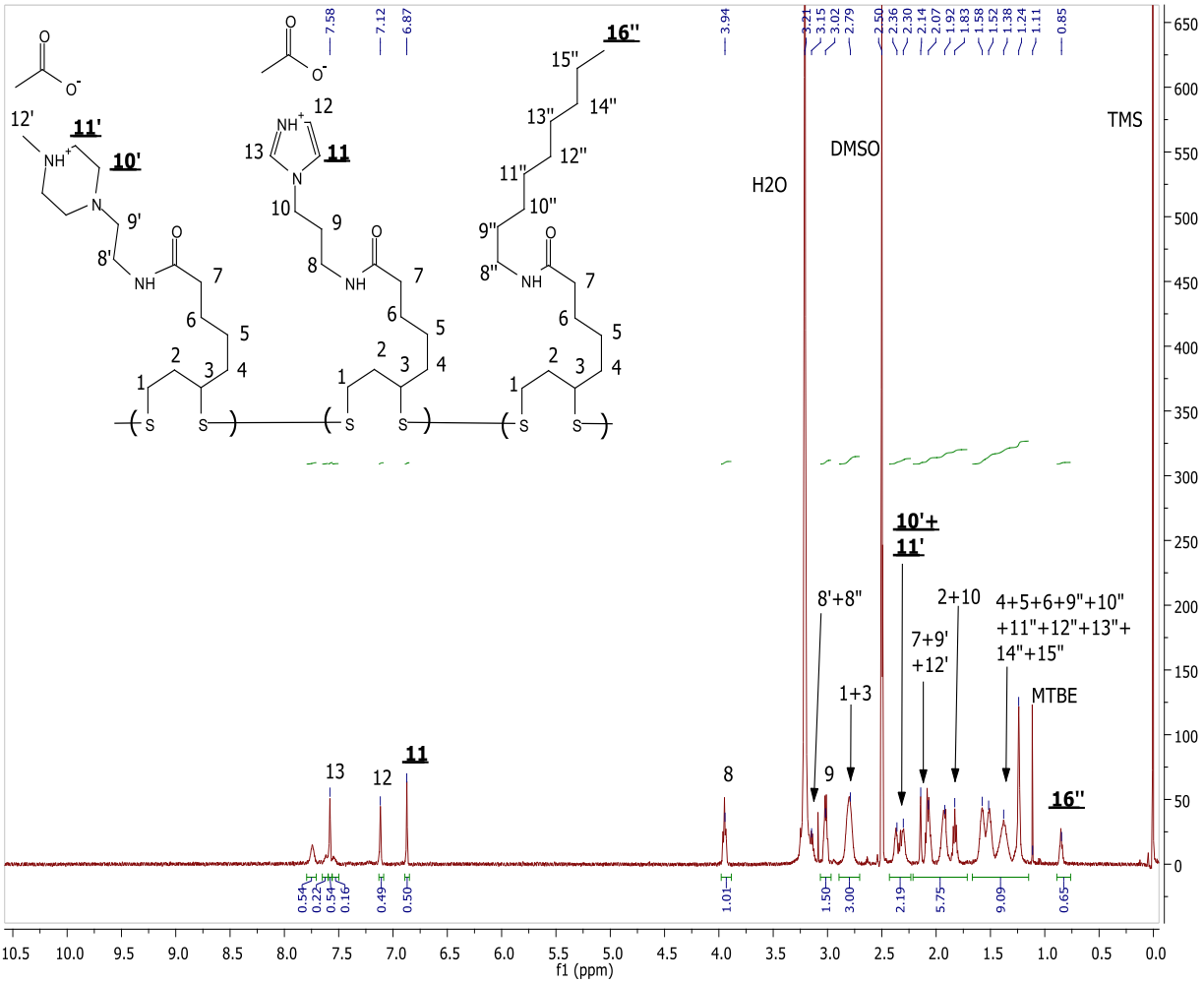

Figure S2.32 ^{1}H NMR of C2-Im-H5 multifunctional polymer in DMSO-*d*6 obtained from post-polymerization functionalization. Diagnostic peaks used to determine incorporated functional groups ratios are bolded and underlined.

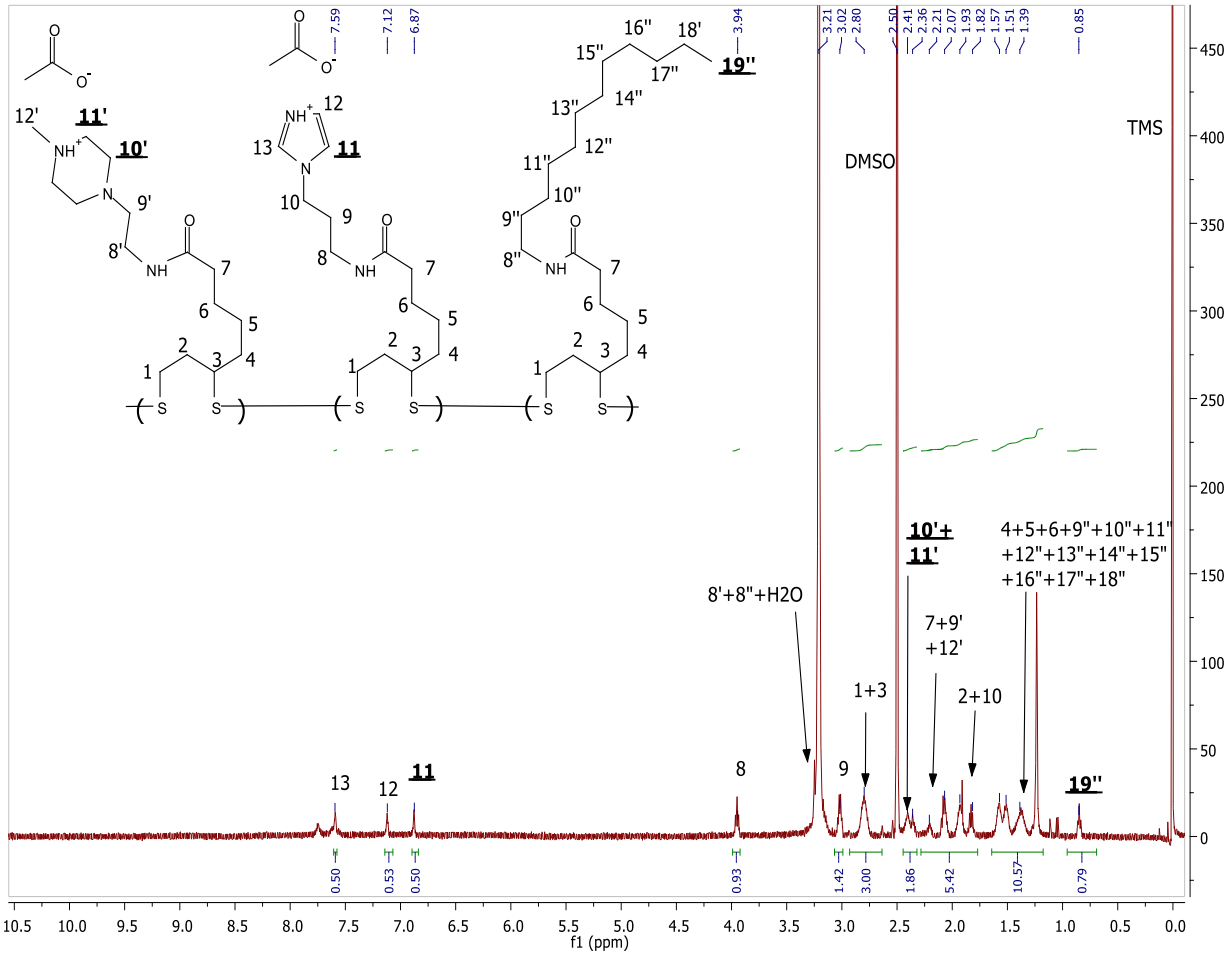

Figure S2.33 ^{1}H NMR of C2-Im-H6 multifunctional polymer in DMSO-*d*6 obtained from post-polymerization functionalization. Diagnostic peaks used to determine incorporated functional groups ratios are bolded and underlined.

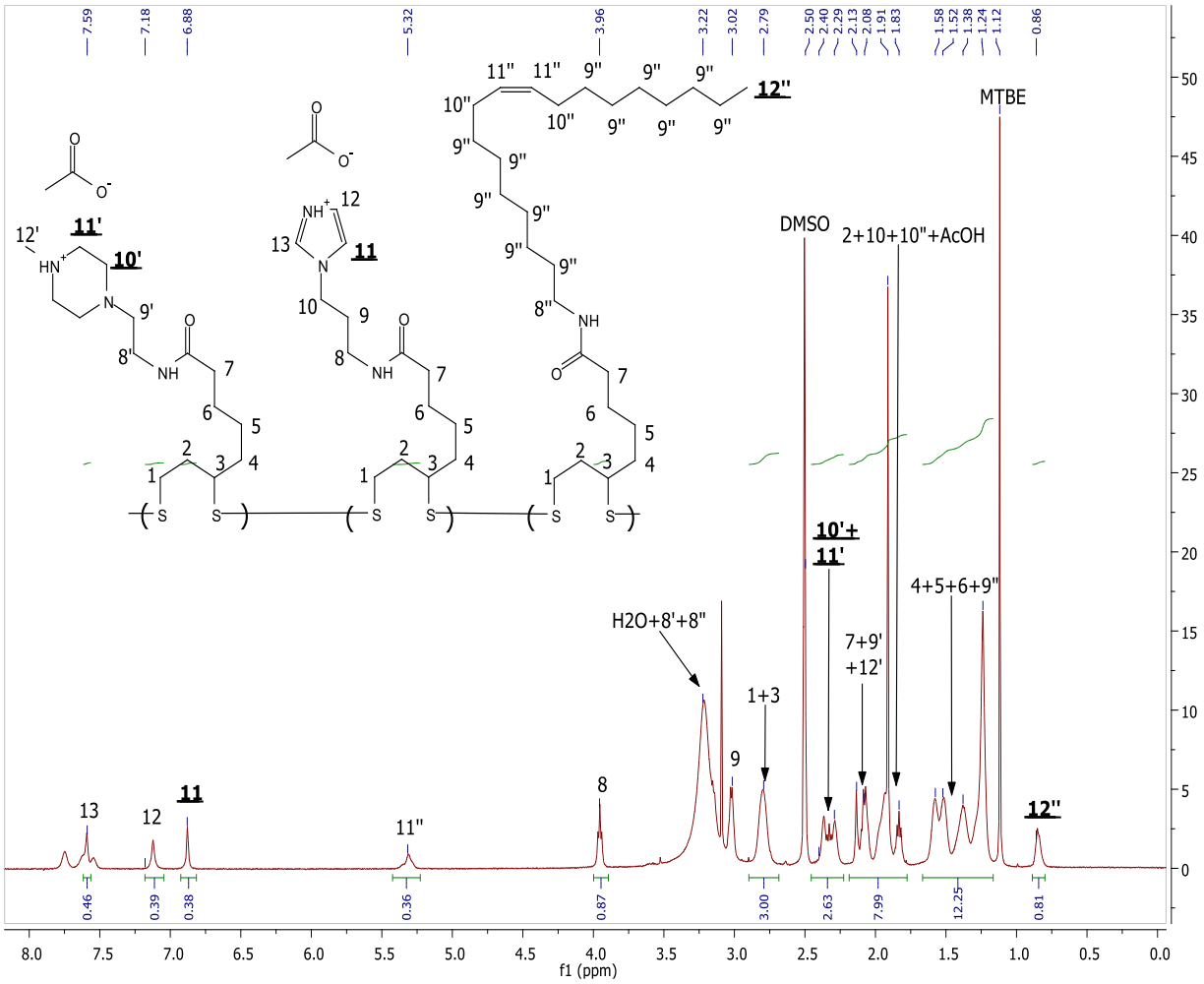

Figure S2.34 ^{1}H NMR of C2-Im-H7 multifunctional polymer in DMSO-*d*6 obtained from post-polymerization functionalization. Diagnostic peaks used to determine incorporated functional groups ratios are bolded and underlined.

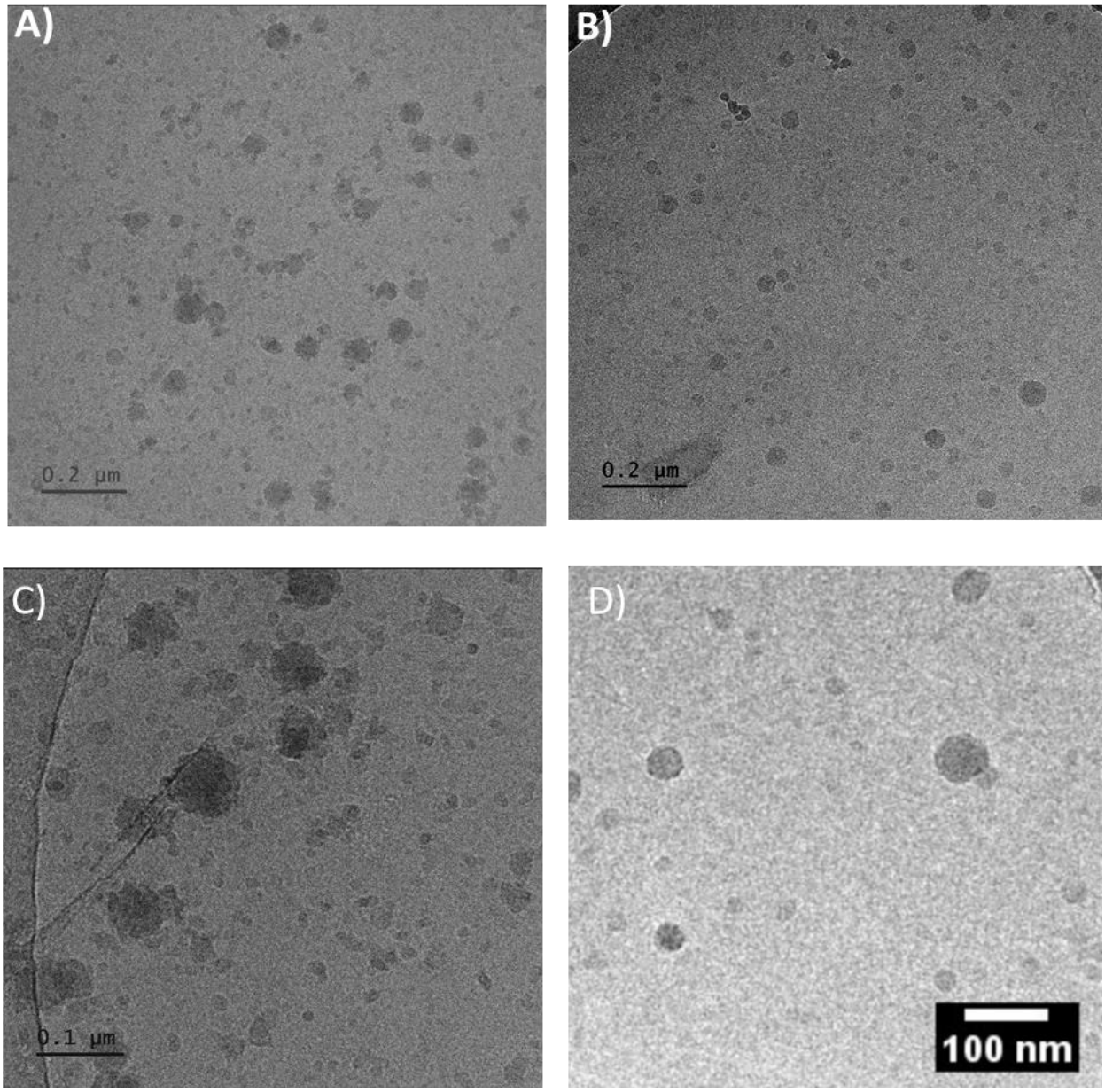

Figure S2.35 Additional Cryo-TEM Images of EGFP mRNA-polymer nanoparticles with: **A**) C1-Im-H1 polymer, **B**) C1-Im-H4 polymer, **C**) C1-Im-H1 polymer at higher amplification, and **D**) zoomed image of C1-Im-H4 polymer. C1-I-H4 nanoparticles have more defined spheroidal character whereas C1-Im-H1 nanoparticles demonstrate clustering behavior to form irregular nanoparticle polyplexes. Scale bars represent 0.2 µm for **A**) and **B**); scale bar represents 0.1 µm for **C**) and **D**).

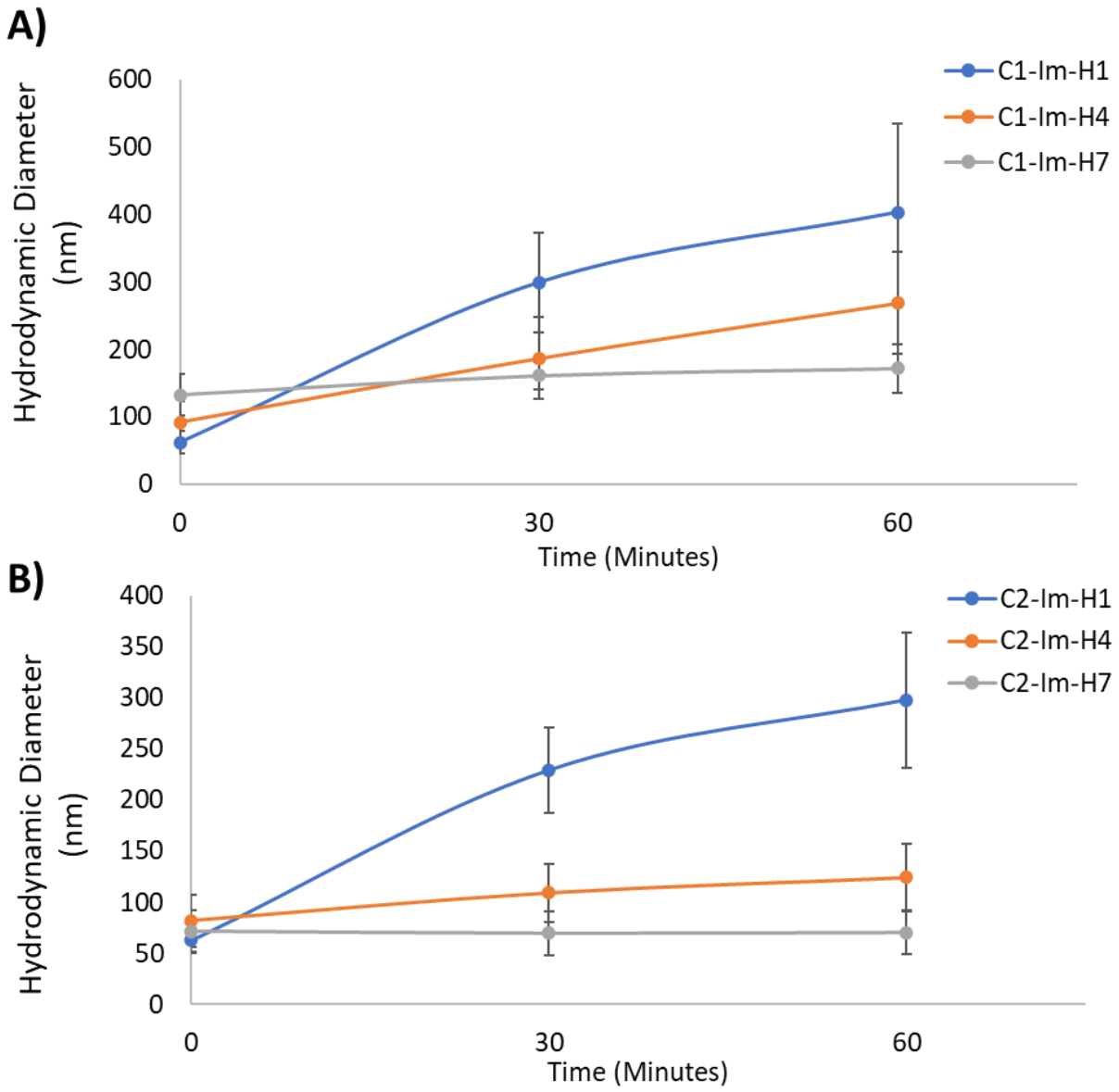

Figure S2.36 Nanoparticle aggregation, as measured by DLS, of multifunctional polymer nanoparticles without mRNA. **A**) Polymeric nanoparticles containing C1 amino- groups. **B**) Polymeric nanoparticles containing C2-amino groups.

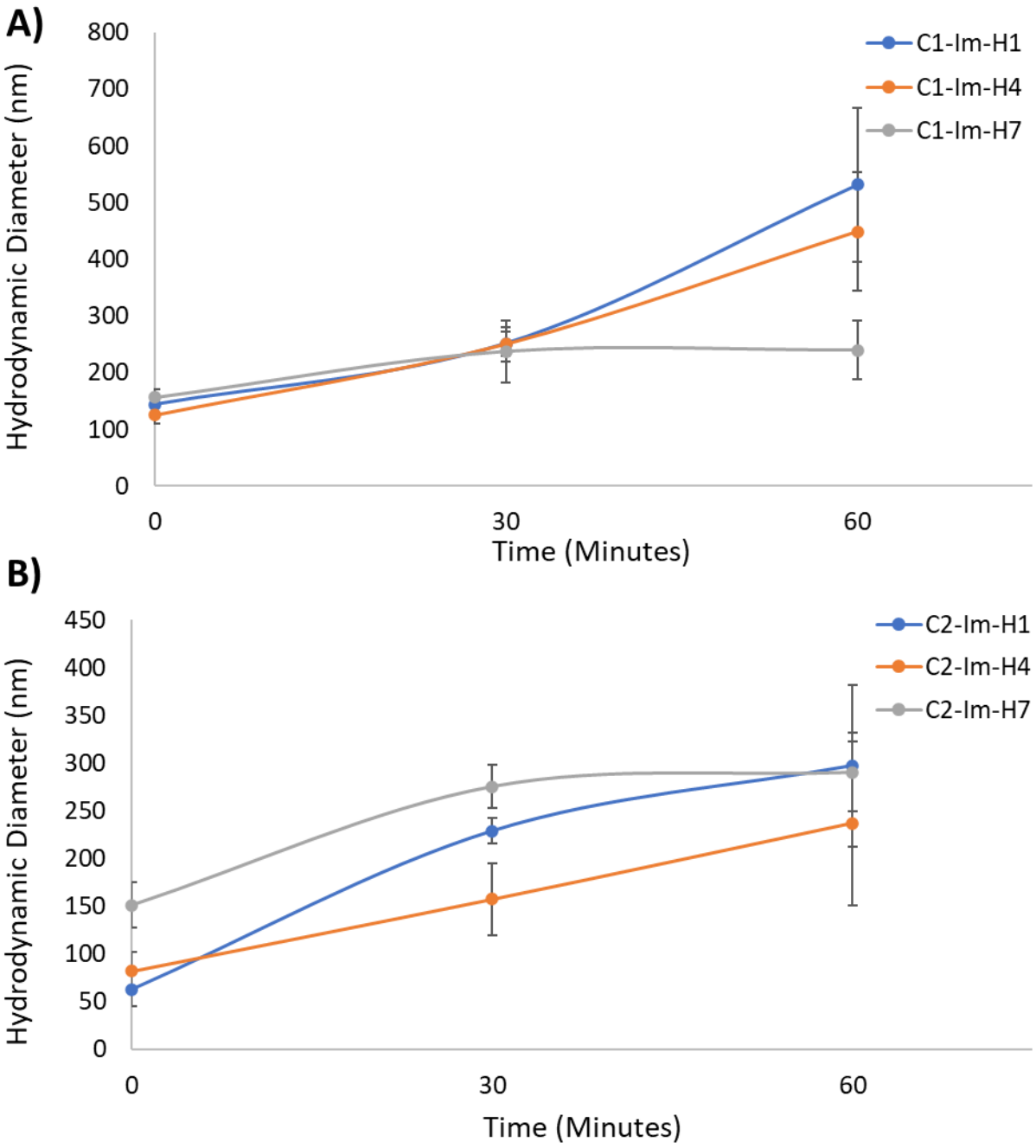

Figure S2.37 Nanoparticle aggregation, as measured by DLS, of multifunctional polymer nanoparticles with EGFP mRNA. **A**) Polymeric nanoparticles containing C1 amino-groups. **B**) Polymeric nanoparticles containing C2-amino groups.

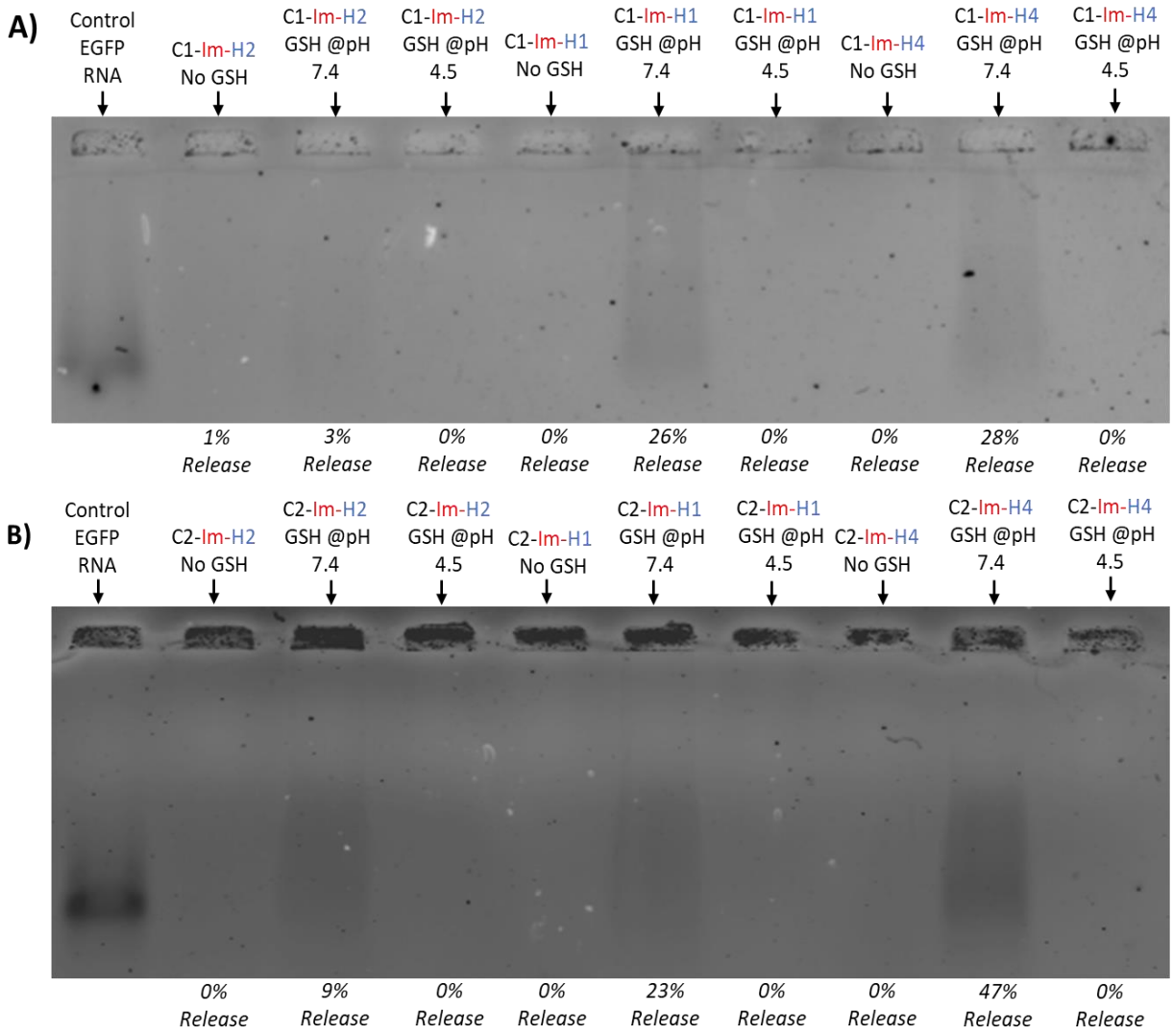

Figure S2.38 *Ex vivo* depolymerization reactions for **A)** C1-Im-H2, C1-Im-H1, and C1-Im-H4 polymeric nanoparticles containing EGFP mRNA and **B)** C2-Im-H2, C2-Im-H1, and C2-Im-H4 polymeric nanoparticles. Polymeric nanoparticles were incubated with 10 mM GSH at either pH 7.4 or 4.5. Quantified mRNA released is written under relevant samples. All samples were incubated in 50% DMSO-50% Buffer for 12 hours at 37 °C.

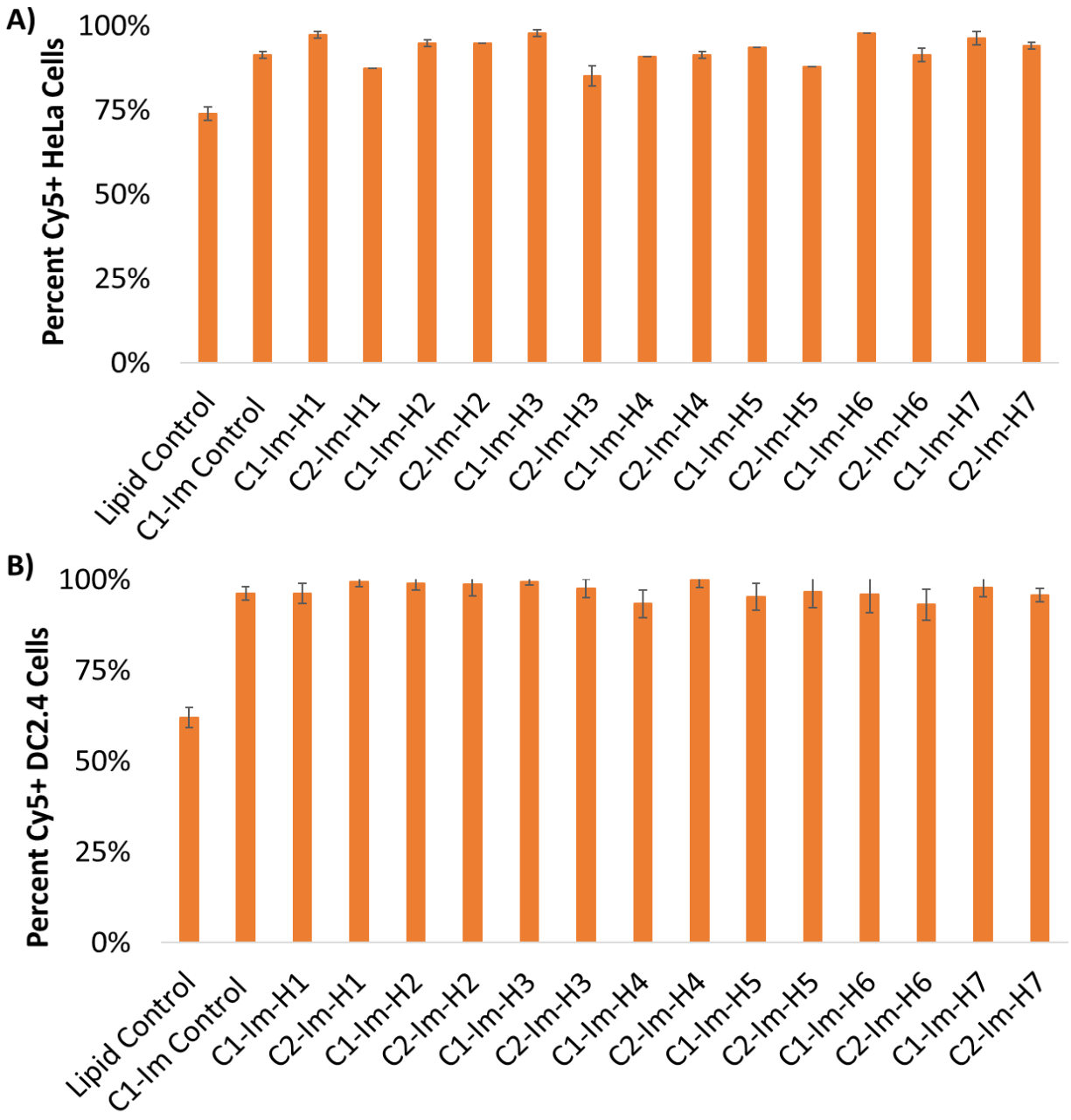

Figure S2.39 Percent of Cy5+ cells after treatment with multifunctional polymer-mRNA nanoparticles containing Cy5-labeled mRNA for **A**) HeLa cells and **B**) DC2.4 cells. Cy5+ cells determined by flow cytometry 6 hours after nanoparticle administration. All nanoparticles formualated at an N/P ratio of 5 and 150 ng of mRNA was administered per 5K cells. Lipofectamine MessengerMAX was used as a lipid control. n=3 for all sample treatments.

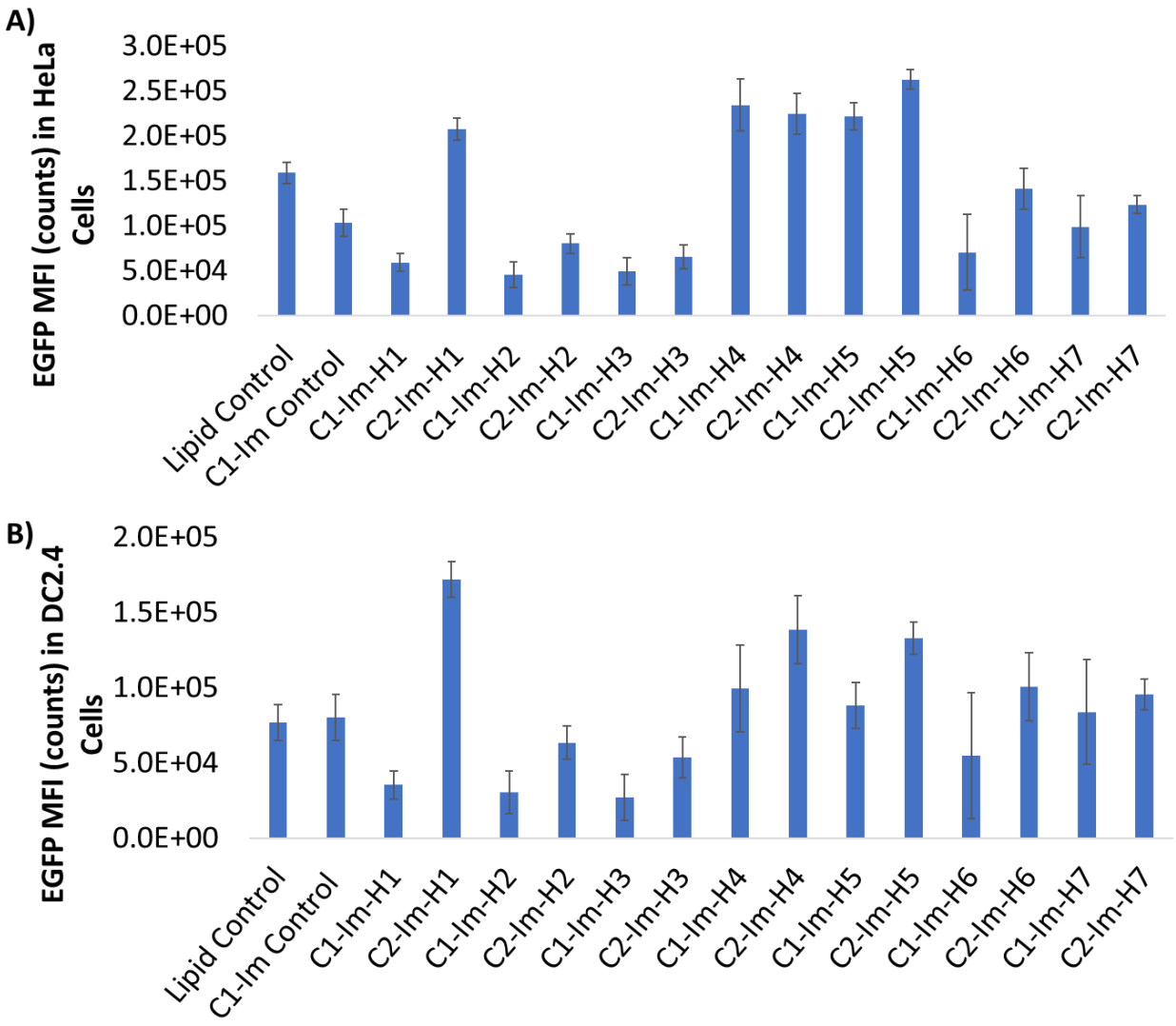

Figure S2.40 Cellular EGFP expression (Mean Fluorescence Intensity [MFI] in counts) after treatment with multifunctional polymer-mRNA nanoparticles containing Cy5-labeled mRNA for **A**) HeLa cells and **B**) DC2.4 cells. EGFP+ cells determined by flow cytometry 48 hours after nanoparticle administration. All nanoparticles formulated at an N/P ratio of 5 and 150 ng of mRNA was administered per 5K cells. Lipofectamine MessengerMAX was used as a lipid control. n=3 for all sample treatments.

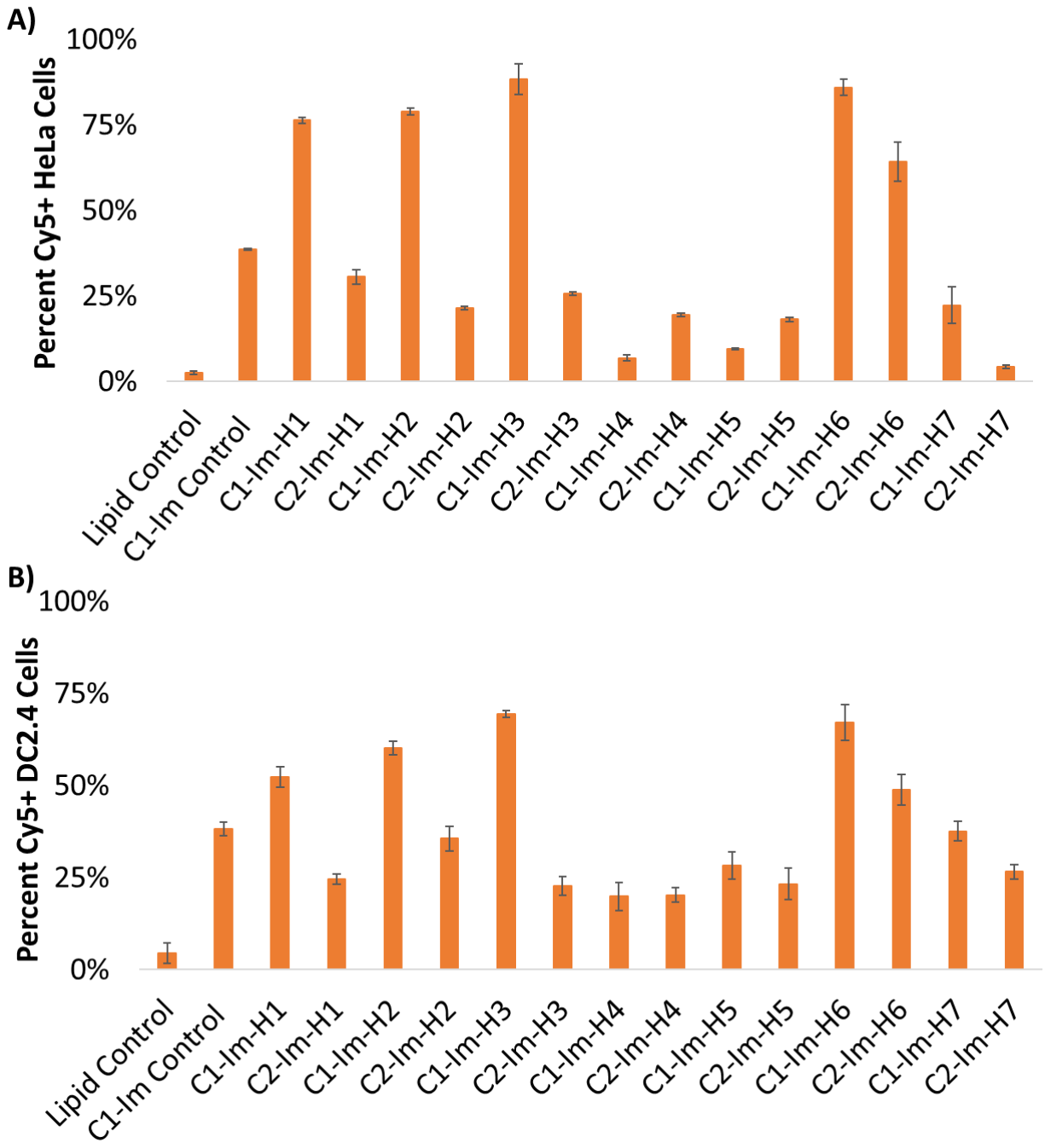

Figure S2.41 Percent of Cy5+ cells after treatment with multifunctional polymer-mRNA nanoparticles containing Cy5-labeled mRNA for **A**) HeLa cells and **B**) DC2.4 cells. Cy5+ cells determined by flow cytometry 48 hours after nanoparticle administration. All nanoparticles formulated at an N/P ratio of 5 and 150 ng of mRNA was administered per 5K cells. Lipofectamine MessengerMAX was used as a lipid control. n=3 for all sample treatments.

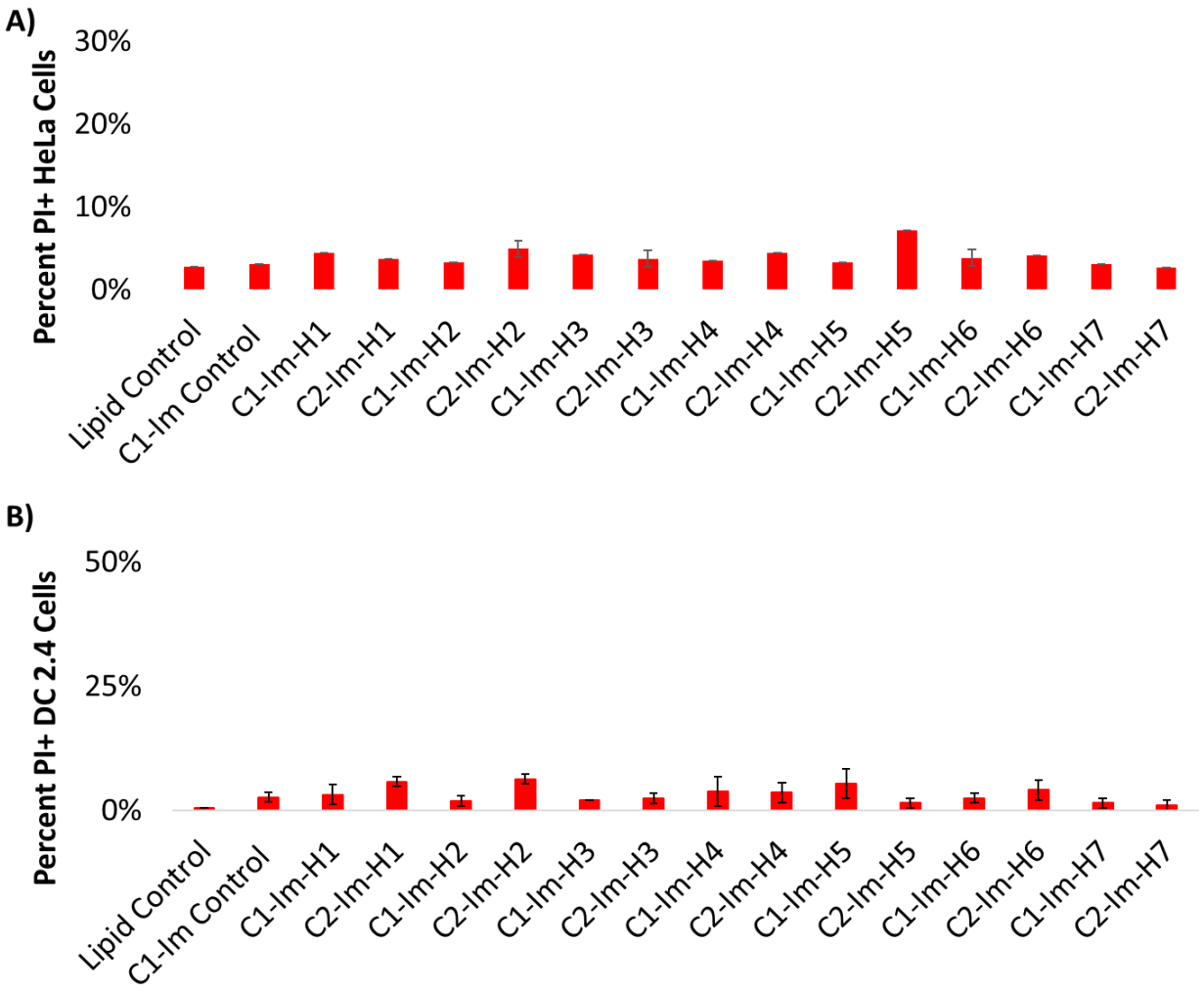

Figure S2.42 Percent of PI+ cells after treatment with multifunctional polymer-mRNA nanoparticles for **A**) HeLa cells and **B**) DC2.4 cells. PI+ cells determined by flow cytometry 6 hours after nanoparticle administration. All nanoparticles formualated at an N/P ratio of 5 and 150 ng of mRNA was administered per 5K cells. Lipofectamine MessengerMAX was used as a lipid control. n=3 for all sample treatments.

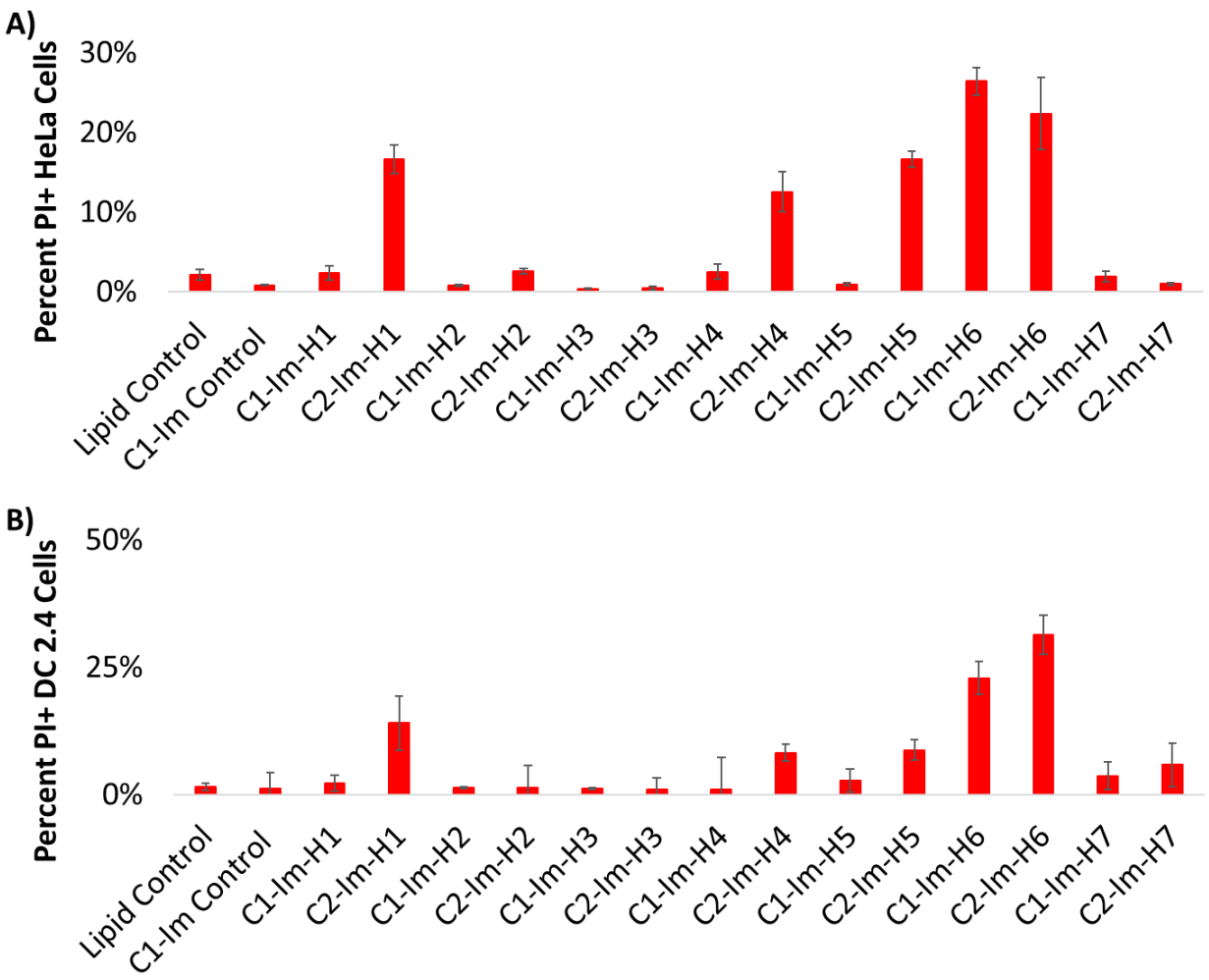

Figure S2.43 Percent of PI+ cells after treatment with multifunctional polymer-mRNA nanoparticles for **A**) HeLa cells and **B**) DC2.4 cells. PI+ cells determined by flow cytometry 48 hours after nanoparticle administration. All nanoparticles formulated at an N/P ratio of 5 and 150 ng of mRNA was administered per 5K cells. Lipofectamine MessengerMAX was used as a lipid control. n=3 for all sample treatments.

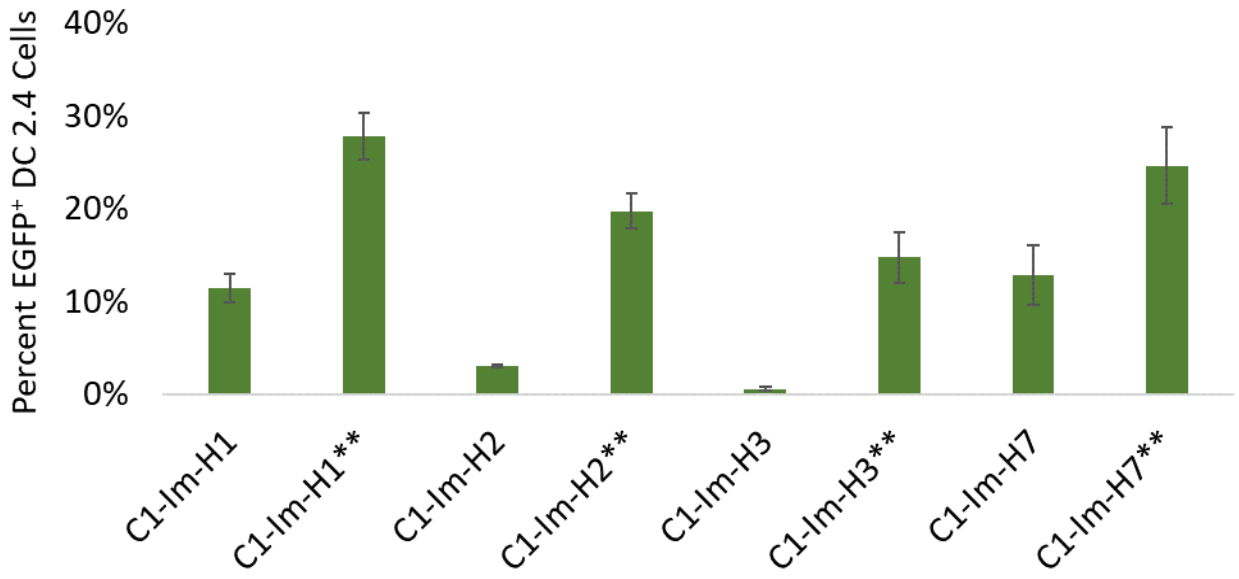

Figure S2.44 Comparison of EGFP+ cells treated with polymeric nanoparticles containing C1-Im-H1, C1-Im-H2, and C1-Im-H3 vectors and supplemental chloroquine (25 μM; chloroquine-containing samples denoted by **). Additional chloroquine provided a minor increase in the number of EGFP+ cells, but EGFP expression is not comparable to best-performing vectors. n=3 for all sample treatments.

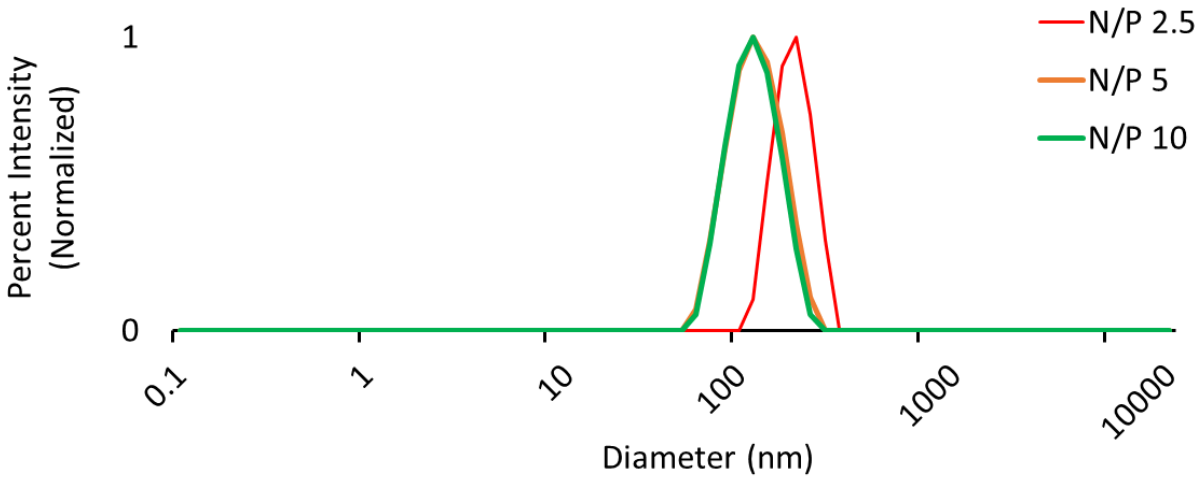

Figure S2.45 Representative DLS signals for OVA mRNA-polymer nanoparticles generated using C2-Im-H1 multifunctional polydisulfide at different N/P ratios. Nanoparticles were complexed and analyzed in pH 4.0 sodium acetate buffer.

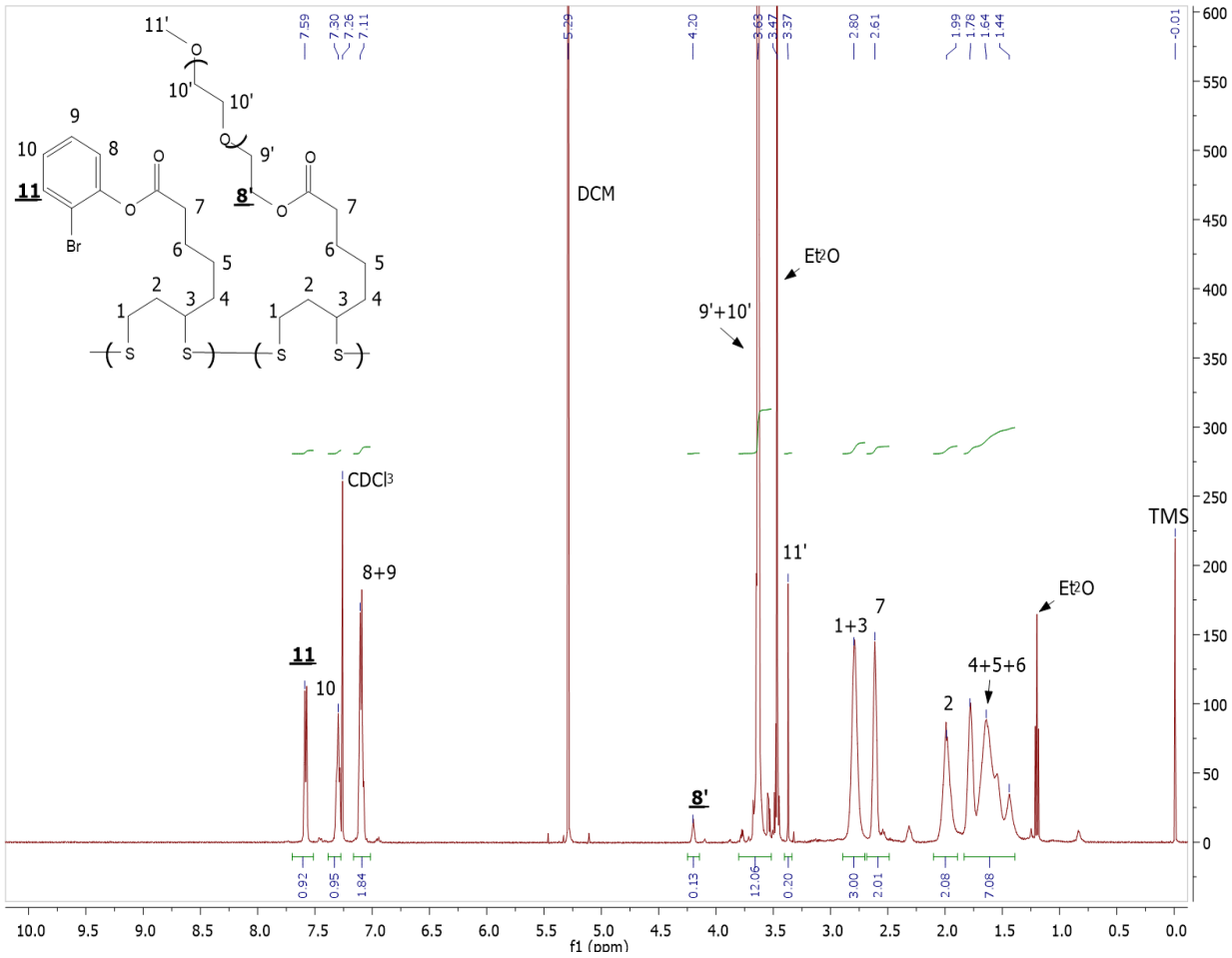

Figure S2.46 ^{1}H NMR of **M2**+LA(PEG 2K) copolymer in $CDCl_3$. Diagnostic peaks used to determine incorporation ratios are bolded and underlined.

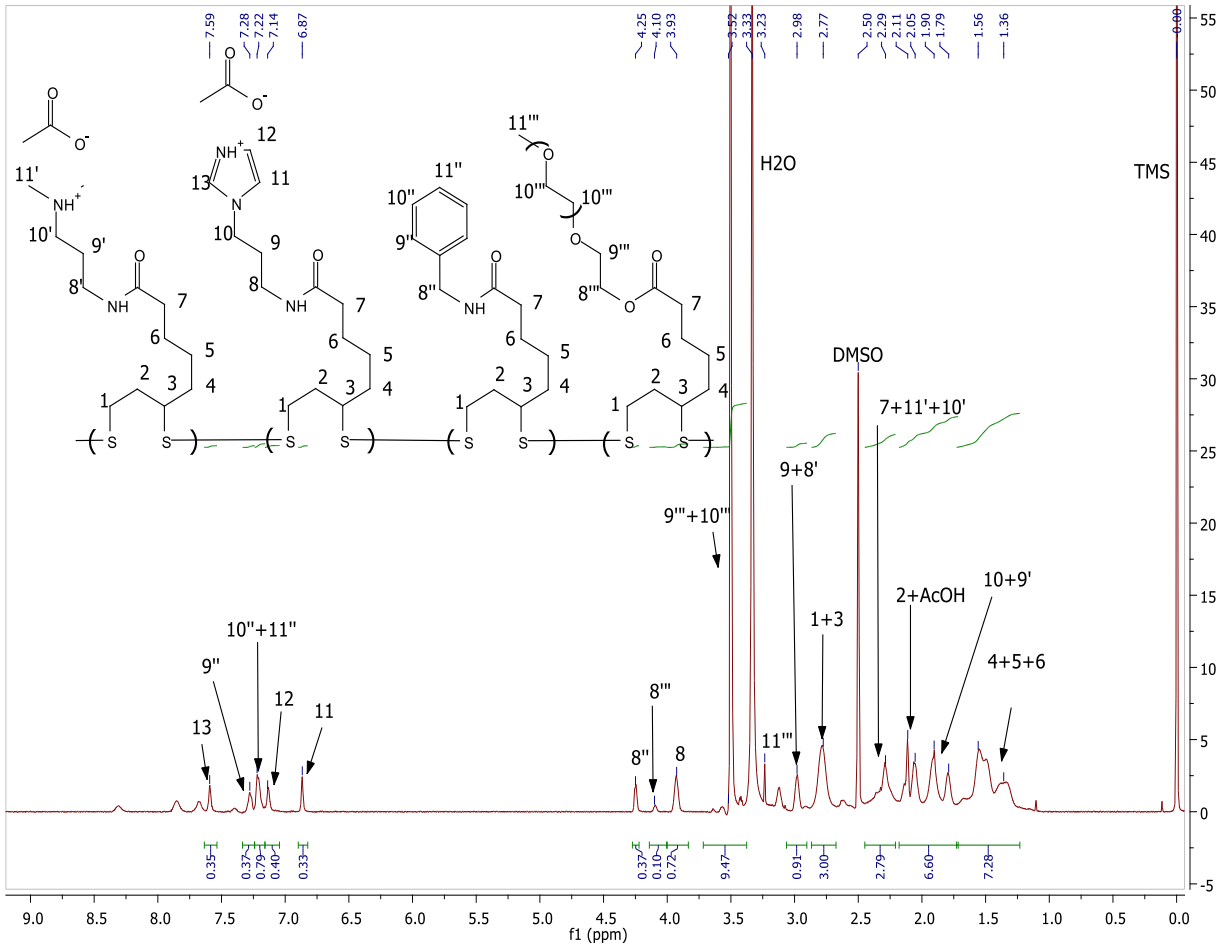

Figure S2.47 ^{1}H NMR of C1-Im-H1-7%PEG in DMSO-*d*6.

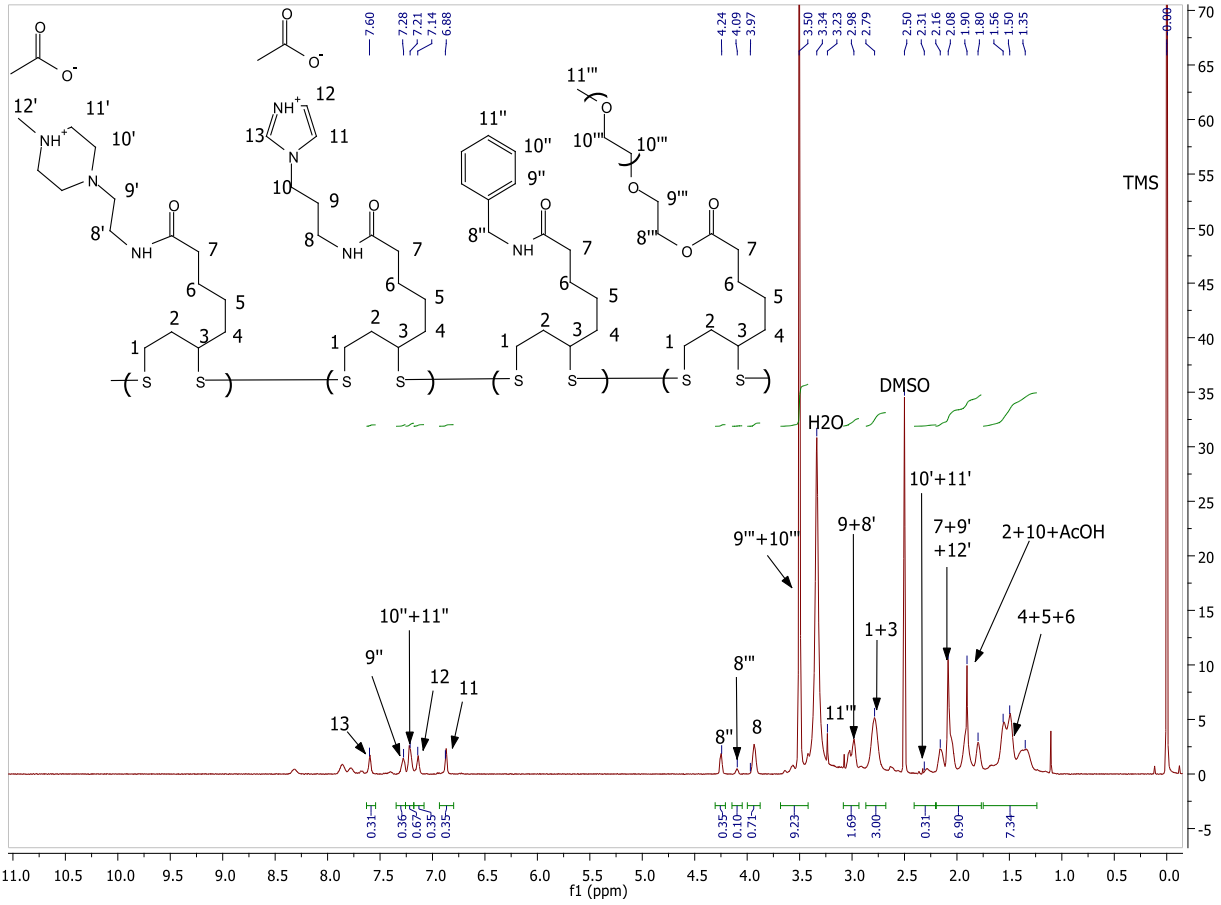

Figure S2.48 ^{1}H NMR of C2-Im-H1-7%PEG in DMSO-*d6*.

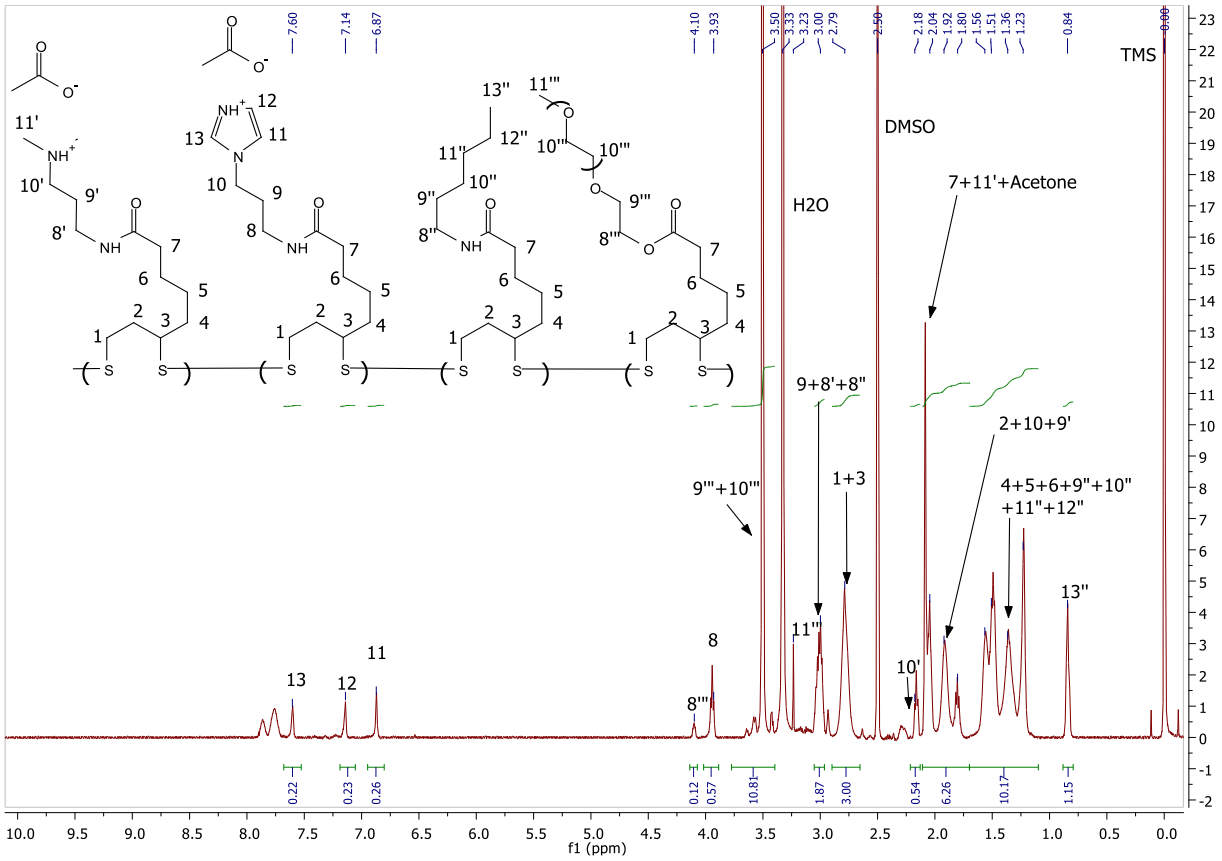

Figure S2.49 ^{1}H NMR of C1-Im-H4-7%PEG in DMSO-*d*6.

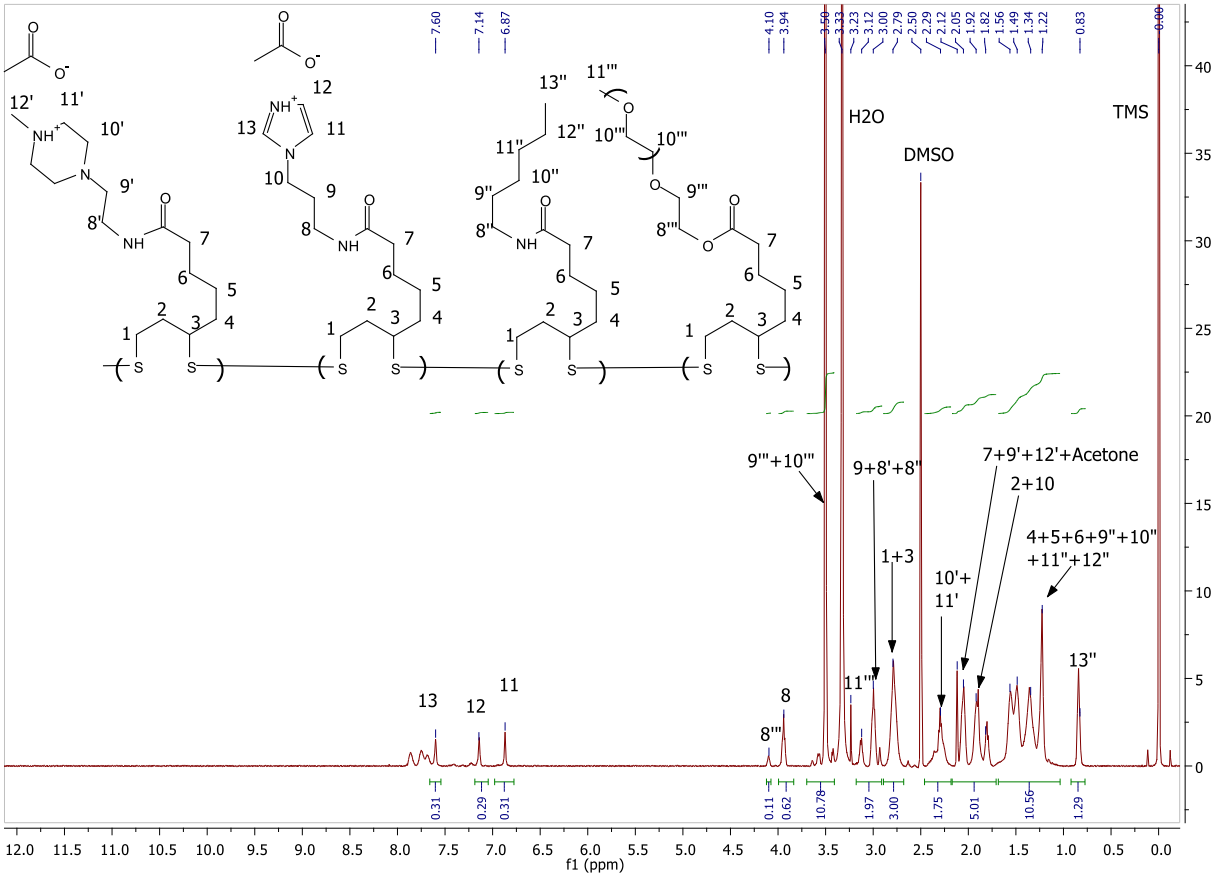

Figure S2.50 ^{1}H NMR of C2-Im-H4-7%PEG in DMSO-*d*6.

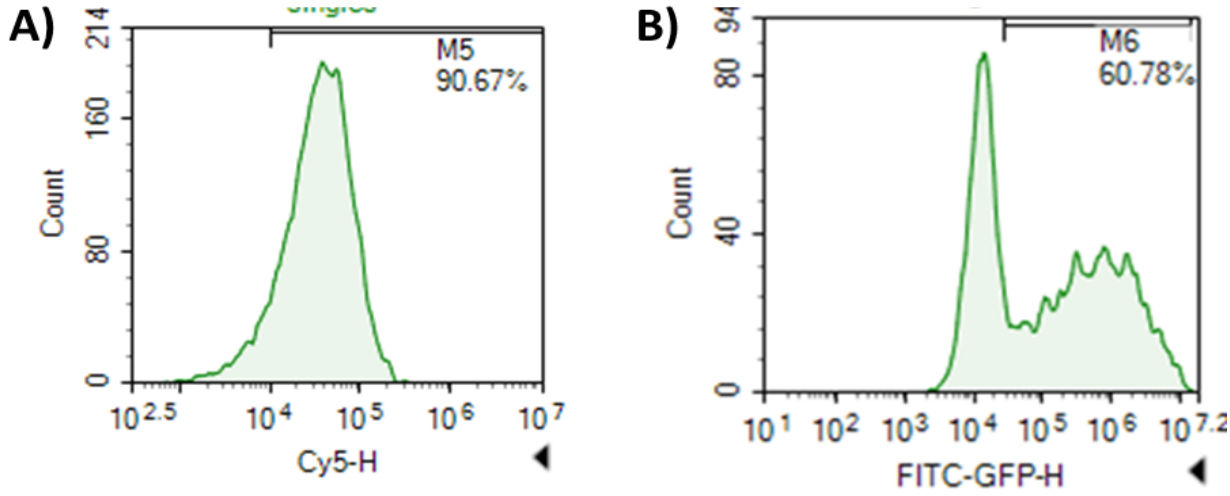

Figure S2.51 A) Representative flow cytometry plot depicting histology gates and for determining number of Cy5+ HeLa cells and **B)** EGFP+ HeLa cells.

Table S2.1. Summary of all **M2** aminolysis conditions using different amine-containing species.

Amine	**Aminolysis Reaction Temperature:**	**% Conversion (via ^{1}H NMR):**
1-(3-Aminopropyl)imidazole (Im)	30 °C	97%
3-Dimethylaminopropylamine (C1)	30 °C	99%
1-(2-Aminoethyl)-4-methylpiperazine (C2)	30 °C	99%
Benzylamine (H1)	30 °C	97%
Tyramine (H2)	30 °C	99%
Tryptamine (H3)	30 °C	98%
Hexylamine (H4)	30 °C	92%
Nonylamine (H5)	35 °C	95%
Dodecylamine (H6)	40 °C	92%
Oleylamine (H7)	40 °C	97%

Table S2.2 Summary of all post-polymerization multifunctional polymers generated from poly(**M2**)disulfide.

Target Amine Ratio	Aminolysis Reaction Temperature:	Estimated Ratio in Polymer (from ^{1}H NMR):	% Yield
100% Im	30 °C	100% Im	53.4%
20% C1: 80% Im	30 °C	16% C1: 82% Im	68.7%
25% C1: 50% Im: 25% H1	30 °C	28% C1: 37% Im: 23% H1	72.6%
25% C1: 50% Im: 25% H2	30 °C	25% C1: 48% Im: 23% H2	70.5%
25% C1: 50% Im: 25% H3	30 °C	20% C1: 43% Im: 20% H3	89.2%
25% C1: 50% Im: 25% H4	30 °C	22% C1: 54% Im: 20% H4	42.0%
25% C1: 50% Im: 25% H5	35 °C	25% C1: 48% Im: 22% H5	40.4%
25% C1: 50% Im: 25% H6	45 °C	23% C1: 28% Im: 36% H6	58.1%
25% C1: 50% Im: 25% H7	40 °C	29% C1: 37% Im: 32% H7	65.3%
25% C2: 50% Im: 25% H1	30 °C	26% C2: 46% Im: 22% H1	78.7%
25% C2: 50% Im: 25% H2	30 °C	26% C2: 48% Im: 22% H2	68.2%
25% C2: 50% Im: 25% H3	30 °C	28% C2: 42% Im: 21% H3	79.9%
25% C2: 50% Im: 25% H4	30 °C	28% C2: 46% Im: 26% H4	41.8%
25% C2: 50% Im: 25% H5	35 °C	27% C2: 50% Im: 22% H5	43.7%
25% C2: 50% Im: 25% H6	45 °C	23% C2: 50% Im: 26% H6	62.6%
25% C2: 50% Im: 25% H7	40 °C	33% C2: 38% Im: 27% H7	70.2%

Table S2.3 Summary of EGFP mRNA-multifunctional polymer nanoparticles as determined by DLS. All nanoparticles complexed and measured in pH 4 sodium acetate buffer.

Multifunctional Polymer Composition:	Z-Average Diameter (nm):	Dispersity (*D*):
C1-Im	223.6 +/- 3.8	0.23
C1-Im-H1	143.3 +/- 3.8	0.20
C1-Im-H2	149.8 +/- 5.6	0.18
C1-Im-H3	142.9 +/- 9.6	0.25
C1-Im-H4	124.8 +/- 2.8	0.21
C1-Im-H5	112.0 +/- 8.1	0.26
C1-Im-H6	112.6 +/- 5.0	0.29
C1-Im-H7	156.2 +/- 4.4	0.19
C2-Im-H1	137.3 +/- 4.1	0.24
C2-Im-H2	130.9 +/- 3.4	0.25
C2-Im-H3	135.2 +/- 4.5	0.23
C2-Im-H4	146.6 +/- 5.3	0.27
C2-Im-H5	116.5 +/- 4.3	0.26
C2-Im-H6	145.2 +/- 4.1	0.27
C2-Im-H7	151.0 +/- 6.2	0.31

Table S2.4 Stability of multifunctional polymer nanoparticles without mRNA after switching from pH 4.0 buffer to PBS (pH 7.4), characterized by DLS.

Multifunctional Polymer Composition:	Time (Minutes):	Z-Average Diameter (nm):	Dispersity (*D*):
C1-Im-H1	0	61.0	0.30
C1-Im-H1	30	299.4	0.25
C1-Im-H1	60	403.7	0.42
C1-Im-H4	0	92.1	0.44
C1-Im-H4	30	186.8	0.42
C1-Im-H4	60	268.9	0.32
C1-Im-H7	0	132.6	0.21
C1-Im-H7	30	161.0	0.67
C1-Im-H7	60	171.7	0.17
C2-Im-H1	0	62.4	0.15
C2-Im-H1	30	228.9	0.13
C2-Im-H1	60	297.5	0.20
C2-Im-H4	0	81.8	0.38
C2-Im-H4	30	109.1	0.28
C2-Im-H4	60	124.0	0.28
C2-Im-H7	0	71.6	0.32
C2-Im-H7	30	69.72	0.38
C2-Im-H7	60	70.39	0.38

Table S2.5 Stability of multifunctional polymer nanoparticles formulated with EGFP mRNA after switching from pH 4.0 buffer to PBS (pH 7.4), characterized by DLS.

Multifunctional Polymer Composition:	Time (Minutes):	Z-Average Diameter (nm):	Dispersity (*D*):
C1-Im-H1	0	143.3	0.20
C1-Im-H1	30	251.4	0.29
C1-Im-H1	60	531.4	0.26
C1-Im-H4	0	124.8	0.21
C1-Im-H4	30	250.3	0.19
C1-Im-H4	60	448.8	0.22
C1-Im-H7	0	156.2	0.19
C1-Im-H7	30	237.2	0.22
C1-Im-H7	60	239.7	0.19
C2-Im-H1	0	137.3	0.24
C2-Im-H1	30	189.1	0.19
C2-Im-H1	60	388.6	0.19
C2-Im-H4	0	146.6	0.27
C2-Im-H4	30	157.2	0.28
C2-Im-H4	60	237.0	0.28
C2-Im-H7	0	151.0	0.31
C2-Im-H7	30	275.4	0.26
C2-Im-H7	60	290.2	0.27

Table S2.6 Summary of model multifunctional polymer nanoparticles formulated with OVA mRNA in pH 4.0 buffer, characterized by DLS.

Sample:	N/P Ratio:	Z-Average Diameter (nm):	Dispersity (D):
C2-Im-H1	2.5	217.5	0.18
C2-Im-H1	5	132.2	0.10
C2-Im-H1	10	118.7	0.22

2.8 Small Molecule Characterization Data (^{1}H NMR, ^{13}C NMR, LC-MS, ESI-MS, GPC)

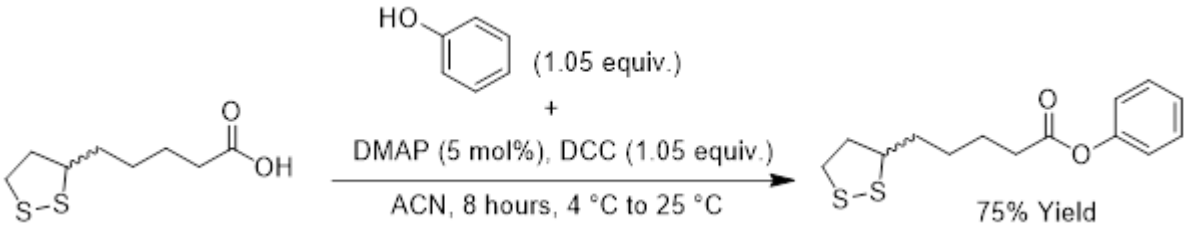

Scheme S2.1. Synthesis of **M1.**

M1 Yield: 5.13 grams, 75%
^{1}H NMR ($CDCl_3$, 500 MHz): δ(ppm)= 7.40-7.30 (t, *J*= 8.5 Hz, 2H), 7.25-7.17 (t, *J*= 7.5 Hz 1H), 7.12-7.00 (d, *J*= 8.5 Hz, 2H), 3.65-3.50 (quint, *J*= 6.5 Hz, 1H), 3.25-3.05 (m, 2H), 2.62-2.53 (t, *J*= 7.5 Hz, 2H), 2.51-2.41 (m, 1H), 1.98-1.87 (m, 1H), 1.85-1.69 (m, 4H), 1.65-1.50 (m,2H); ^{13}C NMR ($CDCl_3$, 500 MHz): δ(ppm)= 171.80, 150.60, 129.39, 125.74, 121.51, 56.24, 40.19, 38.47, 34.55, 34.06, 28.64, 24.59; LC-MS: $C_{14}H_{18}O_2S_2$ [M+H$^+$], Calculated 283.07, Found 282.0. The LC-MS, ^{1}H and ^{13}C NMR spectra of **M1** are attached below:

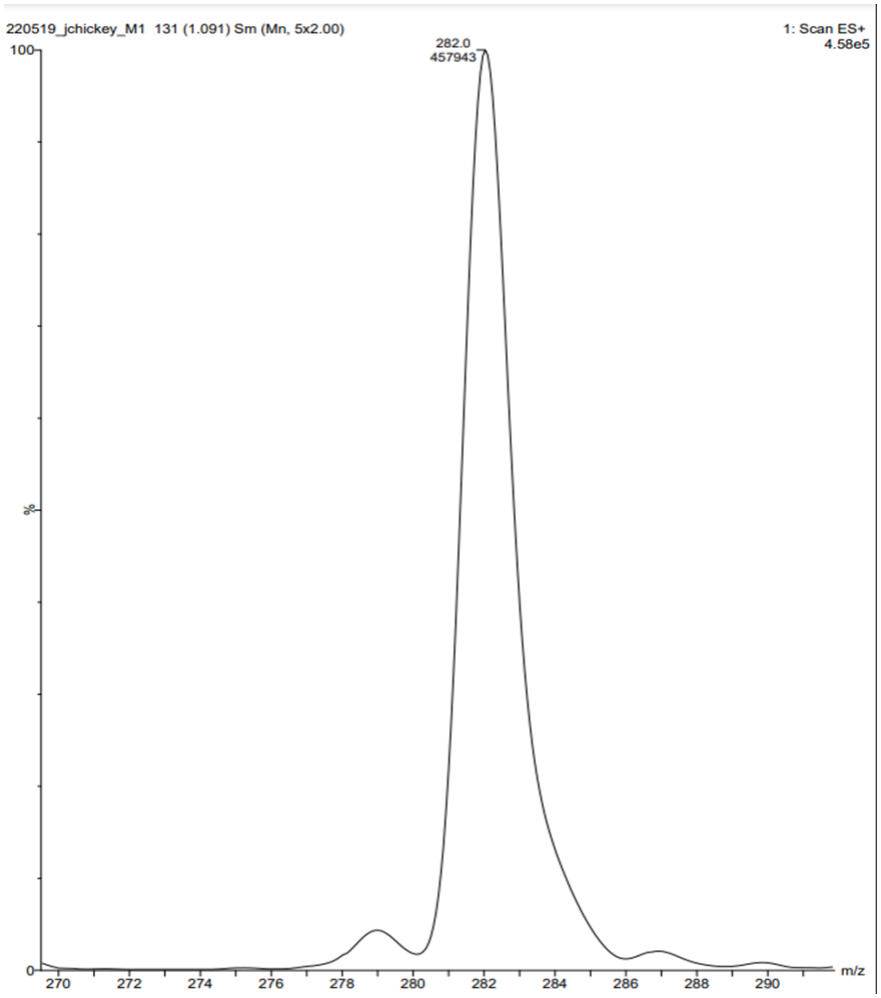

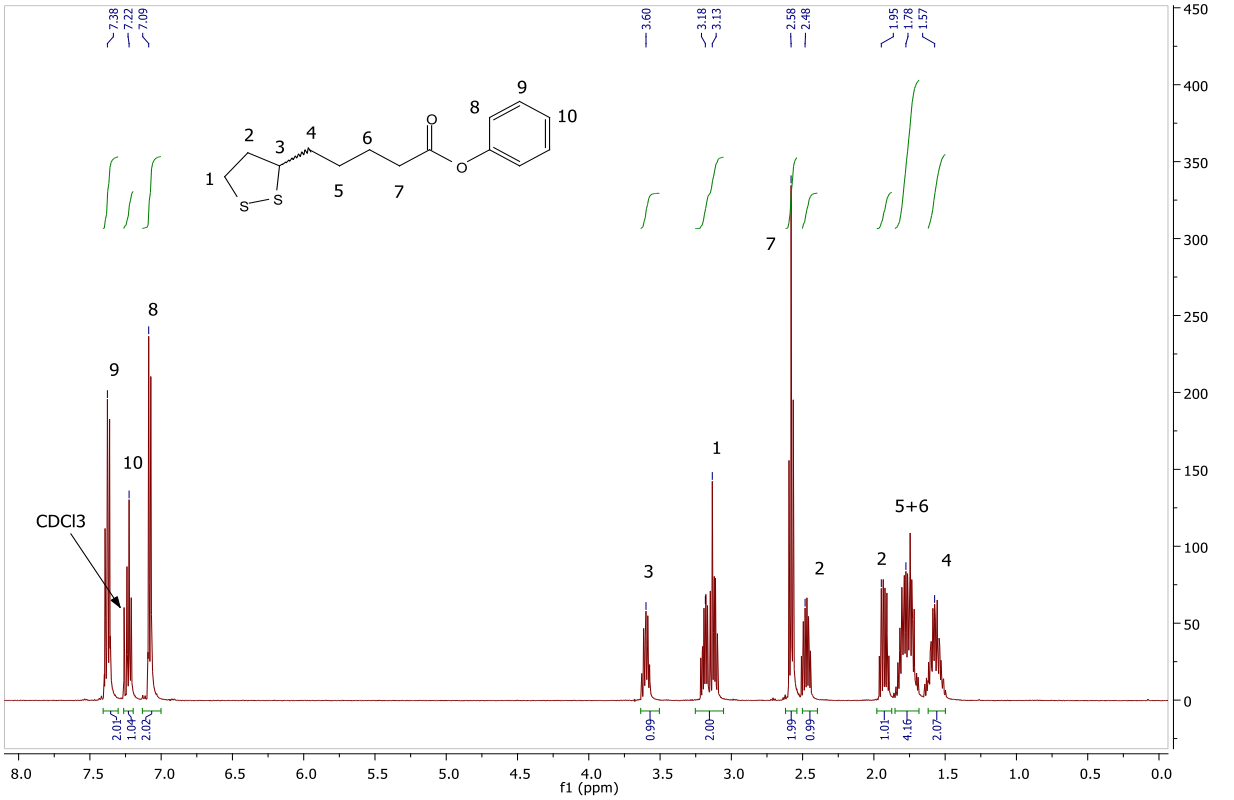
7.38
7.22
7.09
3.60
3.18
3.13
2.58
2.48
1.95
1.78
1.57
CDCl3
f1 (ppm)

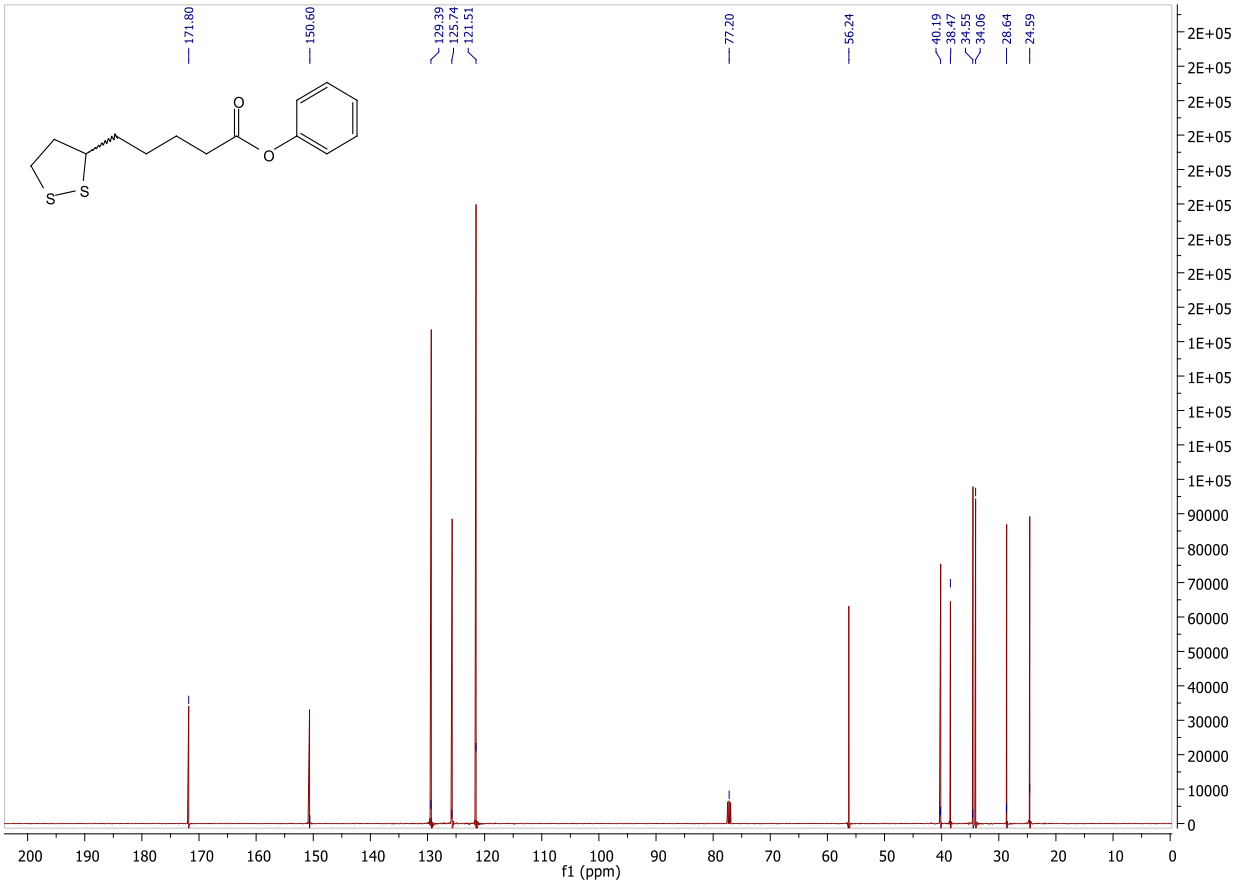
171.80
150.60
129.39
125.74
121.51
77.20
56.24
40.19
38.47
34.55
34.06
28.64
24.59
f1 (ppm)

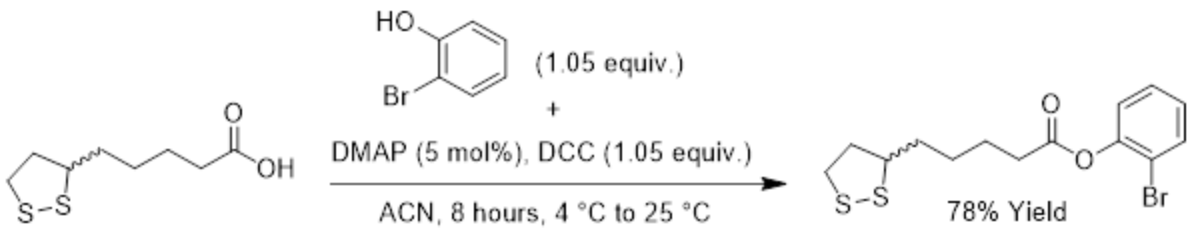

Scheme S2.2. Synthesis of **M2.**

M2 Yield: 6.80 grams, 78%
^{1}H NMR ($CDCl_3$, 500 MHz): δ(ppm)= 7.63-7.57 (d, *J*= 6.5 Hz, 1H), 7.36-7.30 (t, *J*= 8.0 Hz, 1H), 7.16-7.10 (m, 2H), 3.64-3.56 (quint, *J*= 6.0 Hz, 1H), 3.25-3.05 (m, 2H), 2.67-2.62 (t, *J*= 7.0 Hz, 2H), 2.52-2.44 (m, 1H), 1.97-1.89 (m, 1H), 1.88-1.71 (m, 4H), 1.66-1.55 (m,2H); ^{13}C NMR ($CDCl_3$, 500 MHz): δ(ppm)= 171.19, 148.40, 133.55, 128.69, 127.52, 124.02, 116.39, 56.47, 40.51, 38.81, 35.09, 34.13, 28.88, 24.70; LC-MS: $C_{14}H_{17}BrO_2S_2$ [M+H$^+$], Calculated 360.99., Found 361.8. The LC-MS, ^{1}H and ^{13}C NMR spectra of **M2** are attached below:

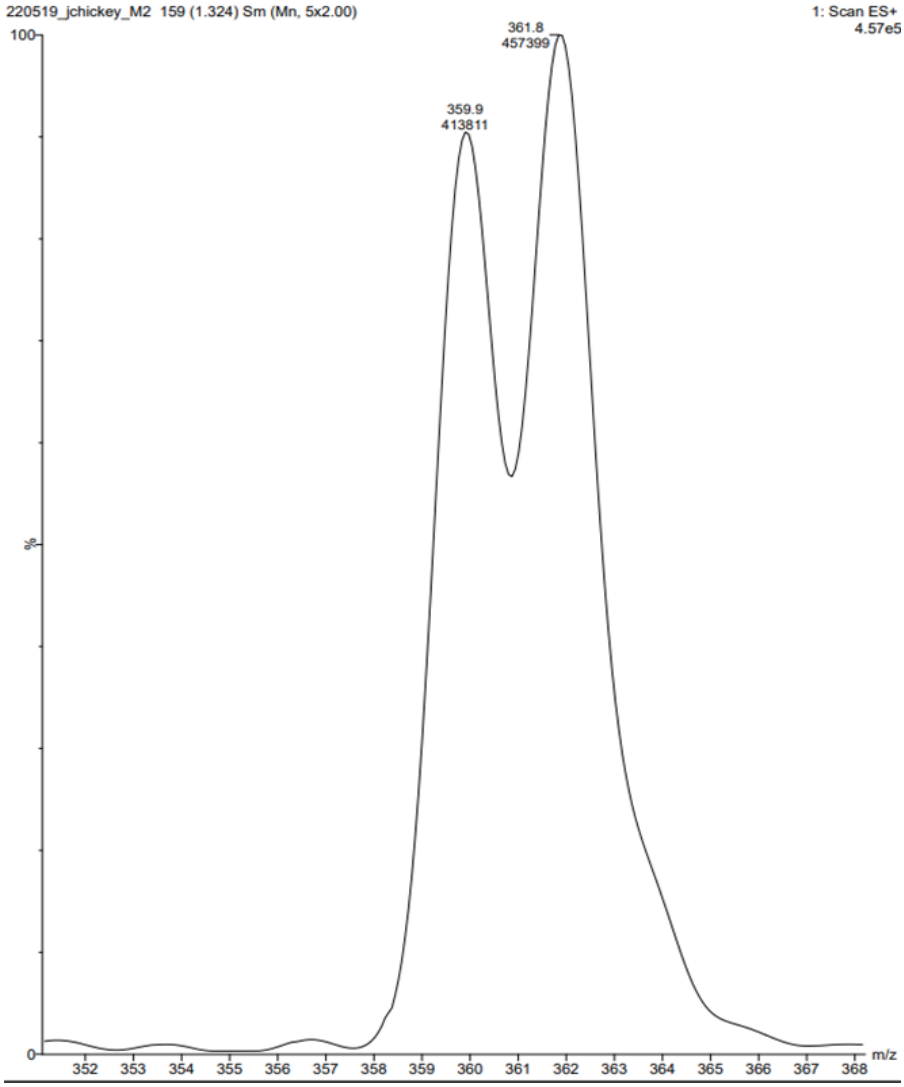

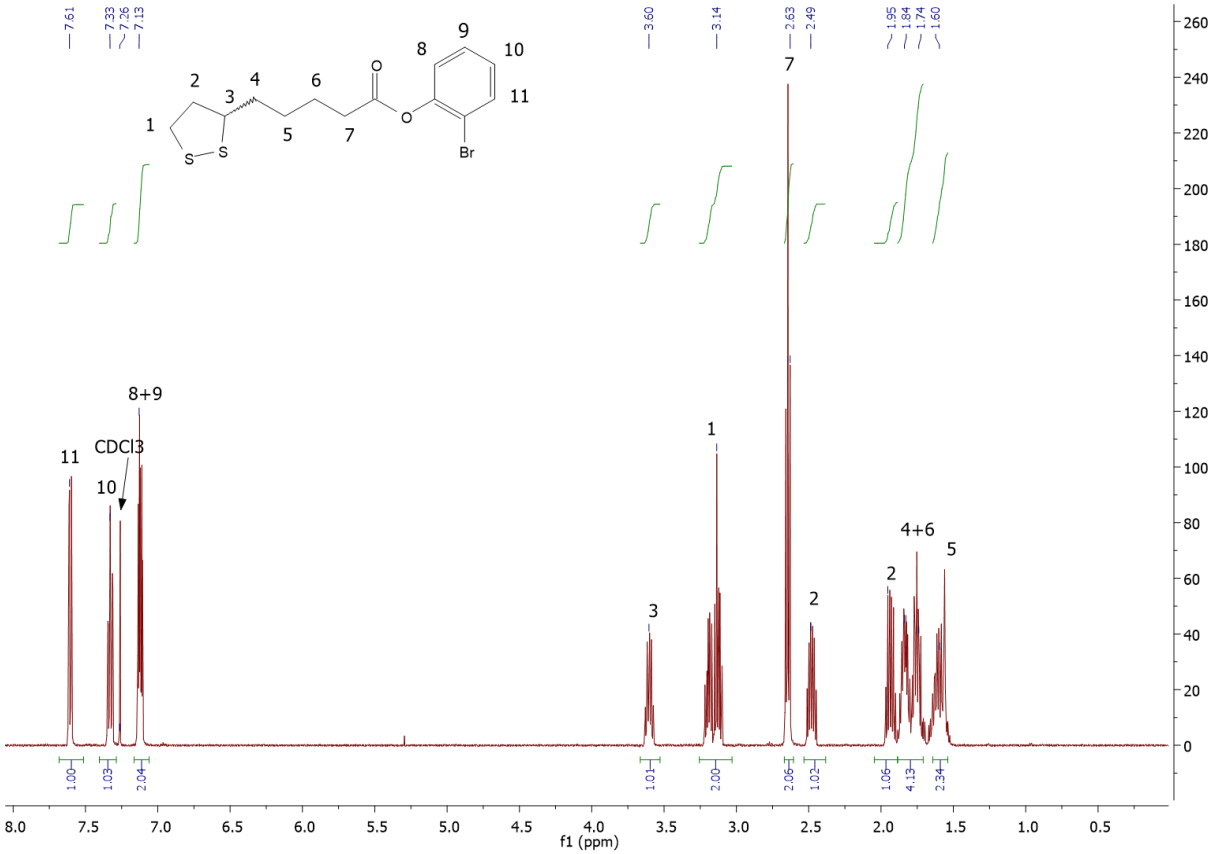
7.61
7.33
7.26
7.13
3.60
3.14
2.63
2.49
1.95
1.84
1.74
1.60
8+9
11
CDCl3
10
1
7
3
2
4+6
5
1.00
1.03
2.04
1.01
2.00
2.06
1.02
1.06
4.13
2.34
f1 (ppm)

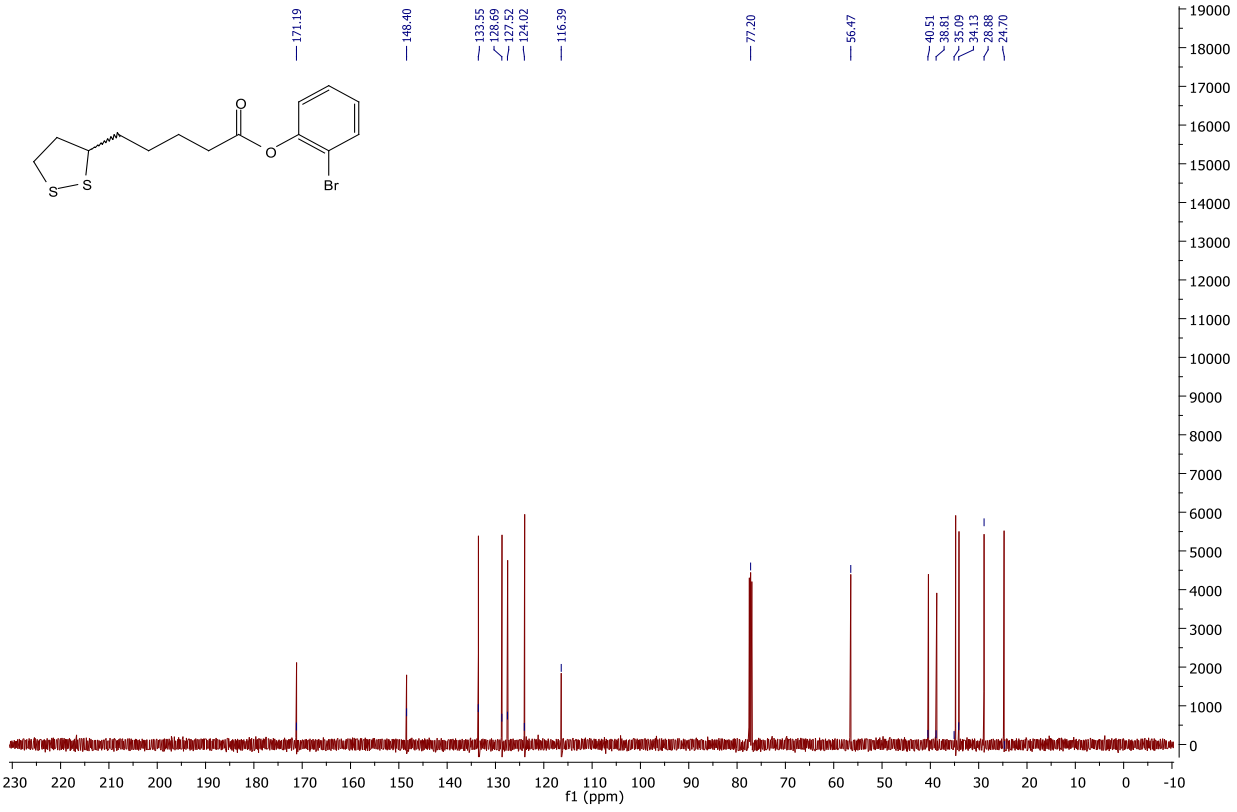
171.19
148.40
133.55
128.69
127.52
124.02
116.39
77.20
56.47
40.51
38.81
35.09
34.13
28.88
24.70
f1 (ppm)

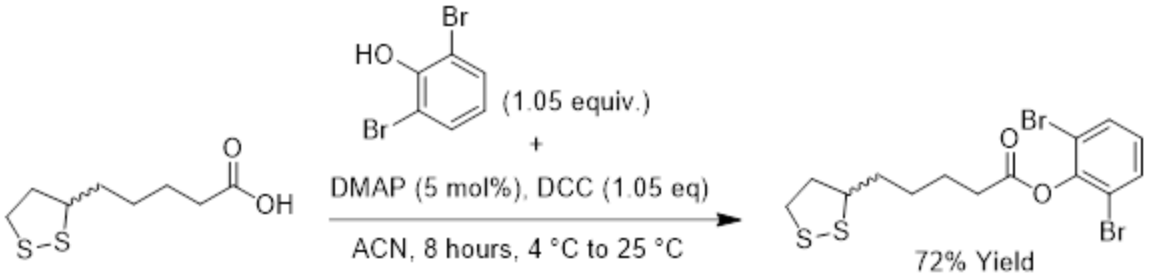

Scheme S2.3. Synthesis of **M3.**

M3 Yield: 7.64 grams, 72%
^{1}H NMR ($CDCl_3$, 500 MHz): δ(ppm)= 7.55-7.47 (d, *J*= 8.5 Hz, 2H), 7.00-6.93 (t, *J*= 8.0 Hz, 1H), 3.61-3.50 (quint, *J*= 6.5 Hz, 1H), 3.20-3.03 (m, 2H), 2.70-2.63 (t, *J*= 7.0 Hz, 2H), 2.48-2.38 (m, 1H), 1.94-1.87 (m, 1H), 1.86-1.77 (m, 2H), 1.76-1.66 (m, 2H), 1.65-1.48 (m,2H); ^{13}C NMR ($CDCl_3$, 500 MHz): δ(ppm)= 169.56, 146.07, 132.31, 128.14, 117.75, 56.26, 40.17, 38.49, 34.50, 33.60, 28.65, 24.43; LC-MS: $C_{14}H_{16}Br_2O_2S_2$ [M+H$^+$], Calculated 439.89, Found 439.8. The LC-MS, ^{1}H and ^{13}C NMR spectra of **M3** are attached below:

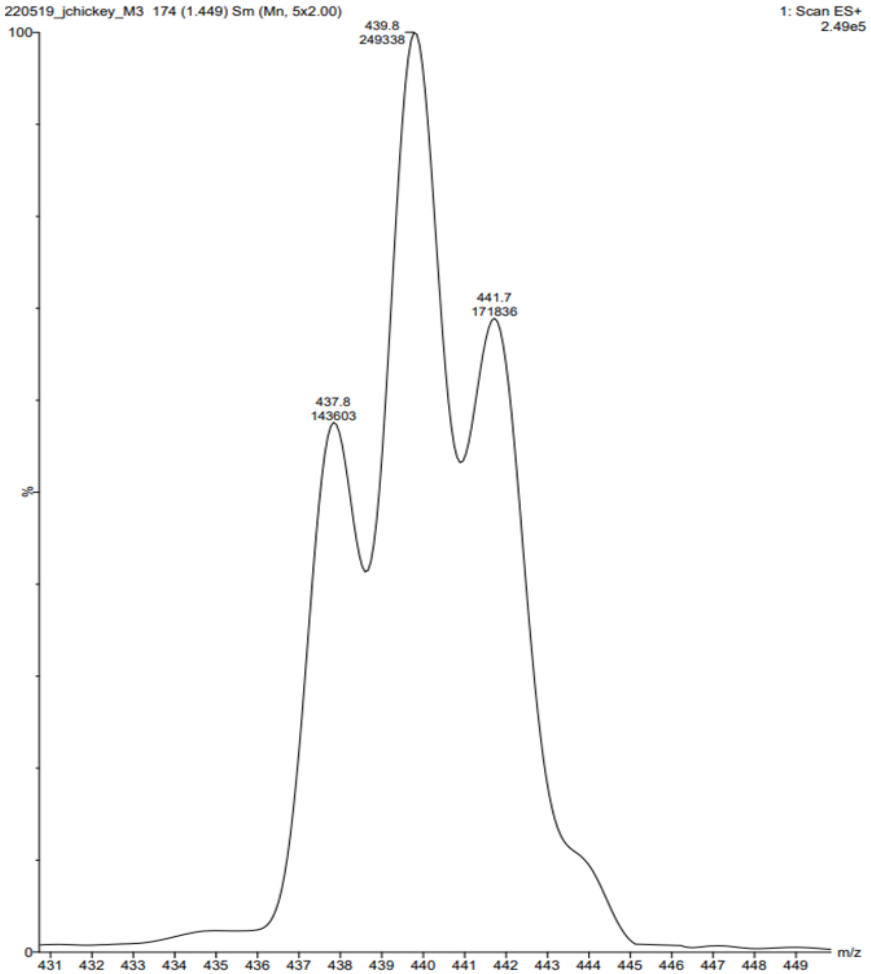

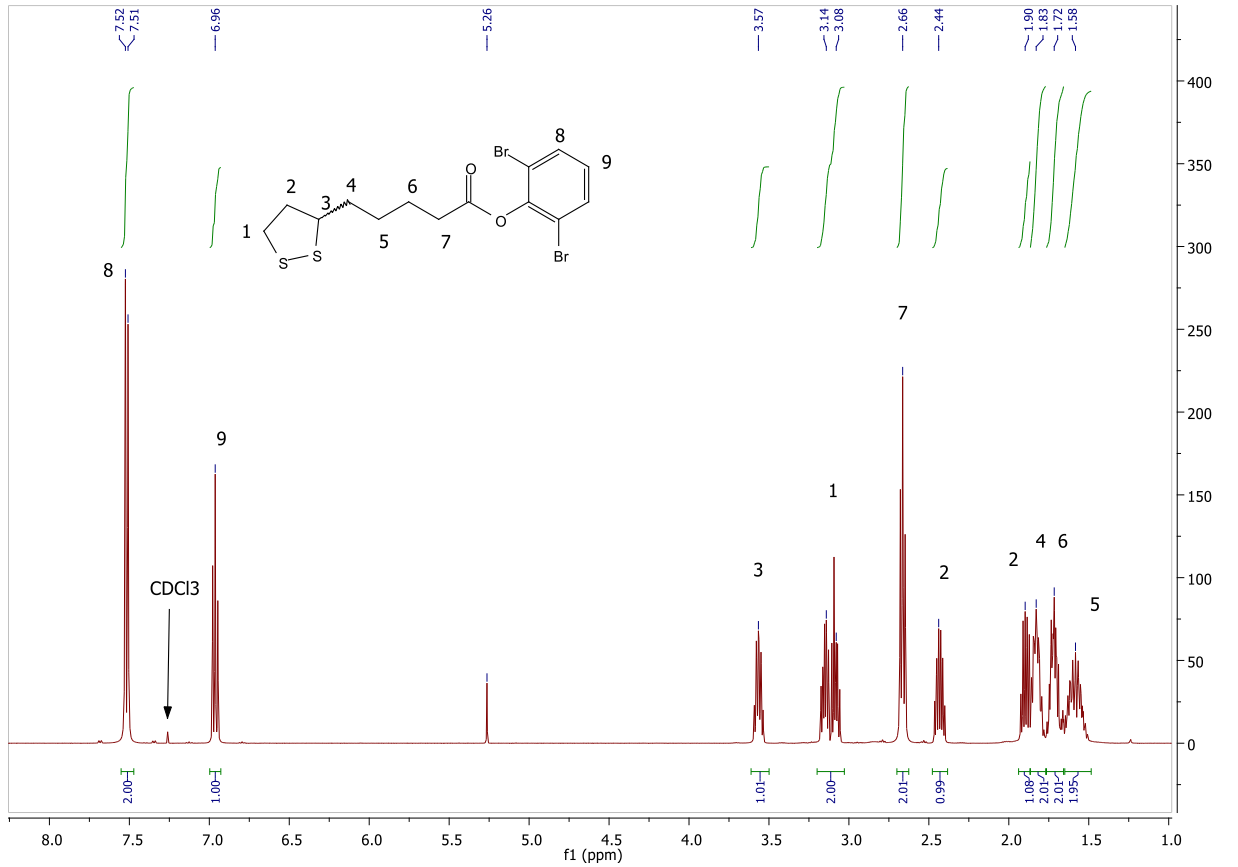
7.52
7.51
6.96
5.26
3.57
3.14
3.08
2.66
2.44
1.90
1.83
1.72
1.58
CDCl3
f1 (ppm)

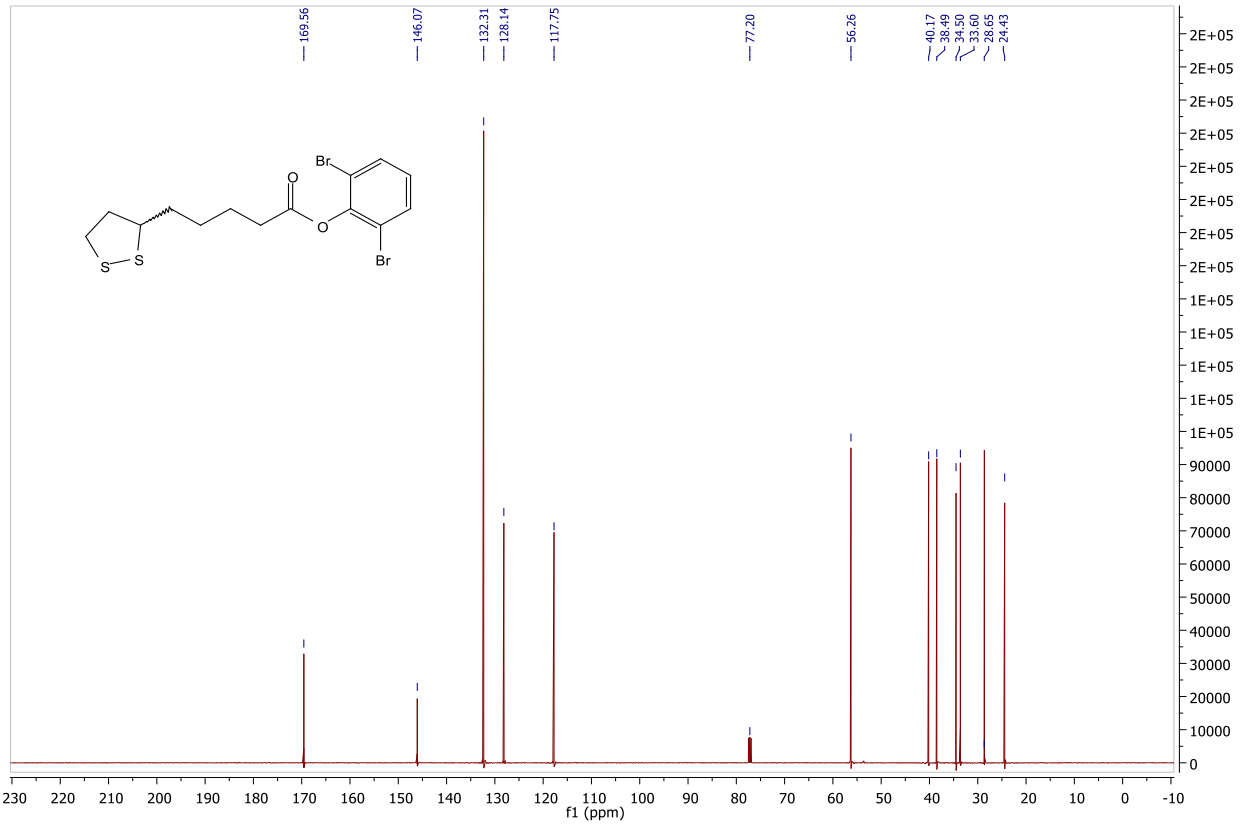
169.56
146.07
132.31
128.14
117.75
77.20
56.26
40.17
38.49
34.50
33.60
28.65
24.43
f1 (ppm)

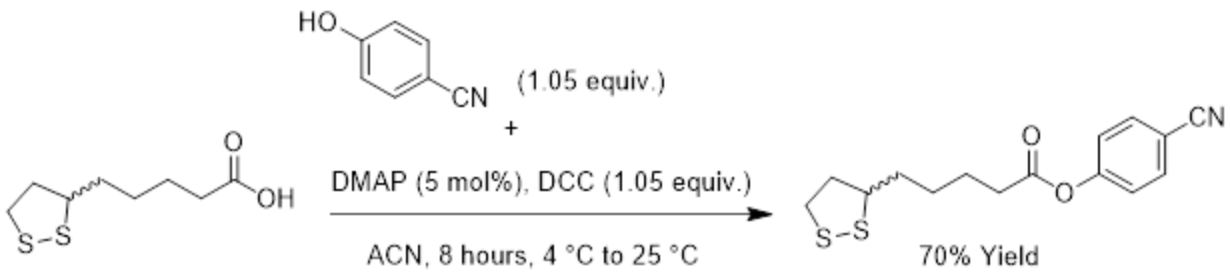

Scheme S2.4. Synthesis of **M4.**

M4 Yield: 5.21 grams, 70%

^{1}H NMR ($CDCl_3$, 500 MHz): δ(ppm)= 7.73-7.65 (d, *J*= 9.0 Hz, 2H), 7.25-7.17 (d, *J*= 9.0 Hz, 2H), 3.65-3.55 (quint, *J*= 6.5 Hz, 1H), 3.24-3.07 (m, 2H), 2.65-2.58 (t, *J*= 7.5 Hz, 2H), 2.52-2.43 (m, 1H), 1.97-1.87 (m, 1H), 1.83-1.768 (m, 4H), 1.63-1.50 (m, 2H); ^{13}C NMR ($CDCl_3$, 500 MHz): δ(ppm)= 171.13, 154.03, 133.74, 122.81, 118.32, 109.77, 56.34, 40.34, 38.61, 34.63, 34.15, 28.72, 24.54; LC-MS: $C_{15}H_{17}NO_2S_2$ [M+H$^+$], Calculated 307.07, Found 307.0. The LC-MS, ^{1}H and ^{13}C NMR spectra of **M4** are attached below:

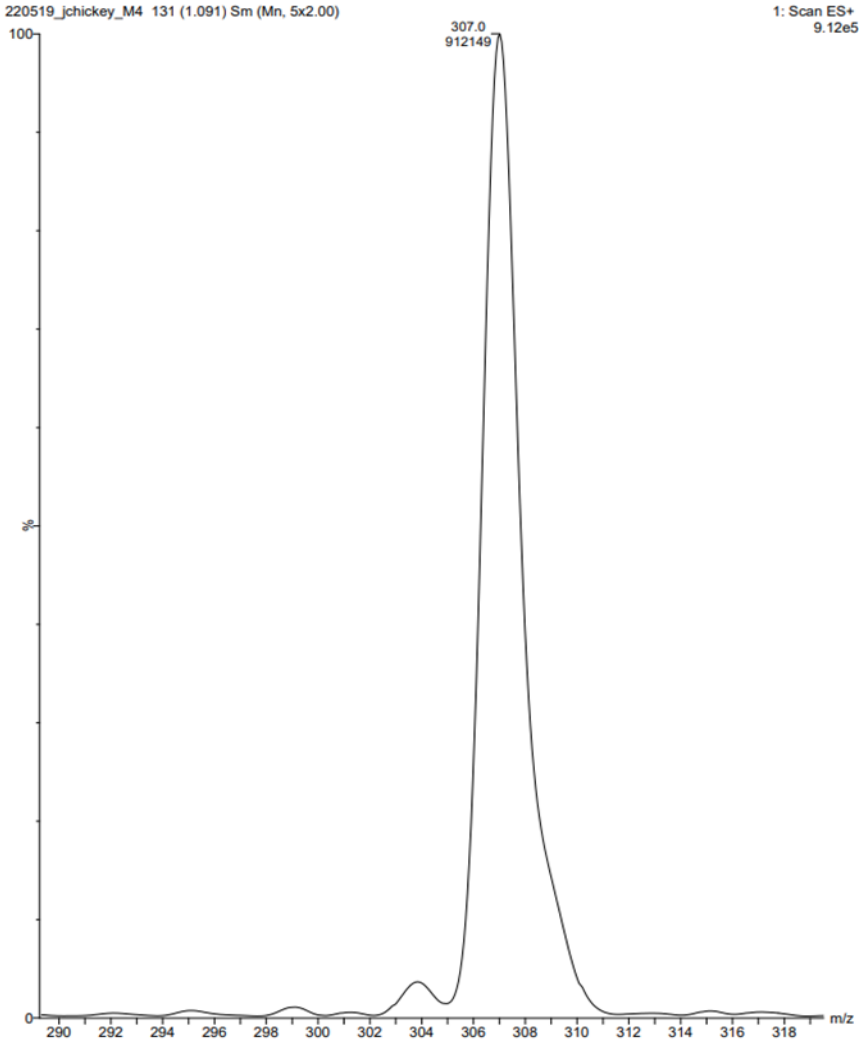

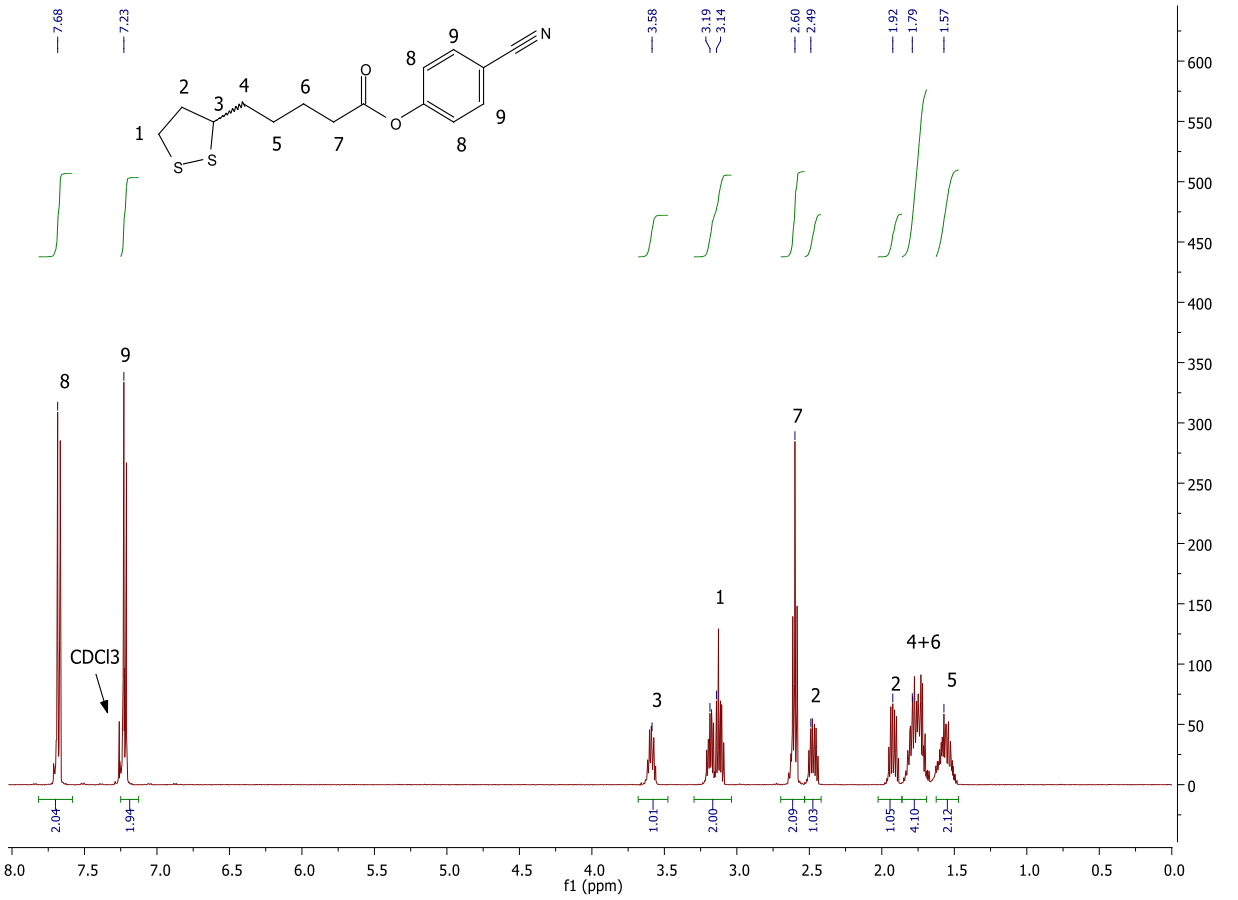
7.68
7.23
3.58
3.19
3.14
2.60
2.49
1.92
1.79
1.57
CDCl3
f1 (ppm)

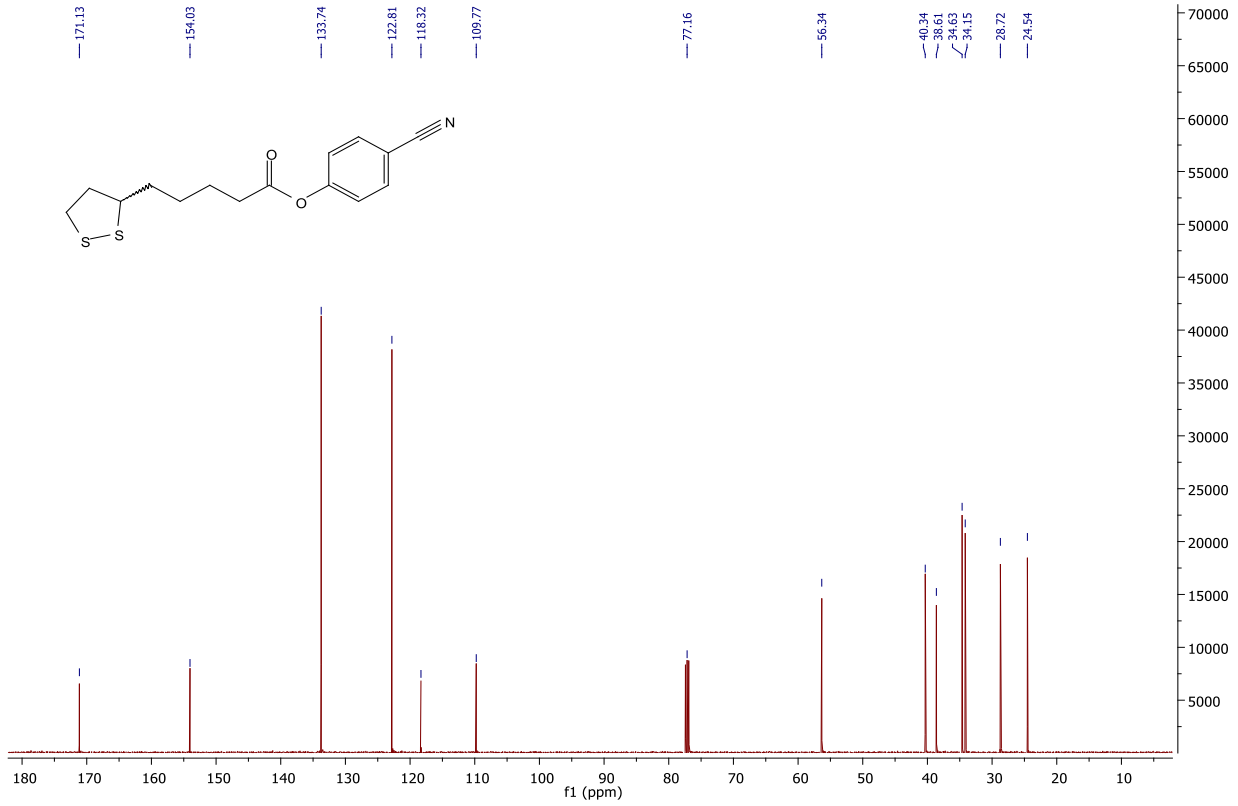
171.13
154.03
133.74
122.81
118.32
109.77
77.16
56.34
40.34
38.61
34.63
34.15
28.72
24.54
f1 (ppm)

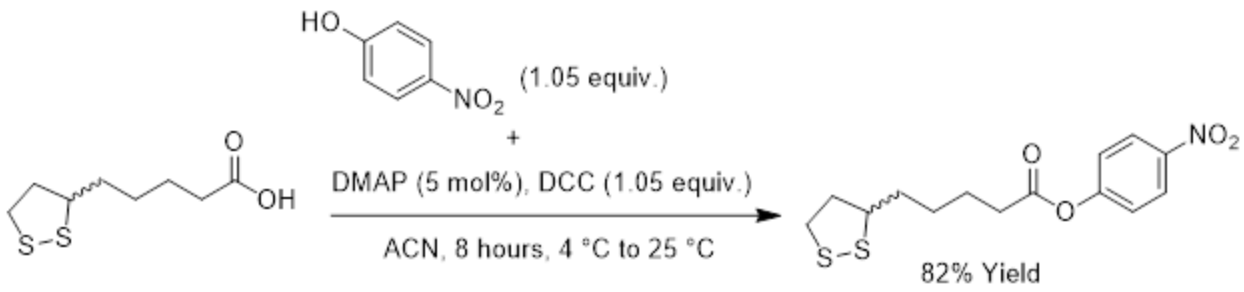

Scheme S2.5. Synthesis of **M5.**

M5 Yield: 6.50 grams, 82%
^{1}H NMR ($CDCl_3$, 500 MHz): δ(ppm)= 8.32-8.20 (d, *J*= 9.5 Hz, 2H), 7.30-7.25 (d, *J*= 9.0 Hz, 2H), 3.65-3.55 (quint, *J*= 6.5 Hz, 1H), 3.25-3.07 (m, 2H), 2.66-2.59 (t, *J*= 7.5 Hz, 2H), 2.53-2.43 (m, 1H), 1.97-1.89 (m, 1H), 1.86-1.70 (m, 4H), 1.64-1.50 (m, 2H); ^{13}C NMR ($CDCl_3$, 500 MHz): δ(ppm)= 170.96, 155.55, 145.41, 125.23, 22.47, 56.33, 40.32, 38.60, 34.61, 34.16, 28.67, 24.53; LC-MS: $C_{15}H_{17}NO_4S_2$ [M+H$^+$], Calculated 327.06, Found 326.9. The LC-MS, ^{1}H and ^{13}C NMR spectra of **M5** are attached below:

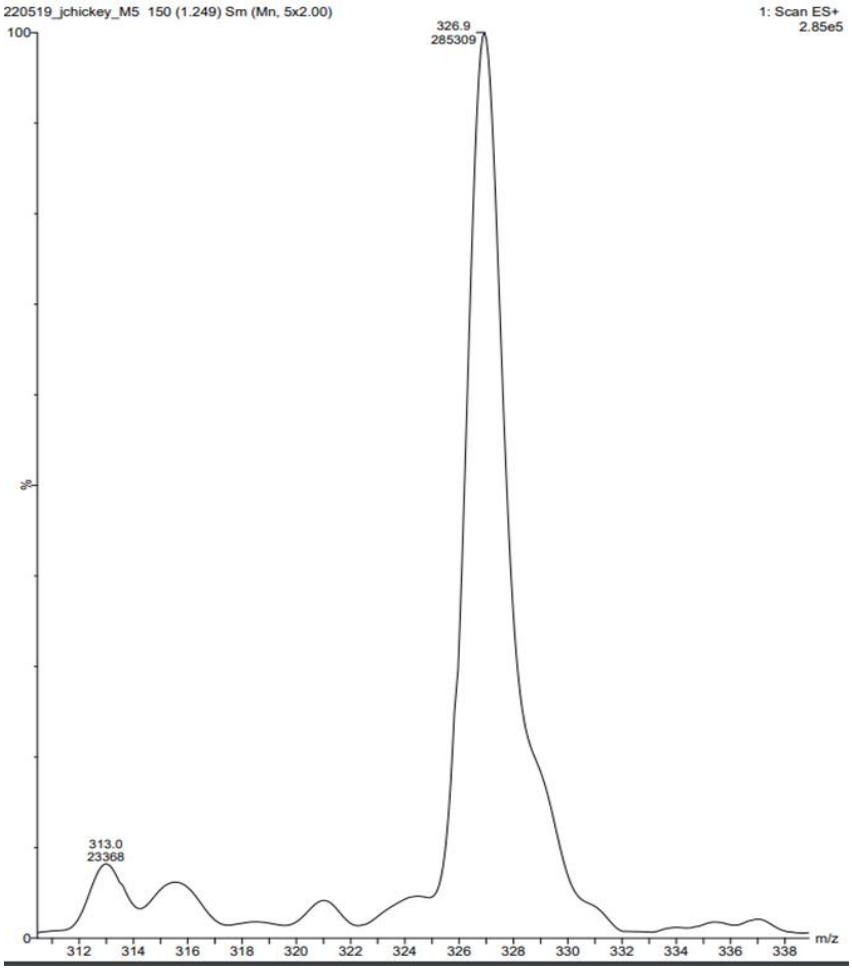

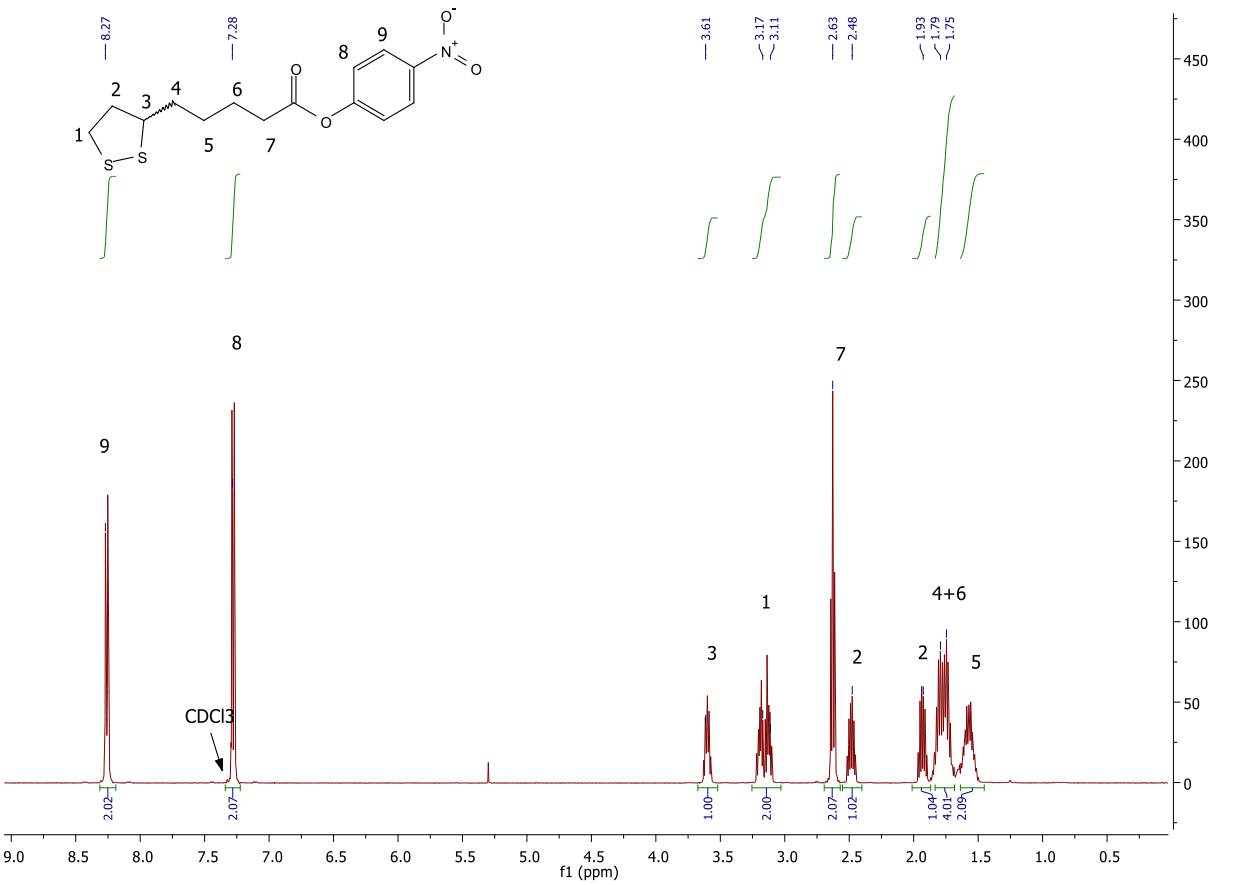
8.27
7.28
3.61
3.17
3.11
2.63
2.48
1.93
1.79
1.75
9
8
7
1
4+6
3
2
2
5
CDCl3
2.02
2.07
1.00
2.00
2.07
1.02
1.04
4.01
2.09
f1 (ppm)

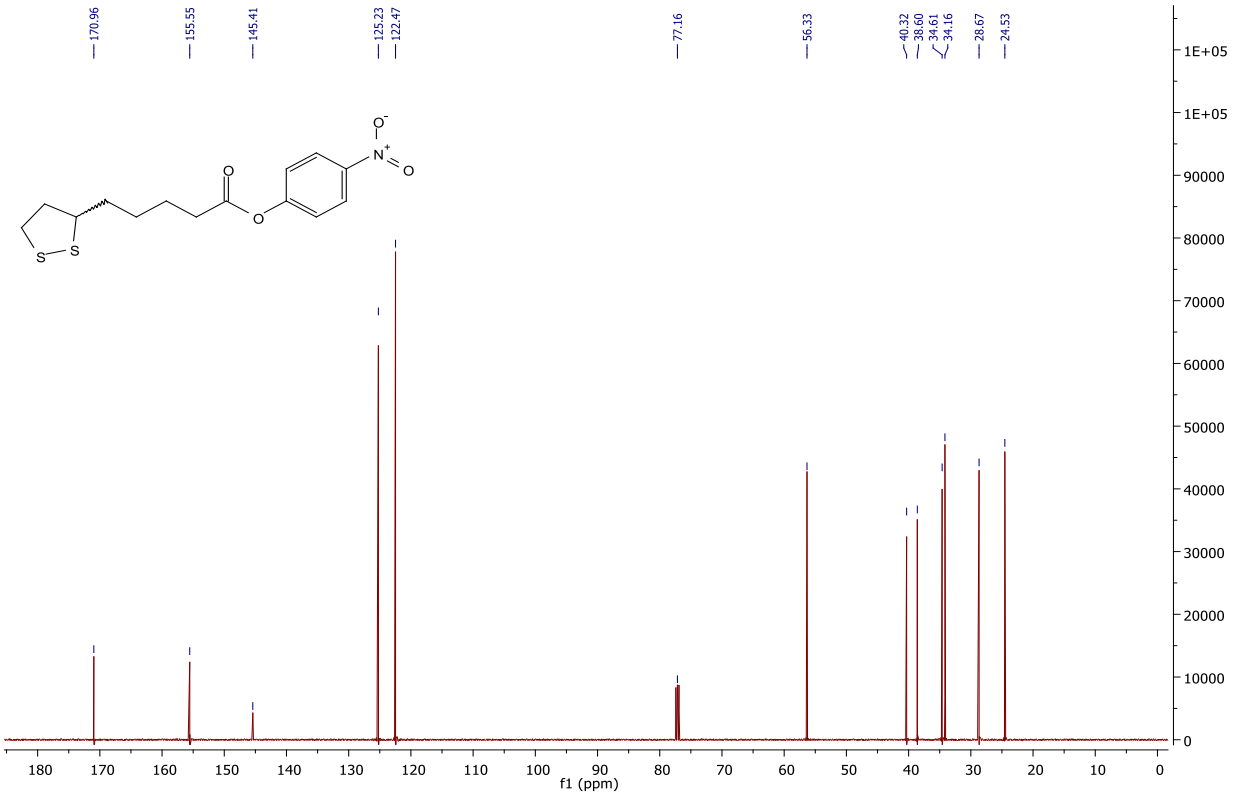
170.96
155.55
145.41
125.23
122.47
77.16
56.33
40.32
38.60
34.61
34.16
28.67
24.53
f1 (ppm)

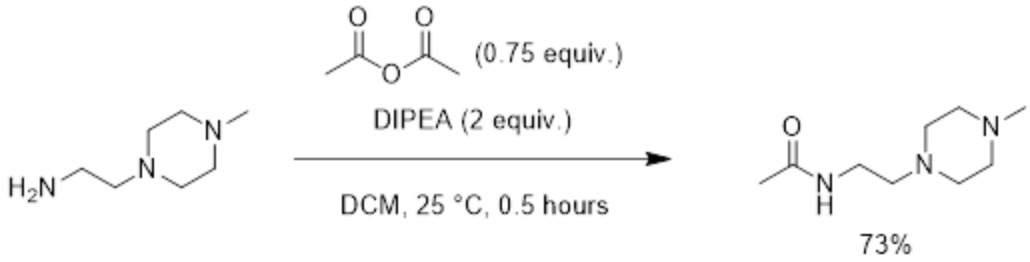

Scheme S2.6. Synthesis of N-Acetyl C2**.**

N-Acetyl C2 Yield: 284 mgs, 73%
^{1}H NMR ($CDCl_3$, 500 MHz): δ(ppm)= 6.30-5.85 (s, 1H), 3.35-3.25 (q, *J*= 6.0 Hz, 2H), 2.65-2.35(m, 10H), 2.28-2.25 (s, 3H), 1.98-1.93 (s, 3H); ^{13}C NMR ($CDCl_3$, 500 MHz): δ(ppm)= 120.26, 56.60, 55.11, 52.89, 46.11, 36.08, 23.43; ESI-MS: $C_9H_{19}N_3O$ [M+H$^+$], Calculated 186.15, Found 186.2. The ESI-MS, ^{1}H spectra, ^{13}C NMR spectra, and pH titration plot of N-Acetyl C2 are attached below:

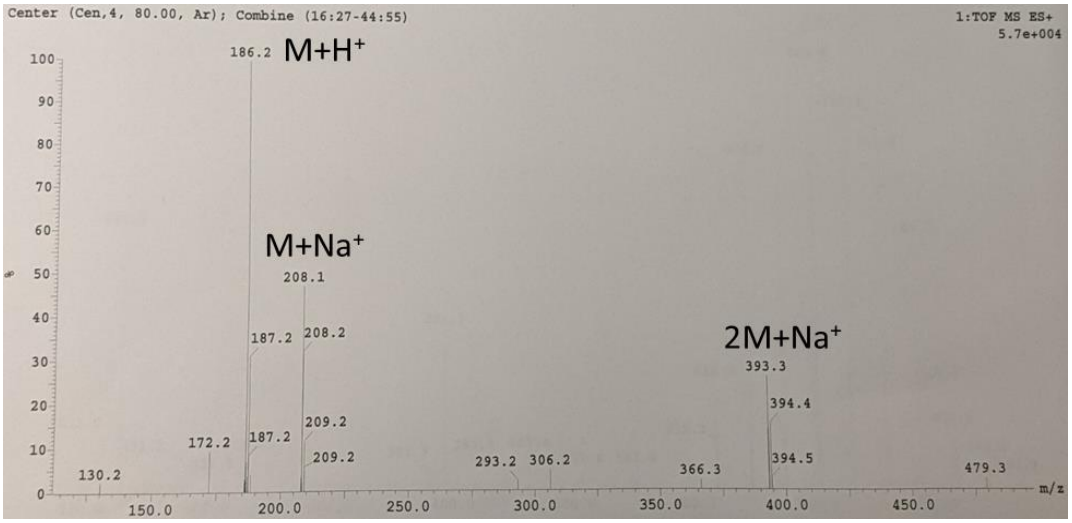

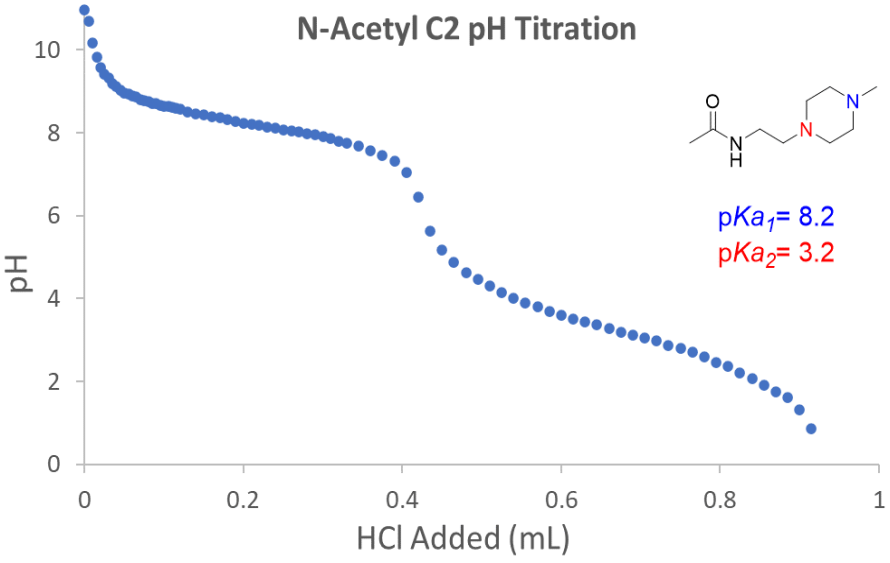

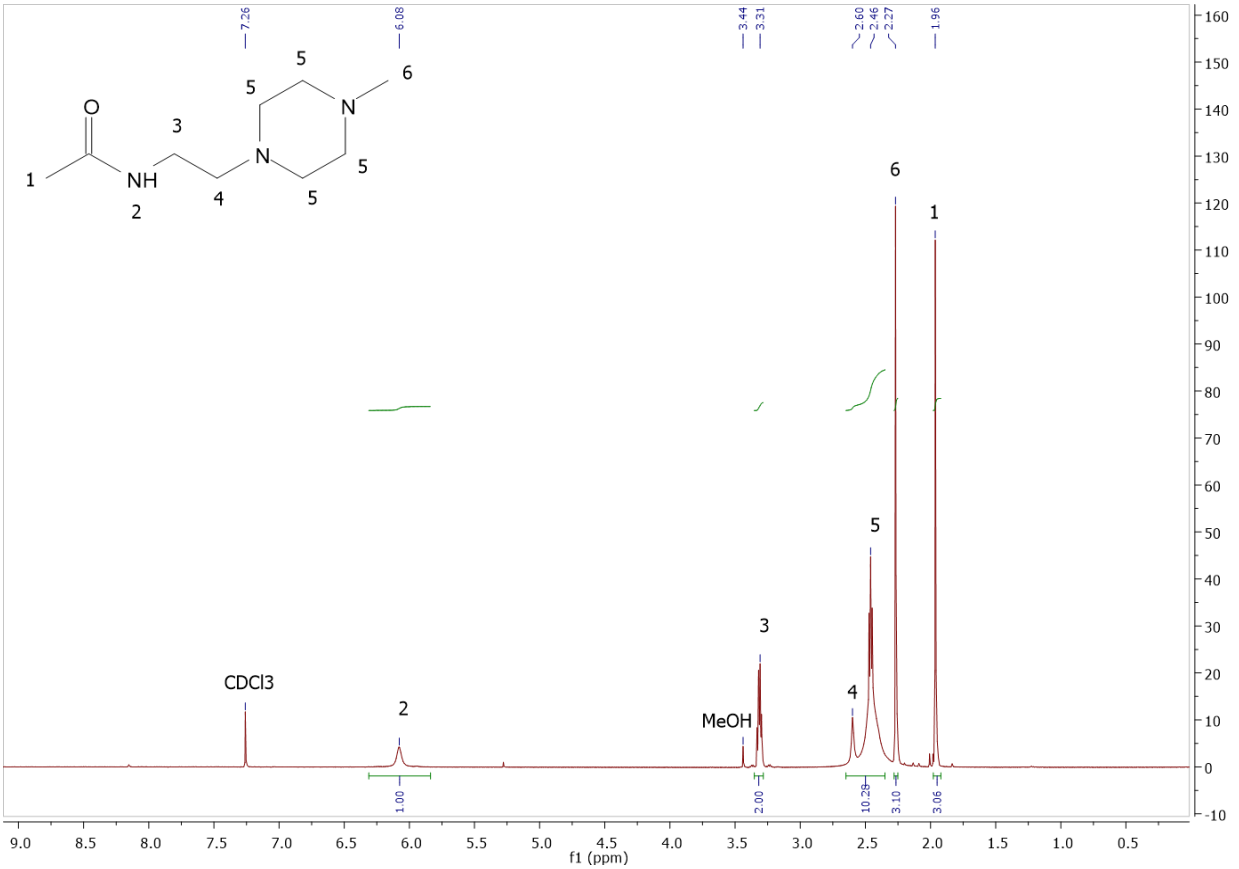
7.26
6.08
3.44
3.31
2.60
2.46
2.27
1.96
CDCl3
MeOH
1.00
2.00
10.29
3.10
3.06
f1 (ppm)

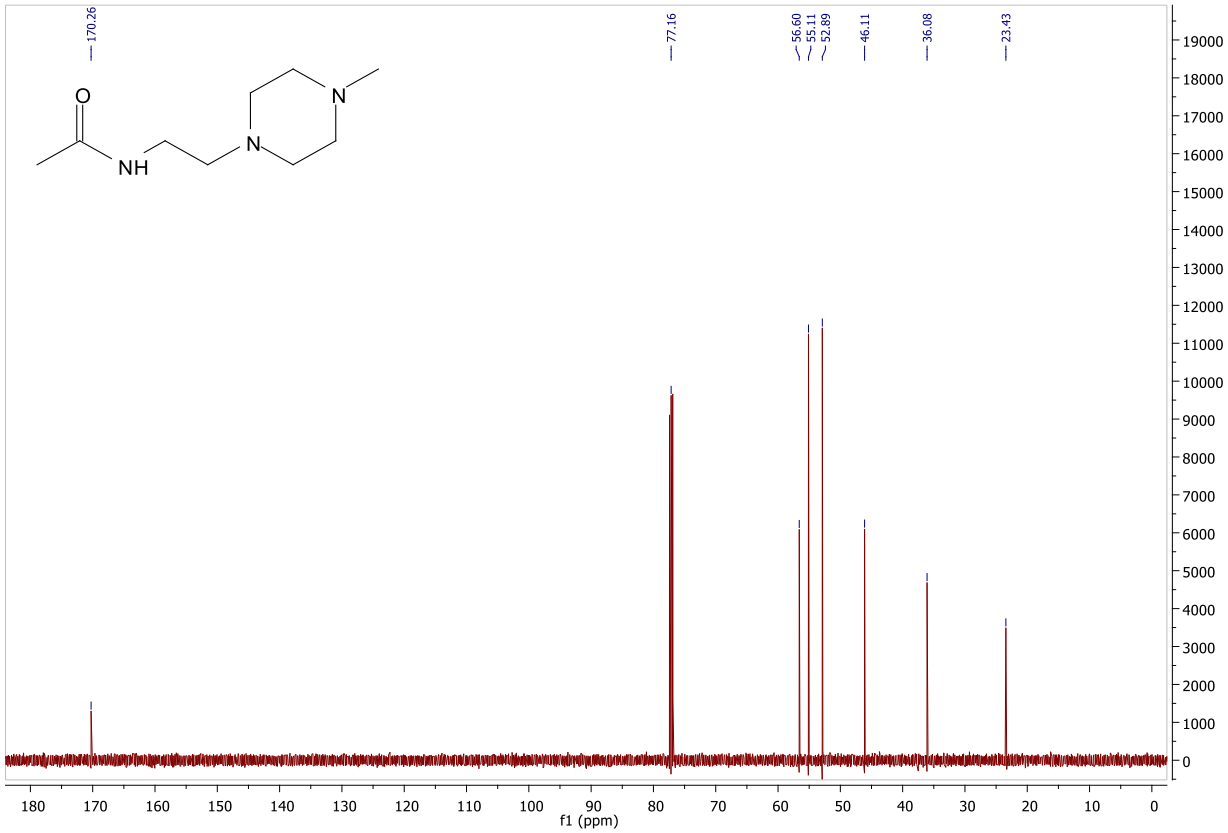
170.26
77.16
56.60
55.11
52.89
46.11
36.08
23.43
f1 (ppm)

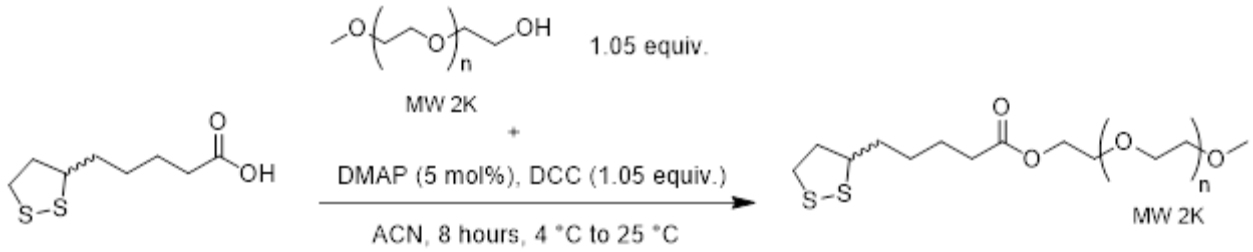

Scheme S9. Synthesis of LA(PEG 2K) Monomer

M1 Yield: 10.1 grams, 45% Yield
^{1}H NMR ($CDCl_3$, 500 MHz): δ(ppm)= 3.93-3.85 (br, 2H), 3.70-3.15 (br, 172H), 3.13-2.95 (s, 3H), 2.90-2.75 (m, 2H), 2.20-2.10 (m, 1H), 2.07-1.99 (t, *J*=7.5 Hz, 2H), 1.65-1.53 (m, 1H), 1.43-1.30 (m, 4H), 1.22-1.07 (m, 2H); ^{13}C NMR ($CDCl_3$, 500 MHz): δ(ppm)= 172.18, 71.08, 69.72, 68.25, 62.53, 58.06, 55.39, 39.36, 37.61, 33.76, 32.99, 27.82, 23.77; The GPC spectrum, ^{1}H spectra, and ^{13}C NMR spectra for LA(PEG 2K) are attached below:

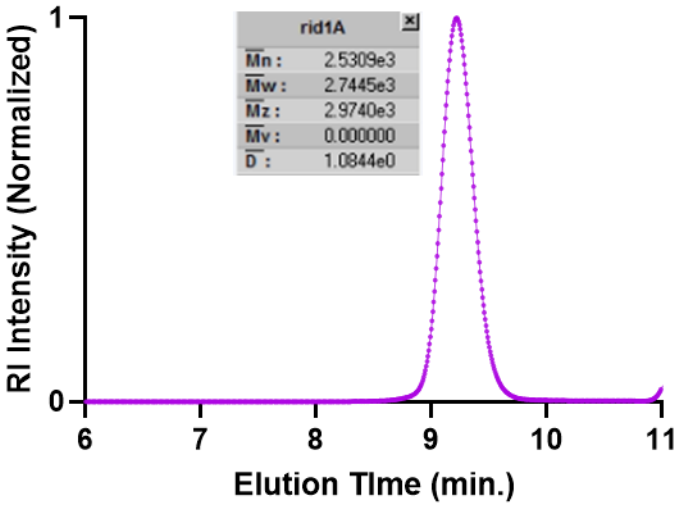

GPC: *M*w = 2.53 kDa, *Đ*=1.08

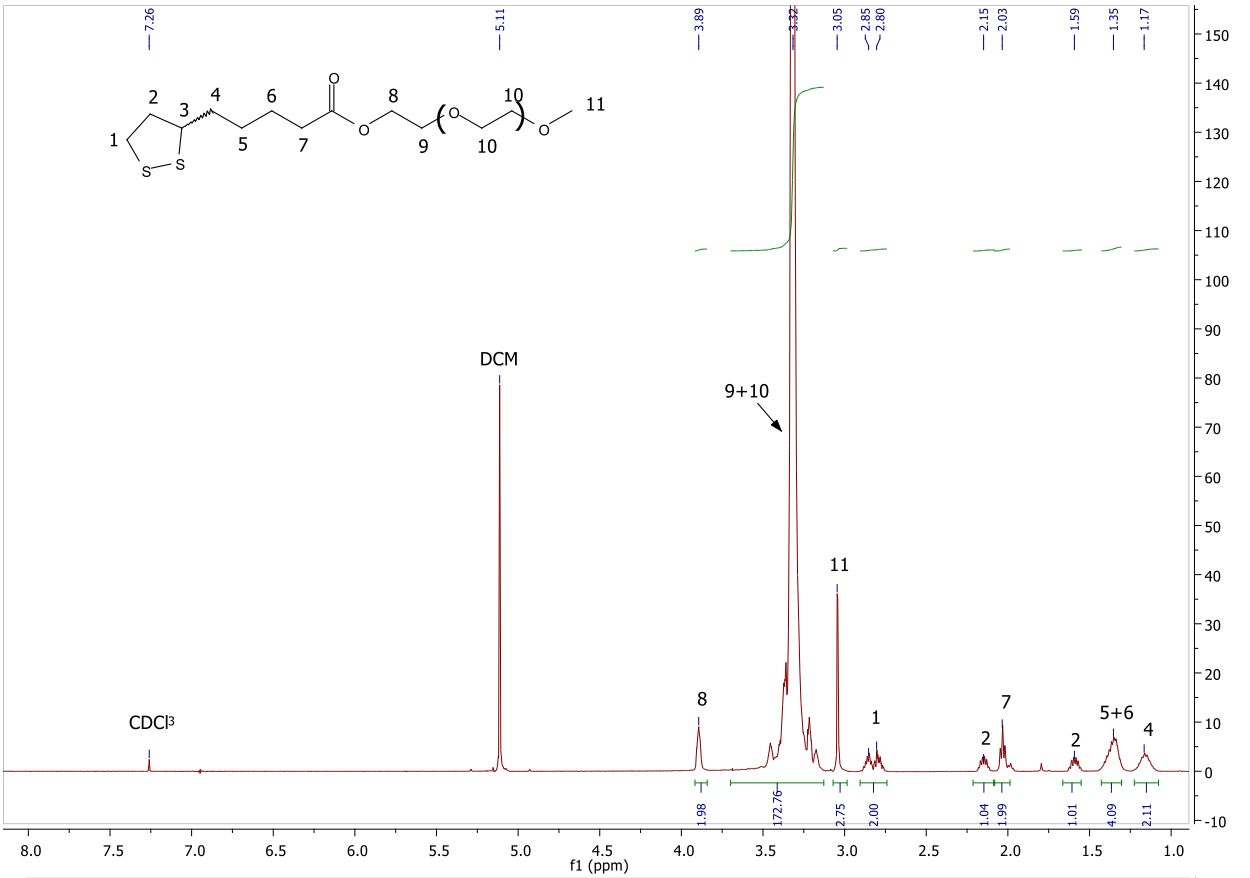
7.26
5.11
3.89
3.22
3.05
2.85
2.80
2.15
2.03
1.59
1.35
1.17
DCM
9+10
11
CDCl3
8
1
7
2
2
5+6
4
1.98
172.76
2.75
2.00
1.04
1.99
1.01
4.09
2.11
f1 (ppm)

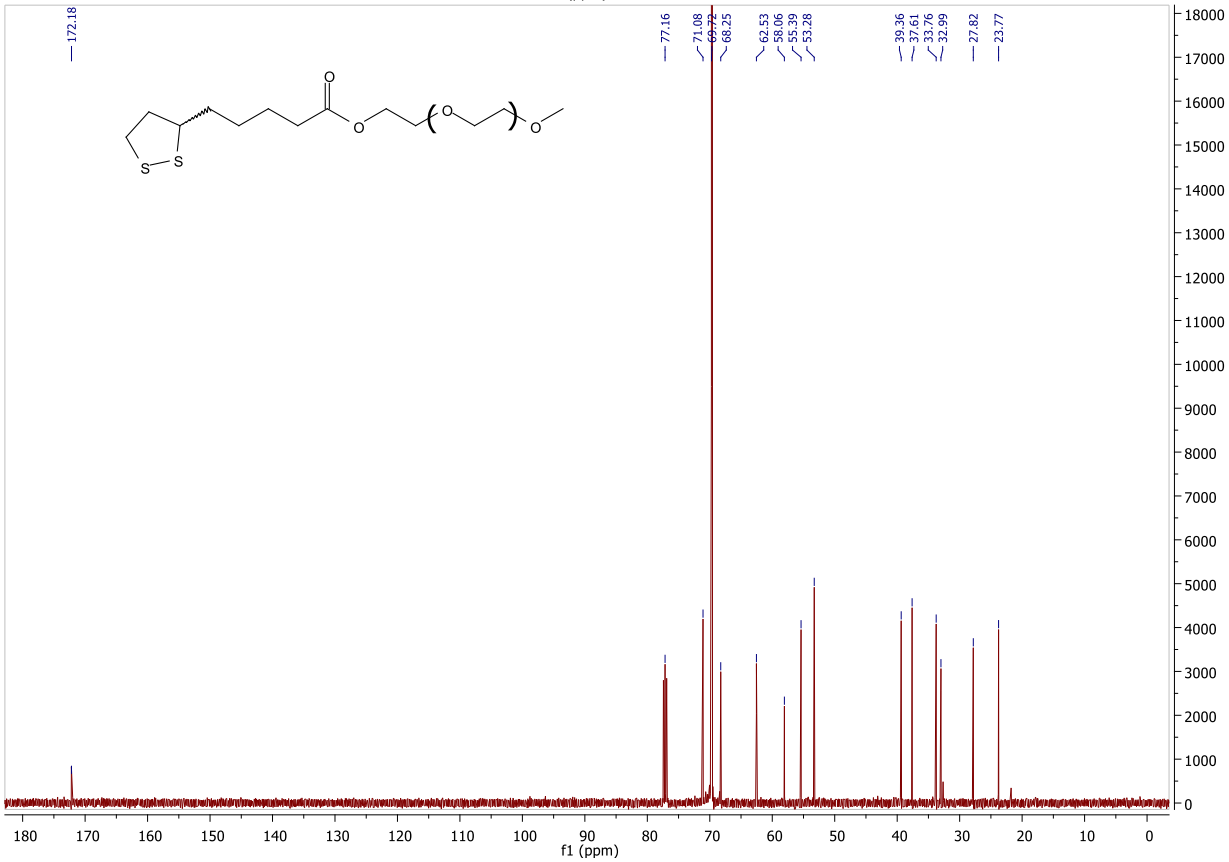
172.18
77.16
71.08
69.72
68.25
62.53
58.06
55.39
53.28
39.36
37.61
33.76
32.99
27.82
23.77
f1 (ppm)

Chapter 3: Dendronized Polypeptide Polymers for CRISPR-Cas9 Gene Editing *In Vitro* and mRNA Delivery *In Vivo*

***Addendum**: Alexander C. Eldredge contributed substantially to this work, particularly in vector synthesis, the optimization of in vitro conditions for sgRNA and Cas9 mRNA codelivery using the described nanoparticles, and quantifying luciferase expression from Fluc mRNA nanoparticle-treated mouse organs. These aspects of this work reflect his contributions to the project.*

3.1 Introduction

The development of new CRISPR-associated protein 9 (CRISPR-Cas9) delivery vehicles has accelerated in recent years, most notably utilizing lipid nanoparticles (LNPs) to carry CRISPR-Cas9 encoding machinery or CRISPR-Cas9 RNPs to target cells for gene editing.[1-3] However, despite the prominent successes of LNPs, there are still fundamental limitations to lipid-based nanocarriers.[4] The development of other effective tissue-specific CRISPR-Cas9 delivery vehicles remains an obstacle to the implementation of novel life-saving CRISPR-Cas9 gene therapies. Previous works have utilized cationic polymers to deliver CRISPR-Cas9-encoding plasmids[5-6] or co-deliver Cas9-mRNA and sgRNA simultaneously[7] to conduct gene editing. However, these construct designs predominantly utilize linear or minimally branched polymers for nanoparticle complexation and delivery, omitting numerous other potential polymer architectures for CRISPR-Cas9 gene editing applications.

Synthetic cationic dendrimers are frequently used to deliver individual RNA species but have not been used for RNA-codelivery-mediated CRISPR-Cas gene editing (from

simultaneous codelivery of Cas9 mRNA and sgRNA). As a result, relatively little is known about cationic dendrimer tissue-specificity in CRISPR-Cas9 gene editing applications. Moreover, dendronized polymers, or polymers with linear backbones and numerous dendrons attached, possess increased chain flexibility that is advantageous for nucleic acid complexation and delivery.[8] Exploration into this family of cationic polymers would determine their gene delivery capability, determine nanoparticle characteristics when complex with mRNA,[9] and examine *in vivo* localization characteristics.

Among the three CRISPR-Cas gene editing approaches, RNA-mediated CRISPR-Cas9 gene editing offers many advantages over CRISPR-Cas9 plasmid-based gene editing. Unlike Cas9-encoding plasmids, Cas9 mRNA does not require nuclear localization and promoter activation to undergo an additional transcription step.[10] When delivered exogenously, Cas9 mRNA can begin translation immediately after entry into the cytosol, generating multiple copies of the Cas9 protein from a single Cas9 mRNA molecule. These numerous Cas9 proteins can assemble with exogenously delivered sgRNA molecules to form complete RNPs capable of gene editing. This transient CRISPR-Cas9 expression avoids prolonged CRISPR-Cas9 activity commonly obtained from plasmid-based delivery and reduces potential off-target gene editing resulting from extended CRISPR-Cas9 expression.[11-12]

Previous works utilizing thiol-reducible dendronized linear polypeptide polymers (denpols) have shown excellent success in nanoparticle complexation and subsequent delivery of both small-interfering RNA (siRNA) and mRNA for fibroblast cells and dendritic cells *in vitro*.[13-14] These multifunctional polymer dendrons were functionalized with either histidine, a common pH-responsive motif to promote endosomal escape upon nanoparticle uptake into endosomes/lysosomes,[15-16] or tryptophan groups for nanoparticle

hydrophobicity and additional RNA interactions.[17-18] Through previous experimental determination, a ratio of two histidines for every tryptophan (2:1) has shown optimal *in vitro* RNA delivery efficacy.[13-14] Additionally, each amino acid functional group contains a cationic amine to complex with RNA phosphate groups through electrostatic interactions.[19] Lastly, thiol-reducible disulfide linkages are prevalent within the polymer backbone to facilitate polymer degradation upon nanoparticle uptake into the cytosol and interaction with cellular thiols.[20-21] Altogether, these various functionalities facilitate RNA-polymer complexation, endosomal escape, and ensure biodegradation upon entry into cells. Moreover, tetraethylene glycol incorporation into the linear polymer backbone was previously explored to alter polymer flexibility, provide spacing between dendrimers, affect nanoparticle complexation, and subsequent nucleic acid delivery efficacy when applied to RNA delivery models.[22]

While denpols have been used to deliver siRNA and mRNA independently, they have not yet been used for the simultaneous delivery of large and small RNA species. Herein, we utilized two specific second-generation denpols, **G2 2:1** and **50% TEG G2 2:1** (see Scheme 3.1A), to complex with only sgRNA or with a Cas9 mRNA-sgRNA mixture, forming two distinct RNA-containing nanoparticle species for *in vitro* delivery (see Scheme 3.1B). Resulting RNA delivery and CRISPR-Cas9 gene editing efficacy of these two different nanoparticle species were evaluated using EGFP-expressing model cell lines. Finally, *in vivo* biodistribution of this class of polymeric nanoparticles was examined using firefly luciferase (Fluc) mRNA for tissue-specific localization.

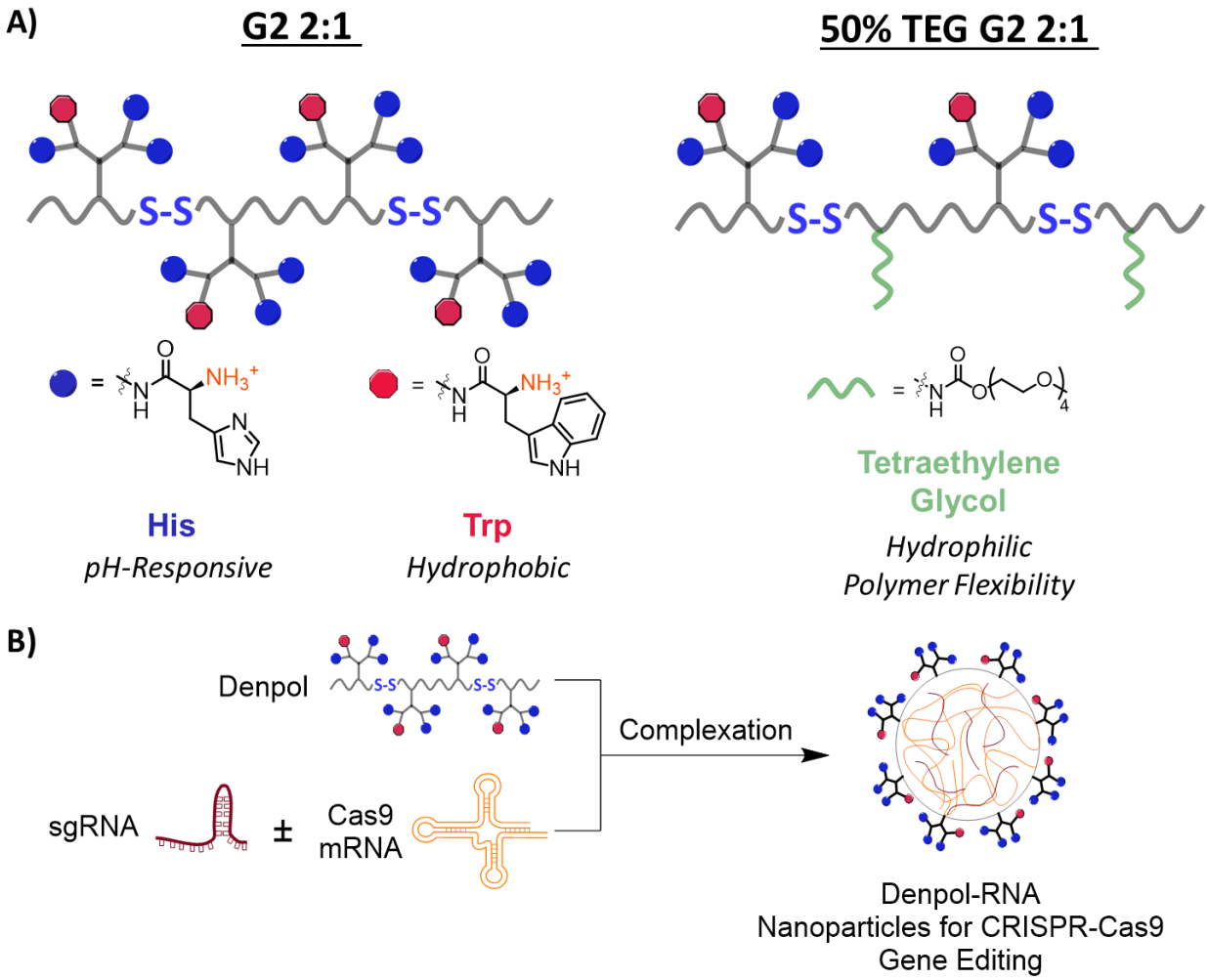

Scheme 3.1. Simplified denpol structures and formulation approach to generate denpol-RNA polymeric nanoparticles. **A)** Structure of **G2 2:1** (left) and **50% TEG G2 2:1** (right) denpols used for RNA delivery in this work. Cationic amines for RNA complexation are colored in orange, histidine motifs are blue, tryptophan residues are red, and tetraethylene glycol functionalities are green. **B)** General complexation scheme to generate denpol-RNA polymeric nanoparticles. Denpol-RNA nanoparticles containing sgRNA alone or sgRNA and Cas9 mRNA are examined.

3.2 Results and Discussion

Both **G2 2:1** or **50% TEG G2 2:1** cationic linear dendronized polymers were synthesized using previous procedures and confirmed using ^{1}H NMR (See Polymer Characterization Data). Additionally, three different *egfp*-targeting sgRNA sequences were

generated (See Table S3.1) and validated in a modified cell line that endogenously expresses both Cas9 protein and EGFP (detailed further below; See Figures S3.2-3.4).

With denpol vectors synthesized and a validated *egfp*-targeting sgRNA, we proceeded to validate denpol-sgRNA nanoparticle generation and nanoparticle cell delivery. To confirm that denpol vectors can independently complex with sgRNA, the validated *egfp*-targeting sgRNA was complexed with **G2 2:1** or **50% TEG G2 2:1** denpols at different N/P ratios. Both vectors demonstrated RNA complexation at N/P ratios above 2.5 via GE assay (Figure S3.5). Nanoparticle sizes at an N/P ratio of 30 were characterized by both DLS (See Figure 3.1A; See Table S3.2) and cryogenic transmission electron microscopy (cryo-TEM, Figure 3.1B).

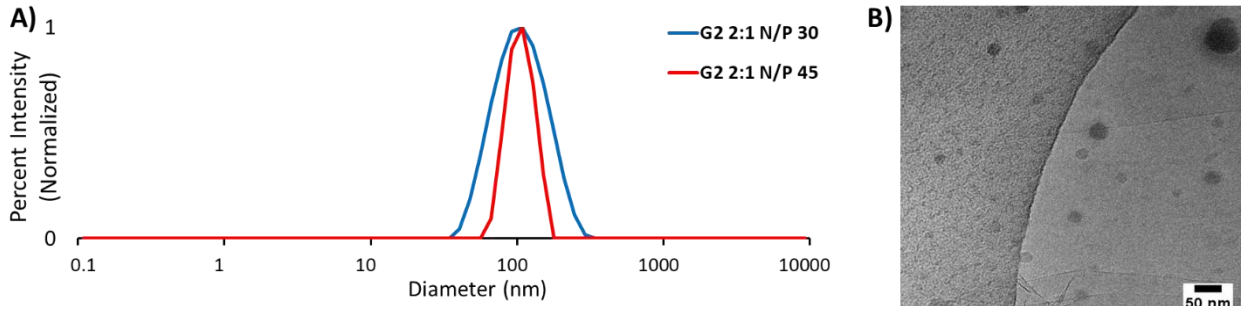

Figure 3.1 DLS and cryo-TEM characterization of denpol-sgRNA nanoparticles. **A)** Representative DLS spectra for **G2 2:1** denpol-sgRNA nanoparticles formulated at N/P ratios of 30 (blue) and 45 (red). **B)** Representative cryo-TEM image for **G2 2:1** denpol-sgRNA nanoparticles formulated at an N/P ratio of 30. Scale bar represents 50 nm.

With nanoparticle generation confirmed, a model cell line was needed to validate sgRNA delivery. By placing a gene of interest within a lentiviral vector, desired genes can be introduced into the genome of immortalized cells. This gene can subsequently be knocked out using exogenously provided CRISPR-Cas9 machinery. In works using this approach, robust gene editing is observed regardless of the number of genomic insertions from lentiviral transduction.[23] Following this, a model NIH-3T3 cell line constitutively

expressing nuclear localization signal-conjugated Cas9 protein (NLS-Cas9) and EGFP was generated via lentiviral transduction and isolated using fluorescence-assisted cell sorting (See Figure S3.6). Exogenous sgRNA was delivered into the cytosol using denpol-sgRNA nanoparticles. After nanoparticle decomplexation in the cytosol, this sgRNA complexed with natively expressed Cas9 protein to edit *egfp* genes; knockout efficiency was determined via flow cytometry (measuring EGFP-negative cells; Figure 3.2A).

At a lower N/P ratio of 10, nanoparticles from both **G2 2:1** and **50% TEG G2 2:1** exhibited lower gene editing (40% and 28%, respectively) compared to higher N/P ratios. At an N/P ratio of 30, nanoparticles formulated from both **G2 2:1** and **50% TEG G2 2:1** resulted in 58% and 43% gene editing, as determined by EGFP reduction (See Figure 3.2B; See Figure S3.7). Similarly, at an N/P ratio of 45, both denpol vectors resulted in >50%

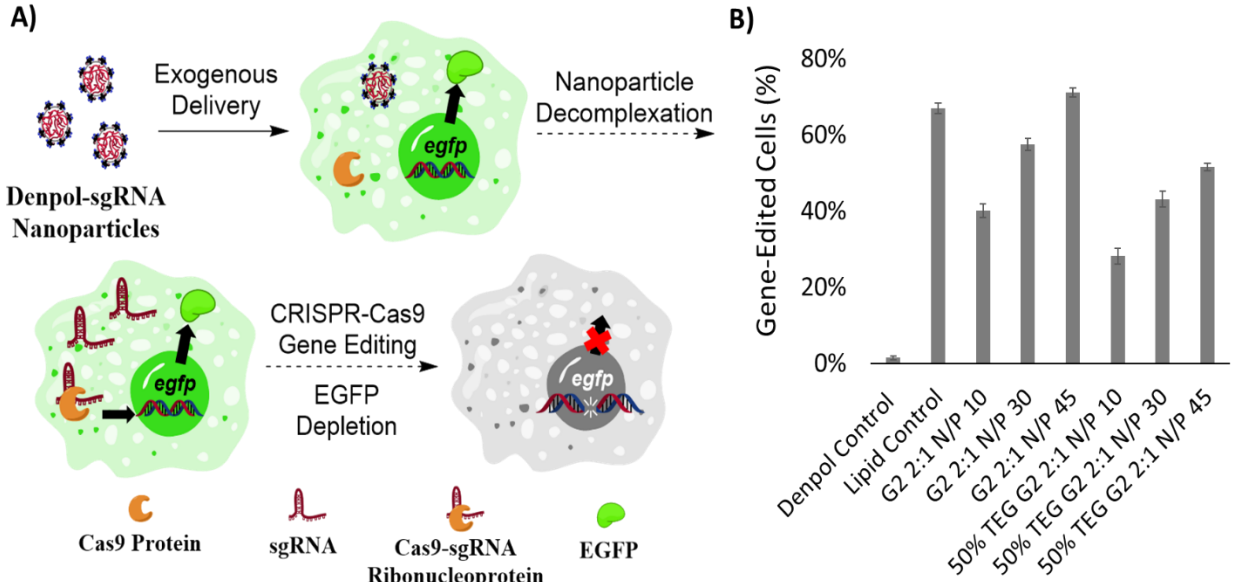

Figure 3.2 *egfp* gene editing from denpol-sgRNA nanoparticles. **A)** Flow through scheme for the delivery of denpol-sgRNA nanoparticles to NLS-Cas9-EGFP-expressing NIH 3T3 cells and subsequent gene editing. **B)** Percent *egfp*-gene-edited NLS-Cas9 and EGFP co-expressing cells after treatment with denpol-RNA nanoparticles at different N/P ratios in serum-free conditions. n=3 for all sample treatments. Lipofectamine P2000 was used as lipid control.

gene editing. The most optimal formulation containing **G2 2:1** denpol was at an N/P ratio of 45, resulting in >70% of all cells being edited. Furthermore, gene editing with these nanoparticles was also observed in the presence of serum during cell transfection (See Figure S3.8).

With sgRNA delivery established, the codelivery of Cas9 mRNA and sgRNA with denpols was further assessed. With no pre-existing CRISPR-Cas9 machinery present within cells, this delivery method should generate Cas9 protein *in situ* alongside exogenously provided sgRNA, assembling all CRISPR-Cas9 components from the cargo of a single nanoparticle. Polymeric nanoparticles containing Cas9 mRNA and *egfp*-targeting sgRNA were formulated with **G2 2:1** or **50% TEG G2 2:1** denpol vectors and characterized by DLS (See Figure 3.3A; See Table S3.3), zeta potential (See Table S3.4), and cryo-TEM (See Figure 3.3B). For initial screens, a 1:7 w/w ratio of Cas9 mRNA and sgRNA was used for codelivery nanoparticle experiments. Notably, formulation using **G2 2:1** or **50% TEG G2 2:1** denpols generated 275-350 nm nanoparticles according to DLS. No significant size difference was

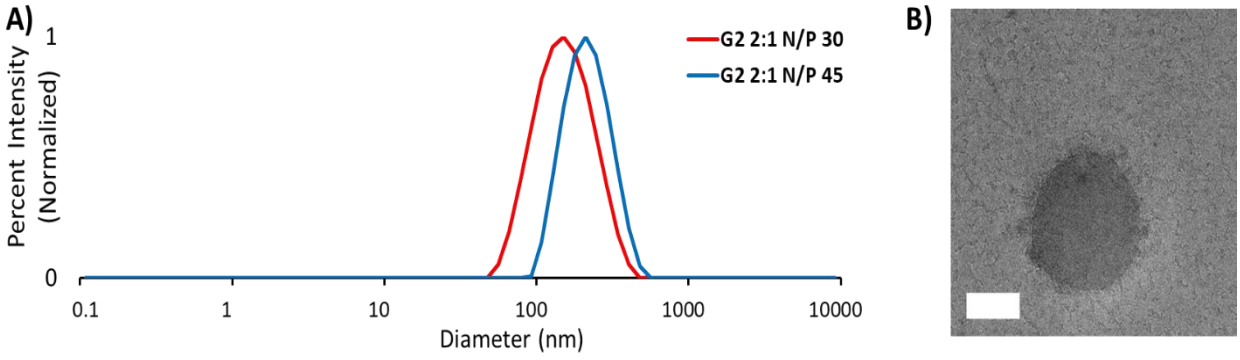

Figure 3.3 DLS and cryo-TEM characterization of denpol-Cas9 mRNA-sgRNA nanoparticles. **A)** Representative DLS spectra for **G2 2:1** denpol-Cas9 mRNA-sgRNA nanoparticles formulated at N/P ratios of 30 (red) and 45 (blue). **B)** Representative cryo-TEM image for **G2 2:1** denpol-Cas9 mRNA-sgRNA nanoparticles formulated at an N/P ratio of 30. Scale bar (white bar) represents 100 nm.

observed between the **G2 2:1** and **50% TEG G2 2:1,** suggesting that tetraethylene glycol functionalization does not drastically alter polyplex size.

To test the viability of these polymeric nanoparticles for *egfp* gene editing, another NIH-3T3 model cell line constitutively expressing EGFP was generated via lentiviral transduction (See Figure S3.9). Denpol-Cas9 mRNA-sgRNA polymeric nanoparticles were administered to these EGFP-expressing NIH-3T3 cells using a similar methodology, and EGFP reduction/gene editing was quantified by flow cytometry (See Figure 3.4A; See Figure S3.10). Notably, polymeric nanoparticle-mediated codelivery of Cas9 mRNA and *egfp*-targeting sgRNA resulted in >70% EGFP editing at N/P ratios of 30 and 45 in serum-free conditions (See Figure 3.4B). The nominal difference in gene editing for both **G2 2:1**- and **50% TEG G2 2:1**- containing nanoparticles at N/P 30 or 45 suggests that the TEG backbone functionalization and increased backbone flexibility have minimal effect on overall gene editing efficacy for this approach. Additionally, like independent sgRNA delivery, increased N/P ratios resulted in higher gene editing efficacy, with the N/P ratio of 45 showing higher gene editing efficacy in both delivery models.

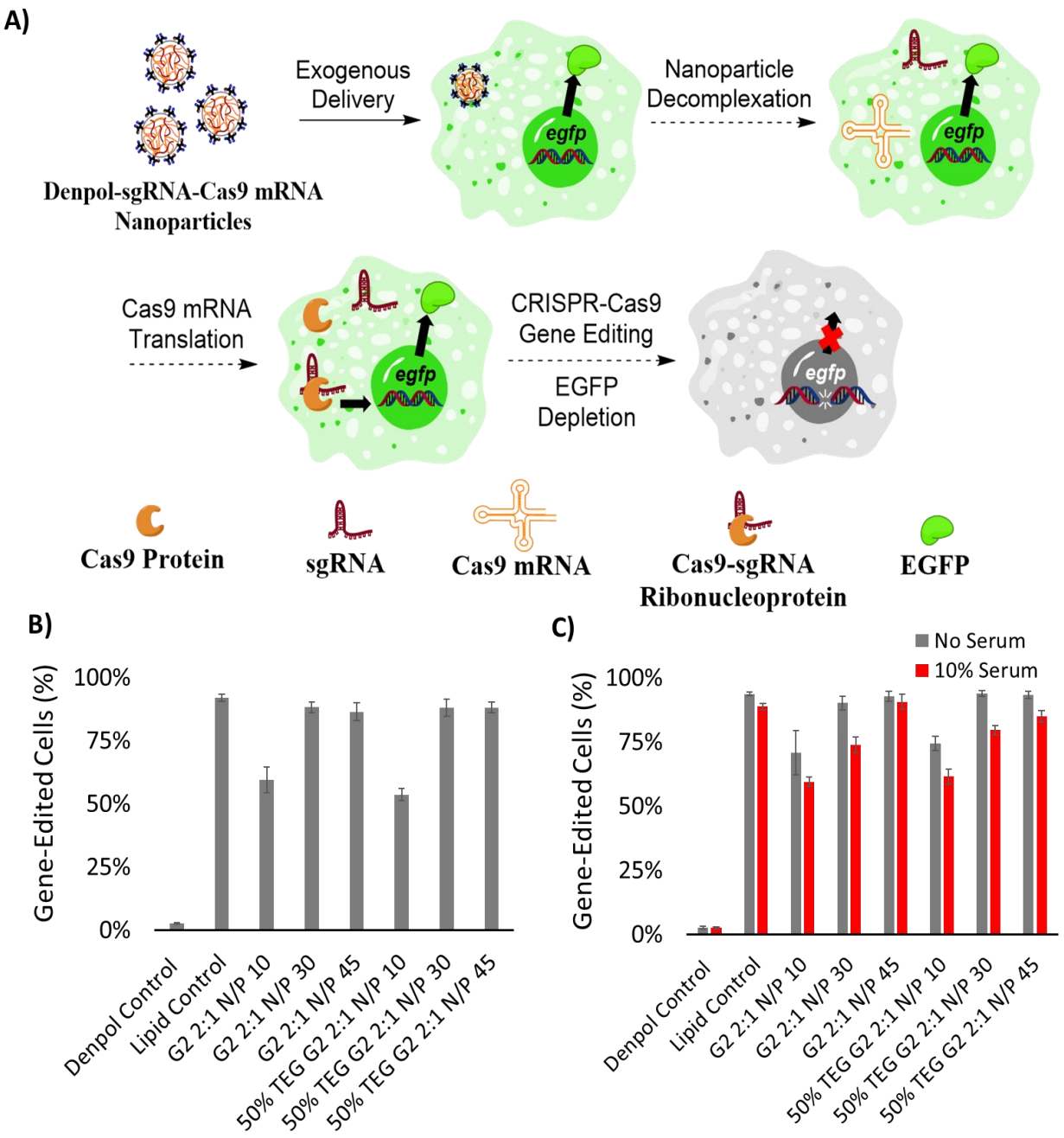

Figure 3.4 *egfp* gene editing from denpol-Cas9 mRNA-sgRNA nanoparticles. **A)** Flow through scheme for the delivery of denpol-Cas9 mRNA-sgRNA nanoparticles to EGFP-expressing NIH 3T3 cells and subsequent gene editing. **B)** Percent *egfp*-gene-edited NIH 3T3 cells after treatment with denpol-RNA nanoparticles at different N/P ratios in serum-free conditions. n=3 for all sample treatments. **C)** Percent *egfp*-gene-edited NIH 3T3 cells after treatment with denpol-RNA nanoparticles at different N/P ratios in serum-rich conditions. Lipofectamine P2000 was used as lipid control. n=3 for all sample treatments.

Exploring this codelivery approach further, polymeric nanoparticles containing both Cas9 mRNA and sgRNA were also administered to cells in a serum-rich environment during initial nanoparticle administration to test transfection viability in the presence of serum proteins. From this, only a minor reduction in *egfp* gene editing efficacy was observed (See Figure 3.4C). At an N/P ratio of 45, both **G2 2:1** and **50% TEG G2 2:1**-containing polymeric nanoparticles resulted in 93% gene editing in serum-free conditions. In the presence of serum, gene editing efficacy was reduced to 90% and 85%, respectively, indicating that serum proteins do not drastically reduce transfection efficacy as shown in other nanoparticle systems.[24] A dose-dependent gene editing relationship was also observed, with lower gene editing efficacy at lower overall RNA loads (See Figure S3.11).

Additionally, a 1:10 w/w ratio of Cas9 mRNA and sgRNA was also tested and similarly obtained comparable levels of gene editing at N/P ratios of 30 and 45 for both denpol vectors (See Figure 3.5). Moreover, an EGFP-expressing HEK 293T cell line was generated through similar lentiviral transduction and treatment with denpol-Cas9 mRNA-sgRNA nanoparticles also resulted in gene editing (See Figures S3.12-3.14), indicating that this methodology is applicable to other cell lines. Altogether, we anticipate that utilizing other sgRNAs can target other genes in treatment models using this RNA codelivery approach.

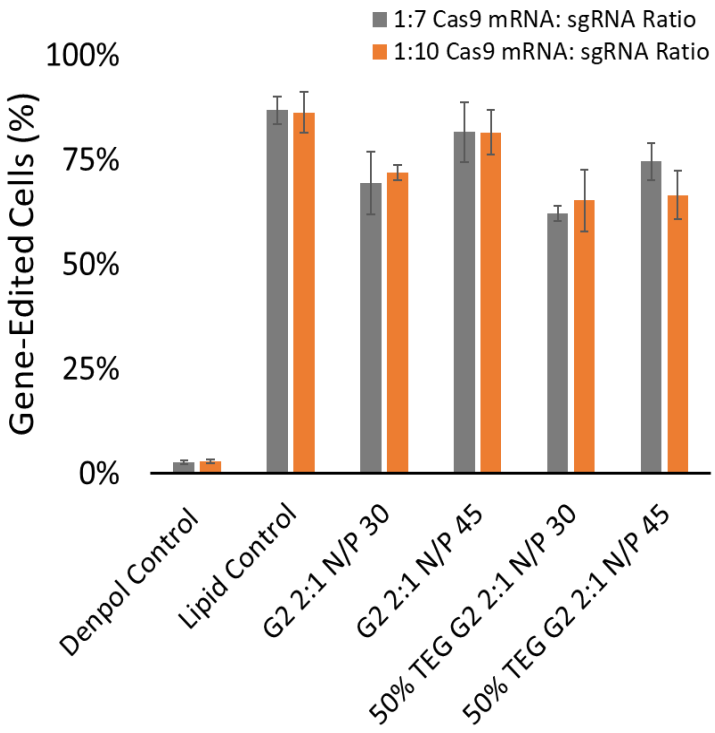

Figure 3.5 *egfp* gene editing with different mRNA:sgRNA ratios. Percent *egfp*-gene edited NIH 3T3 cells after treatment with denpol-RNA nanoparticles containing different 1:7 and 1:10 w/w ratios of Cas9 mRNA to sgRNA. All cells treated in serum-free conditions. Lipofectamine P2000 was used as lipid control. n=3 for all samples,

With RNA-codelivery-mediated CRISPR-Cas9 gene editing demonstrated *in vitro*, the tissue specificity of this class of RNA-polymer nanoparticles was tested *in vivo*. When examining size-dependent *in vivo* nanoparticle distribution, nanoparticles >200 nm tend to localize to the liver and spleen.[25-26] When Cas9 mRNA-sgRNA were formulated with **G2 2:1** at a ratio of 30, >200 nm nanoparticles were obtained by DLS, suggesting that this class of nanoparticle may similarly localize to the liver and spleen *in vivo*.

To test this, denpol polymer vectors were formulated with Cy5-labeled Fluc mRNA and the resulting nanoparticles were characterized by DLS (See Table S3.5). These nanoparticles were then administered to C57BL/6 mice via tail vein injection. After six hours, nanoparticle localization and mRNA expression characteristics were determined by

IVIS *in vivo* imaging. Mice treated with **G2 2:1**- and **50% TEG G2 2:1**-Fluc mRNA nanoparticles at an N/P of 30 showed excellent luciferase expression, with localization frequently away from the site of injection (See Figure 3.6; See Figure S3.15). Luciferase activity is also observed 24 hours post-injection in **G2 2:1**-Fluc mRNA nanoparticles, suggesting that this delivery methodology is capable of prolonged expression of cargo mRNA (See Figure S3.16). One more vector was synthesized, 8%PEG **G2 2:1,** complexed with Fluc mRNA and administered to mice in a similar manner. Good luciferase expression was also obtained for this vector, with expression potentially localized to lymph nodes (See Figure S3.19).[27]

Imaging of individual organs indicated that nanoparticle expression was localized to the lungs and spleen of injected animals (See Figure 3.7). For mice treated with **G2 2:1**-Fluc mRNA nanoparticles at an N/P ratio of 30, the lungs and spleen comprised 59% and 34% of all organ luciferase expression, respectively (See Figure S3.17A+B). These two organs together comprised 93% of all organ luciferase expression, with nominal expression from the liver, heart, and kidneys of treated mice. This organ localization profile is highly indicative of uptake by antigen-presenting cells (APCs) and migration to lymph nodes/the spleen.[28-29] This result is consistent with other similar nanoparticle designs.[29-30]

Interestingly Cy5 fluorescent dye, which was directly conjugated to Fluc mRNA, was located predominantly within the liver of treated mice (See Figure S3.17C+D). These same livers possessed nominal Fluc mRNA expression, indicating minimal cellular uptake by hepatocytes or premature degradation in the liver. With the naturally high levels of glutathione found in the liver, we hypothesize that Cy5 accumulation in the liver may be

the result of premature polyplex degeneration due to high exogenous thiols present in the liver;[31] degraded Fluc mRNA would release lipophilic Cy5 dye that accumulates in the hepatocytes.

The safety profiles of **G2 2:1-** and **50% TEG G2 2:1**-Fluc mRNA nanoparticles were also examined in these mice. After injection with denpol-Cas9 mRNA-sgRNA nanoparticles at an N/P of 30, an aspartate aminotransferase (AST) assay was performed on serum 4 days post-injection. AST activity was not significantly affected by nanoparticle administration (See Figure S3.18), suggesting that nanoparticles from **G2 2:1-** and **50% TEG G2 2:1** denpols are highly biocompatible for mRNA, and Cas9 mRNA-sgRNA codelivery applications.

Altogether, the luciferase expression of nanoparticles from all denpol derivatives suggests that these nanoparticle derivatives are highly promising mRNA delivery and CRISPR-Cas9 mRNA-sgRNA codelivery vehicles for immunology project designs. Despite the relatively short lifetimes of some antigen-presenting cells,[32] there is growing interest in CRISPR-Cas9 gene editing in macrophages,[33] monocytes,[34] and dendritic cells.[35] CRISPR-Cas modifications in these cells have demonstrated promise in the treatment of inflammatory diseases such as irritable bowel disease,[36] or to engineer immune tolerance after organ transplantation.[35] Some of these designs already utilize linear polymers to mediate CRISPR-Cas9 delivery,[35, 37] but have not utilized dendronized polymer architectures. With the excellent RNA-codelivery-mediated CRISPR-Cas9 gene editing capability and favorable *in vivo* nanoparticle safety profile described within this work, we

suggest that these denpol vectors, and cationic dendritic polymers more broadly, are very promising nanoparticle tools for future immune cell CRISPR-Cas9 gene editing therapies.

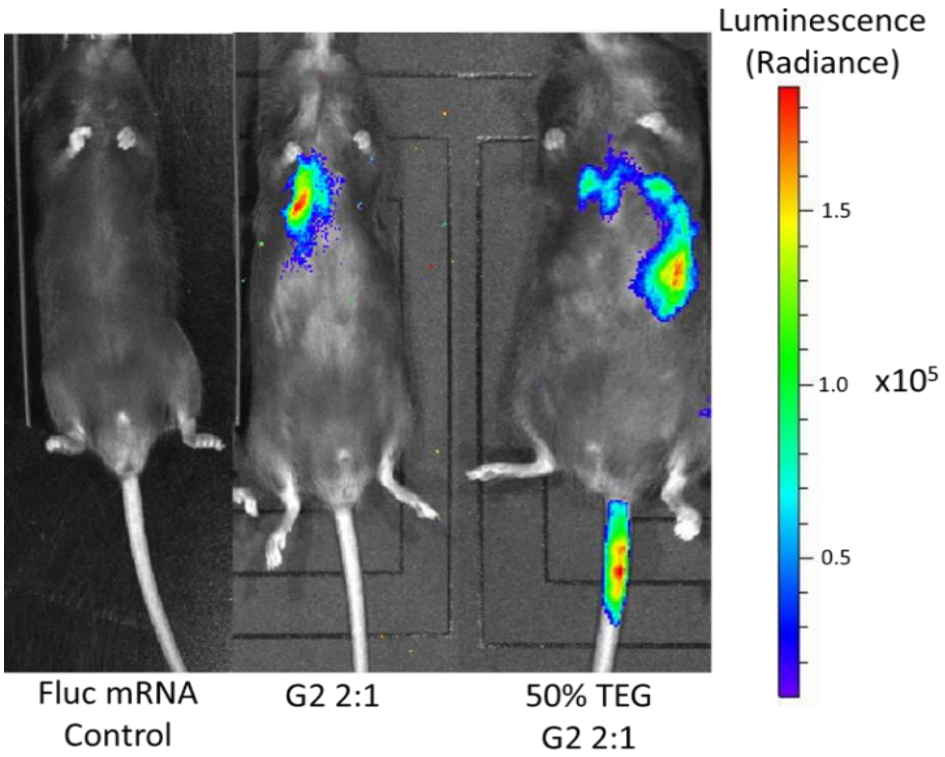

Figure 3.6 *In vivo* imaging of C57BL/6 mice injected with denpol-Fluc mRNA polymeric nanoparticles six hours post-injection. All denpol-Cas9 mRNA-sgRNA nanoparticles formulated at an N/P ratio of 30 prior to administration.

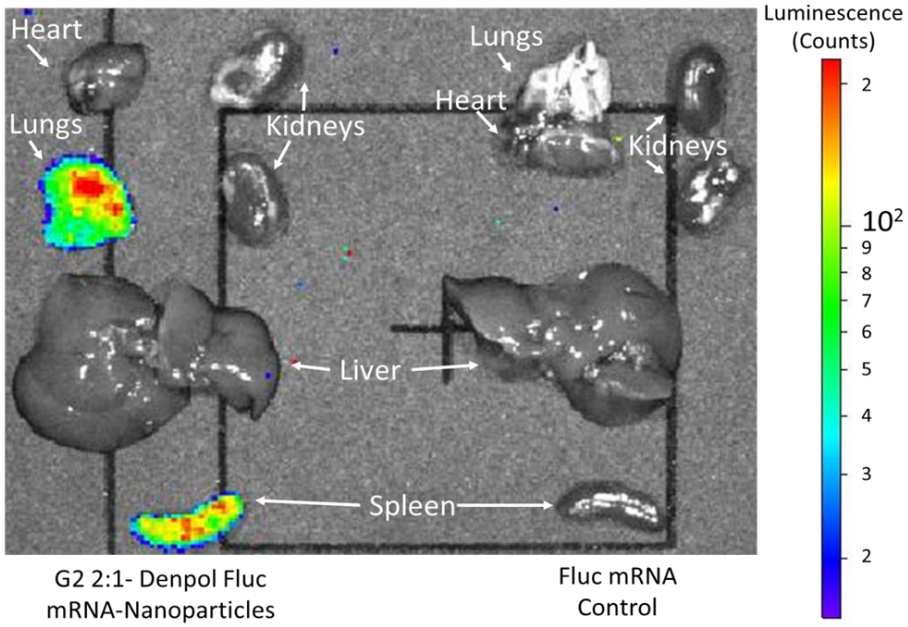

Figure 3.7 Luciferase expression in extracted organs from C57BL/6 mice treated with denpol-Fluc mRNA polymeric nanoparticles. Organs analyzed six hours post-injection. All denpol-Cas9 mRNA-sgRNA nanoparticles formulated at an N/P ratio of 30 prior to administration.

3.3 Conclusions

In this project we explored nanoparticle complexation of both sgRNA and Cas9 mRNA+sgRNA using two different cationic linear dendronized polymer (denpol) species. RNA-encapsulated polymeric nanoparticles could deliver *egfp*-targeting sgRNA alone or sgRNA+Cas9 mRNA cargo together to model EGFP-expressing cells. *In vitro egfp* gene editing efficacy after nanoparticle administration was quantified by measuring EGFP depletion in a simplified flow cytometry protocol. When polymeric nanoparticles containing both Cas9 mRNA and sgRNA were administered *in vitro*, 90% *egfp* gene editing was observed in NIH 3T3 cells. This RNA-codelivery methodology was also applicable in a model HEK 293T cell line, in the presence of serum proteins, and at two different Cas9 mRNA to sgRNA ratios. When complexed with luciferase mRNA and administered *in vivo*, both denpol-mRNA polymeric nanoparticle species demonstrated robust luciferase expression in the lungs and spleens of treated mice. With presumed uptake by immune cells in the spleen, nanoparticles generated from these vectors are extremely promising as vectors for CRISPR-Cas9 gene editing of immune cells and as mRNA delivery vehicles for future immunotherapy applications.

3.4 References

(1) Gillmore, J. D.; Gane, E.; Taubel, J.; Kao, J.; Fontana, M.; Maitland, M. L.; Seitzer, J.; O'Connell, D.; Walsh, K. R.; Wood, K.; Phillips, J.; Xu, Y.; Amaral, A.; Boyd, A. P.; Cehelsky, J. E.; McKee, M. D.; Schiermeier, A.; Harari, O.; Murphy, A.; Kyratsous, C. A.; Zambrowicz, B.; Soltys, R.; Gutstein, D. E.; Leonard, J.; Sepp-Lorenzino, L.; Lebwohl, D., CRISPR-Cas9 In Vivo Gene Editing for Transthyretin Amyloidosis. *New England Journal of Medicine* **2021,** *385* (6), 493-502.

(2) Mirjalili Mohanna, S. Z.; Djaksigulova, D.; Hill, A. M.; Wagner, P. K.; Simpson, E. M.; Leavitt, B. R., LNP-mediated delivery of CRISPR RNP for wide-spread in vivo genome editing in mouse cornea. *Journal of Controlled Release* **2022,** *350*, 401-413.

(3) Han, J. P.; Kim, M.; Choi, B. S.; Lee, J. H.; Lee, G. S.; Jeong, M.; Lee, Y.; Kim, E.-A.; Oh, H.-K.; Go, N.; Lee, H.; Lee, K. J.; Kim, U. G.; Lee, J. Y.; Kim, S.; Chang, J.; Lee, H.; Song, D. W.; Yeom, S. C., In vivo delivery of CRISPR-Cas9 using lipid nanoparticles enables antithrombin gene editing for sustainable hemophilia A and B therapy. *Science Advances* **2022,** *8* (3), eabj6901.

(4) Ghasemiyeh, P.; Mohammadi-Samani, S., Solid lipid nanoparticles and nanostructured lipid carriers as novel drug delivery systems: applications, advantages and disadvantages. *Res Pharm Sci* **2018,** *13* (4), 288-303.

(5) Zhang, Z.; Wan, T.; Chen, Y.; Chen, Y.; Sun, H.; Cao, T.; Songyang, Z.; Tang, G.; Wu, C.; Ping, Y.; Xu, F. J., Cationic Polymer-Mediated CRISPR/Cas9 Plasmid Delivery for Genome Editing. *Macromolecular Rapid Communications* **2019,** *40* (5), e1800068.

(6) Feng, Y.; Guo, Z.; Chen, J.; Zhang, S.; Wu, J.; Tian, H.; Chen, X., Cationic polymer synergizing with a disulfide-containing enhancer achieved efficient nucleic acid and protein delivery. *Biomaterials Science* **2022**.

(7) Abbasi, S.; Uchida, S.; Toh, K.; Tockary, T. A.; Dirisala, A.; Hayashi, K.; Fukushima, S.; Kataoka, K., Co-encapsulation of Cas9 mRNA and guide RNA in polyplex micelles enables genome editing in mouse brain. *Journal of Controlled Release* **2021,** *332*, 260-268.

(8) Kretzmann, J. A.; Ho, D.; Evans, C. W.; Plani-Lam, J. H. C.; Garcia-Bloj, B.; Mohamed, A. E.; O'Mara, M. L.; Ford, E.; Tan, D. E. K.; Lister, R.; Blancafort, P.; Norret, M.; Iyer, K. S., Synthetically controlling dendrimer flexibility improves delivery of large plasmid DNA. *Chemical Science* **2017,** *8* (4), 2923-2930.

(9) Arno, M. C.; Williams, R. J.; Bexis, P.; Pitto-Barry, A.; Kirby, N.; Dove, A. P.; O'Reilly, R. K., Exploiting topology-directed nanoparticle disassembly for triggered drug delivery. *Biomaterials* **2018,** *180*, 184-192.

(10) Lino, C. A.; Harper, J. C.; Carney, J. P.; Timlin, J. A., Delivering CRISPR: a review of the challenges and approaches. **2018,** *25* (1), 1234-1257.

(11) Oude Blenke, E.; Evers, M. J. W.; Mastrobattista, E.; van der Oost, J., CRISPR-Cas9 gene editing: Delivery aspects and therapeutic potential. *Journal of Controlled Release* **2016,** *244*, 139-148.

(12) Transient editing catches the eye. *Nature Biomedical Engineering* **2021,** *5* (2), 127-127.

(13) Zeng, H.; Little, H. C.; Tiambeng, T. N.; Williams, G. A.; Guan, Z., Multifunctional Dendronized Peptide Polymer Platform for Safe and Effective siRNA Delivery. *Journal of the American Chemical Society* **2013,** *135* (13), 4962-4965.
(14) Oldenhuis, N. J.; Eldredge, A. C.; Burts, A. O.; Ryu, K. A.; Chung, J.; Johnson, M. E.; Guan, Z., Biodegradable Dendronized Polymers for Efficient mRNA Delivery. *ChemistrySelect* **2016,** *1* (15), 4413-4417.
(15) Erazo-Oliveras, A.; Muthukrishnan, N.; Baker, R.; Wang, T. Y.; Pellois, J. P., Improving the endosomal escape of cell-penetrating peptides and their cargos: strategies and challenges. *Pharmaceuticals (Basel)* **2012,** *5* (11), 1177-1209.
(16) Chang, K.-L.; Higuchi, Y.; Kawakami, S.; Yamashita, F.; Hashida, M., Efficient Gene Transfection by Histidine-Modified Chitosan through Enhancement of Endosomal Escape. *Bioconjugate Chemistry* **2010,** *21* (6), 1087-1095.
(17) Riley, K. E.; Hobza, P., On the Importance and Origin of Aromatic Interactions in Chemistry and Biodisciplines. *Accounts of Chemical Research* **2013,** *46* (4), 927-936.
(18) Warren, G. M.; Meir, A.; Wang, J.; Patel, D. J.; Greene, E. C.; Shuman, S., Structure–activity relationships at a nucleobase-stacking tryptophan required for chemomechanical coupling in the DNA resecting motor-nuclease AdnAB. *Nucleic Acids Research* **2021,** *50* (2), 952-961.
(19) Tang, M. X.; Szoka, F. C., The influence of polymer structure on the interactions of cationic polymers with DNA and morphology of the resulting complexes. *Gene Therapy* **1997,** *4* (8), 823-832.
(20) Hwang, C.; Sinskey, A. J.; Lodish, H. F., Oxidized Redox State of Glutathione in the Endoplasmic Reticulum. *Science* **1992,** *257* (5076), 1496-1502.
(21) Kim, T. I.; Kim, S. W., Bioreducible polymers for gene delivery. *Reactive & Functional Polymers* **2011,** *71* (3), 344-349.
(22) Raghupathi, K.; Kumar, V.; Sridhar, U.; Ribbe, A. E.; He, H.; Thayumanavan, S., Role of Oligoethylene Glycol Side Chain Length in Responsive Polymeric Nanoassemblies. *Langmuir* **2019,** *35* (24), 7929-7936.
(23) Yuen, G.; Khan, F. J.; Gao, S.; Stommel, J. M.; Batchelor, E.; Wu, X.; Luo, J., CRISPR/Cas9-mediated gene knockout is insensitive to target copy number but is dependent on guide RNA potency and Cas9/sgRNA threshold expression level. *Nucleic Acids Research* **2017,** *45* (20), 12039-12053.
(24) Cherng, J. Y.; van de Wetering, P.; Talsma, H.; Crommelin, D. J.; Hennink, W. E., Effect of size and serum proteins on transfection efficiency of poly ((2-dimethylamino)ethyl methacrylate)-plasmid nanoparticles. *Pharmaceutical Research* **1996,** *13* (7), 1038-1042.
(25) Albanese, A.; Tang, P. S.; Chan, W. C., The effect of nanoparticle size, shape, and surface chemistry on biological systems. *Annual Review of Biomedical Engineering* **2012,** *14*, 1-16.
(26) Mandl, H. K.; Quijano, E.; Suh, H. W.; Sparago, E.; Oeck, S.; Grun, M.; Glazer, P. M.; Saltzman, W. M., Optimizing biodegradable nanoparticle size for tissue-specific delivery. *Journal of Controlled Release* **2019,** *314*, 92-101.
(27) Harrell, M. I.; Iritani, B. M.; Ruddell, A., Lymph node mapping in the mouse. *Journal of Immunological Methods* **2008,** *332* (1-2), 170-174.
(28) Bronte, V.; Pittet, M. J., The spleen in local and systemic regulation of immunity. *Immunity* **2013,** *39* (5), 806-818.

(29) Fromen, C. A.; Robbins, G. R.; Shen, T. W.; Kai, M. P.; Ting, J. P. Y.; DeSimone, J. M., Controlled analysis of nanoparticle charge on mucosal and systemic antibody responses following pulmonary immunization. *Proceedings of the National Academy of Sciences* **2015,** *112* (2), 488-493.
(30) Saito, E.; Gurczynski, S. J.; Kramer, K. R.; Wilke, C. A.; Miller, S. D.; Moore, B. B.; Shea, L. D., Modulating lung immune cells by pulmonary delivery of antigen-specific nanoparticles to treat autoimmune disease. *Science Advances* **2020,** *6* (42), eabc9317.
(31) Kaplowitz, N., The importance and regulation of hepatic glutathione. *Yale Journal of Biology and Medicine* **1981,** *54* (6), 497-502.
(32) Patel, A. A.; Ginhoux, F.; Yona, S., Monocytes, macrophages, dendritic cells and neutrophils: an update on lifespan kinetics in health and disease. *Immunology* **2021,** *163* (3), 250-261.
(33) Luo, Y.-L.; Xu, C.-F.; Li, H.-J.; Cao, Z.-T.; Liu, J.; Wang, J.-L.; Du, X.-J.; Yang, X.-Z.; Gu, Z.; Wang, J., Macrophage-Specific in Vivo Gene Editing Using Cationic Lipid-Assisted Polymeric Nanoparticles. *ACS Nano* **2018,** *12* (2), 994-1005.
(34) Hiatt, J.; Cavero, D. A.; McGregor, M. J.; Zheng, W.; Budzik, J. M.; Roth, T. L.; Haas, K. M.; Wu, D.; Rathore, U.; Meyer-Franke, A.; Bouzidi, M. S.; Shifrut, E.; Lee, Y.; Kumar, V. E.; Dang, E. V.; Gordon, D. E.; Wojcechowskyj, J. A.; Hultquist, J. F.; Fontaine, K. A.; Pillai, S. K.; Cox, J. S.; Ernst, J. D.; Krogan, N. J.; Marson, A., Efficient generation of isogenic primary human myeloid cells using CRISPR-Cas9 ribonucleoproteins. *Cell Reports* **2021,** *35* (6), 109105.
(35) Zhang, Y.; Shen, S.; Zhao, G.; Xu, C.-F.; Zhang, H.-B.; Luo, Y.-L.; Cao, Z.-T.; Shi, J.; Zhao, Z.-B.; Lian, Z.-X.; Wang, J., In situ repurposing of dendritic cells with CRISPR/Cas9-based nanomedicine to induce transplant tolerance. *Biomaterials* **2019,** *217*, 119302.
(36) Yan, X.; Pan, Q.; Xin, H.; Chen, Y.; Ping, Y., Genome-editing prodrug: Targeted delivery and conditional stabilization of CRISPR-Cas9 for precision therapy of inflammatory disease. *Science Advances* **2021,** *7* (50), eabj0624.
(37) Wan, T.; Pan, Q.; Ping, Y., Microneedle-assisted genome editing: A transdermal strategy of targeting NLRP3 by CRISPR-Cas9 for synergistic therapy of inflammatory skin disorders. *Science Advances* **2021,** *7* (11), eabe2888.

3.5 Experimental Protocols

Chemical Reagents: Unless otherwise noted, all reagents were used as received from commercial suppliers without further purification. All chemical reactions were performed in HPLC-grade solvent unless otherwise noted. Protected amino acids were purchased from Advanced ChemTech (Louisville, KY) and Aroz Technologies, LLC (Cincinnati, OH). Coupling reagents were purchased from GL Biochem Ltd. (Shanghai,

China). Lipofectamine 2000 was purchased from Invitrogen (Carlsbad, CA). Aspartate Aminotransferase (AST) Activity Assay Kit was purchased directly from Abcam (ab105135). All aqueous solutions used for nanoparticle complexation were made using DEPC-treated water to prevent RNAse contamination. sgRNAs were synthesized using an Engen sgRNA Synthesis Kit (NEB; # E3322V) according to the manufacturer's protocols. Generated sgRNA sequences are provided in the Supporting Information (Table S1). Cas9 mRNA was purchased directly from TriLink Biotechnologies (#L-7606-100) and diluted in 20 μM Sodium Citrate buffer (pH 6.4) before use. Cy5-labelled luciferase mRNA was purchased directly from TriLink Biotechnologies (#L-7202) with custom Cy5-functionalization and similarly diluted before use.

General Instrument Information: Nuclear Magnetic Resonance (NMR) spectra were recorded on 500 MHz or 600 MHz Bruker spectrometers at 25 °C with chemical shifts reported in ppm and coupling constants in Hertz (Hz). ^{1}H NMR chemical shifts were referenced to D_2O. Denpol-RNA polyplex sizes and zeta potential values were measured at 633 nm using a Zetasizer dynamic light scattering instrument (Malvern, UK) at 25 °C with a detection angle of 173°. Flow cytometry experiments determining *egfp* knockout/ gene editing were conducted on a NovoCyte flow cytometer (ACEA Biosciences, San Diego; PMT voltage of 300 V) using NovoExpress Software. Fluorescence assisted cell sorting experiments (FACS) for lentiviral transduction experiments were conducted on either a Beckton Dickinson FACSAria Fusion flow cytometer (BD Biosciences, USA) or Beckton DickinsonFACSAria II flow cytometer (BD Biosciences, USA). For both instruments, the argon ion excitation laser emitted at 488nm and PMT voltage was set to 300V. Sorting gates were manually determined based on the background fluorescence of GFP-negative cells

and the intensity of EGFP expression on transduced cells. Denpol-RNA nanoparticle complexation assays were performed using agarose gel electrophoresis and imaged on a Typhoon 9410 system (GE).

Plasmids: psPAX2 plasmid was a gift from Didier Trono (Addgene plasmid #12260; RRID: Addgene _12260), pMD2.G was a gift from Didier Trono (Addgene plasmid #12259; RRID: Addgene_12259), lentiCas9-EGFP was a gift from Phil Sharp & Feng Zhang (Addgene plasmid # 63592; RRID:Addgene_63592), and pLJM1-EGFP was a gift from David Sabatini (Addgene plasmid #19319; RRID: Addgene_19319). All plasmids were transformed into competent DH5α cells through heat-shock transformation and streaked onto plates containing lysogeny broth (LB; TEKNOVA, #L9135) with 1% agarose (Alfa Aesar, #J66501) and 150 μg/mL ampicillin (CHEM IMPEX, #00516). Plates were incubated at 37 °C overnight to yield colonies that contained relevant plasmid. Individual colonies were grown in LB containing 150 μg/mL ampicillin under continuous agitation. Resulting cultures were then lysed and plasmid DNA was extracted by NucleoBond Xtra Midiprep EF Midiprep protocols (Macherey-Nagel, #740420.10).

Cell Lines and Culturing: NIH-3T3 cells were a generous gift from Professor Young Jik Kwon (Department of Chemical Engineering, UC Irvine, CA). HEK293T and HEK 293FT cells were generously provided by Professor Jennifer Prescher (Department of Chemistry, UC Irvine, CA). Unless otherwise indicated, all cell lines used were grown in complete low glucose DMEM (for NIH 3T3 cells; Gibco, #11885084) or high glucose DMEM (for HEK293FT and HEK293T cells; Gibco, #119650092) containing 10% v/v Fetal Bovine Serum (FBS; Sigma, #12207C) and 1X antibiotic-antimycotic solution (Gibco, #15240062).

Trypsin (Gibco, #25200056) was used to dislodge cells for routine passaging. All cell lines are prophylactically treated with Mycoplasma Removal Agent (MB Biosciences, #3050044) to prevent mycoplasma contamination.

Cryo-TEM: : **G2 2:1**-sgRNA polymer nanoparticles samples were prepared from resuspended or extracted solutions onto Quantifoil R2/2 (Electron Microscopy Sciences) grids that were layered with graphene oxide following an established procedure.[1] **G2 2:1**-Cas9 MRNA-sgRNA nanoparticles were loaded onto quantifoil grids without graphene oxide pretreatment. Vitrification was carried out by an automatic plunge freezer ME GP2 (Leica Microsystems) with 3 μL of sample. Grid preparation was performed at 95% humidity. After loading the sample, grids were let to sit for 3 minutes before being blotted for 3 seconds prior to plunging into liquid propane. Cryo-TEM samples were then placed on a Gatan cryo-TEM holder and imaged on a JEOL 2100F TEM using a Schottky type field emission gun operating at 200 keV. Images were recorded using SerialEM low dose imaging mode with a Gatan OneView CMOS camera at 4k × 4k resolution.

sgRNA Synthesis and Characterization: sgRNA was generated according to the EnGen®sgRNA Synthesis Kit protocol; ssDNA Oligo (generated from IDT), *S. pyrogenes* Cas9 tracrRNA Scaffold Oligo, RNase-free water, and EnGen 2X sgRNA Reaction Mix were combined and incubated at 37 °C for 40 minutes. After incubation this mixture was treated with DNase (provided in EnGen®sgRNA Synthesis Kit) and the resulting RNA mixture was purified by GeneJET RNA Cleanup and Concentration Micro Kit (Thermo Scientific, #K0841) to yield purified sgRNA. Generated sgRNAs were analyzed by 10% TBE-Urea gel electrophoresis; sgRNA were mixed with 1 volumetric equivalent of 2X RNA Loading Dye

(NEB, #BO363S) and incubated at 90 °C for ten minutes. Resulting denatured mixes were loaded into a pre-cast Mini-PROTEAN TBE-Urea gel (10%; Bio-Rad, #456-6033) and run in 1X TBE running buffer for 75 minutes at 180 volts. The resulting gel was rinsed with fresh 1X TBE buffer, stained with Gel-Red (Biotium, #41002) and analyzed by a Typhoon 8600 Imager (Molecular Dynamics, Israel). Image contrast was adjusted in ImageQuant Software.

Denpol Synthesis and Characterization: Typical procedure for denpol functionalization was as follows: G2 and 50% TEG G2 denpol backbones were synthesized and dendronized according to literature procedures. For final denpol functionalization, in a 1-dram vial equipped with a stir bar, the specified denpol (10.0 mg/ 1.00 equiv.) was dissolved in 1 mL of DMF. After the denpol was completely dissolved, Boc-His(Boc)-OH, and Boc-Trp(Boc)-OH were added in the corresponding ratios. After all reagents had been solubilized, ByBOP (10.00 equiv.) and DIPEA (12.00 equiv.) were added, and the 1-dram vial was sealed with nitrogen and stirred over-night. After 12 h, 3 mL of MeOH was added to the reaction, and the mixture was purified via dialysis (MWCO = 6 – 8 kDa) against MeOH for 12 h. After 12 h, the mixture was concentrated in vacuo (no heating), yielding a solid film. The Boc groups were removed by suspending the solid mixture of TFA (1.5 mL), DCM (0.75 mL), and TIPS (0.1 mL) and stirring for 4 h under nitrogen. The mixture was concentrated in vacuo (no heating), resuspending in methanol, and then precipitated in cold ether. The precipitate was pelleted via centrifugation, and the supernatant was discarded. The precipitate was purified via dialysis (MWCO = 6 – 8 kDa) in MeOH for 24 hours and then concentrated in vacuo. All denpols were characterized by ^{1}H NMR. The final functionalization ratio was calculated using the same methodology as previously reported.[2]

Denpol-sgRNA Nanoparticle Complexation and Gel Electrophoresis: The binding of sgRNA to denpols was studied through agarose gel electrophoresis. After nanoparticle formulation 2.5 μL 6X loading dye was added to each sample and 10 μL of the mixture was loaded to each well in a 1% agarose gel with 1X GelRed dye. Gel electrophoresis was run in TAE buffer at 60 V for 45 minutes and the gel was visualized under a UV transilluminator.

Denpol-RNA Polymer Nanoparticle Formulation: To generate nanoparticles, denpol stock solutions (10 mgs/ mL in DI H_2O) were mixed with RNA stock solutions (20 μM Sodium Citrate buffer, pH 6.4) via pipette at defined cationic amine to phosphate (N/P) ratios. Resulting nanoparticle solutions were continuously mixed for another 30 seconds before the addition of desired buffer and further incubation at 25 ˚C. For dynamic light scattering and zeta potential experiments, phosphate buffered saline (PBS; pH 7.4) was used to disperse denpol-RNA nanoparticles and were incubated in PBS for at least 10 minutes prior to measurements. For cellular transfection experiments, OptiMEM was used to disperse nanoparticles and nanoparticles were incubated for at least 20 minutes before administering to cells.

Dynamic Light Scattering Characterization: After formulation, denpol-RNA nanoparticles were resuspended in PBS and denpol-RNA polymeric nanoparticle sizes were measured at 633 nm using a Zetasizer Nano ZS dynamic light scattering instrument (Malvern Instruments, Malvern, UK) at 25 ˚C with detection angle of 173°.

Lentivirus Generation, Cell Transduction Protocol, and FACS Sorting: All lentiviral particles were generated using previously established procedures.[3] HEK293FT

($1x10^6$ cells) were seeded onto poly-L-lysine-treated (Millipore, #P8920) 60mm tissue-culture treated plate and set to adhere overnight in complete media. The following day, media was exchanged for OptiMEM (Gibco, #31985-070) containing 50 μM chloroquine (Sigma, #50-63-5) and cells were incubated at 37 °C for eight hours before switching back to complete media for another eight hours. After this period, lentiviral packaging plasmids pMD2.G (10 μg) and psPAX2 (10 μg) were co-assembled with Lenti-Cas9-eGFP plasmid (20 μg) in Lipofectamine P2000 (Invivogen, #11668019) in OptiMEM and transfected into 50 μM-chloroquine-treated HEK293T cells. After eight hours of incubation, Lipofectamine-containing media was removed and fresh media containing 10% serum was added to the treated plate. Supernatant from these plates were harvested after 48 hours and 72 hours and concentrated via 100K-MWCO Centricon filters (Millipore, #ACS510012) to obtain concentrated lentivirus. Aliquoted lentivirus was snap-frozen and stored at -80 °C. NIH-3T3 cells were plated at 2.0 x 10^3 cells/well in 48-well plates and adhered overnight at 37 °C. Adhered cells were incubated with 5 μL of 8 μg/mL Polybrene (28728-55-4) in OptiMEM along with concentrated lentivirus for 24 hours and grown for an additional 72 hours in complete media. Treated cells were then trypsinized and sorted by FACS to obtain stable lentivirally-transduced cell populations. This protocol was repeated with pLJM1-eGFP expression plasmid (20 μg) and the same packaging plasmids to obtain lentiviral particles containing pLJM1-eGFP plasmid. Both NIH-3T3 cells and HEK293T were similarly transduced and sorted FACS to obtain stable lentivirally-transduced cell populations.

For all lentiviral-transduced cell populations, cells were sorted by either a Beckton Dickinson FACSAria Fusion flow cytometer or Beckton Dickinson FACSAria II flow cytometer. For both instruments, the argon ion excitation laser emitted at 488nm and PMT

voltage was set to 300V. Sorting gates were manually determined based on the background fluorescence of EGFP-negative cells and the intensity of EGFP expression on transduced cells. Subsequent pooled cell populations were grown using normal tissue culture conditions.

***In Vitro* Transfection Experiment**s: For sgRNA delivery experiments, a total of 200 ng of *egfp*-targeting sgRNA was added for each well. Similarly, for Cas9 mRNA-sgRNA codelivery experiments a total of 200 ng of RNA was added to each well, with either a 1:7 or 1:10 w/w ratio of Cas9 mRNA to sgRNA comprising the final RNA quantity.

For *in vitro* nanoparticle transfection experiments, lentivirally-transduced NIH 3T3 cells were plated at a density of 5,000 cells/ well in 96-well plates 24 hours prior to treatment. During transfection media was removed, formulated nanoparticle solutions were added to each corresponding cell well, and treated cells were incubated at 25 ˚C for 5 minutes under gentle mixing. Afterwards, for serum-free conditions, an additional 100 µL of OptiMEM was added to each cell well and incubated for 8 hours at 37 ˚C. For serum-containing conditions, an additional 100 µL of OptiMEM containing 10% FBS was added to each cell well and incubated for 8 hours at 37 ˚C. All nanoparticle treatments were performed in triplicate. Following the initial 8-hour incubation all media was removed and replaced with complete DMEM with 10% FBS. Treated cells were cultured for 5 days before flow cytometry analysis. After 120 hours of culturing has concluded, media in cell wells were removed and replaced with trypsin to dislodge cells. Trypsinized cells were quenched with complete DMEM and analysed by flow cytometry to determine the number of gene-edited, EGFP-negative, cells.

***In Vivo* Nanoparticle Delivery:** C57BL/6 mice were purchased from Jackson Laboratories. Mouse studies were conducted in accordance with federal guidelines and were approved by the Institutional Animal Care and Use Committee at the University of California Irvine. 4 weeks old (~25 g) C57BL/6 mice were treated with Cy5-labelled luciferase mRNA complexed with denpols at (N/P = 30) via vein tail injection at a single mRNA dose of 15 μg/mouse (150 μL solution). Six hours post-injection, D-luciferin substrate was administered via intraperitoneal injection 10-20 minutes prior to imaging. For IVIS imaging, animals were anesthetized with isoflurane in a separate chamber and then moved to a dark IVIS imaging chamber (PerkinElmer, USA) while being kept under isoflurane anaesthesia using nose cones and a heated stage. For organ-specific imaging, treated mice were sacrificed, organs were excised, and organs were similarly imaged using an IVIS camera.

AST assay from Denpol-Fluc mRNA Nanoparticle-Treated C57BL/6 Mice: AST assay kit was purchased directly from abcam (ab 105135) and used according to the manufacturer's protocols. AST assay was performed using the blood of mice 4 days following injection of mice treated with denpol-Fluc mRNA polymeric nanoparticles (formulated at an N/P ratio of 30). AST kit was used according to the manufacturer's protocols.

3.6 References for Experimental Protocols

(1) Patterson, J. P.; Sanchez, A. M.; Petzetakis, N.; Smart, T. P.; Epps, T. H., 3rd; Portman, I.; Wilson, N. R.; O'Reilly, R. K., A simple approach to characterizing block copolymer

assemblies: graphene oxide supports for high contrast multi-technique imaging. *Soft Matter* **2012,** *8* (12), 3322-3328.
(2) Oldenhuis, N. J.; Eldredge, A. C.; Burts, A. O.; Ryu, K. A.; Chung, J.; Johnson, M. E.; Guan, Z., Biodegradable Dendronized Polymers for Efficient mRNA Delivery. *ChemistrySelect* **2016,** *1* (15), 4413-4417.
(3) Sanjana, N. E.; Shalem, O.; Zhang, F., Improved vectors and genome-wide libraries for CRISPR screening. *Nature Methods* **2014,** *11* (8), 783-784.

3.7 Supplementary Figures

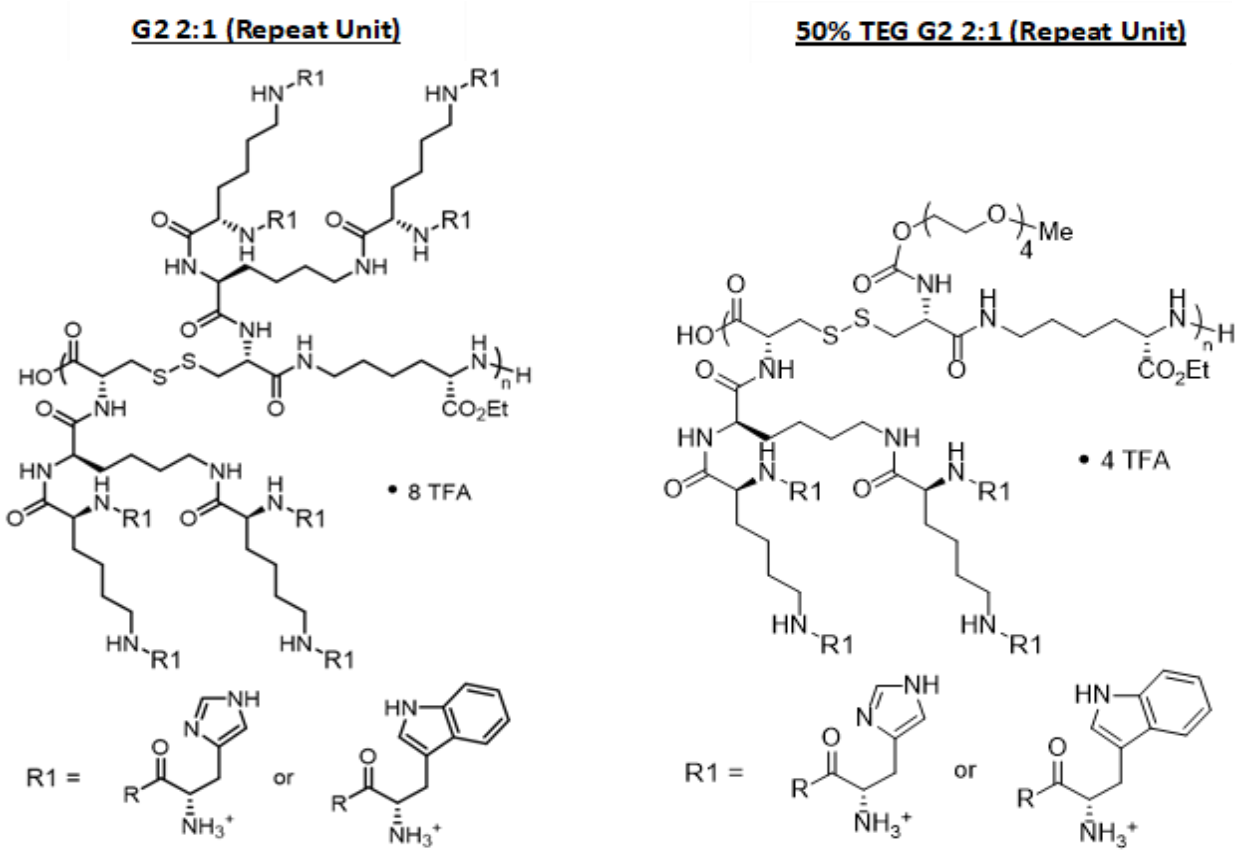

Figure S3.1 Expanded denpol structures for polymer repeat units of **G2 2:1** (left) and **50% TEG G2 2:1** (right).

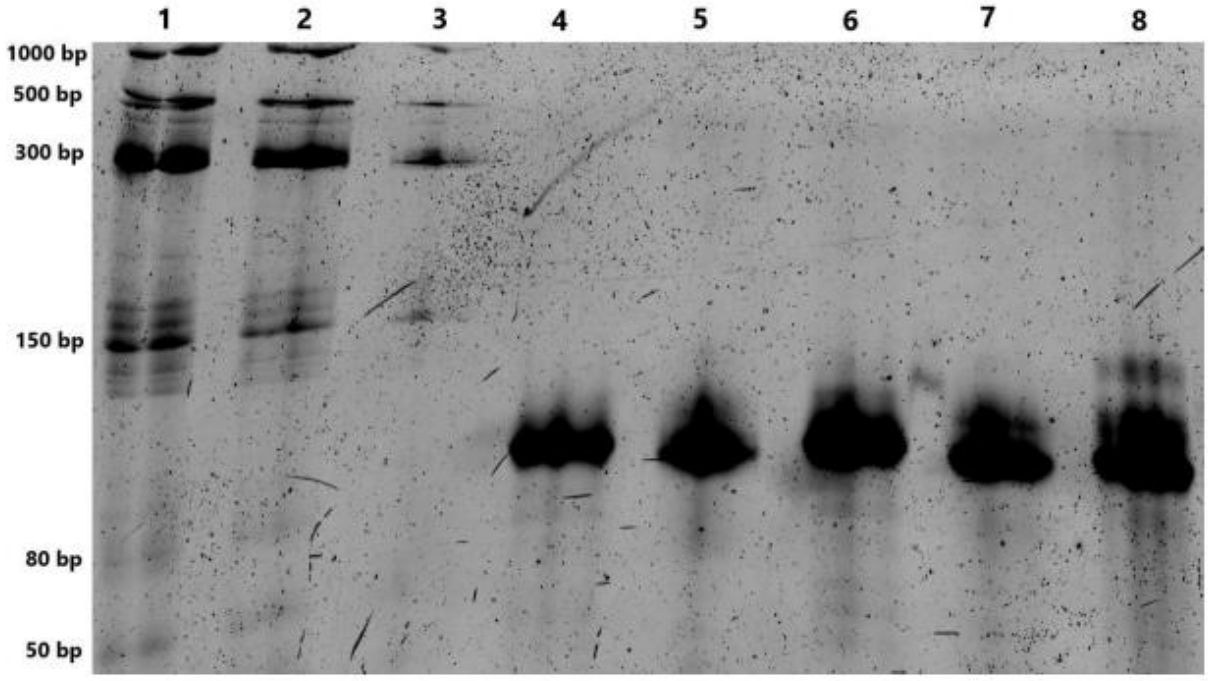

Figure S3.2 10% TBE-Urea gel of various synthesized and purified sgRNAs. Wells **1**-**3** all contain ssRNA ladder in varying amounts. Well **4** contains SG1 sgRNA, well **5** contains SG4 sgRNA (not shown in this work), well **6** contains SG2 sgRNA, well **7** contains SG3 sgRNA, and well **8** contains control sgRNA (generated from scrambler ssDNA provided by NEB).

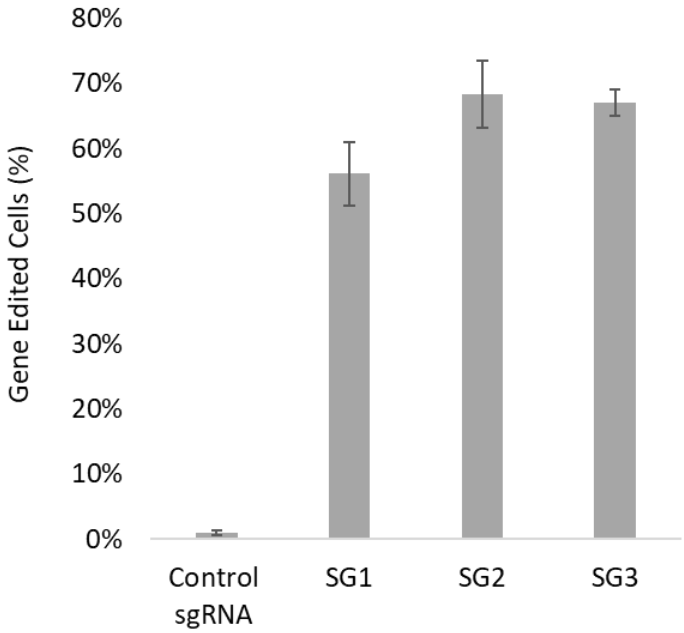

Figure S3.3 *egfp* gene editing efficiency with different sgRNA species in Lenti-Cas9-EGFP-transduced NIH-3T3 cells. Lipofectamine 2000 was used as delivery vehicle for all sgRNA samples.

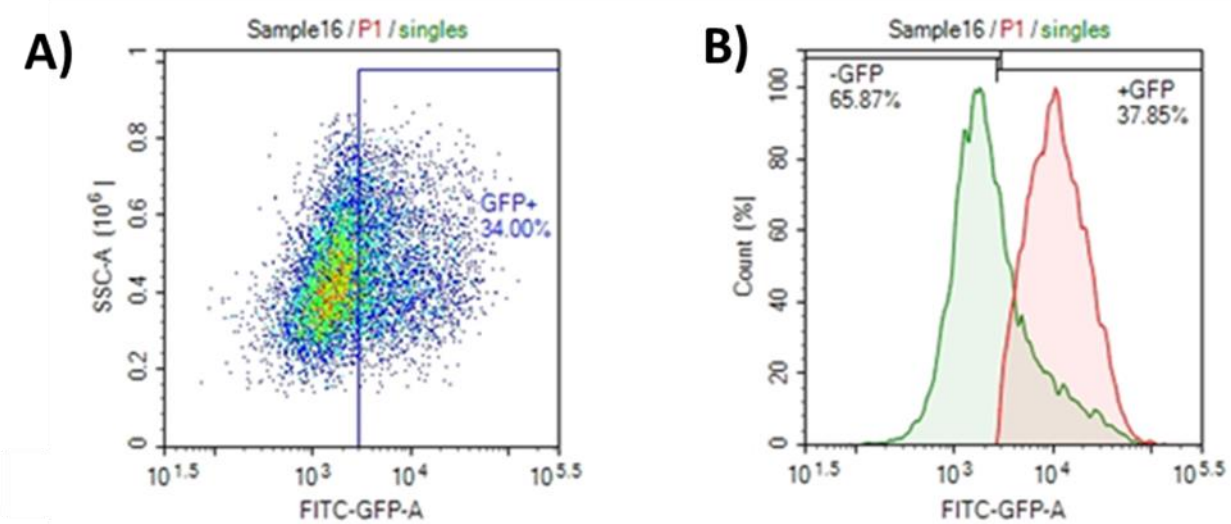

Figure S3.4 Representative flow cytometry **A)** density plot for sorting sgRNA-treated Lenti-Cas9-EGFP-transduced NIH-3T3 cells (From Figure S3.3; SG3 sgRNA used for A). **B)** Representative histogram with gating to sort EGFP-negative/ gene edited Lenti-Cas9-EGFP-transduced NIH-3T3 cells after sgRNA-treatment. sgRNA-treated/ gene edited cells are shown in green and overlayed with nontreated Lenti-Cas9-EGFP-transduced NIH-3T3 cells (red).

Figure S3.5 Gel electrophoresis assay for denpol-sgRNA complexes at various N/P ratios. Exact N/P ratios for given wells are listed above gel images. Minimum N/P ratio for complete binding and polyplex formation is achieved at an N/P of 2.5 for both **G2 2:1** (left) and **50% TEG G2 2:1** (right).

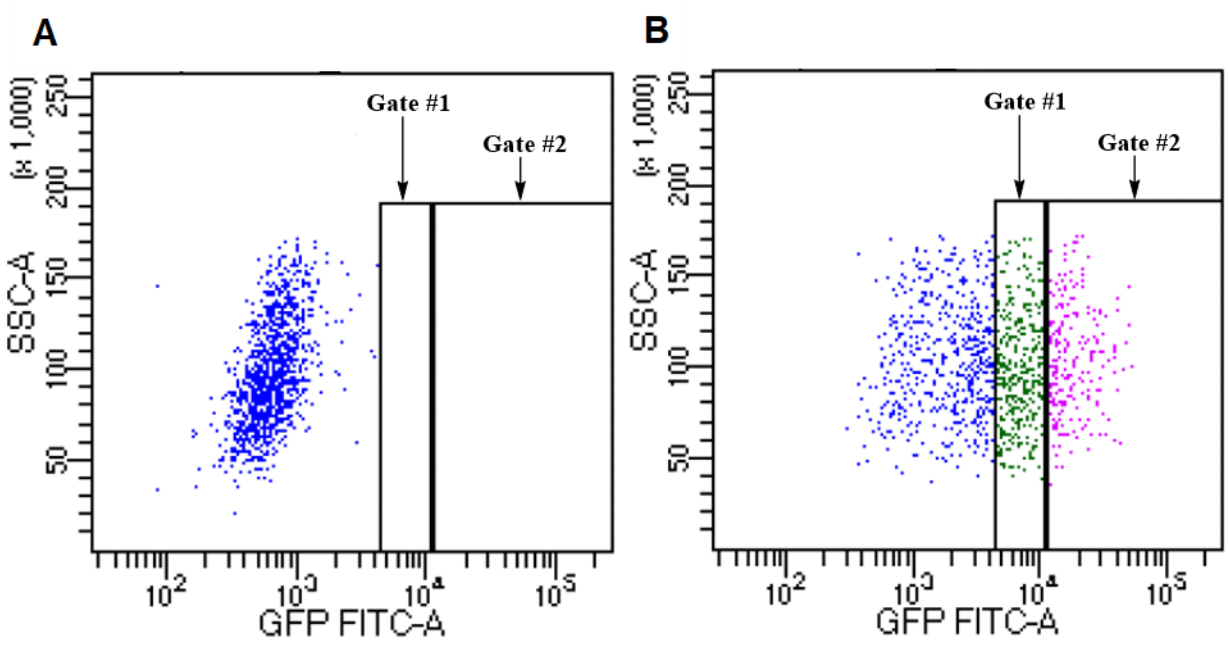

Figure S3.6 FACS gates for Control NIH-3T3 cells (A; left) and Lenti-Cas9-EGFP-transduced NIH-3T3 cells (B; right) using a Beckton Dickinson FACSAria Fusion flow cytometer. EGFP+ cells within gate #2 were pooled, expanded, and used for future gene editing experiments. Flow cytometer argon ion excitation laser emitted at 488nm and PMT voltage was set to 300V.

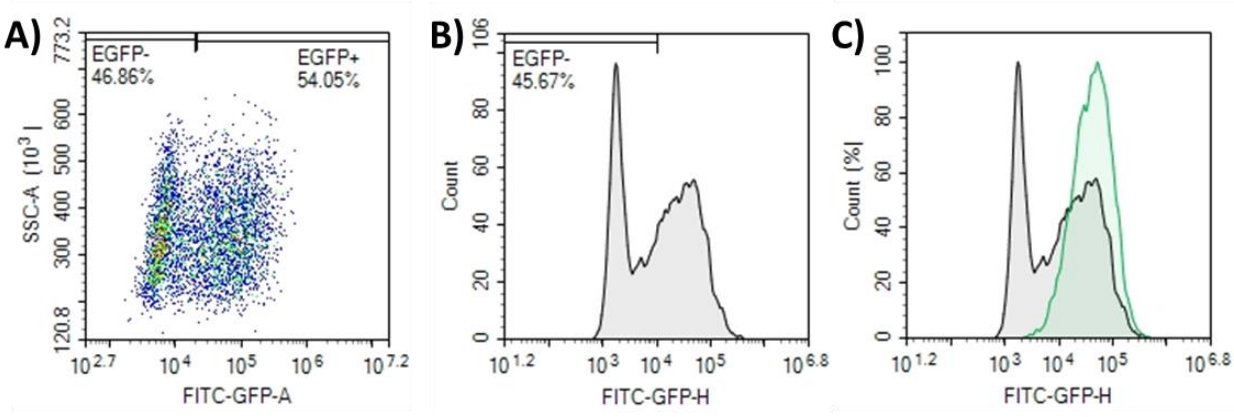

Figure S3.7 Representative flow cytometry **A)** density plot for sorting denpol-sgRNA nanoparticle-treated Lenti-Cas9-EGFP-transduced NIH-3T3 cells (from Figure 3.2; SG3 sgRNA used for A). **B)** Representative histogram with gating to sort EGFP-negative/ gene edited Lenti-Cas9-EGFP-transduced NIH-3T3 cells after denpol-sgRNA nanoparticle treatment. **C)** sgRNA-treated/ gene edited cells (gray) overlayed with control, EGFP+ Lenti-Cas9-EGFP-transduced NIH-3T3 cells (green).

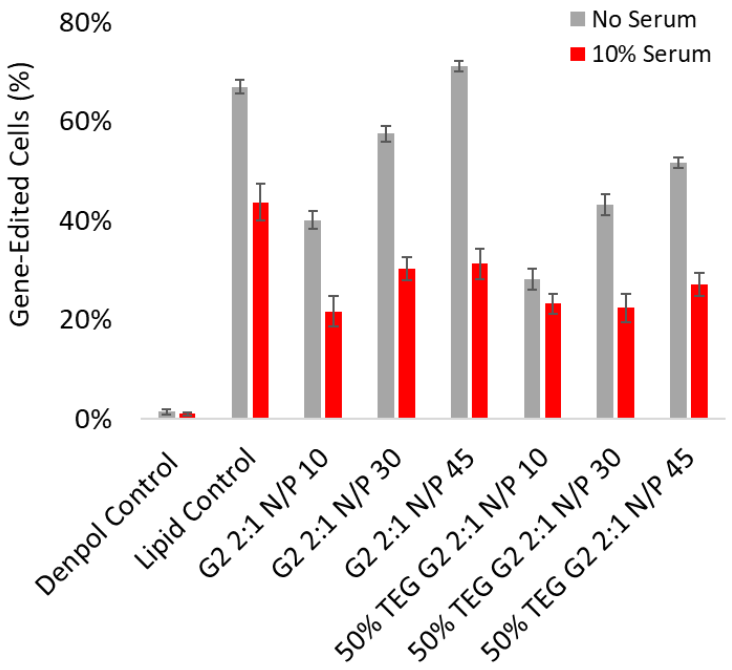

Figure S3.8 *egfp* gene editing efficiency using **G2 2:1** or **50% TEG G2 2:1** denpol-sgRNA nanoparticles (SG3 sgRNA) at different N/P ratios with Lenti-Cas9-EGFP-transduced NIH-3T3 cells. Nanoparticle samples were formulated with serum (red) or without (gray). Lipofectamine P2000 was used as lipid control. n=3 for all samples.

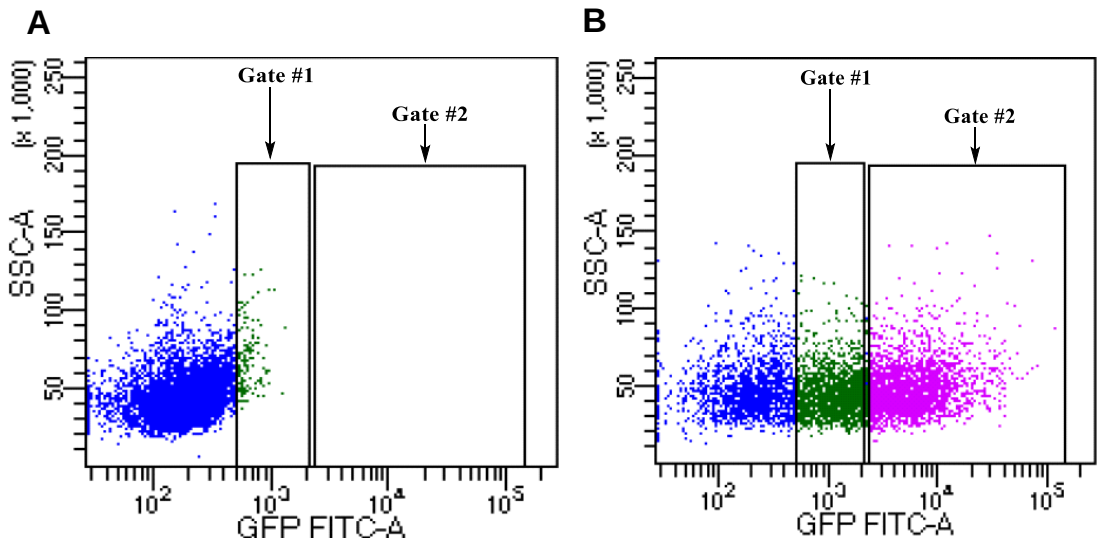

Figure S3.9 FACS gates for Control NIH-3T3 cells (A; left) and Lenti-pLJM1-EGFP -transduced NIH-3T3 cells (B; right) using a Beckton Dickinson FACSAria Fusion flow cytometer. EGFP+ cells within gate #2 were pooled, expanded, and used for future gene editing experiments. Flow cytometer argon ion excitation laser emitted at 488nm and PMT voltage was set to 300V.

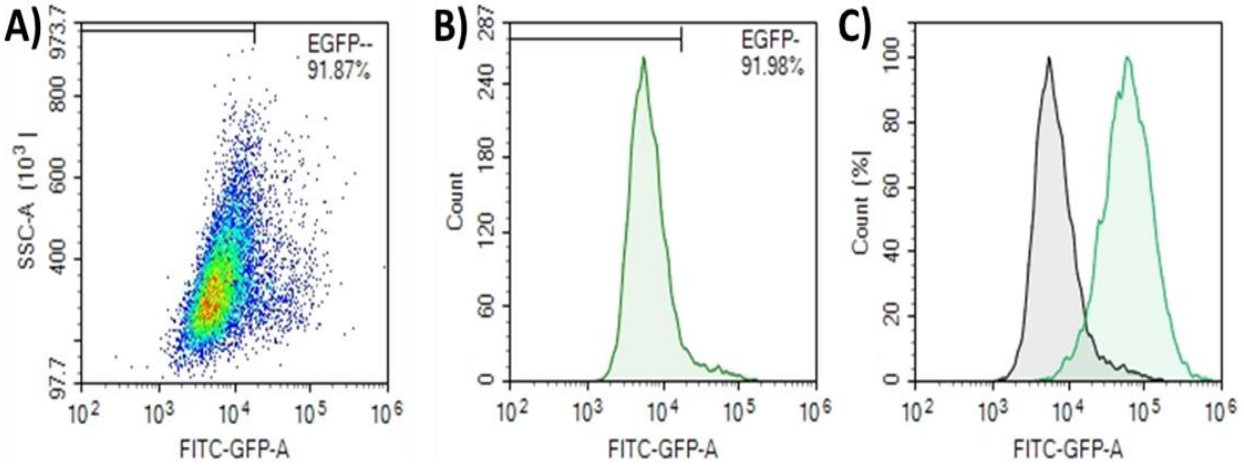

Figure S3.10 Representative flow cytometry **A)** density plot for sorting denpol-Cas9 mRNA-sgRNA nanoparticle-treated in Lenti-pLJM1-EGFP -transduced NIH-3T3 cells. **B)** Representative histogram with gating to sort EGFP-negative/ gene edited Lenti-pLJM1-EGFP -transduced NIH-3T3 cells denpol-Cas9 mRNA-sgRNA nanoparticle treatment. **C)** Cas9 mRNA-sgRNA-treated/ gene edited cells (gray) overlayed with nontreated EGFP+ Lenti-pLJM1-EGFP -transduced NIH-3T3 cells (green).

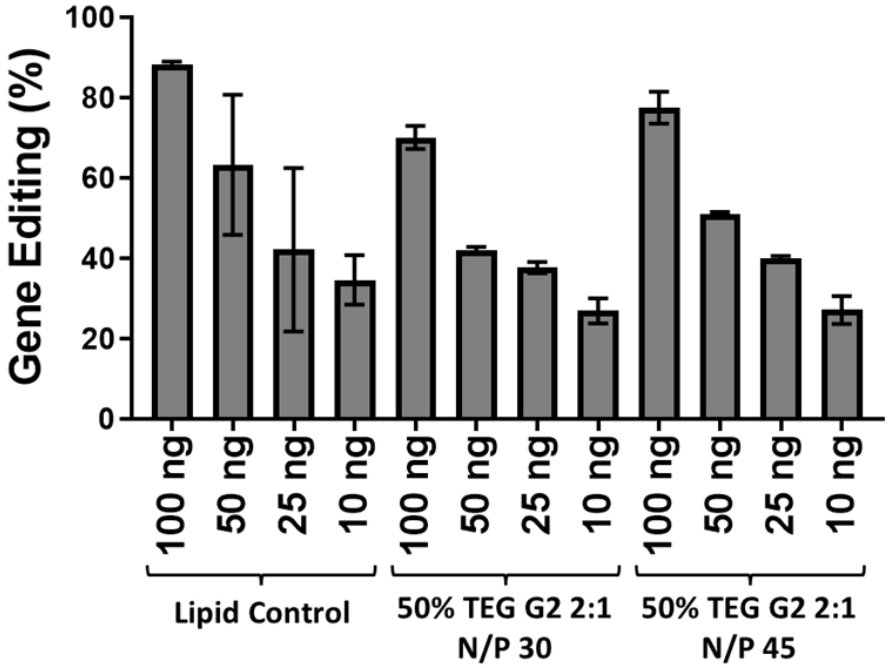

Figure S3.11 *egfp* gene editing efficiency (with both Cas9 mRNA and SG3 sgRNA) in Lenti-pLJM1-EGFP -transduced NIH-3T3 cells using lipid control and **50% TEG G2 2:1**-RNA nanoparticles at different N/P ratios. n=3 for all samples. All formulations used a 1:10 w/w Cas9 mRNA to sgRNA ratio. Overall RNA dosage affects gene efficacy. Lipofectamine P2000 was used as lipid control.

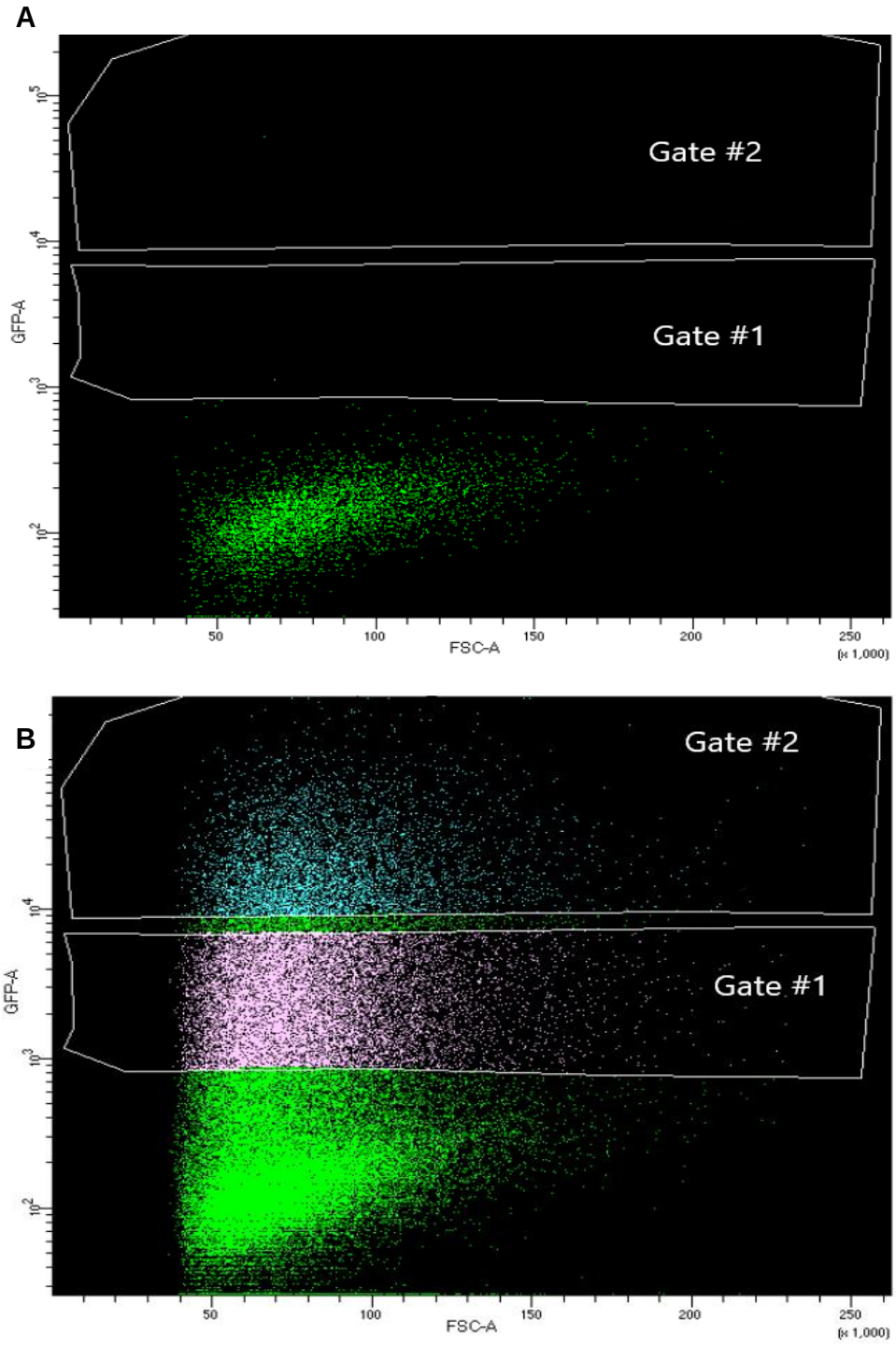

Figure S3.12 FACS gates for **A**) Control HEK293T cells (left) and **B**) Lenti-pLJM1-EGFP - transduced HEK293T cells (right) using a Beckton DickinsonFACSAria II flow cytometer. EGFP+ cells within gate #2 were pooled, expanded, and used for future gene editing experiments. Flow cytometer argon ion excitation laser emitted at 488nm and PMT voltage was set to 300V.

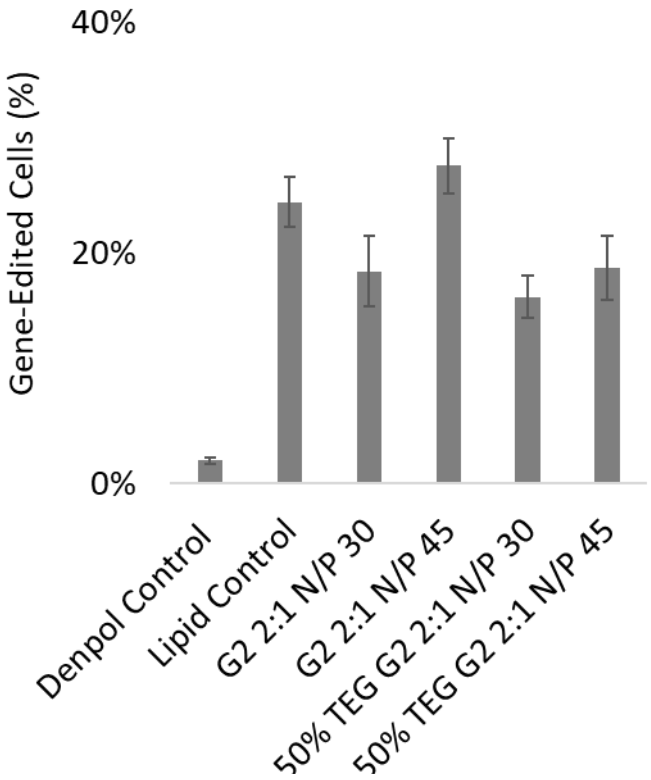

Figure S3.13 *egfp* gene editing efficiency (with both Cas9 mRNA and SG3 sgRNA) in Lenti-pLJM1-EGFP -transduced HEK293T cells using lipid control and denpol-RNA nanoparticles at different N/P ratios. Lipofectamine P2000 was used as lipid control. n=3 for all samples.

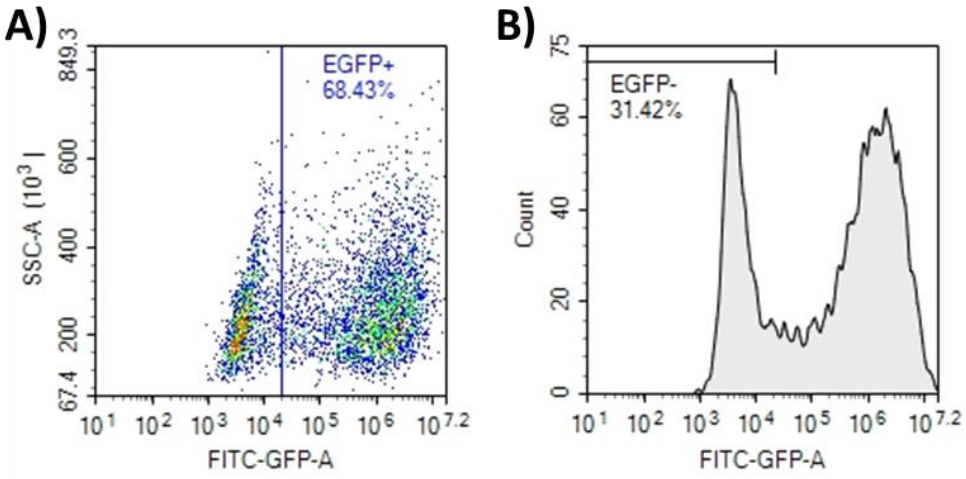

Figure S3.14 Representative flow cytometry **A)** density plot for sorted denpol-Cas9 mRNA-sgRNA nanoparticle-treated Lenti-pLJM1-EGFP-transduced HEK293T cells. **B)** Representative histogram with gating to sort EGFP-negative/ gene edited Lenti-pLJM1-EGFP -transduced HEK293T cells denpol-Cas9 mRNA-sgRNA nanoparticle treatment.

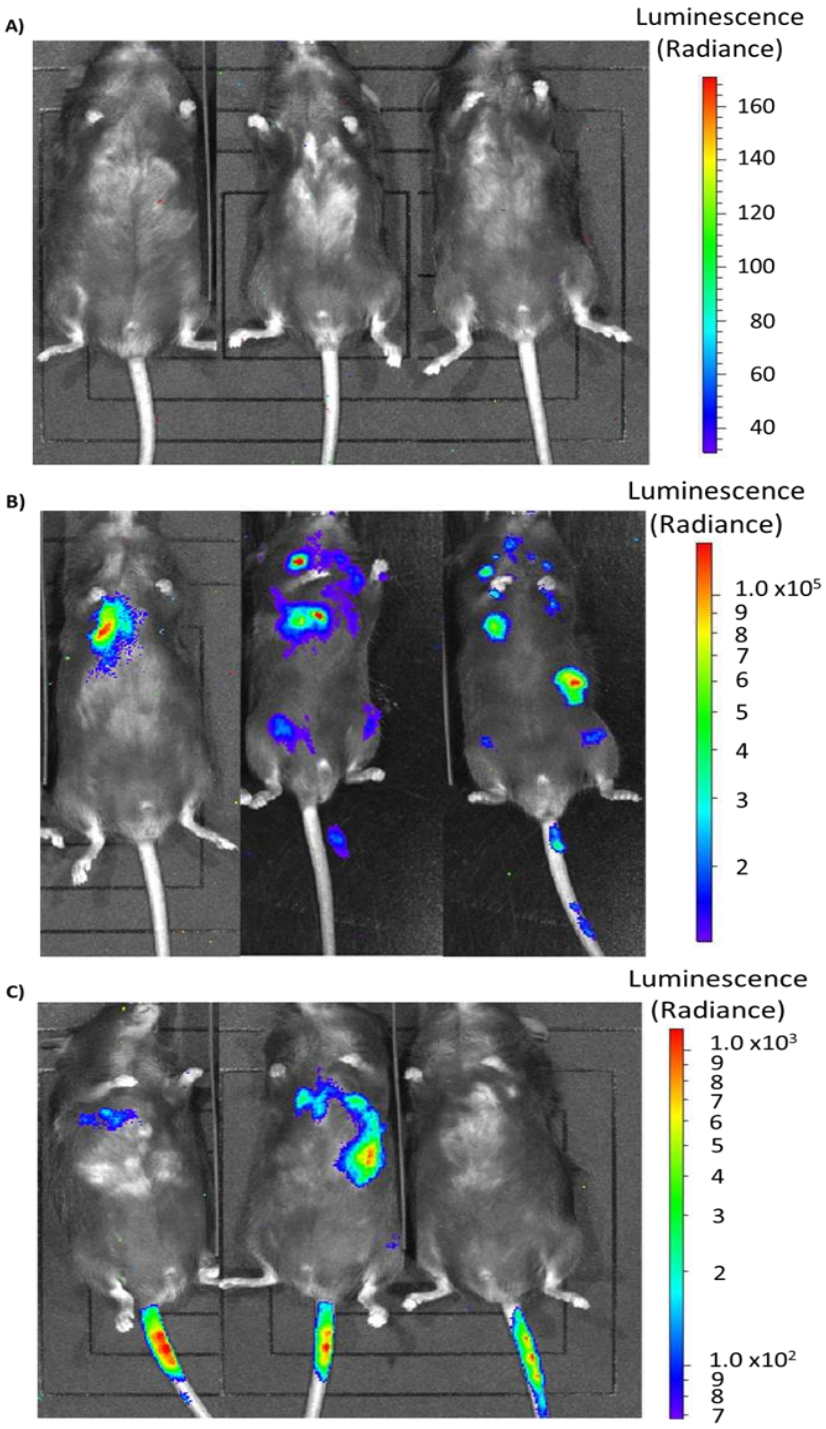

Figure S3.15 *In vivo* luciferase expression in mice six hours post-injection with: **A)** PBS control, **B) G2 2:1** denpol-Fluc mRNA nanoparticles formulated at an N/P of 30, C) **50% TEG G2 2:1** denpol-Fluc mRNA nanoparticles formulated at an N/P of 30. All nanoparticles were administered via tail vein injection and luciferin was administered intraperitoneally 10 minutes prior to imaging.

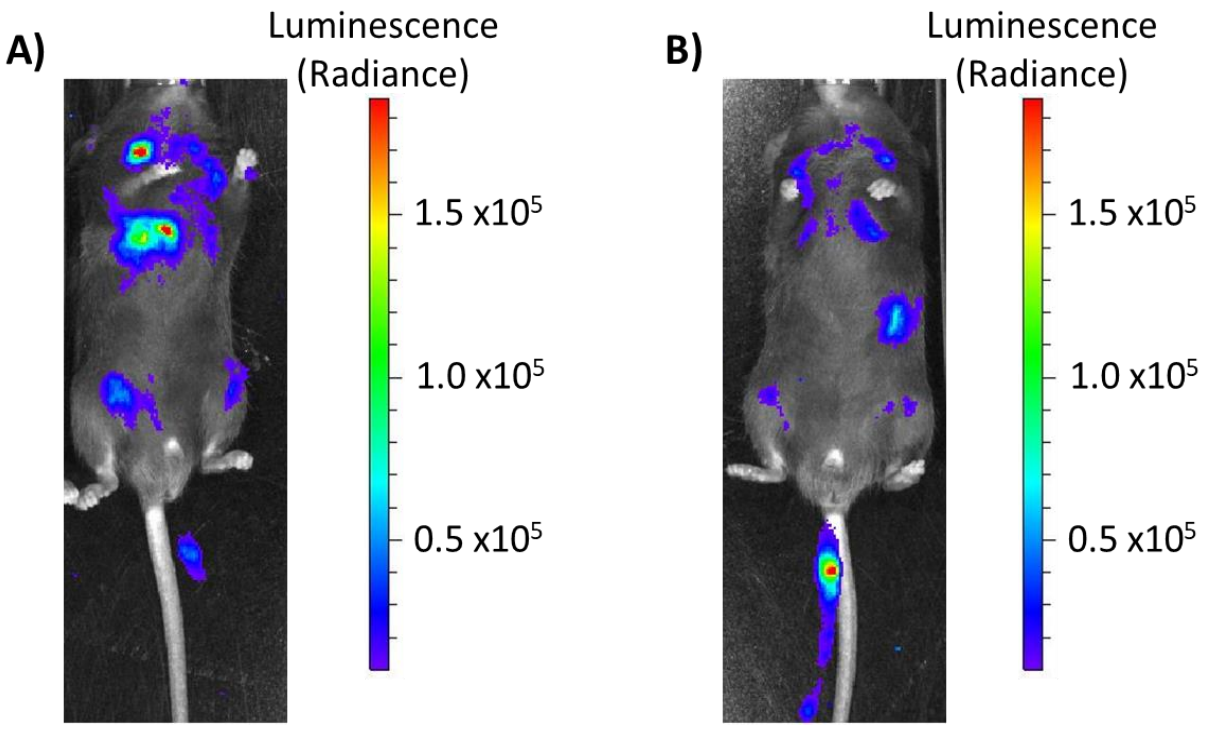

Figure S3.16 *In vivo* luciferase expression in mice **A)** six hours post injection with **G2 2:1** denpol-Fluc mRNA nanoparticles formulated at an N/P of 30 and **B)** 24 hours post injection with **G2 2:1** denpol-Fluc mRNA nanoparticles formulated at an N/P of 30. Luciferin was administered intraperitoneally 10 minutes prior to imaging.

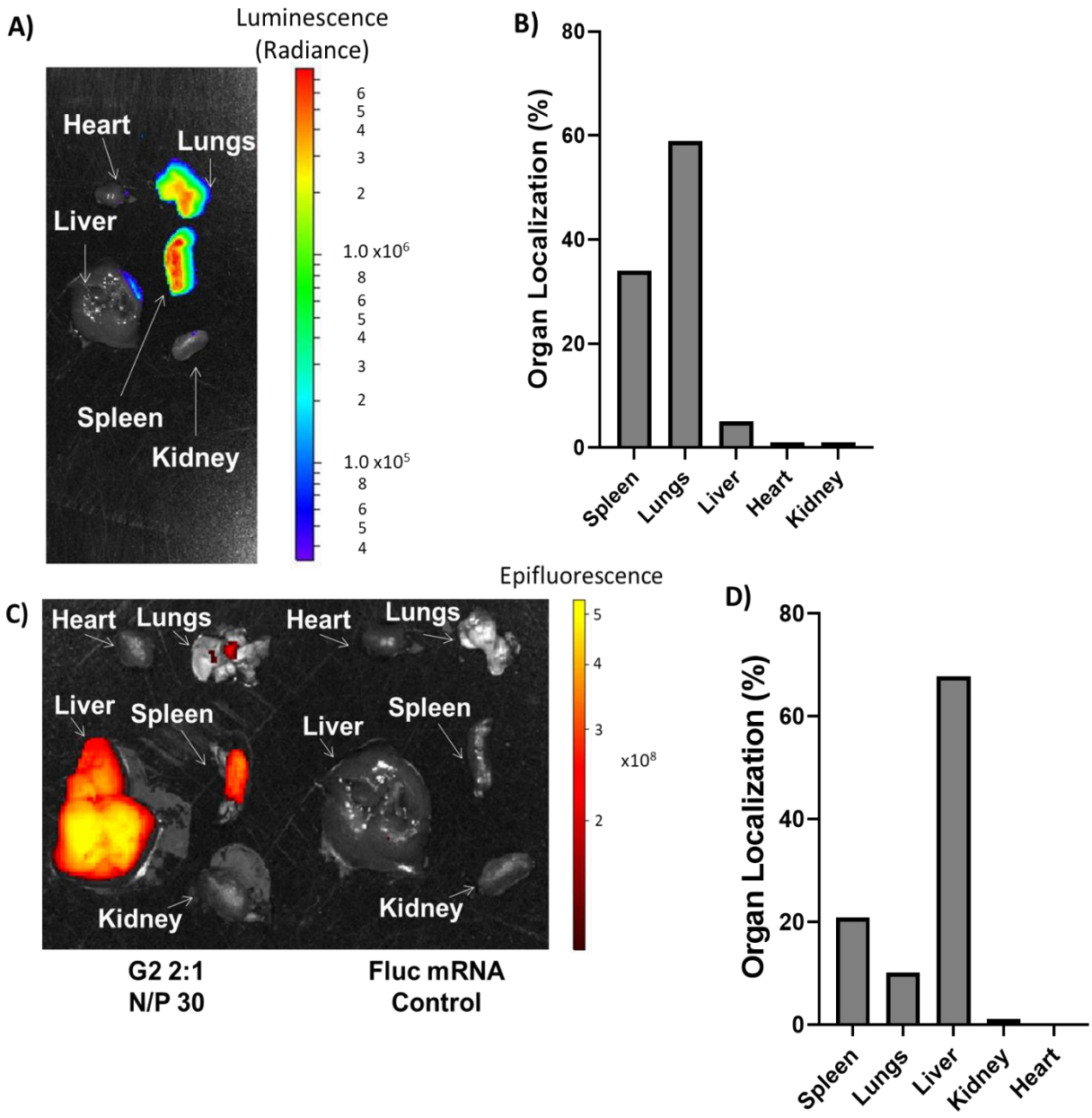

Figure S3.17 A) Organ-specific luciferase expression from mice six hours post injection with **G2 2:1** denpol-Fluc mRNA nanoparticles formulated at an N/P of 30. **B)** Luciferase expression quantified from A. **C)** Organ-specific Cy5 epifluorescence from mice six hours post injection with **G2 2:1** denpol-Fluc mRNA nanoparticles formulated at an N/P of 30. **D)** Cy5 epifluorescence quantified from C.

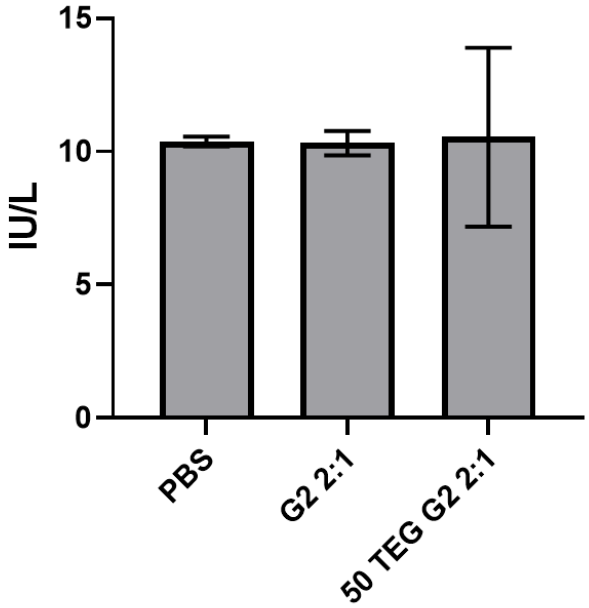

Figure S3.18 Hepatic function of mice treated with denpol-Fluc mRNA polymeric nanoparticles, as measured by aspartate transamidase (AST) levels in blood (IU/L). Mice were injected with 15 µg of Fluc mRNA/ mouse and denpol-Fluc mRNA nanoparticles were formulated at an N/P ratio of 30. N=3 mice per group.

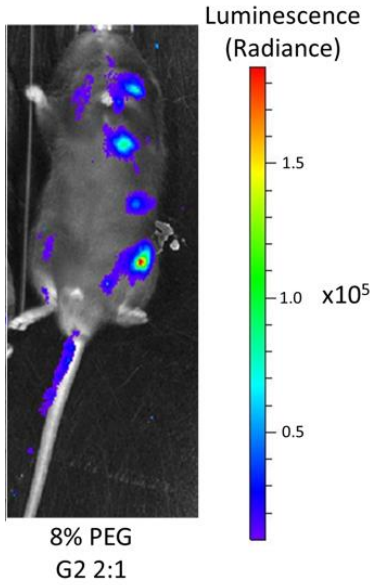

Figure S3.19 *In vivo* luciferase expression in mice six hours post-injection with 8%PEG **G2 2:1** denpol-Fluc mRNA nanoparticles formulated at an N/P of 30. Nanoparticles were administered via tail vein injection and luciferin was administered intraperitoneally 10 minutes prior to imaging.

Table S3.1 ssDNA Oligonucleotide sequences used for sgRNA generation via EnGen® sgRNA Synthesis Kit. For ssDNA oligonucleotide sequences, T7 promoter sequences are green, target gene sequences are red, and primer extension sequences are blue. For sgRNA sequences, crRNA sequences are red and tracrRNA sequences are blue. SG3 sgRNA was used for all future gene editing experiments.

egfp-Targeting sgRNA Name	ssDNA Oligo Sequence (5'-3')	Final sgRNA Sequence (5'-3')
SG1	ttctaatacgactcactatagg cgagggcgatgccacctagtt ttagagctaga	ggcgagggcgaugccaccuaguuuuagagcuagaa auagcaaguuaaaauaaggcuaguccguuaucaacu ugaaaaaguggcaccgagucggugcuuuu
SG2	ttctaatacgactcactatagg gcgaggagctgttcaccggtttt tagagctaga	gggcgaggagcuguucaccgguuuuagagcuagaa auagcaaguuaaaauaaggcuaguccguuaucaacu ugaaaaaguggcaccgagucggugcuuuu
SG3	ttctaatacgactcactataggt ggtgcagatgaacttcagtttta gagctaga	gguggugcagaugaacuucaguuuuagagcuagaa auagcaaguuaaaauaaggcuaguccguuaucaacu ugaaaaaguggcaccgagucggugcuuuu

Table S3.2 Denpol-sgRNA nanoparticle sizes (diameter, in nm) and dispersity values at various N/P ratios. All polyplexes analyzed in PBS, pH 7.4 solution. Nanoparticles formulated with **G2 2:1** at N/P ratios of 30 and 45 are also found in Figure 1A.

Sample:	Z-Average Diameter (nm):	Dispersity (*D*):
G2 2:1 N/P 30	149.2	0.10
G2 2:1 N/P 45	143.8	0.33
50% TEG G2 2:1 NP 30	320.1	0.14
50% TEG G2 2:1 NP 45	258.9	0.27

Table S3.3 Denpol-Cas9 mRNA-sgRNA nanoparticle sizes (diameter, in nm) and dispersity values at various N/P ratios. All polyplexes are at a 1:7 Cas9 mRNA to sgRNA w/w ratio and analyzed in PBS, pH 7.4 solution.

Sample:	Z-Average Diameter (nm):	Dispersity (*D*):
G2 2:1 N/P 30	276.0	0.16
G2 2:1 N/P 45	350.4	0.15
50% TEG G2 2:1 NP 30	298.0	0.12
50% TEG G2 2:1 NP 45	316.8	0.14

Table S3.4 Denpol-Cas9 mRNA-sgRNA nanoparticle zeta potential (in mV) at an N/P of 30. All polyplexes are at a 1:7 Cas9 mRNA to sgRNA w/w ratio and analyzed in PBS, pH 7.4 solution.

Sample:	Zeta Potential (mV):
G2 2:1 N/P 30	+11.5
50% TEG G2 2:1 NP 30	+9.6

Table S3.5 Denpol-Fluc mRNA nanoparticle sizes (diameter, in nm) and dispersity values at an N/P ratio of 30. All polyplexes are analyzed in PBS (pH 7.4) solution.

Sample:	Z-Average Diameter (nm):	Dispersity (*D*):
G2 2:1 N/P 30	180.7	0.01
50% TEG G2 2:1 NP 30	224.4	0.09

3.8 Polymer Characterization Data (^{1}H NMR)

G2 2:1 (64 H 36 W)

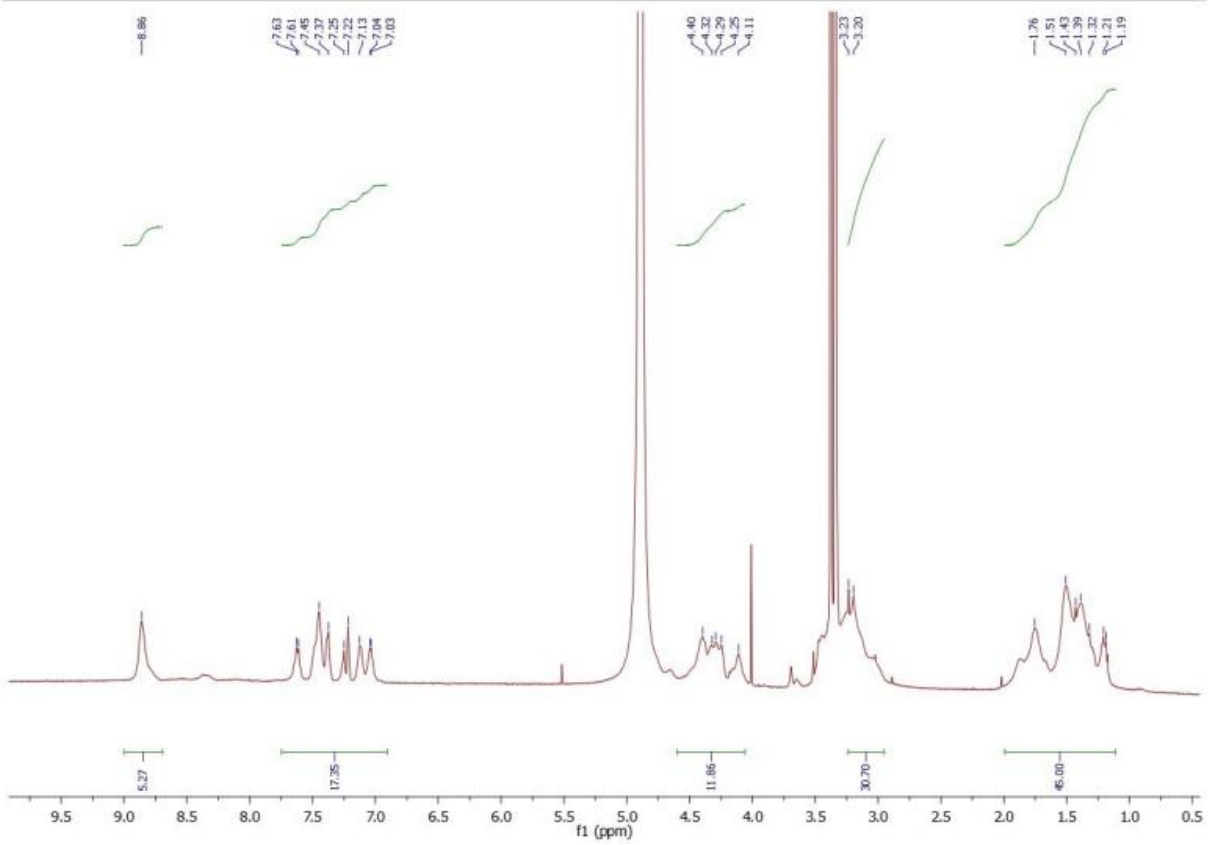

G2 2:1 (64 H 36 W): Boc-His(Boc)-OH (16.00 equiv.) and Boc-Trp(Boc)-OH (8.00 equiv.). Clear colorless solid. 82% isolated yield.

G2 2:1: ^{1}H NMR (600 MHz, MeOH) δ 8.75 (s, 5.27H), 7.83 – 6.82 (m, 18H), 4.60 – 4.04 (m, 11.89H), 3.09 (m, 15H),2.12 – 1.05 (m, 45H).

50% TEG G2 2:1 (63 H 37 W)

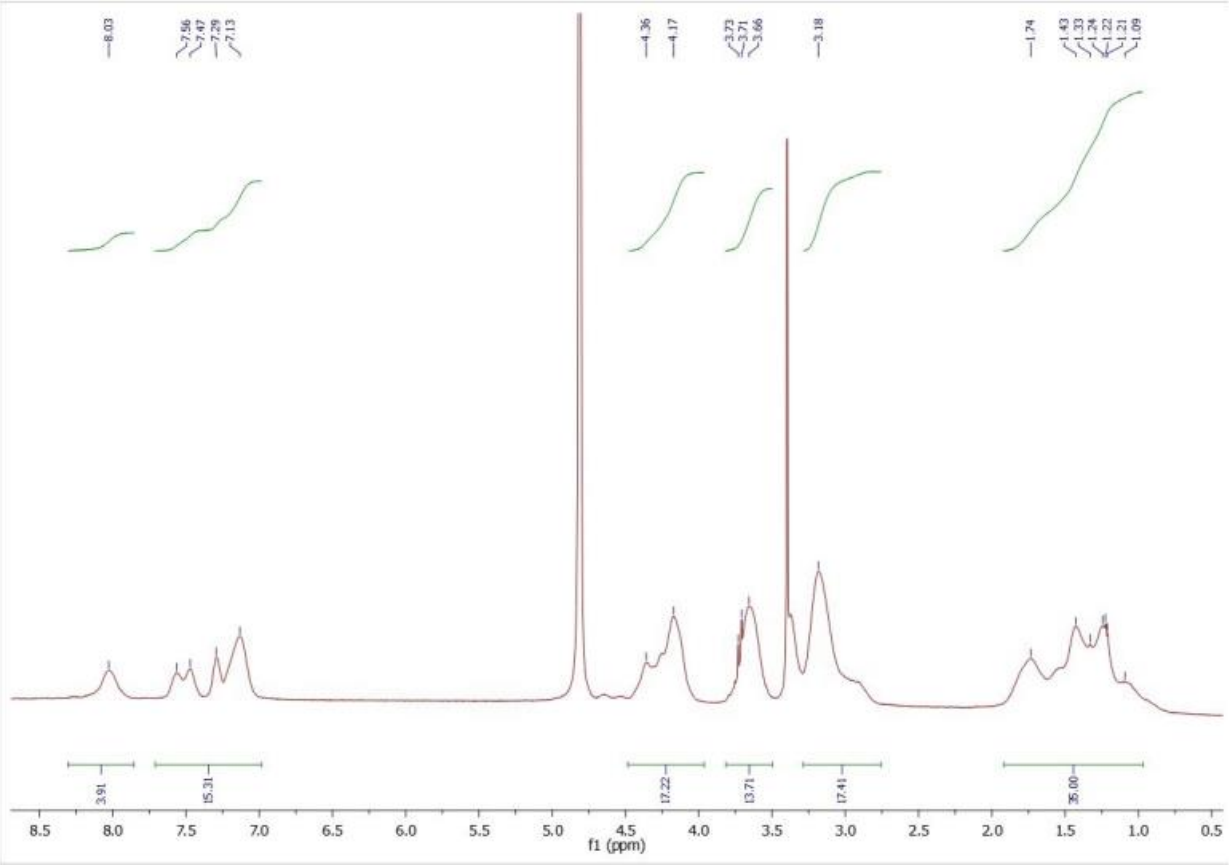

50 TEG G2 2:1 (63 H 37 W): Boc-His(Boc)-OH (16.00 equiv.) and Boc-Trp(Boc)-OH (8.00 equiv.). Clear colorless solid. 71% isolated yield.

50 TEG G2 2:1: ^{1}H NMR (600 MHz, D2O), δ 8.03 (s, 3.91H), 7.37 (m, 15.31H), 4.27 (m, 17.22H), 3.93 – 3.53 (m, 13.71H), 3.18 (m, 17.41H), 2.11 – 0.74 (m, 35H).

8% PEG G2 2:1 (61 H 39 W)

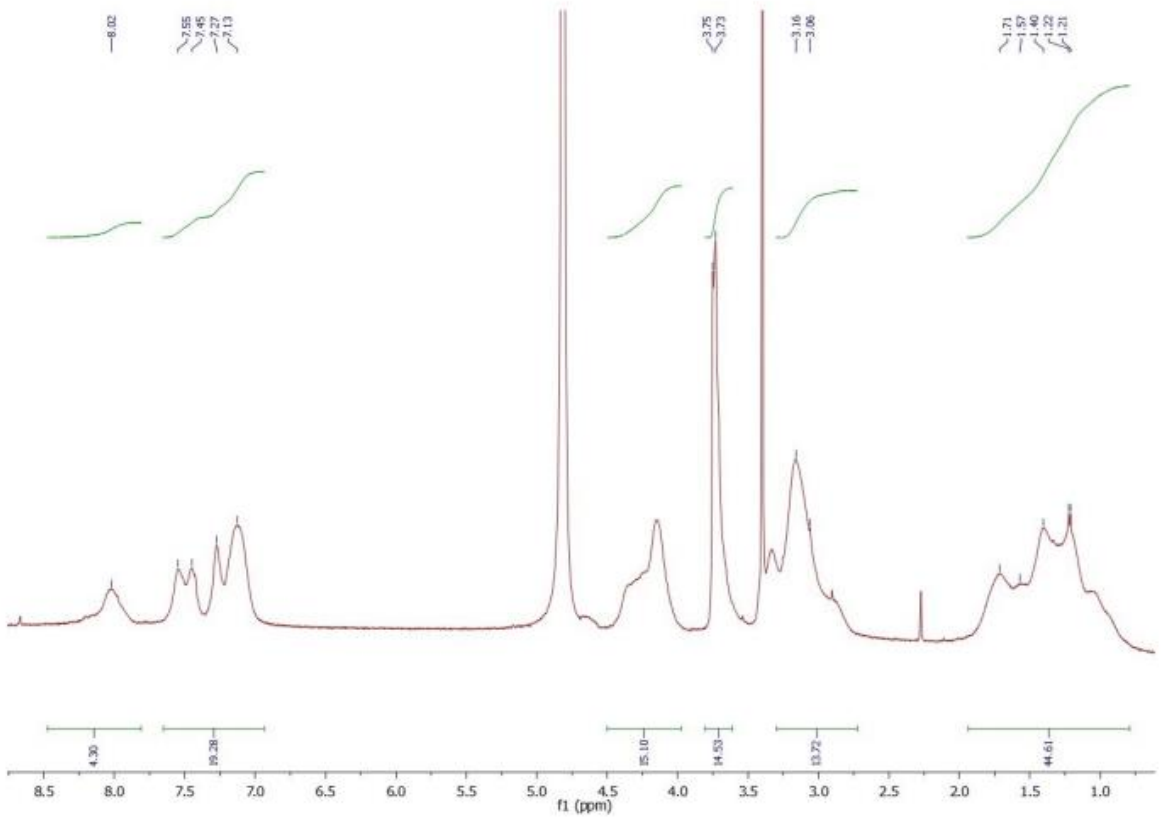

8% PEG G2 2:1 (61 H 39 W): Boc-His(Boc)-OH (16.00 equiv.) and Boc-Trp(Boc)-OH (8.00 equiv.). Clear colorless solid. 54% isolated yield.

8% PEG G2 2:1 (61 H 39 W): ^{1}H NMR (600 MHz, D2O), δ 8.02 (s, 4.3H), 7.35 (m, 19.28H), 4.15 (s, 15.1H), 3.74 (d, J = 10.3 Hz, 14.53H), 3.11 (m, 13.72H), 2.11-0.63 (m, 44.61H).

CHAPTER 4: Cryopolymerization-Generated Polydisulfides: Progress Towards Polyanionic and Polycationic Approaches to mRNA Delivery

4.1 Introduction

Polydisulfide polymers from lipoic acid (LA) are quickly becoming popular biomaterials for many biological applications. However, the lack of facile polydisulfide polymerization methodologies greatly limits the potential of these bioreducible polymers, particularly as RNA delivery vehicles. While biocompatible polydisulfides have been synthesized previously, this methodology has almost exclusively been applied to aqueous-soluble guanidinium-containing LA monomers.[1-3] This room temperature aqueous-phase polymerization methodology is robust but requires a concentrated buffer that would likely not be applicable with anionic LA monomers (due to potential complexation with cationic buffer components). Development of a polymerization methodology that can reliably polymerize both poly(anionic)disulfides and poly(cationic)disulfides from LA-derived monomers without a concentrated buffered solution would greatly aid in generating more polydisulfide polymers designs for biological applications, including RNA delivery.

Fortunately, Lu et al. pioneered an approach to generate both poly(anionic)disulfides and poly(cationic)disulfides from LA-derived monomers without concentrated buffering conditions. By freezing a protein with a solvent-exposed cysteine/thiol and a LA-derived monomer at physiological pH, Lu and coworkers were able to generate protein-polydisulfide polymer conjugates with controlled polymerization kinetics.[4] Moreover, this cryopolymerization methodology was used to generate both protein-poly(anionic)disulfide and protein-poly(cationic)disulfide conjugates, the latter of

which demonstrated cell-penetrating capability when delivering conjugated EGFP protein as a payload to cells.

While this cryopolymerization methodology has shown promise, it has not yet been used to generate LA-derived poly(anionic)disulfides or poly(cationic)disulfides at larger scales or for RNA delivery applications. Although poly(anionic)disulfides would obviously be negatively charged and not have favorable electrostatic interactions with nucleic acids, utilizing poly(anionic)disulfides for RNA delivery is not without precedent: biodegradable anionic polymers, notably sodium alginate, are frequently formulated with plasmid DNA and a crosslinking agent (most commonly Ca^{2+}) to generate DNA-loaded hydrogels/nanoparticles for cell delivery.[5-7] In these designs, calcium ions cross-link both polymer carboxylate groups and phosphate groups of plasmid DNA to entangle the two species within a nanoparticle/hydrogel. However, sodium alginate's ionizable carboxylate units have an estimated pK_a range of 3.4-3.7,[8] which is well outside the optimal pH range of endosomes/lysosomes (pH 5.0-7.0), lowering endosomal escape efficiency. In contrast, LA has a pK_a of 4.7, which is substantially closer to the lysosomal pH range of 5-7. A poly(anionic)disulfide polymer derived from LA monomer should similarly cross-link to phosphate groups of nucleic acids (See Scheme 4.1) and facilitate a stronger proton sponge effect for enhanced nanoparticle delivery. Additionally, chemical motifs other than thiol-reducible disulfides could be incorporated into this poly(anionic)disulfide polymerization system, providing more synthetic flexibility than the defined chemical motifs found in sodium alginate.

Poly(amino)disulfide polymers with cationic groups have already been successfully generated using this cryopolymerization methodology. Expanding on this further, by

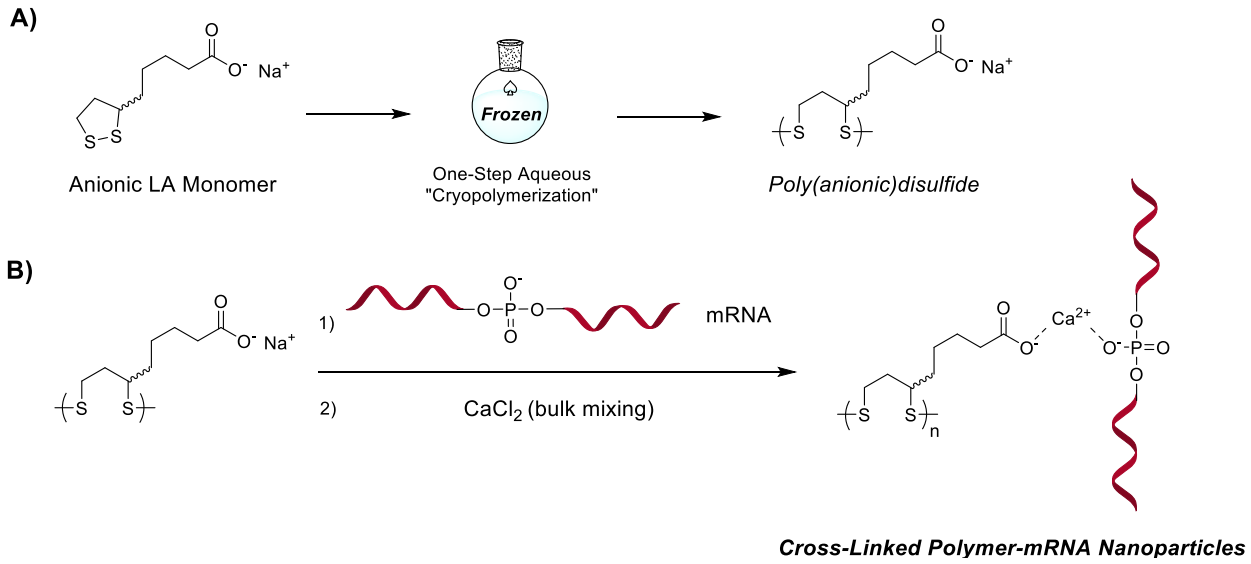

Scheme 4.1 Approach to generating poly(anionic)disulfide-mRNA nanoparticles for RNA delivery. **A)** Synthesis approach to generating poly(anionic)disulfide from LA monomer. **B)** Crosslinking carboxylate-containing poly(anionic)disulfides and phosphate groups of mRNA should result in polymer-mRNA nanoparticles.

conjugating different amine-containing groups to LA derivatives, poly(amino)disulfide polymers can be generated that possess both cationic amines for RNA complexation and ionizable amines to promote endosomal escape (See Scheme 4.2). Copolymerization of both cationic and ionizable LA-derived monomers could also be explored. This cryopolymerization methodology was herein utilized to generate both

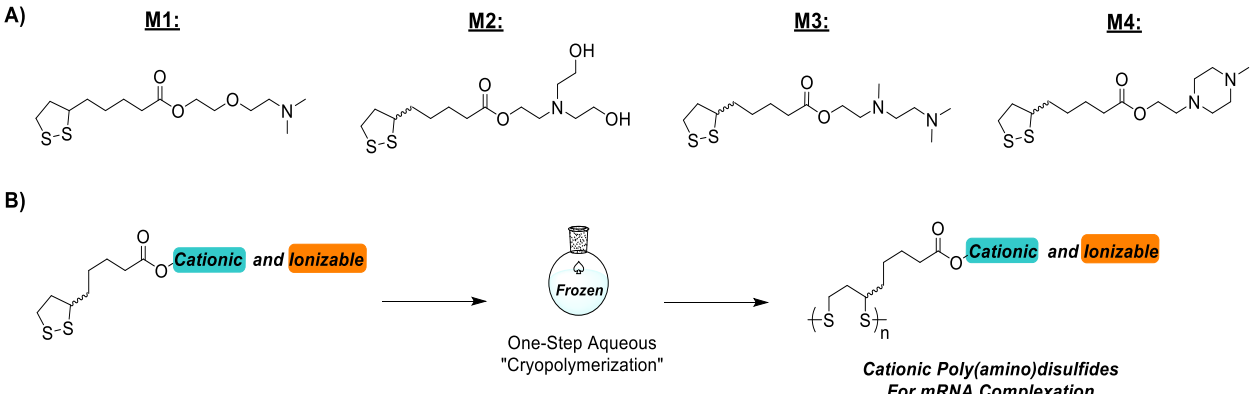

Scheme 4.2 Approach to generating cationic poly(amino)disulfide-mRNA nanoparticles for RNA delivery. **A)** Cationic monoamine or diamine-containing LA monomers examined in this study. **B)** Cryopolymerization of cationic monomers should result in poly(amino)disulfides capable of mRNA complexation.

poly(anionic)disulfide and poly(amino)disulfide polymers for LA-derived monomers at larger scale than previously reported. Subsequent polydisulfide polymers were complexed with a model mRNA through two different methodologies to form polymeric nanoparticles capable of delivering mRNA *in vitro*.

4.2 Results and Discussion

The aqueous-phase LA cryopolymerization methodology reported previously has only been applied to small-scale protein-polydisulfide polymer conjugates;[4] larger-scale polymerization conditions needed to be explored first before RNA delivery could be investigated. We began by freezing different concentrations of aqueous sodium lipoate

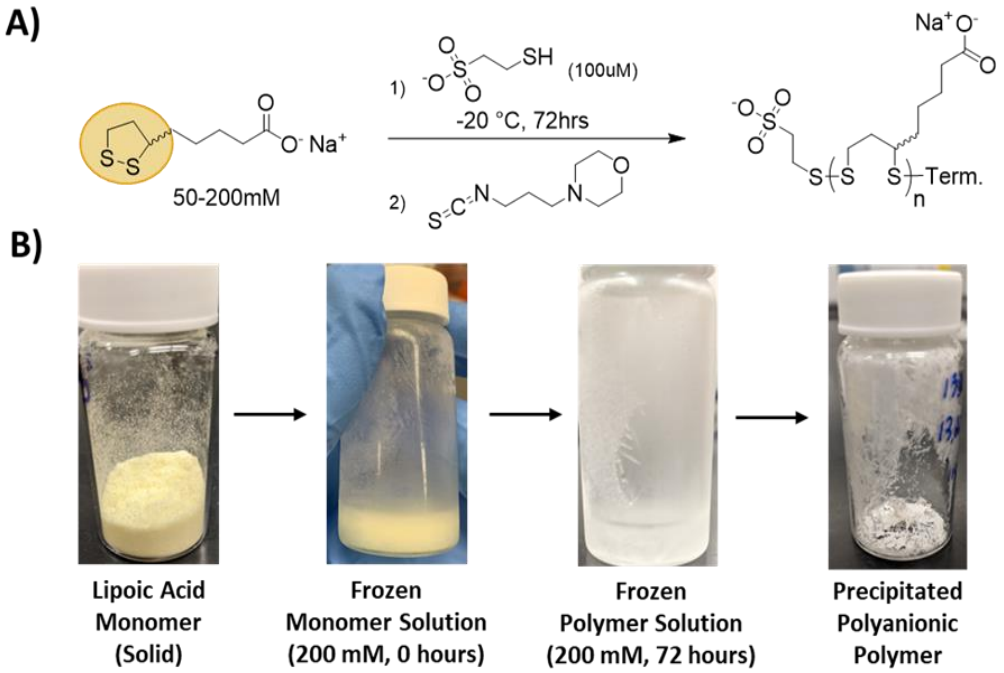

Figure 4.1 Cryopolymerization of lipoic acid at scaled conditions. **A**) Synthetic procedure to generate anionic poly(**M0**)disulfide. **B**) Monomer polymerization can readily be visualized by disappearance of monomer chromophore/color throughout cryopolymerization. Anti-solvent addition results in polymer precipitation.

monomer (conjugate base of LA; **M0**) solution at pH 7.4 in scintillation vials. After 72 hours of freezing at -20 °C a colorimetric change was observed (See Figure 4.1), indicating that the ring-opening of **M0** had occurred. Subsequent treatment of the frozen polymer solutions with a miscible anti-solvent resulted in the precipitation of the corresponding poly(anionic)disulfide in decent yield (See Table 4.1). Subsequent GPC analysis confirmed that poly(**M0**)disulfide polymers had been generated. Additional ^{1}H NMR analysis further indicated poly(**M0**)disulfide product (See Figure 4.2). With this initial success,

Table 4.1 Results from cryopolymerization of different lipoic acid solution at pH 7.4 under scaled conditions.

Monomer Feedstock Concentration:	Polymer *Mn* (kDa):	Dispersity (D):	Yield:
50 mM	*3.91*	*1.9*	36%
75 mM	*4.78*	*1.7*	30%
100 mM	*63.3*	*1.8*	59%
200 mM	*92.2*	*1.5*	88%

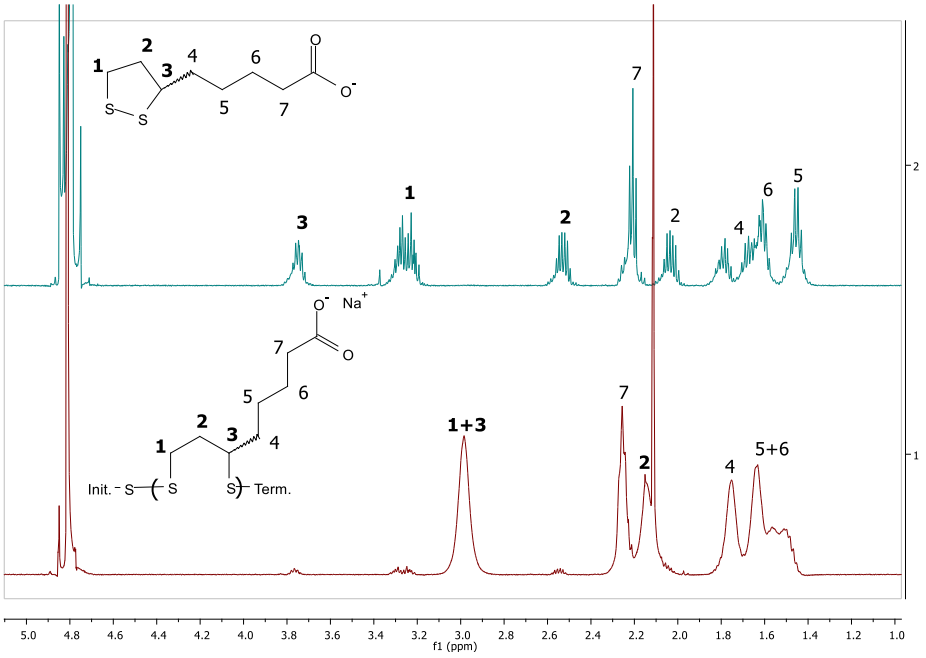

Figure 4.2 ^{1}H NMR (in D_2O) overlay of **M0** monomer and poly(**M0**)disulfide after cryopolymerization.

cryopolymerizaton of **M0** was also tested at pH 10, yielding polymer (See Figure S4.1) and validating that this technique can be applied to two separate pH conditions.

With poly(**M0**)disulfide generated, formulations containing polymer, EGFP mRNA, and calcium chloride (cross-linking agent) were generated and characterized by DLS. Bulk formations of these components yielded nanoparticles with diameters between 60-185 nm depending on the quantity of calcium cross-linker used (See Table 4.2). While nanoparticles were formed, more refined nano/microparticle design approaches using sodium alginate and calcium cross-linking agent utilize electrospray jets[5] or microfluidic flow devices[9-11] to generate more uniform nanoparticles with larger quantities of cross-linker. Attempted bulk formulations of these nanoparticles with large (excess) quantities of calcium resulted in visible aggregation. In future formulation designs, more sophisticated mixing strategies will need to be implemented to obtain more defined nanoparticles.

Table 4.2 DLS results from poly(**M0**)disulfide-EGFP mRNA-Ca^{2+} cross-linked nanoparticles. A 100:1 w/w ratio of polymer to mRNA was utilized for all formulations. Calcium equivalents were calculated with respect to the sum of all carboxylate groups of polymers and phosphate groups of mRNA. All nanoparticles formulated through bulk mixing.

Stoichiometric Ca^{2+} Equivalents:	Z-Ave. Diameter (nm):	PDI:
0.25	62.8	0.34
0.5	141.9	0.27
0.75	184.2	0.34

Regardless, bulk-formulated nanoparticles with limited cross-linker were tested as RNA delivery vehicles *in vitro*. Due to the broad buffering capacity of the poly(**M0**)disulfide polymer (See Figure S4.2), these nanoparticles should be capable of absorbing protons in cellular endosomes, enhancing the proton sponge effect. To test this EGFP mRNA, calcium

chloride, and varying quantities of poly(**M0**)disulfide were formulated, generating nanoparticles that were administered to DC2.4 cells. After 48 hours, these cells were analysed by flow cytometry to determine EGFP expression (See Figure 4.3). Compared to equivalent sodium alginate nanoparticles, poly(**M0**)disulfide-containing nanoparticles generated six times more EGFP+ cells when a 200/1 w/w ratio of polymer to mRNA was used. There is also an observable dose-dependent relationship observed between the amount of poly(**M0**)disulfide added to each nanoparticle formulation and the resulting number of EGFP+ cells. For cells treated with a 100/1 w/w ratio of poly(**M0**)disulfide to

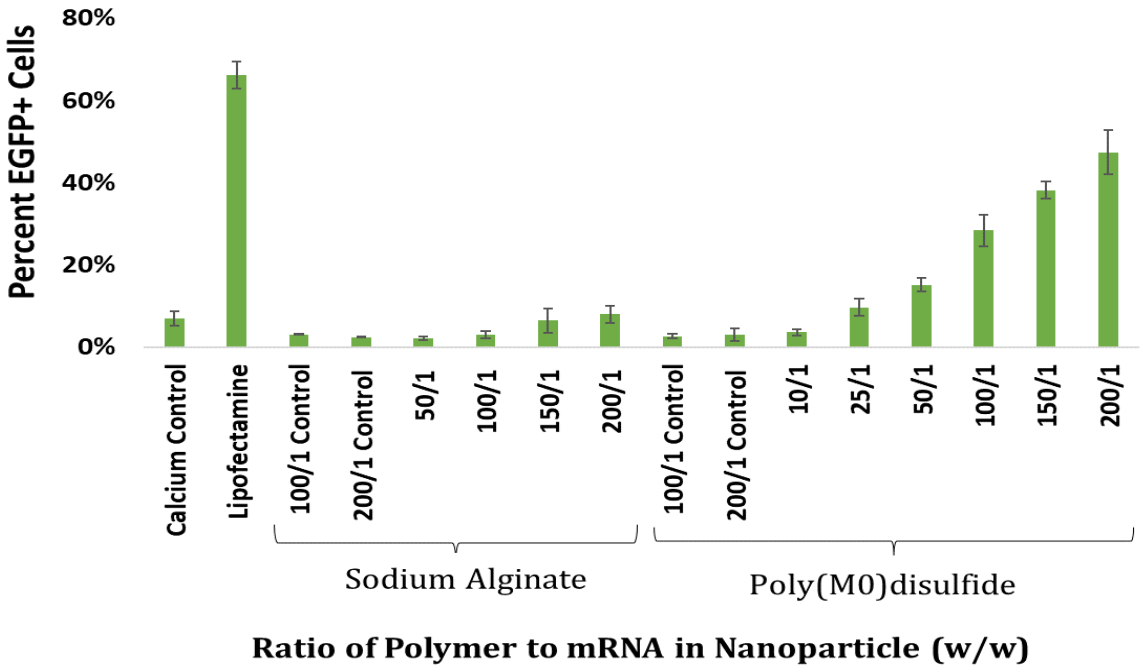

Figure 4.3 EGFP expression after treatment with cross-linked poly(**M0**)disulfide-EGFP mRNA nanoparticles. Percent EGFP+ DC2.4 cells after 48 hours of treatment with Ca^{2+} cross-linked poly(**M0**)disulfide-EGFP mRNA nanoparticles. Calcium ions formulated with mRNA used as control; Lipofectamine used as positive control. 100/1 and 200/1 control samples are respective polymer and EGFP mRNA formulations without Ca^{2+} crosslinking. 50/1, 100/1, 150/1, and 200/1 samples represent Ca^{2+} cross-linked polycarboxylate-EGFP mRNA nanoparticles formulated at different polymer/EGFP mRNA w/w ratios. All nanoparticles were generated by bulk mixing using 0.5 stoichiometric equivalents of Ca^{2+} ions (with respect to the sum of all carboxylate and phosphate groups). N=3 for all samples.

mRNA, 28% of resulting cells were EGFP+, while cells treated with a 200/1 w/w ratio of poly(**M0**)disulfide to mRNA were 47% EGFP+. Minimal cytotoxicity was also observed for cells treated with these nanoparticles, as indicated by propidium iodide (PI) staining (See Figure S4.3). These results are very promising, indicating that poly(**M0**)disulfide-containing nanoparticles are more capable at delivering mRNA than standard sodium alginate formulations, even at equivalent polymer: nucleic acid ratios.[5] However, optimized formulation conditions are needed before this nanoparticle delivery method is investigated further.

Cationic poly(amino)disulfide polymers were also investigated using this cryopolymerization methodology (See Figure 4.4A). Four different cationic monomers

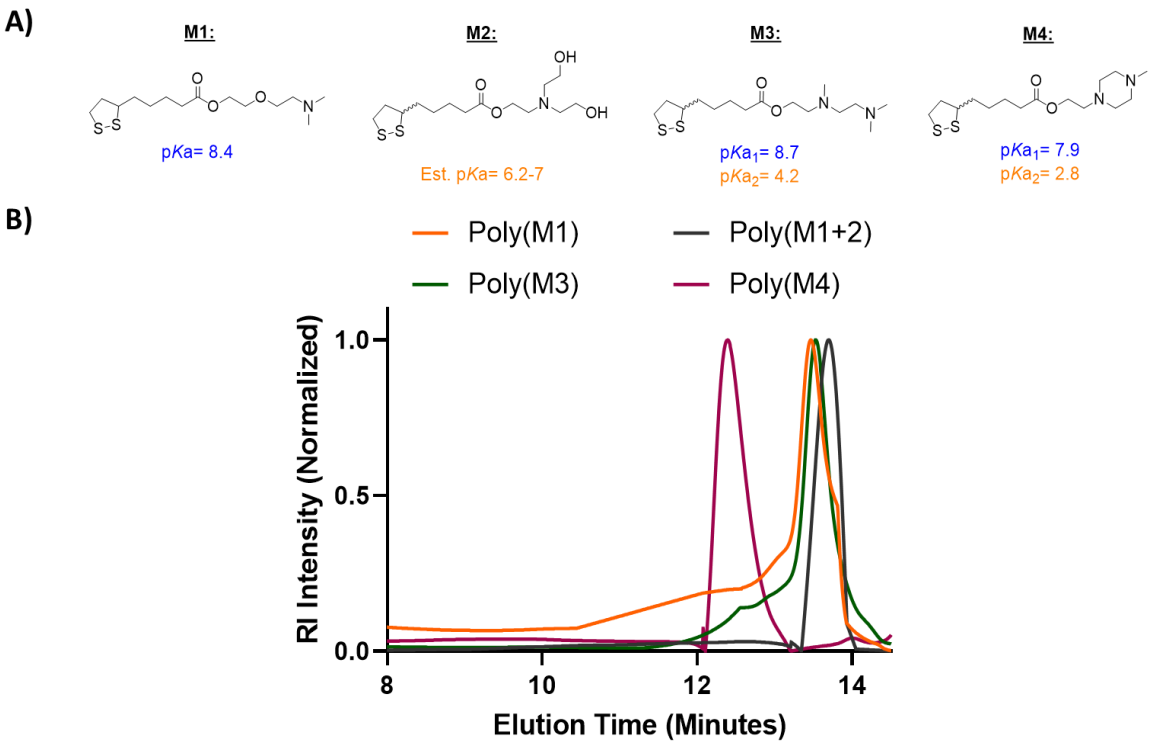

Figure 4.4 Amine-containing LA derivatives generate cationic poly(disulfides). **A)** Amine-containing LA derivative monomers and their respective conjugate acid p*K*a values. **B)** GPC traces of cryopolymerized cationic poly(amino)disulfides.

(**M1**-**M4**) were synthesized and titrated to determine approximate p*K*a values for each amino group. Monomers were then cryopolymerized to yield poly(**M1**)-, poly(**M1**+**M2**)-, poly(**M3**)-, and poly(**M4**)disulfides. Polymer generation was validated by both GPC (See Figure 4.4B; See Table S4.2) and ^{1}H NMR (See Figure S4.4-4.7). Due to the cationic nature of these polymers, they should rapidly complex with mRNA through electrostatic interactions to generate nanoparticles. This was initially investigated by gel electrophoresis, with complexation observed above N/P ratios of 2.5 for two of the four representative polymers at pH 7.4 (See Figure 4.5); DLS also confirmed nanoparticle generation at an N/P ratio of 10

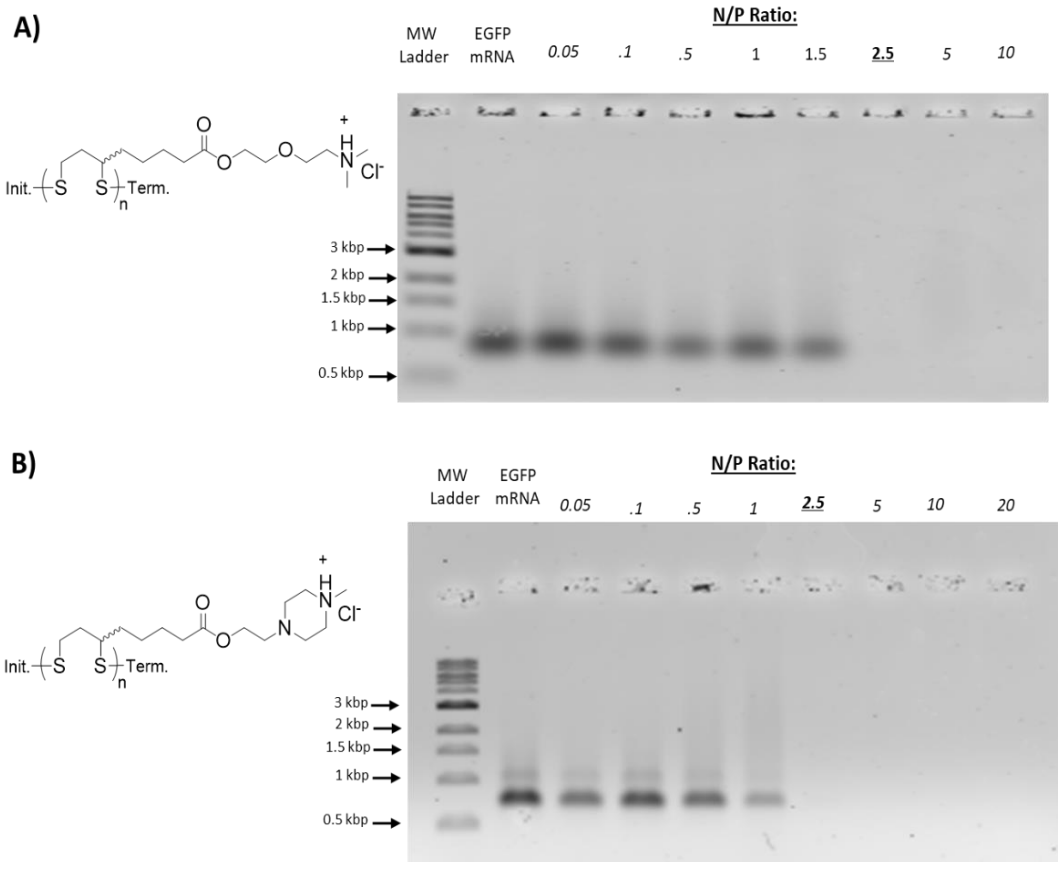

Figure 4.5 Cationic poly(amino)disulfide gel complexation. **A)** Complexation of poly(**M1**)disulfide with EGFP mRNA (in PBS, pH 7.4) at various N/P ratios. **B)** Complexation of poly(**M4**)disulfide with EGFP mRNA (in PBS, pH 7.4) at various N/P ratios. Both polymers demonstrate complete complexation at N/P ratios of 2.5 and above.

(See Table S4.3).

With nanoparticles confirmed, we proceeded with *in vitro* validation of these polymeric nanoparticles. All four cationic poly(amino)disulfides were formulated with EGFP mRNA (at different N/P ratios) and administered to DC2.4 cells. Cells were then isolated after 48 hours of nanoparticle treatment and sorted by flow cytometry to determine the number of EGFP+ cells. From the experimentally determined pK_a values, we predicted that poly(**M1**+**M2**)- and poly(**M3**)disulfide polymers would generate the strongest endosomal escape response and therefore, optimal mRNA delivery profiles. This was confirmed by observed EGFP expression by flow cytometry; nanoparticle treatment with poly(**M1**+**M2**)- and poly(**M3**)disulfide polymers, containing both cationic and ionizable motifs, resulted in the largest number of EGFP+ cells (both ~30% of cells; See Figure 4.6). Interestingly, nanoparticles generated at an N/P ratio of 15 demonstrated the highest degree of EGFP transfection; nanoparticles with an N/P ratio of 30 demonstrated cytotoxicity, as determined by PI staining (See Figure S4.8).

Cellular treatment with polymeric nanoparticles only containing cationic groups (from poly(**M1**)- and poly(**M4**)disulfides) resulted in poor EGFP expression, suggesting that nanoparticles of this design do require ionizable motifs for endosomal escape. Future experiments will need to determine the precise uptake mechanism of these nanoparticles and determine if endosomal entrapment is occurring.

Despite these initial successes, the total number of EGFP+ cells treated with either poly(anionic)disulfide- and poly(amino)disulfide-containing polymeric mRNA nanoparticles is relatively low compared to lipofectamine, a cationic lipid control. Future

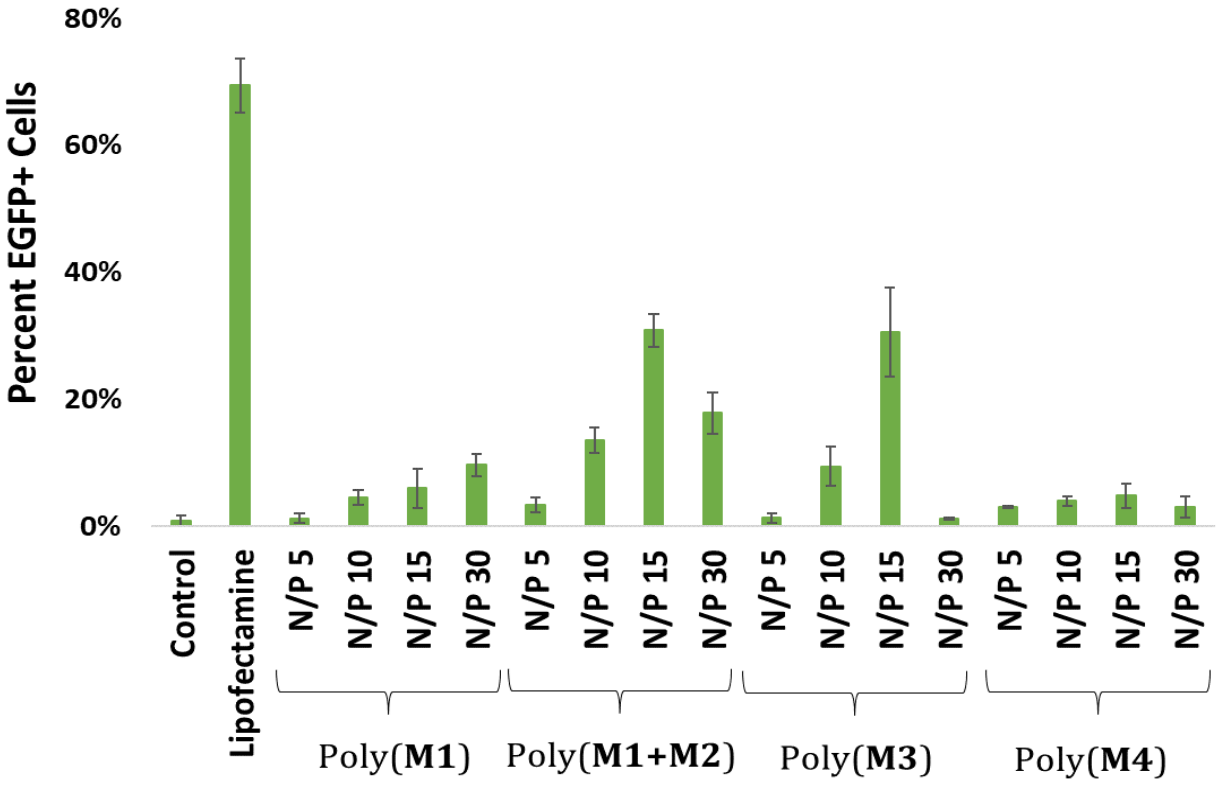

Figure 4.6 EGFP expression after treatment with poly(amino)disulfide-mRNA nanoparticles. Percent EGFP+ DC2.4 cells after 48 hours of treatment with poly(amino)disulfide-EGFP mRNA polymeric nanoparticles at different N/P ratios; EGFP expression determined by flow cytometry. Untreated DC2.4 cells are displayed as control samples; Lipofectamine MessengerMAX was used as positive control. N=3 for all samples.

experiments with both polymer systems will need optimized formulation conditions or potentially new chemical functionalizations to further increase cell transfection efficacy.

4.3 Conclusions

In this project an established cryopolymerization protocol was explored to synthesize both poly(anionic)- and poly(cationic)disulfides from LA-derived monomers at larger scales than previously reported. For poly(anionic)disulfides, a calcium-based crosslinking strategy generated nanoparticles containing mRNA and polymers through

bulk mixing. While many improvements can be made to the outlined bulk mixing methodology described here, treatment of DC2.4 cells with cross-linked EGFP mRNA-poly(anionic)disulfide nanoparticles resulted in 47% EGFP+ cells after 48 hours. Similarly, cationic poly(amino)disulfides can also be generated using this cryopolymerization methodology and amine-containing LA derivatives. Complexation of these cationic poly(amino)disulfides with EGFP mRNA also resulted in nanoparticles by DLS. Treatment of DC2.4 cells resulted in successful EGFP mRNA delivery, depending N/P ratio and if ionizable motifs were present on the polymer. Altogether, the progress made in this project highlights the synthetic potential of the cryopolymerization methodology for generating numerous polydisulfides for biological applications, including RNA delivery.

4.4 References

(1) Bang, E.-K.; Gasparini, G.; Molinard, G.; Roux, A.; Sakai, N.; Matile, S., Substrate-Initiated Synthesis of Cell-Penetrating Poly(disulfide)s. *Journal of the American Chemical Society* **2013,** *135* (6), 2088-2091.

(2) Fu, J.; Yu, C.; Li, L.; Yao, S. Q., Intracellular Delivery of Functional Proteins and Native Drugs by Cell-Penetrating Poly(disulfide)s. *Journal of the American Chemical Society* **2015,** *137* (37), 12153-12160.

(3) Guo, J.; Wan, T.; Li, B.; Pan, Q.; Xin, H.; Qiu, Y.; Ping, Y., Rational Design of Poly(disulfide)s as a Universal Platform for Delivery of CRISPR-Cas9 Machineries toward Therapeutic Genome Editing. *ACS Central Science* **2021,** *7* (6), 990-1000.

(4) Lu, J.; Wang, H.; Tian, Z.; Hou, Y.; Lu, H., Cryopolymerization of 1,2-Dithiolanes for the Facile and Reversible Grafting-from Synthesis of Protein–Polydisulfide Conjugates. *Journal of the American Chemical Society* **2020,** *142* (3), 1217-1221.

(5) Alallam, B.; Altahhan, S.; Taher, M., Electrosprayed Alginate Nanoparticles as CRISPR Plasmid DNA Delivery Carrier: Preparation, Optimization, and Characterization. *Pharmaceuticals (Basel)* **2020,** *13* (8).

(6) You, J.-O.; Peng, C.-A., Calcium-Alginate Nanoparticles Formed by Reverse Microemulsion as Gene Carriers. *Macromolecular Symposia* **2005,** *219* (1), 147-153.

(7) Goldshtein, M.; Shamir, S.; Vinogradov, E.; Monsonego, A.; Cohen, S., Co-assembled Ca2+ Alginate-Sulfate Nanoparticles for Intracellular Plasmid DNA Delivery. *Molecular Therapy - Nucleic Acids* **2019,** *16*, 378-390.
(8) Bastos, L. P. H.; de Carvalho, C. W. P.; Garcia-Rojas, E. E., Formation and characterization of the complex coacervates obtained between lactoferrin and sodium alginate. *International Journal of Biological Macromolecules* **2018,** *120*, 332-338.
(9) Valentin, T. M.; Leggett, S. E.; Chen, P.-Y.; Sodhi, J. K.; Stephens, L. H.; McClintock, H. D.; Sim, J. Y.; Wong, I. Y., Stereolithographic printing of ionically-crosslinked alginate hydrogels for degradable biomaterials and microfluidics. *Lab on a Chip* **2017,** *17* (20), 3474-3488.
(10) Cinel, V. D. P.; Taketa, T. B.; de Carvalho, B. G.; de la Torre, L. G.; de Mello, L. R.; da Silva, E. R.; Han, S. W., Microfluidic encapsulation of nanoparticles in alginate microgels gelled via competitive ligand exchange crosslinking. *Biopolymers* **2021,** *112* (7), e23432.
(11) Rondeau, E.; Cooper-White, J. J., Biopolymer Microparticle and Nanoparticle Formation within a Microfluidic Device. *Langmuir* **2008,** *24* (13), 6937-6945.

4.5 Experimental Protocols

Instruments: Nuclear Magnetic Resonance (NMR) spectra were recorded on 500 MHz Bruker spectrometers at 25 °C with chemical shifts reported in ppm and coupling constants in Hertz (Hz). ^{1}H NMR chemical shifts were referenced to either CD_3OD or D_2O. Number average molecular weight (*Mn*) and Dispersity (*D*) were determined by Gel Permeation Chromatography (GPC). Organic-phase GPC experiments were performed on an Agilent 1100 SEC system using a PLGel 5 μm MIXED-C 300 x 7.5mm column from Agilent Technologies (PN PL1110-6500) and polymer molecular weight was determined with respect to polystyrene standards purchased from Sigma-Aldrich. DMF was used as the eluent at a flow rate of 1mL/min and at a column temperature of 35 °C. All aqueous-phase GPC experiments were performed on an Agilent 1100 SEC system using an Asahipak GF-150 HQ 7.5 x 300 mm column from Shodex (PN SH-F7600002) and polymer molecular weight was determined with respect to polyethylene glycol standards purchased from

Sigma-Aldrich. 90% phosphate buffered saline (PBS): 10% Methanol (MeOH) was used as the eluent at a flow rate of 1.0 mL/min and at a column temperature of 35 °C. EGFP mRNA-polymer nanoparticle sizes were measured at 633 nm using a Zetasizer Nano ZS dynamic light scattering instrument (Malvern Instruments, Malvern, UK) at 25 ˚C with detection angle of 173°. All flow cytometry was performed on a NovoCyte flow cytometer (ACEA Biosciences, San Diego) using NovoExpress Software. All EGFP mRNA-polymer nanoparticles were visualized using a JEOL 2100F TEM utilizing a Schottky type field emission gun operating at 200 keV. All pH measurements were measured using an Accumet Basic AB15 pH probe. Poly(amino)disulfide-mRNA nanoparticle complexation assays were performed using agarose gel electrophoresis and imaged on a Typhoon 9410 system (GE).

Materials: All commercially available chemicals were used without further purification unless otherwise noted and all reactions performed using HPLC grade solvents.

Reagents: All reagents described within have purity denoted as percent purity (%). D,L-α-Lipoic acid (LA; 99.3%) was purchased from Chem-Impex (USA, IL). N,N′-Dicyclohexylcarbodiimide (DCC; 99%), and 4-Dimethylaminopyridine (DMAP; 99%) were purchased from Alfa Aesar. Triethanolamine (>99%), Sodium 2-mercaptoethanesulfonate (>98%), and 3-(4-Morpholino)propyl isocyanate (95%) were purchased from Sigma-Aldrich. 2-[2-(Dimethylamino)ethoxy]ethanol (>98%), 2-[[2-(Dimethylamino)ethyl]methylamino]ethanol (>97%), 4-Methylpiperazine-1-ethanol (>98%), and 2-Iodoacetamide (>98%) were purchased from TCI America.

Monomer (M1-M4) Synthesis Procedure: For monomers **M1**, **M3**, and **M4**: D,L-α-Lipoic acid [2.00 grams; 9.68 mmol; 2 equiv.] was dissolved in 150 mLs of dry, 4 °C -

prechilled acetonitrile (ACN) containing 5 mol% 4-dimethylaminopyridine (DMAP) [0.48 mmol; 6 mgs] and stirred under inert gas until fully dissolved. 1.05 equivalents of N,N′-dicyclohexylcarbodiimide (DCC) [1.05 grams; 5.08 mmol; 1 equiv.] was dissolved in a 15 mLs of dry, 4 °C -prechilled ACN and added dropwise to the solution of LA. The reaction mixture was gradually warmed to 25 °C and stirred for 3 hrs. Afterwards the reaction was filtered, the corresponding amino alcohol (7.26 mmol; 1.5 equiv.) was added, and the reaction was stilled for another 8 hours at 25 °C. After this reaction was placed in a -20 °C freezer for 24 hours and subsequently filtered to remove any residual DCC/ DCU. The solution was then reduced *in vacuo*, resuspended in dichloromethane (DCM), washed with 1M Na_2CO_3 (3X 100 mL washes), followed by Brine (3X 100 mL washes), dried with $MgSO_4$, and filtered. The organic layer was reduced *in vacuo* and loaded on silica for flash chromatography; columns were run with DCM: basified methanol (90% DCM: 9% MeOH: 1% NH_4OH) gradient all monomers eluted in 80-90% basified methanol. Pure monomer appears as a yellow viscous oil.

For **M2** synthesis: D,L-α-Lipoic acid [2.00 grams; 9.68 mmol; 2 equiv.] was dissolved in 150 mLs of dry, 4 °C -prechilled ACN containing 5 mol% 4-dimethylaminopyridine (DMAP) [0.48 mmol; 6 mgs] and stirred under inert gas until fully dissolved. 1.05 equivalents of N,N′-dicyclohexylcarbodiimide (DCC) [1.05 grams; 5.08 mmol; 1 equiv.] was dissolved in a 15 mLs of dry, 4 °C -prechilled ACN and added dropwise to the solution of LA. The reaction mixture was gradually warmed to 25 °C, stirred for 3 hours, then filtered. In a separate 250 mL round bottom flask triethanolamine [24.2 mmol; 5 equiv.] was dissolved in 50 mL of dry CAN and stirred. The previously-filtered LA solution was placed into a 200 mL syringe, fitted to a syringe pump, and added to the stirring solution of triethanolamine

at a rate of 0.4 mL/min. After complete addition the reaction was stirred for 8 hours at 25 °C. After this reaction was placed in a -20 °C freezer for 24 hours and subsequently filtered to remove any residual DCC/ DCU. The solution was then reduced *in vacuo*, resuspended in dichloromethane (DCM), washed with 1M Na_2CO_3 (3X 100 mL washes), followed by Brine (3X 100 mL washes), dried with $MgSO_4$, and filtered. The organic layer was reduced *in vacuo* and loaded on silica for flash chromatography; columns were run with DCM: basified methanol (90% DCM: 9% MeOH: 1% NH_4OH) gradient all monomers eluted in 80-90% basified methanol. Pure monomer appears as a yellow viscous oil.

Poly(anionic/M0)disulfide Polymerization Procedure: Prior to cryopolymerization a fresh stock solution of sodium lipoate (**M0**) was generated by carefully dissolving D,L-α-lipoic acid with 6M or 1M NaOH in water to a pH of 7.4 and final concentration of 200 mM. Depending on the final polymerization concentration, varying quantities of this solution (2 mL for 200 mM, 1 mL for 100 mM, 0.75 mLs for 75 mM, and 0.5 mLs for 50 mM) was added to a fresh scintillation vial and diluted to the final concentration, if appropriate. To this solution sodium 2-mercaptoethanesulfonate (0.2 μmol) initiator was added to final solution concentration of 100 uM and mixed thoroughly. Afterwards the solution was placed in a -20 °C freezer for 72 hours. After visual confirmation of polymerization, the scintillation vial was removed, excess anti-solvent (acetone or acetonitrile) was quickly added to the vial, and the vial was vortexed to yield a white sticky precipitate. The solvent was carefully decanted, residual polymer was rinsed again with anti-solvent, and decanted once more. After very briefly removing residual solvent *in vacuo*, 3-(4-Morpholino)propyl isocyanate (xs) was dissolved in 2 mLs of fresh 80% H_2O-20% MeOH solution, added to the white polymer, and the resulting solution was

vortex for 3-5 minutes. Afterwards the polymer was precipitated in anti-solvent again, resuspended in 1 mL of fresh water, and precipitated in anti-solvent again. After one more wash, the final polymer was reduced *in vacuo* to yield shelf-stable poly(**M0**)disulfide. GPC characterization of poly(**M0**)disulfide was conducted using the aqueous conditions mentioned in the Instruments section above.

Poly(amino/M1-M4)disulfide Polymerization Procedure: Each corresponding monomer (M1-M4; 0.3 mmol; 1 equiv) was added to a clean scintillation vial along with 0.5 mLs of fresh methanol and mixed thoroughly until fully dissolved. To this methanol solution a stoichiometric amount of 3M HCl (0.3 mmol for M1, M2, and M4; 0.6 mmol for M3) was added and gently mixed. Afterwards 2 mLs of DI H_2O was added to the acidified methanol solution and the resulting solution was reduced in vacuo at 28 °C to remove residual methanol. After confirming the pH of each monomer solution was between 4.0-4.5 via pH probe, sodium 2-mercaptoethanesulfonate (0.2 μmol) initiator was added to the solution and gently mixed. The resulting solution was then placed in a -20 °C freezer for 72 hours. After visual confirmation of polymerization, the scintillation vial was removed, excess anti-solvent (acetone) was quickly added to the vial, and the vial was vortexed to yield a white sticky precipitate. The solvent was carefully decanted, residual polymer was rinsed again with anti-solvent, and decanted once more. After very briefly removing residual solvent *in vacuo*, 2-Iodoacetamide (xs) was dissolved in 2 mLs of fresh 80% H_2O-20% MeOH solution, added to the white polymer, and the resulting solution was vortex for 3-5 minutes. Afterwards the polymer was precipitated in anti-solvent again, resuspended in 1 mL of fresh water, and precipitated in anti-solvent again. After one more wash, the final polymer was reduced *in vacuo* to yield shelf-stable poly(amino)disulfides. GPC

characterization of poly(amino)disulfide was conducted using the organic conditions mentioned in the Instruments section above.

Nanoparticle Formulation, DLS, and Gel Electrophoresis Assay Procedure: EGFP mRNA was diluted to a concentration of 50 ng/ μL in 10 mM sodium acetate (NaOAc) buffer (pH 4) or PBS (pH 7.4) prior to use. For cell culture experiments, 150ng of mRNA was administered per well and for dynamic light scattering (DLS) measurements 0.5 μg of EGFP mRNA was used for nanoparticle characterization.

For poly(anionic)disulfide complexation: After the desired amount of mRNA was pipetted into a clear microfuge tube, a correspond quantity of polymer was (10-200 w/w) was also added to the mRNA from a 10 mg/mL sodium alginate stock or poly(**M0**)disulfide stock solution. After a brief mixing of these components, 1 mM stock solution calcium chloride solution (quantity varies; 0.25-0.75 equivalents of Ca^{2+} relative to the sum of all carboxylate and phosphate groups present in each formulation) was quickly pipetted into the mixture and aggressively vortexed for 20 seconds. For DLS measurements and *in vitro* cell delivery experiments, the resulting nanoparticle solution was resuspended in PBS (pH 7.4) prior to analysis/ use.

For poly(amino)disulfide complexation: After the desired amount of mRNA was pipetted into a clear microfuge tube, a correspond quantity of poly(amino)disulfide polymer (from a 5 mg/mL solution) was also added to the mRNA solution and vortexed thoroughly. For all formulations in this work the nitrogen-to-phosphate (N/P) ratio was used as a measure of how many equivalents of polymer to add in polymer-RNA complexations (N quantity was determined from the average number of cationic residues

per repeat unit of polymer). For DLS experiments, the resulting EGFP mRNA-polymer nanoparticles were resuspended in 600 μL of 10 mM NaOAc buffer (pH 4), placed in a clean cuvette, briefly mixed, and incubated at 25 °C for 10 minutes before measurement. DLS measurements were taken measured at 633 nm using Zetasizer Nano ZS dynamic light scattering instrument (Malvern Instruments, Malvern, UK) at 25 ˚C with detection angle of 173 ˚. A minimum of three measurements were taken for each sample and the mean Z-average values were reported. For gel electrophoresis assays, EGFP mRNA-poly(amino)disulfide nanoparticles were formulated in PBS (pH 7.4) as described above and resuspended in additional PBS. Complexed nanoparticles were briefly mixed with loading gel before being separated on a 1% agarose gel. 1kb DNA ladder was purchased from NEB (Catalog # N3232S) and used as the molecular weight ladder for gel electrophoresis assays. For *in vitro* cell delivery assays, EGFP mRNA-poly(amino)disulfide nanoparticles were formulated in a 10 mM NaOAc buffer (pH 4) as mentioned above, then resuspended in OptiMEM (pH 7.4) before administration to cells.

***In Vitro* Cell Delivery:** DC2.4 transfections were performed in triplicate within cell culture-treated clear-bottom 96-well plates (Corning). After passaging, cells were seeded at a density of 10,000 cells/ 96 well and incubated for 24 hours prior to treatment. The EGFP mRNA-polymer nanoparticles were formulated as mentioned above (for both poly(anionic)disulfide or poly(amino)disulfides; with 150ng of mRNA administered per well), resuspended in 30 μL of PBS or OptiMEM, and gently mixed via pipette for 30 seconds before administering to cells. After an additional 50 μL of OptiMEM was added to each treated well, cells were incubated for 6 hours before media was exchanged with DMEM containing 10% FBS. After 6 hours or 48 hours of incubation media was removed,

cells were trypsinized, and transferred to non-binding V-bottom 96 well microplate plates (Greiner) for flow cytometry analysis. To determine cytotoxicity propidium iodide (PI) was added to sample wells at a final concentration of 2.5 µg/ mL and incubated for at least five minutes prior to flow cytometry analysis. EGFP expression and cytotoxicity (PI fluorescence) were determined using a NovoCyte flow cytometer. For lipid control samples, Cy5-EGFP mRNA (150 ng of mRNA per well; 50 ng/ µL in pH 7.4 PBS) was complexed with Lipofectamine MessengerMAX in OptiMEM under continuous mixing before administering to cells.

4.6 Supplementary Figures

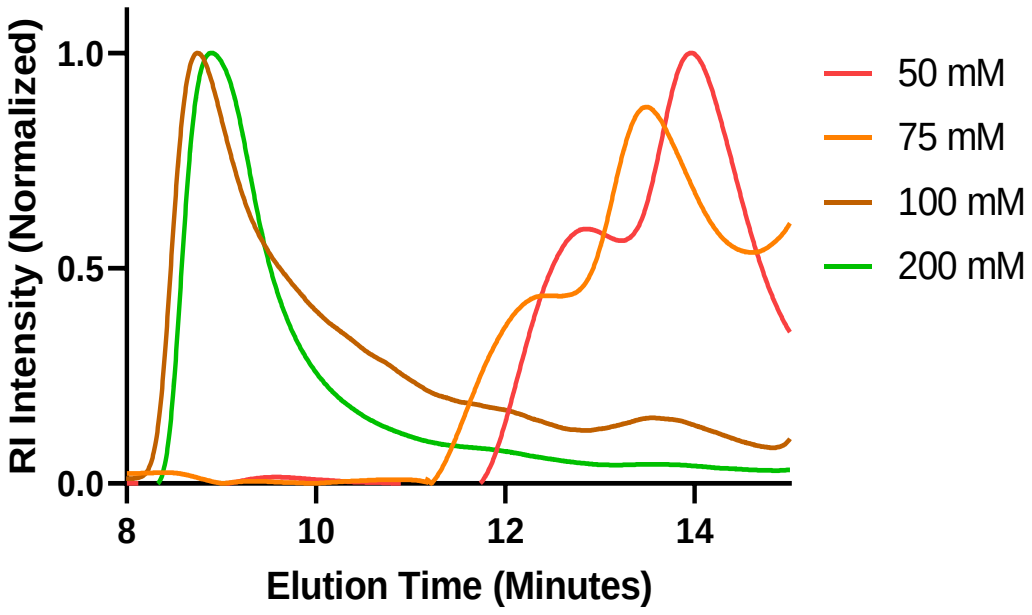

Figure S4.1 GPC traces of cryopolymerized poly(**M0**)disulfides generated from different lipoic acid monomer concentrations at pH 7.4 (50 mM is red, 75 mM is yellow, 100 mM is brown, and 200 mM is green). All polymers were dissolved in and eluted with 90% PBS (pH 7.4) with 10% methanol at a flow rate of 1.0 mL/min.

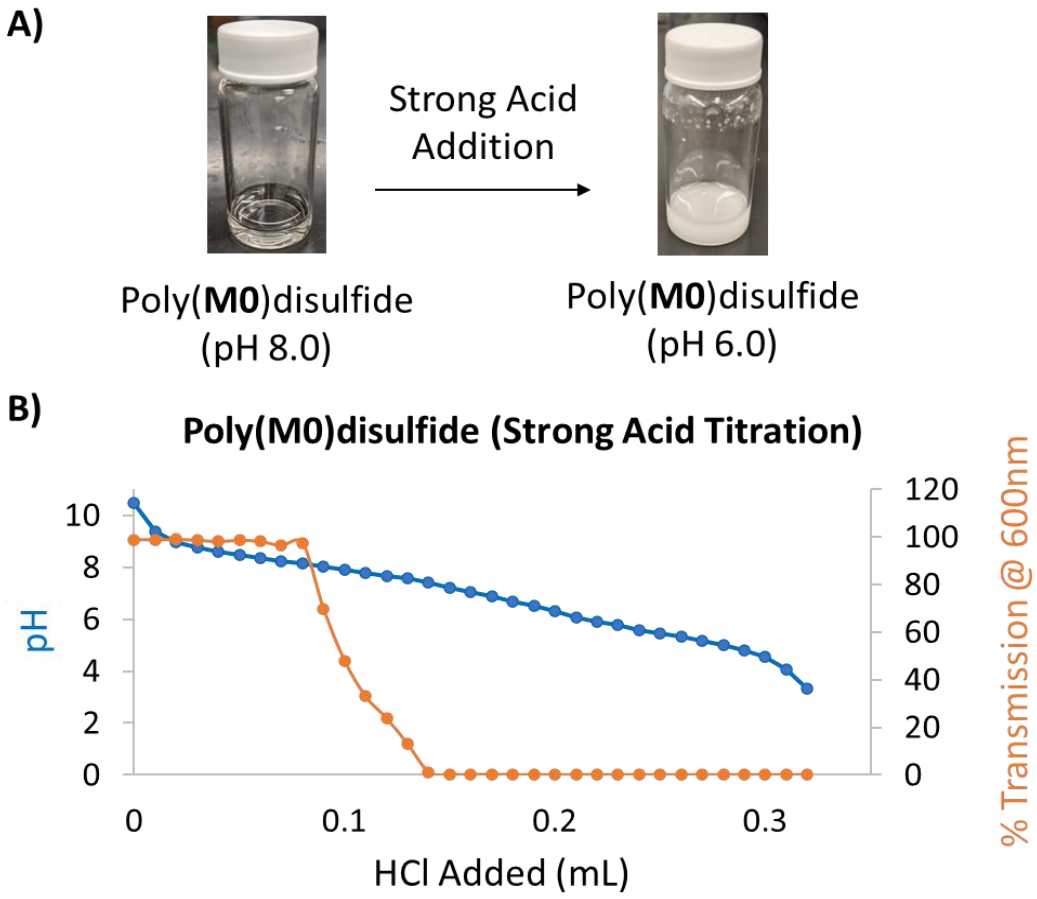

Figure S4.2 Buffering capacity of poly(**M0**)disulfide polymer with 1M HCl strong acid. **A**) Visible turbidity for poly(**M0**)disulfide solutions is observed after strong acid addition to 10 mg/ mL poly(**M0**)disulfide solution. **B**) Plot of pH (blue; left) and turbidity/ Percent transmission at 600 nm (orange; right) vs amount of 1M HCl added. Turbidity is apparent below pH 8.0.

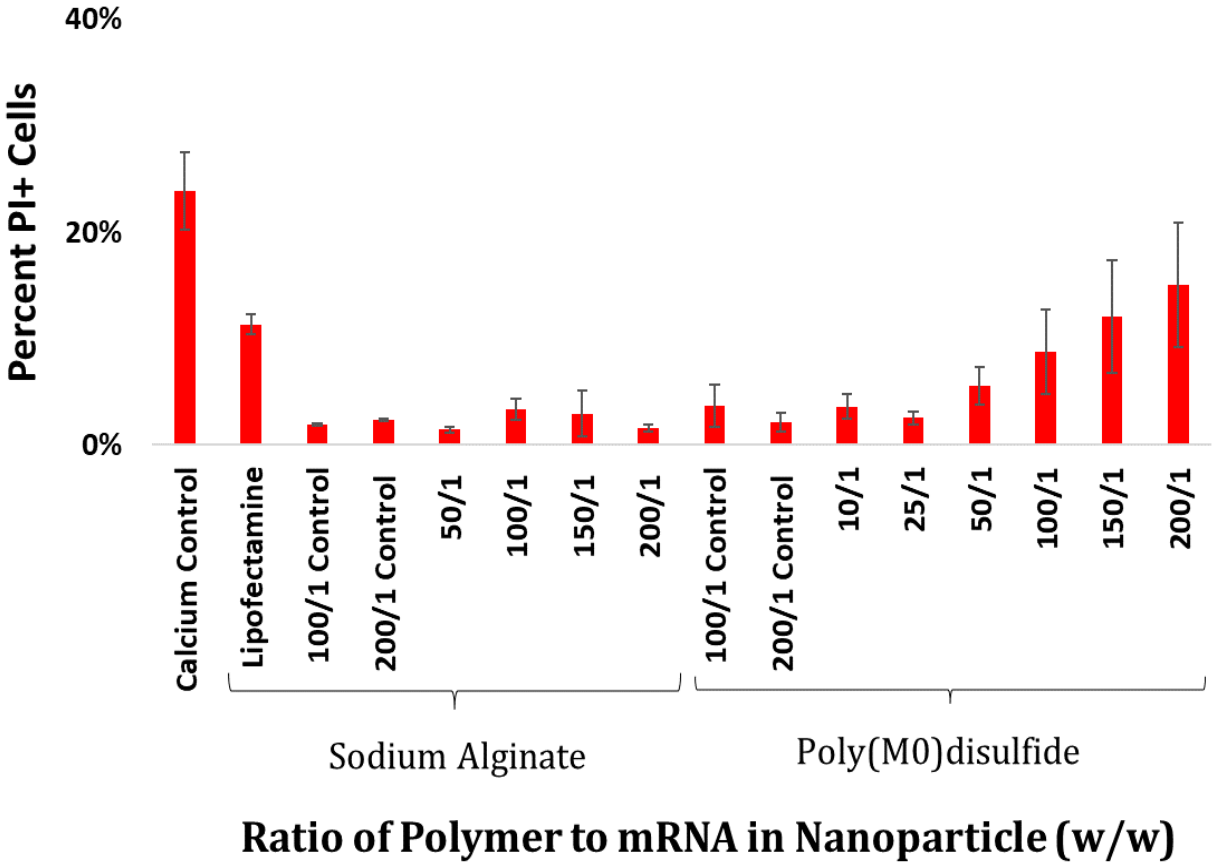

Figure S4.3 Number of PI+ (dead) cells after treatment with cross-linked poly(**M0**)disulfide-EGFP mRNA nanoparticles. Percent PI+ DC2.4 cells after 48 hours of treatment with Ca^{2+} cross-linked poly(**M0**)disulfide-EGFP mRNA nanoparticles. Calcium ions formulated with mRNA used as control; Lipofectamine used as positive control. 100/1 and 200/1 control samples are respective polymer and EGFP mRNA formulations without Ca^{2+} crosslinking. 50/1, 100/1, 150/1, and 200/1 samples represent Ca^{2+} cross-linked polycarboxylate-EGFP mRNA nanoparticles formulated at different polymer/EGFP mRNA w/w ratios. All nanoparticles were generated by bulk mixing using 0.5 stoichiometric equivalents of Ca^{2+} ions (with respect to the sum of all carboxylate and phosphate groups). N=3 for all samples.

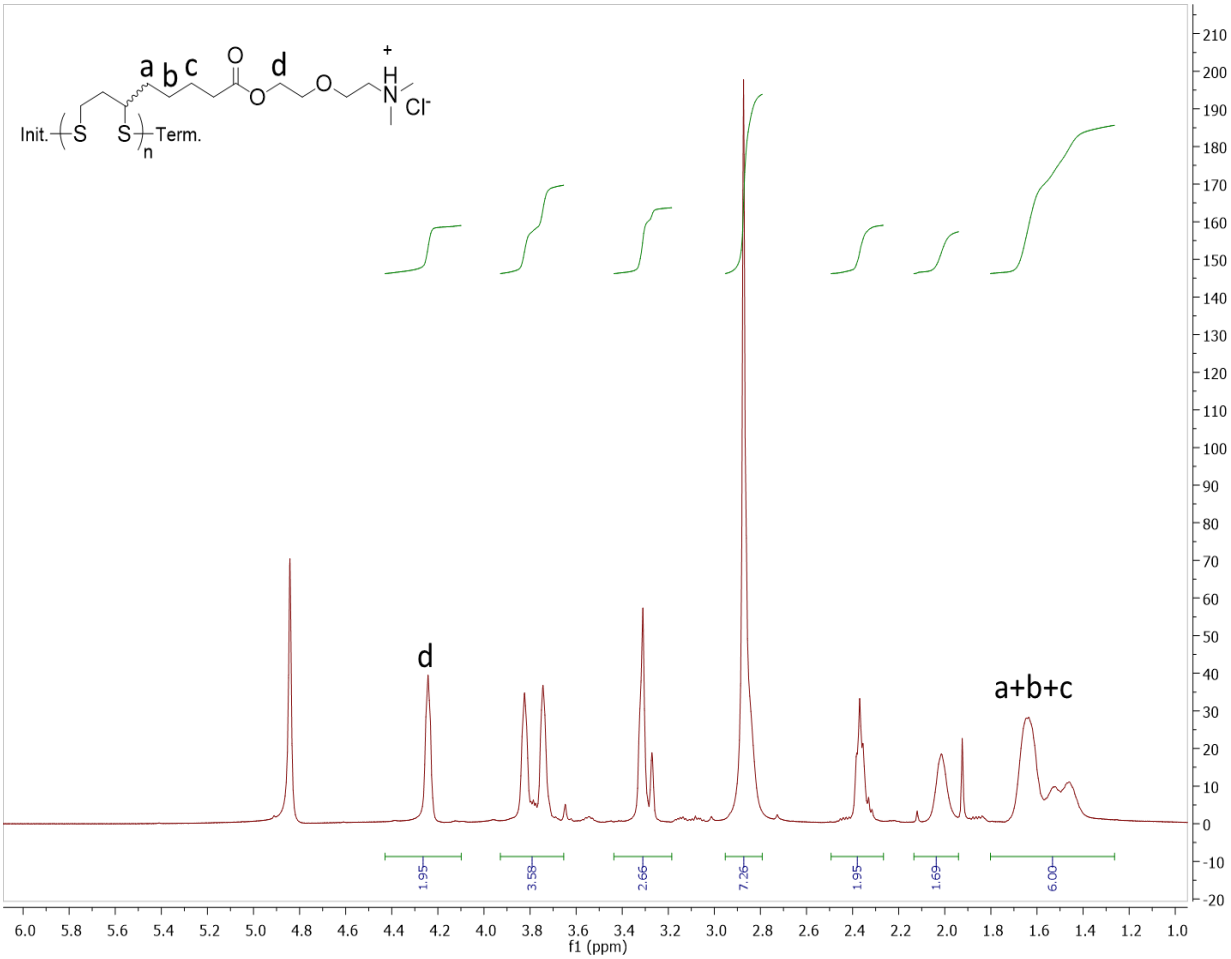

Figure S4.4 Partially annotated ^{1}H NMR (in CD_3OD) spectra of poly(**M1**)disulfide after cryopolymerization. Polymer signals were normalized to proton signals from a, b, and c. Signal d was used as a diagnostic peak for amine-containing motif. Estimated 97.5% **M1** by integration.

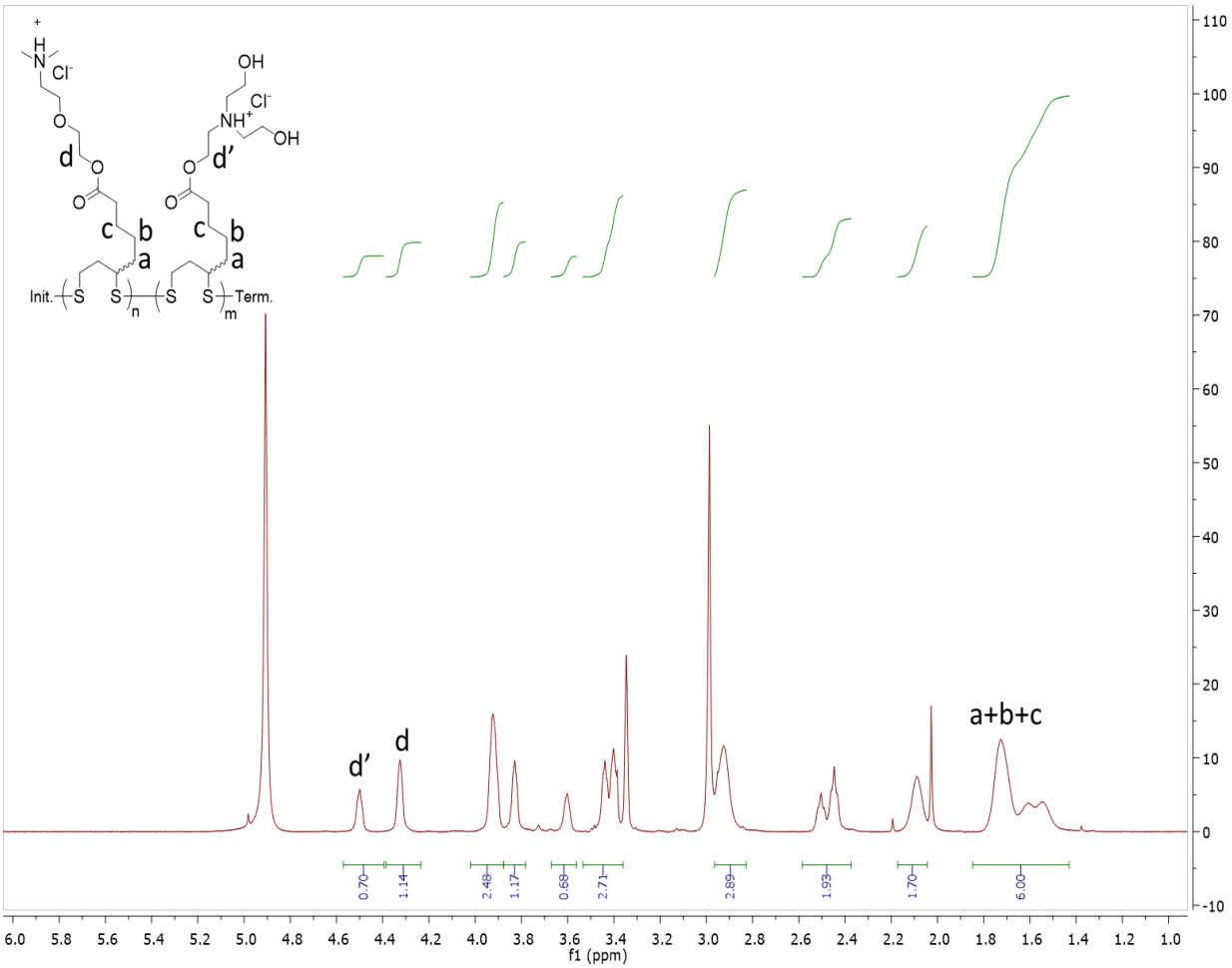

Figure S4.5 Partially annotated ^{1}H NMR (in CD_3OD) spectra of poly(**M1+M2**)disulfide after cryopolymerization. Polymer signals were normalized to proton signals from a, b, and c. Signal d ad d' were used as a diagnostic peak for amine-containing motif. Estimated 61.9% **M1** and 38.0% **M2** by integration.

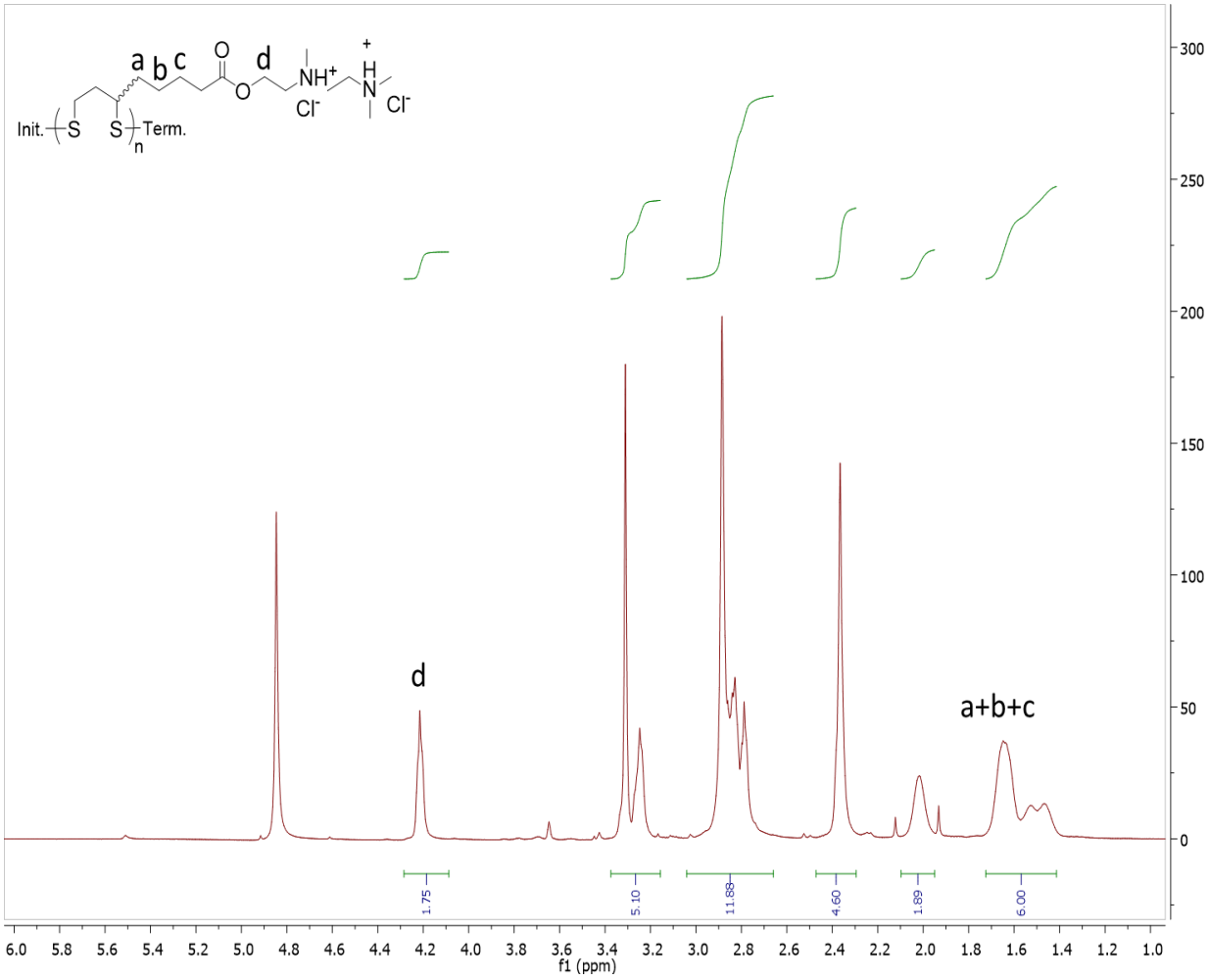

Figure S4.6 Partially annotated ^{1}H NMR (in CD_3OD) spectra of poly(**M3**)disulfide after cryopolymerization. Polymer signals were normalized to proton signals from a, b, and c. Signal d was used as a diagnostic peak for amine-containing motif. Estimated 87.5% **M3** by integration.

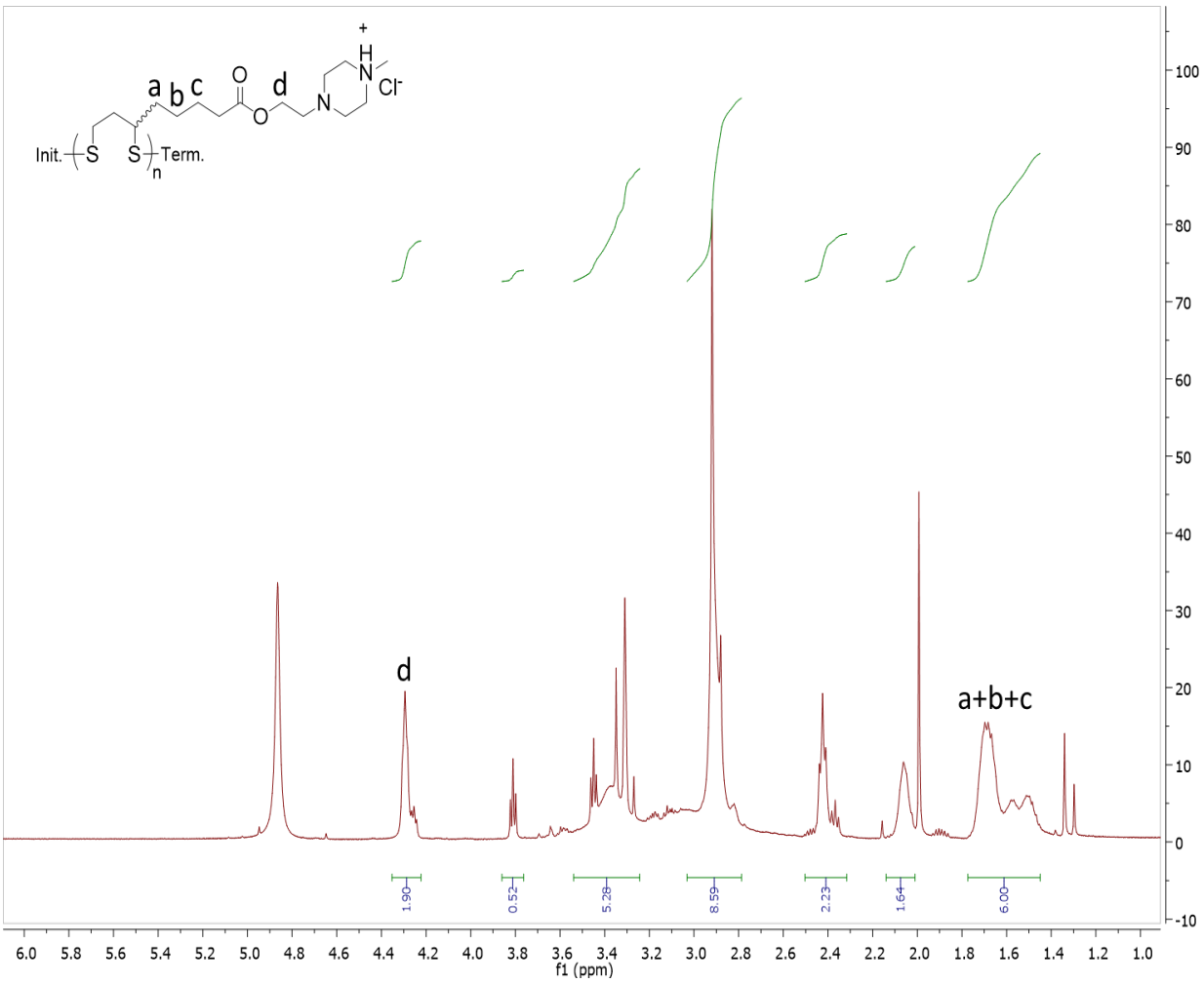

Figure S4.7 Partially annotated ^{1}H NMR (in CD_3OD) spectra of poly(**M4**)disulfide after cryopolymerization. Polymer signals were normalized to proton signals from a, b, and c. Signal d was used as a diagnostic peak for amine-containing motif. Estimated 95.0% **M4** by integration.

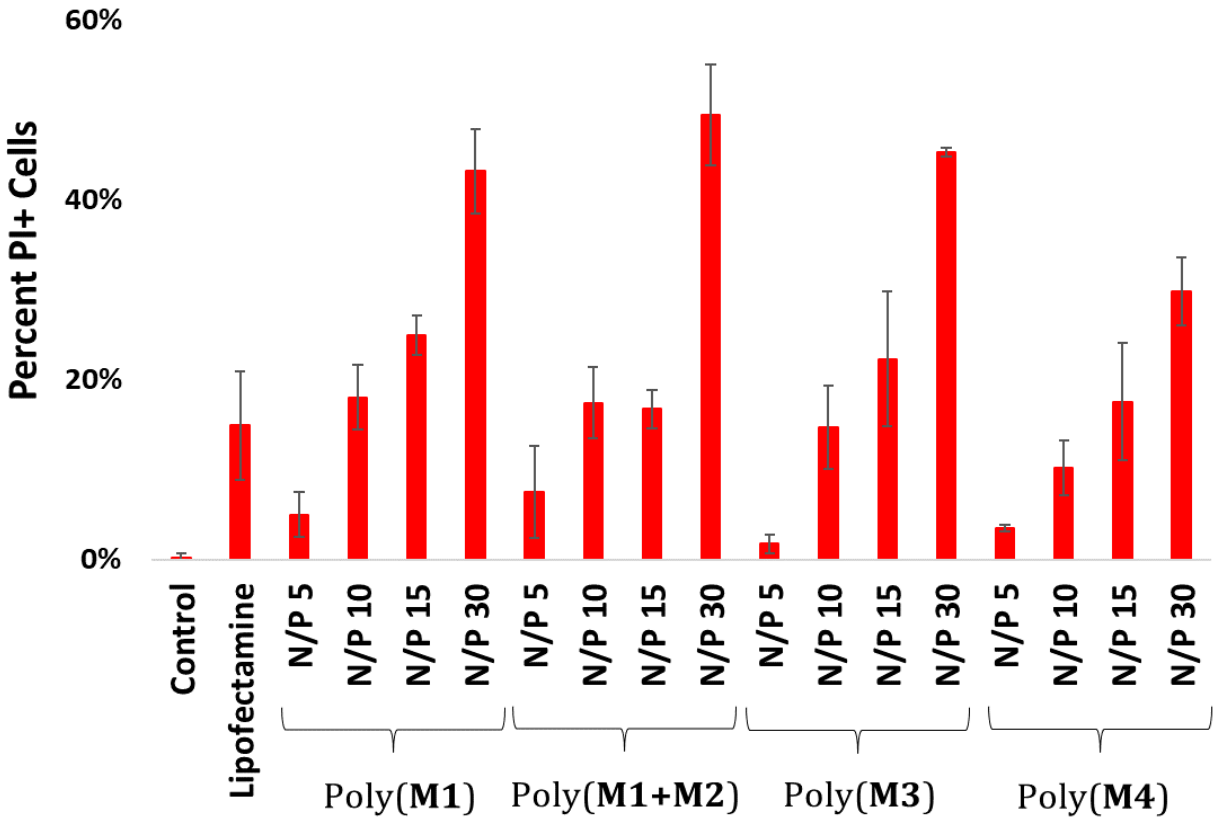

Figure S4.8 PI+ (dead) cells after treatment with poly(amino)disulfide-mRNA nanoparticles. Percent PI+ DC2.4 cells after 48 hours of treatment with poly(amino)disulfide-EGFP mRNA polymeric nanoparticles at different N/P ratios; Number of PI+ cells determined by flow cytometry. Untreated DC2.4 cells are displayed as control samples; Lipofectamine MessengerMAX was used as positive control. N=3 for all samples.

Table S4.1 Results of cryopolymerization of different lipoic acid solutions at pH 10 under scaled conditions.

Monomer Feedstock Concentration:	Polymer *Mn* (Da):	Dispersity (D):	Yield:
50 mM	$3.4x10^3$	1.9	26%
75 mM	$4.1x10^3$	1.8	39%
100 mM	$9.8x10^3$	1.1	58%
200 mM	$1.0x10^4$	1.1	63%

Table S4.2 Yield and polymer characterization (by GPC) of poly(amino)disulfides generated by cryopolymerization. All monomer concentrations prior to cryopolymerization were 150 mM; all cryopolymerizations occurred in aqueous pH 4.0-4.5 conditions.

Monomer :	Polymer *Mn* (kDa):	Dispersity (*D*):	Yield:
M1	*4.65*	*1.42*	60%
M1+M2	*4.59*	*1.04*	48%
M3	*4.88*	*1.28*	62%
M4	*9.41*	*1.10*	67%

Table S4.3 Summary of poly(amino)disulfide-EGFP mRNA nanoparticles as determined by DLS. All nanoparticles complexed in pH 4 sodium acetate buffer at an N/P ratio of 10.

Poly(amino)disulfide Species	Z-Ave. Diameter (nm):	Dispersity (*D*):
Poly(**M1**)-	112.6	0.29
Poly(**M1**+**M2**)-	97.2	0.22
Poly(**M3**)-	82.7	0.18
Poly(**M4**)-	117.9	0.34

4.7 Small Molecule Characterization Data (^{1}H NMR, ^{13}C NMR, ESI-MS, Titration Curves)

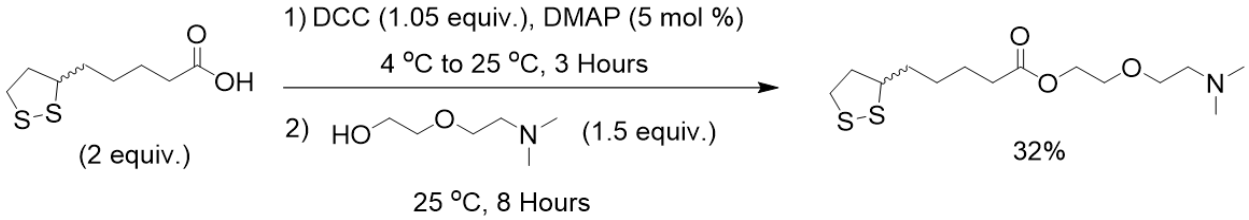

Scheme S4.1 Synthesis of **M1.**

M1 Yield: 0.49 grams, 32%

^{1}H NMR (CD_3OD, 500 MHz): δ(ppm)= 4.25-4.18 (t, *J*= 3.5 Hz, 2H), 3.68-3.64 (t, *J*= 5.0 Hz, 2H), 3.63-3.55 (m, 3H), 3.22-3.07 (m, 2H), 2.59-2.54 (t, *J*= 6.0 Hz, 2H), 2.51-2.44 (sext, *J*= 7.0 Hz, 1H), 2.38-2.34 (t, *J*= 7.5 Hz, 2H), 2.32-2.25 (s, 6H), 1.94-1.86 (sext, *J*= 7.0 Hz, 1H), 1.77-1.60 (m, 4H), 1.54-1.41 (m, 2H); ^{13}C NMR (CD_3OD, 500 MHz): δ(ppm)= 175.00, 69.94, 69.72, 64.50, 59.40, 57.52, 45.84, 41.29, 39.36, 35.70, 34.76, 29.74, 25.74; ESI-MS: $C_{14}H_{27}NO_3S_2$ [M+H$^+$], Calculated 322.14, Found: 321.7; The ESI-MS, ^{1}H and ^{13}C NMR spectra, and pH titration curve of **M1** are attached below:

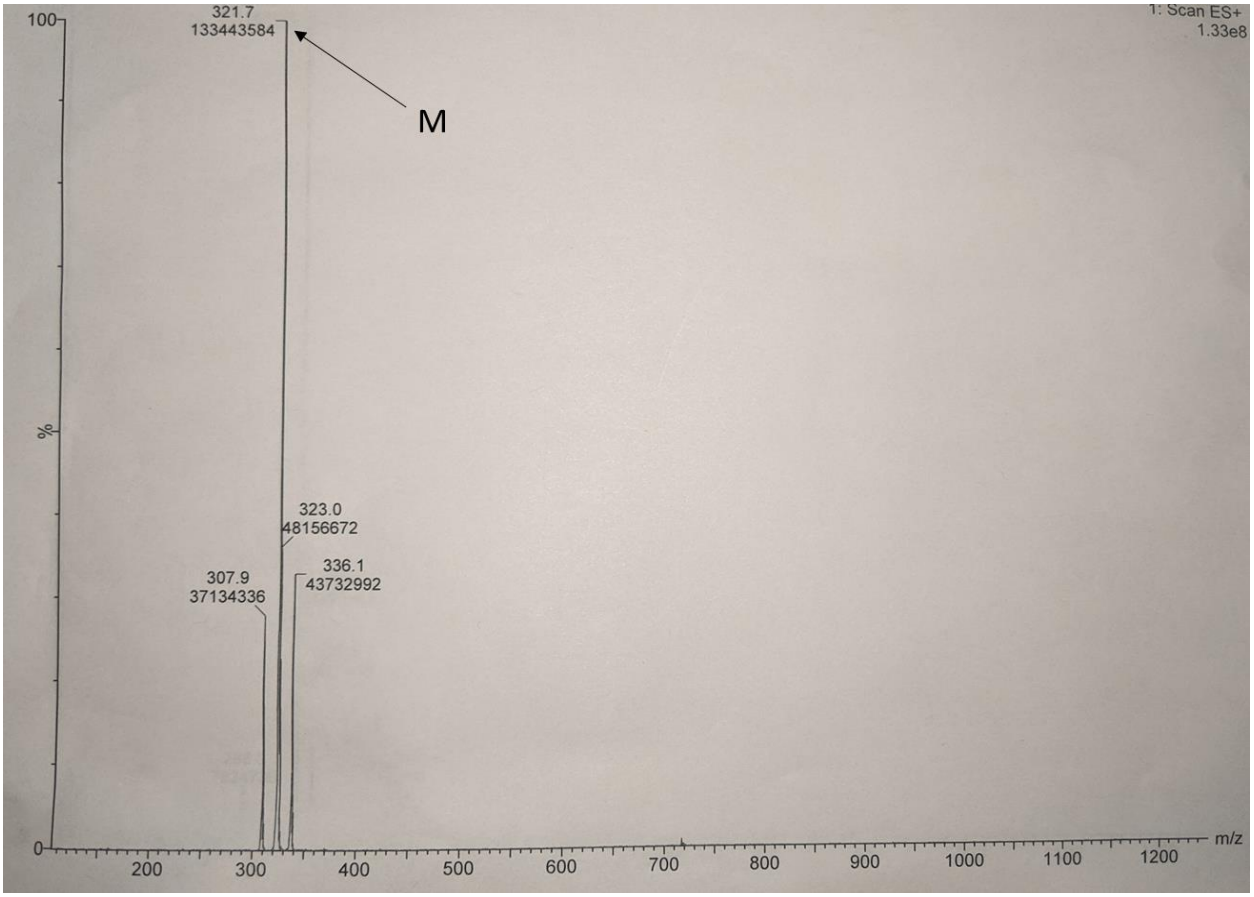

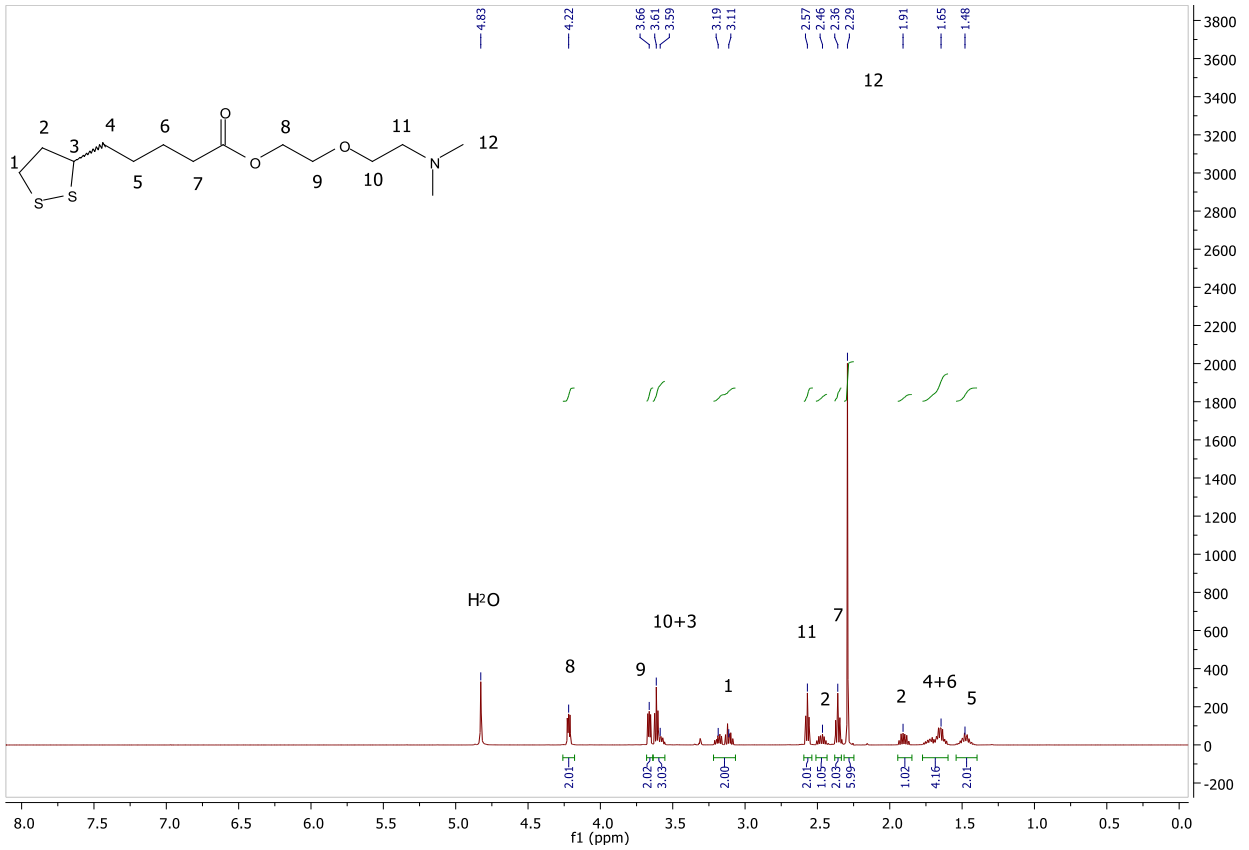
4.83
4.22
3.66
3.61
3.59
3.19
3.11
2.57
2.46
2.36
2.29
1.91
1.65
1.48
12
H2O
10+3
11
7
8
9
1
2
2
4+6
5
f1 (ppm)

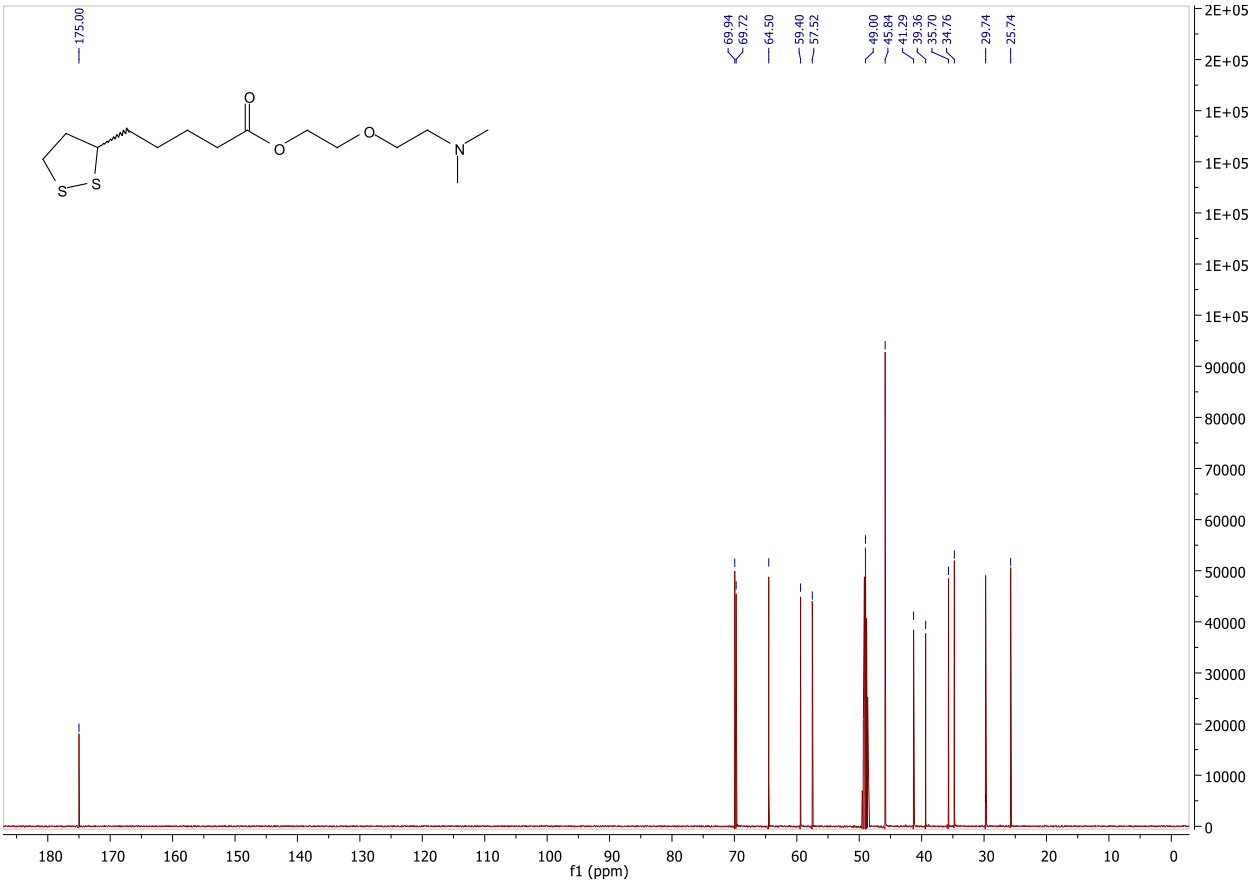
175.00
69.94
69.72
64.50
59.40
57.52
49.00
45.84
41.29
39.36
35.70
34.76
29.74
25.74
f1 (ppm)

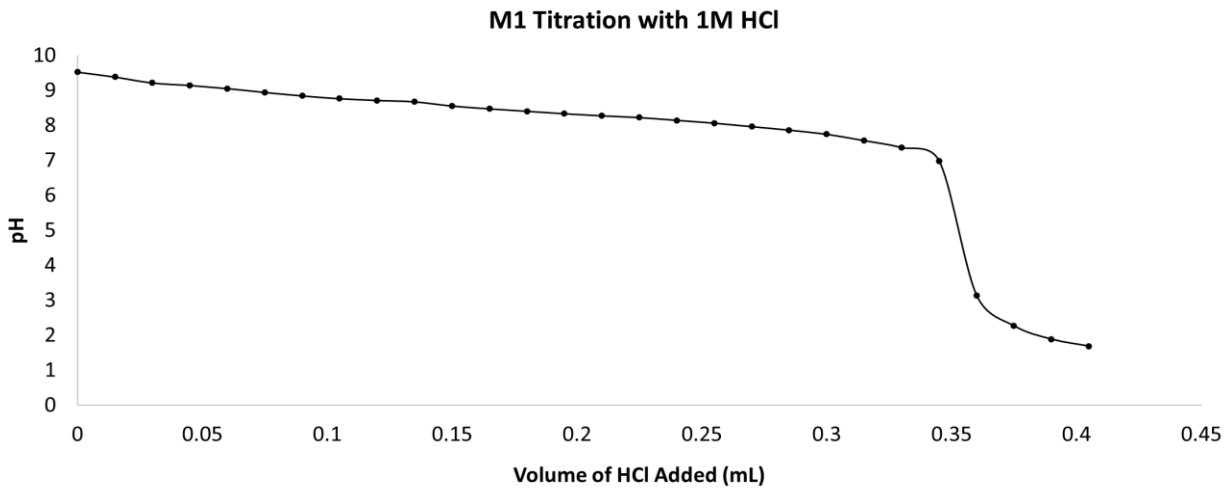
M1 Titration with 1M HCl
pH
Volume of HCl Added (mL)
0
1
2
3
4
5
6
7
8
9
10
0
0.05
0.1
0.15
0.2
0.25
0.3
0.35
0.4
0.45

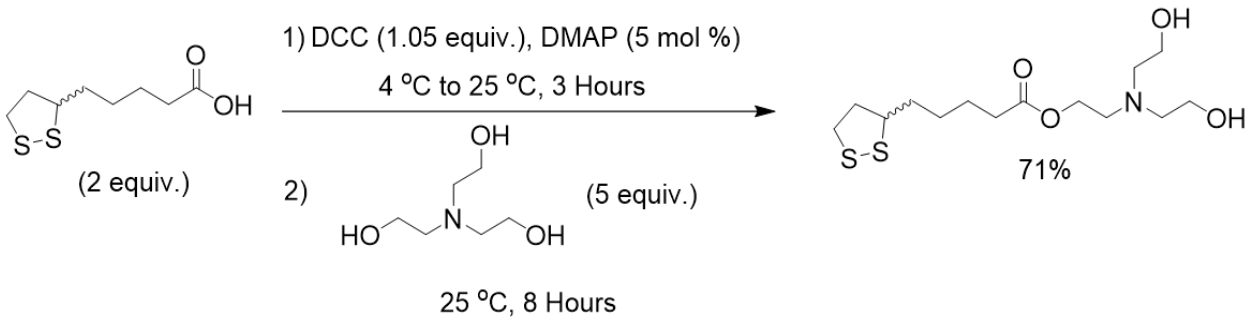

Scheme S4.2 Synthesis of **M2.**

M2 Yield: 1.16 grams, 71%

^{1}H NMR (CD_3OD, 500 MHz): δ(ppm)= 4.23-4.12 (t, *J*= 6.0 Hz, 2H), 3.63-3.54 (m, 5H), 3.22-3.06 (m, 2H), 2.89-2.82 (t, *J*= 6.0 Hz, 2H), 2.77-2.67 (t, *J*= 6.0 Hz, 2H), 2.50-2.43 (sext, *J*= 5.5 Hz, 1H), 2.38-2.32 (t, *J*= 7.5 Hz, 2H), 1.94-1.85 (sext, *J*= 6.5 Hz, 1H), 1.76-1.59 (m, 4H), 1.54-1.41 (m, 2H); ^{13}C NMR (CD_3OD, 500 MHz): δ(ppm)= 175.30, 63.38, 60.81, 58.15, 57.52, 54.42, 41.30, 39.35, 35.70, 34.86, 29.80, 25.73; ESI-MS: $C_{14}H_{27}NO_4S_2$ [M+H$^+$], Calculated 338.14, Found: 337.8; The ESI-MS, ^{1}H and ^{13}C NMR spectra, and pH titration curve of **M2** are attached below:

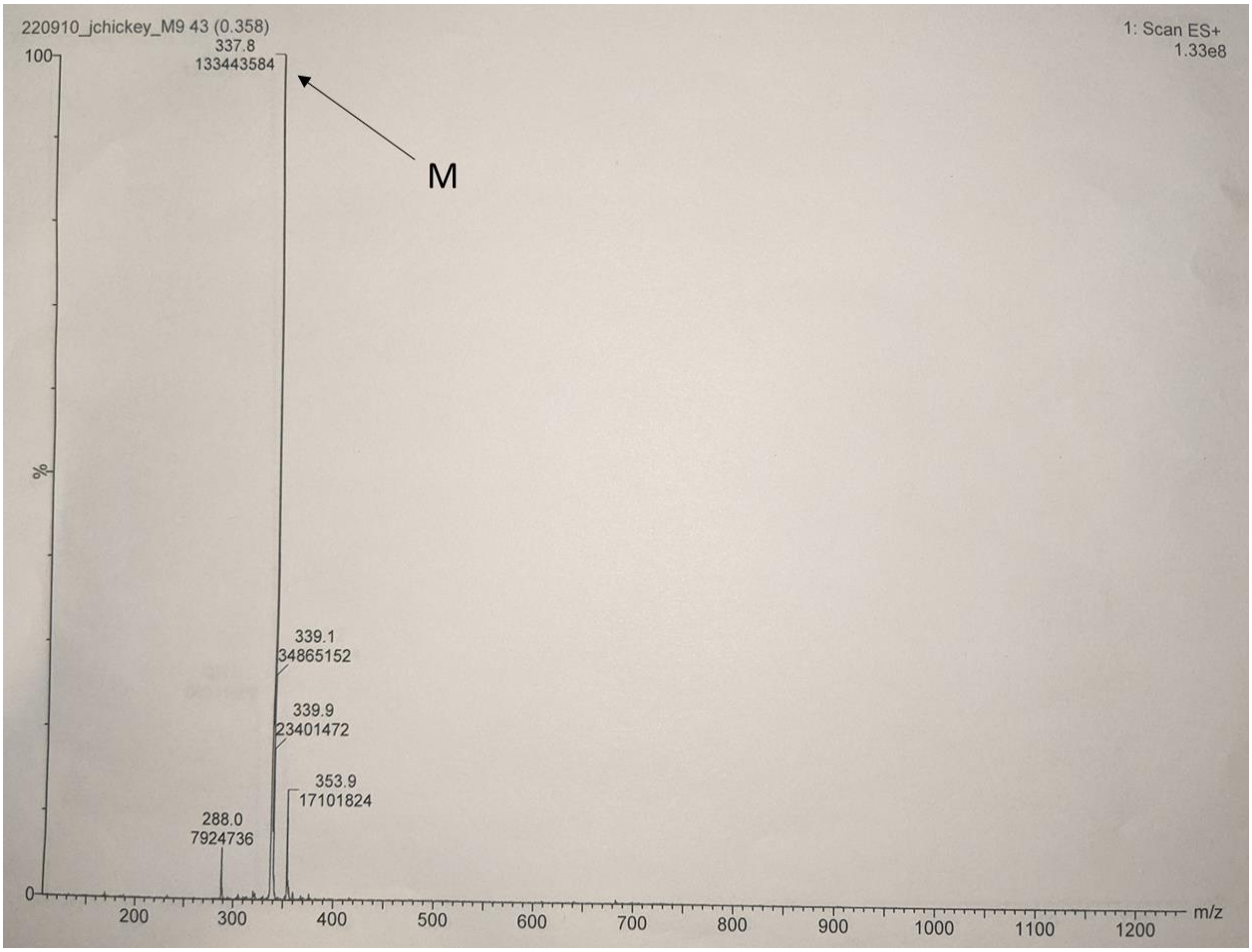

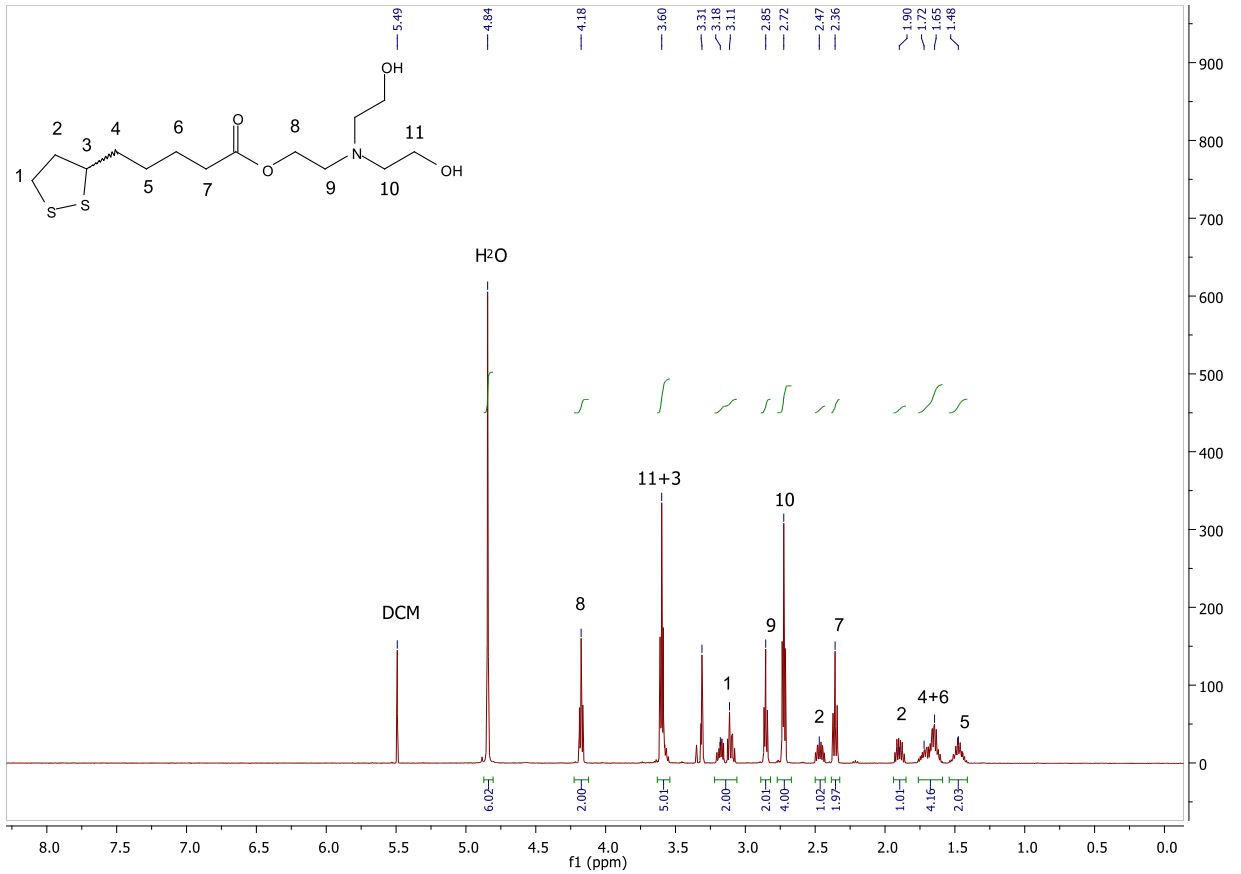
5.49
4.84
4.18
3.60
3.31
3.18
3.11
2.85
2.72
2.47
2.36
1.90
1.72
1.65
1.48
OH
2
3
4
6
O
8
11
1
5
7
O
N
9
10
OH
S
S
H2O
DCM
11+3
10
8
9
7
1
2
2
4+6
5
6.02
2.00
5.01
2.00
2.01
4.00
1.02
1.97
1.01
4.16
2.03
f1 (ppm)

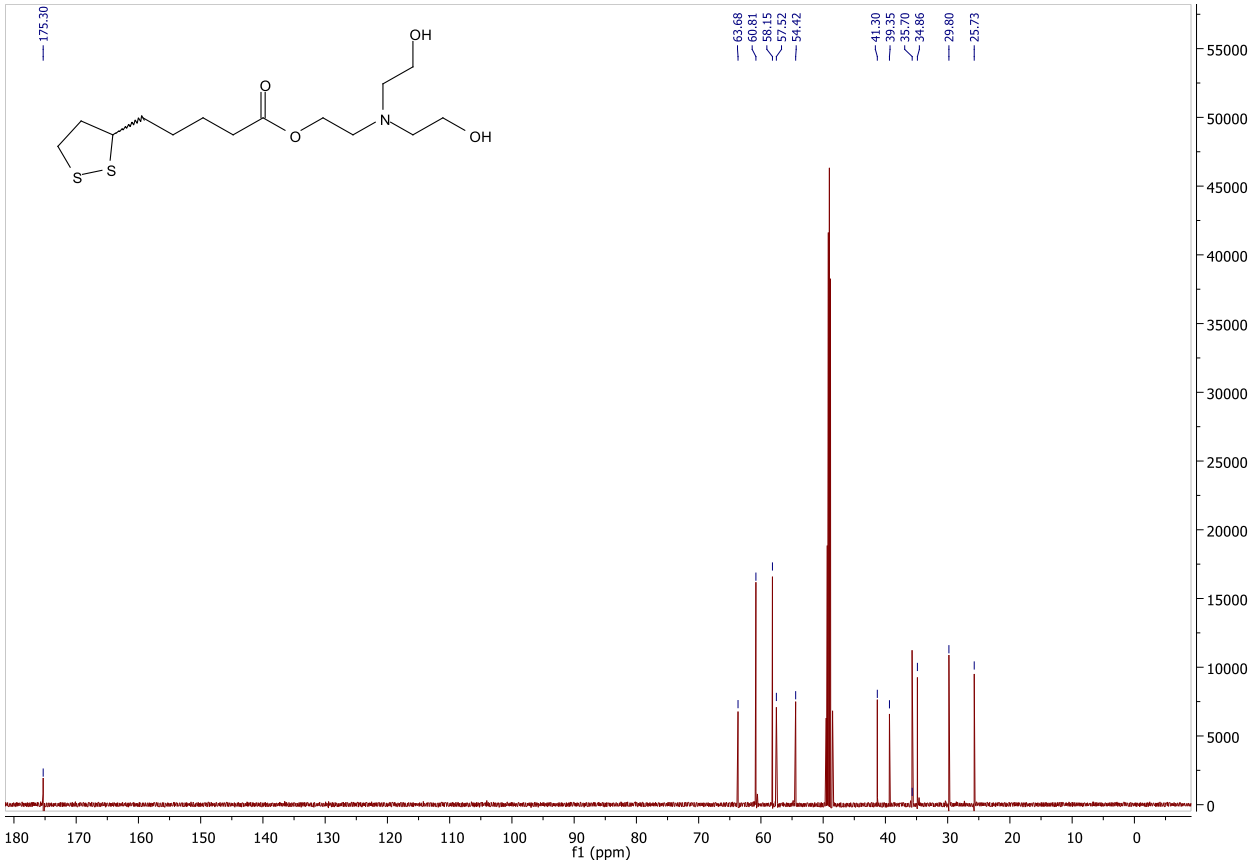
175.30
63.68
60.81
58.15
57.52
54.42
41.30
39.35
35.70
34.86
29.80
25.73
OH
O
N
O
OH
S
S
f1 (ppm)

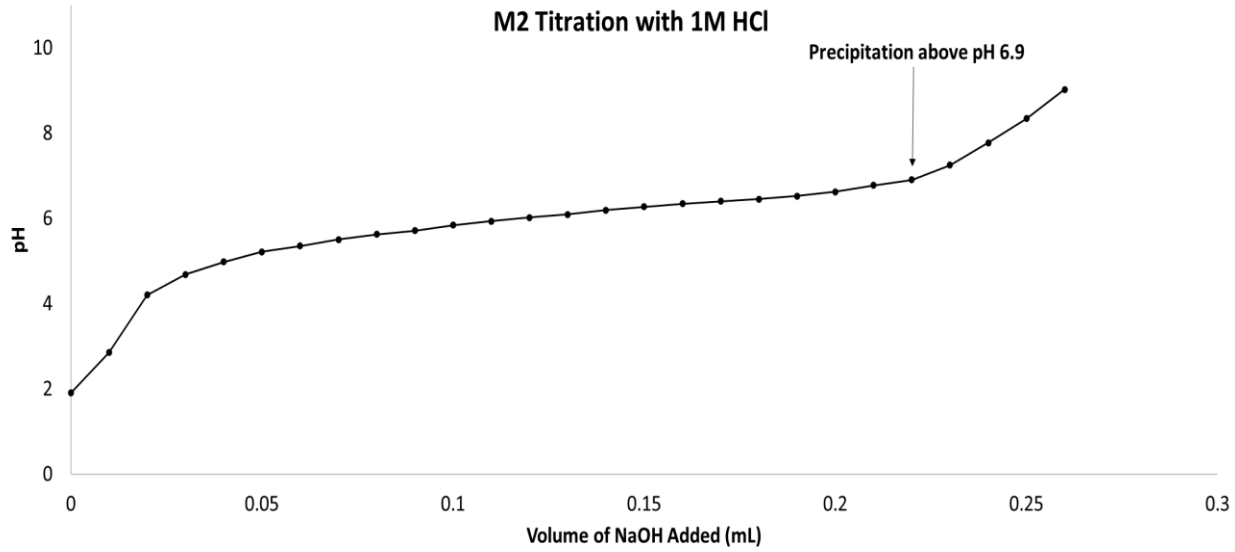
M2 Titration with 1M HCl
Precipitation above pH 6.9
pH
Volume of NaOH Added (mL)
0
2
4
6
8
10
0
0.05
0.1
0.15
0.2
0.25
0.3

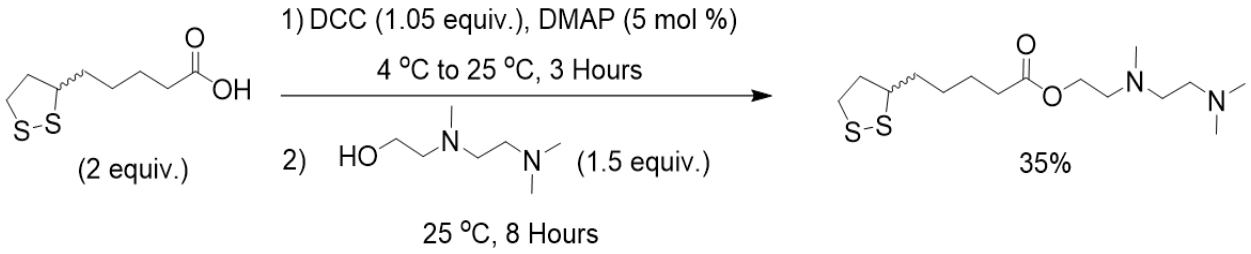

Scheme S4.3 Synthesis of **M3.**

M3 Yield: 0.57 grams, 35%

^{1}H NMR (CD_3OD, 500 MHz): δ(ppm)= 4.25-4.16 (t, *J*= 6.0 Hz, 2H), 3.62-3.54 (quint, *J*= 6.0 Hz, 1H), 3.22-3.07 (m, 2H), 2.74-2.66 (t, *J*= 6.0 Hz, 2H), 2.62-2.56 (t, *J*= 6.5 Hz, 2H), 2.51-2.43 (m, 3H), 2.38-2.34 (t, *J*= 7.0 Hz, 2H), 2.33-2.30 (s, 3H), 2.29-2.25 (s, 6H), 1.94-1.85 (sext, *J*= 7.0 Hz, 1H), 1.77-1.59 (m, 4H), 1.53-1.41 (m, 2H) ; ^{13}C NMR (CD_3OD, 500 MHz): δ(ppm)= 175.02, 62.85, 57.60, 57.54, 57.08, 56.15, 45.77, 43.09, 41.31, 29.38, 25.71, 34.81, 29.79, 25.73; ESI-MS: $C_{15}H_{30}N_2O_2S_2$ [M+H$^+$], Calculated 335.17, Found: 335.0; The ESI-MS, ^{1}H and ^{13}C NMR spectra, and pH titration curve of **M3** are attached below:

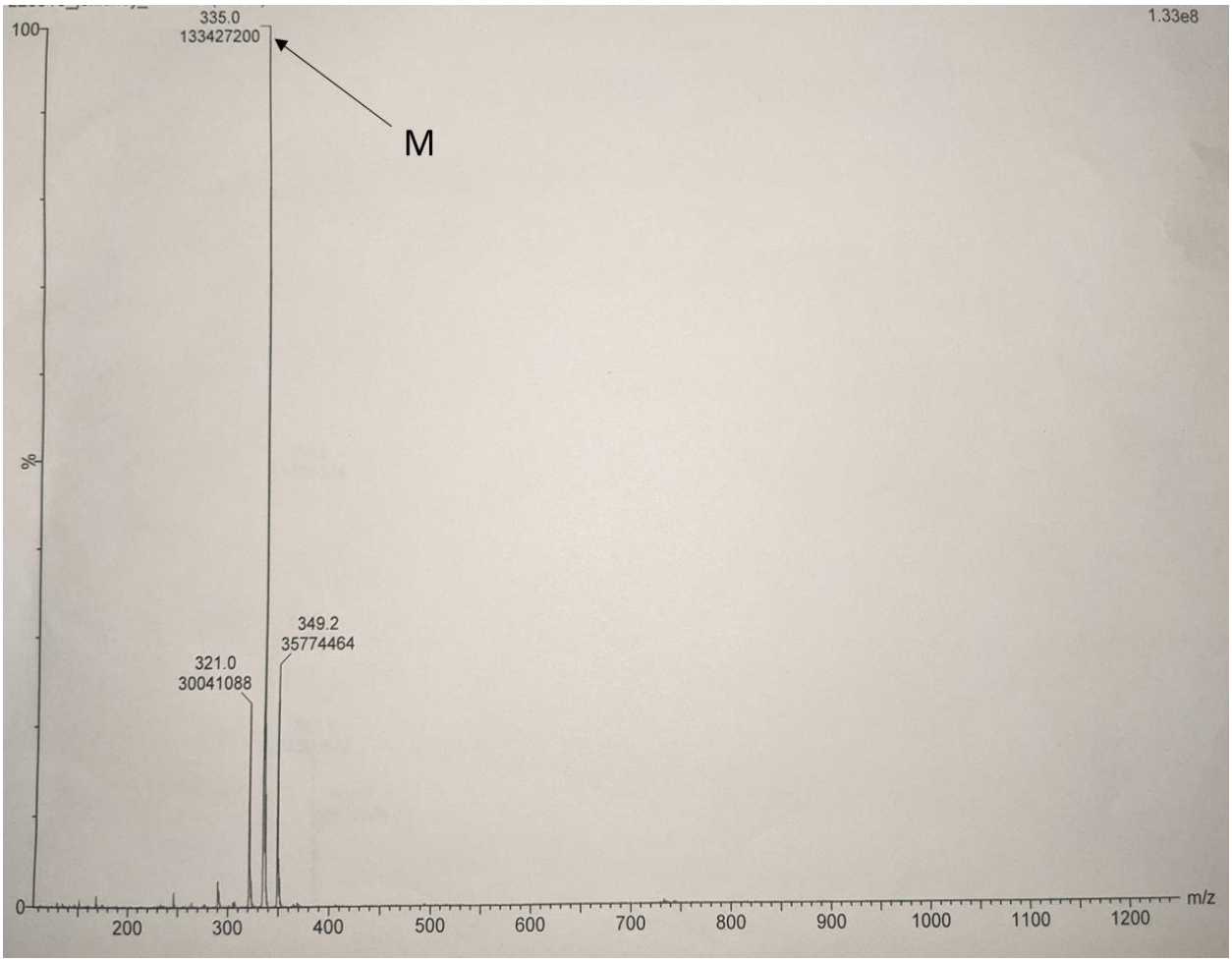

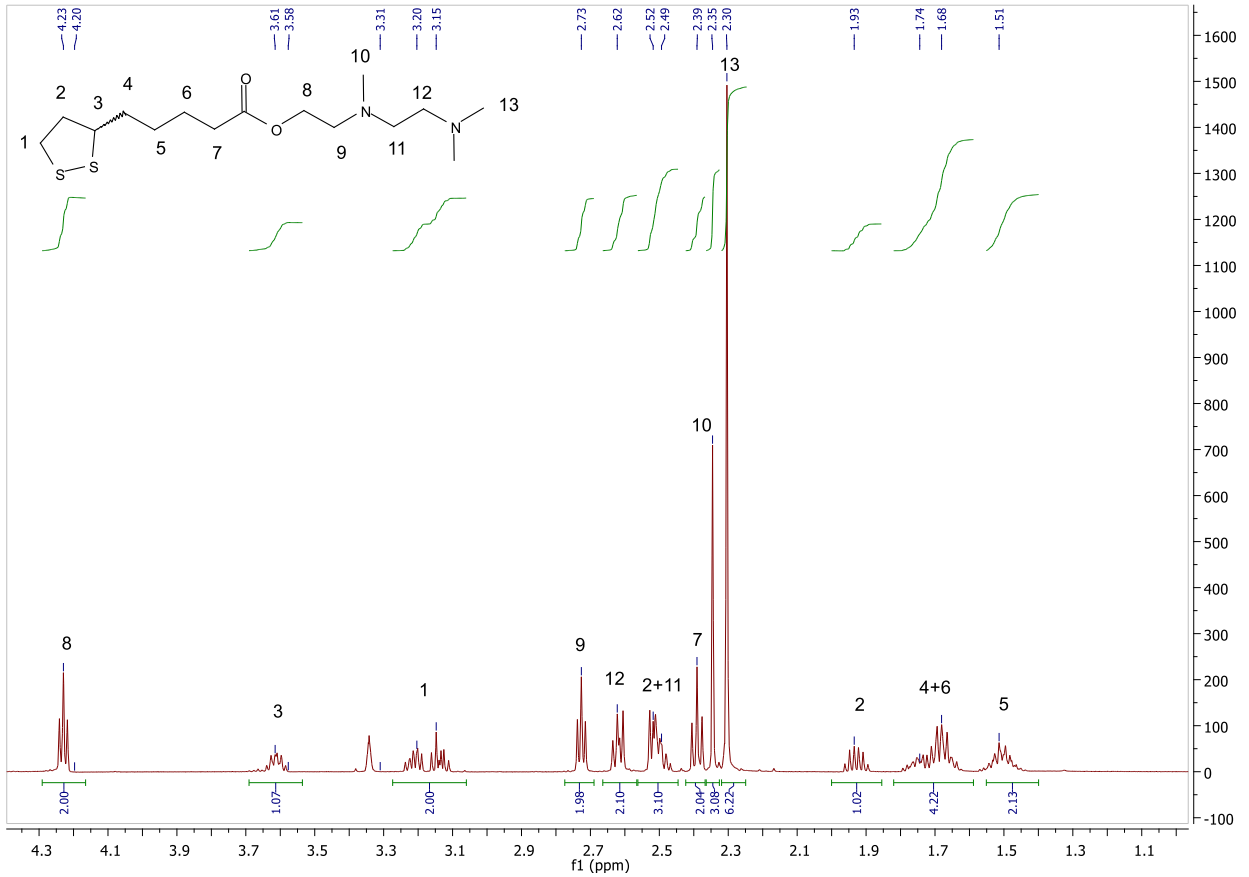
4.23
4.20
3.61
3.58
3.31
3.20
3.15
2.73
2.62
2.52
2.49
2.39
2.35
2.30
1.93
1.74
1.68
1.51
10
13
2
3
4
6
8
12
1
5
7
9
11
S
S
O
N
N
8
3
1
9
12
2+11
7
10
2
4+6
5
2.00
1.07
2.00
1.98
2.10
3.10
2.04
3.08
6.22
1.02
4.22
2.13
f1 (ppm)

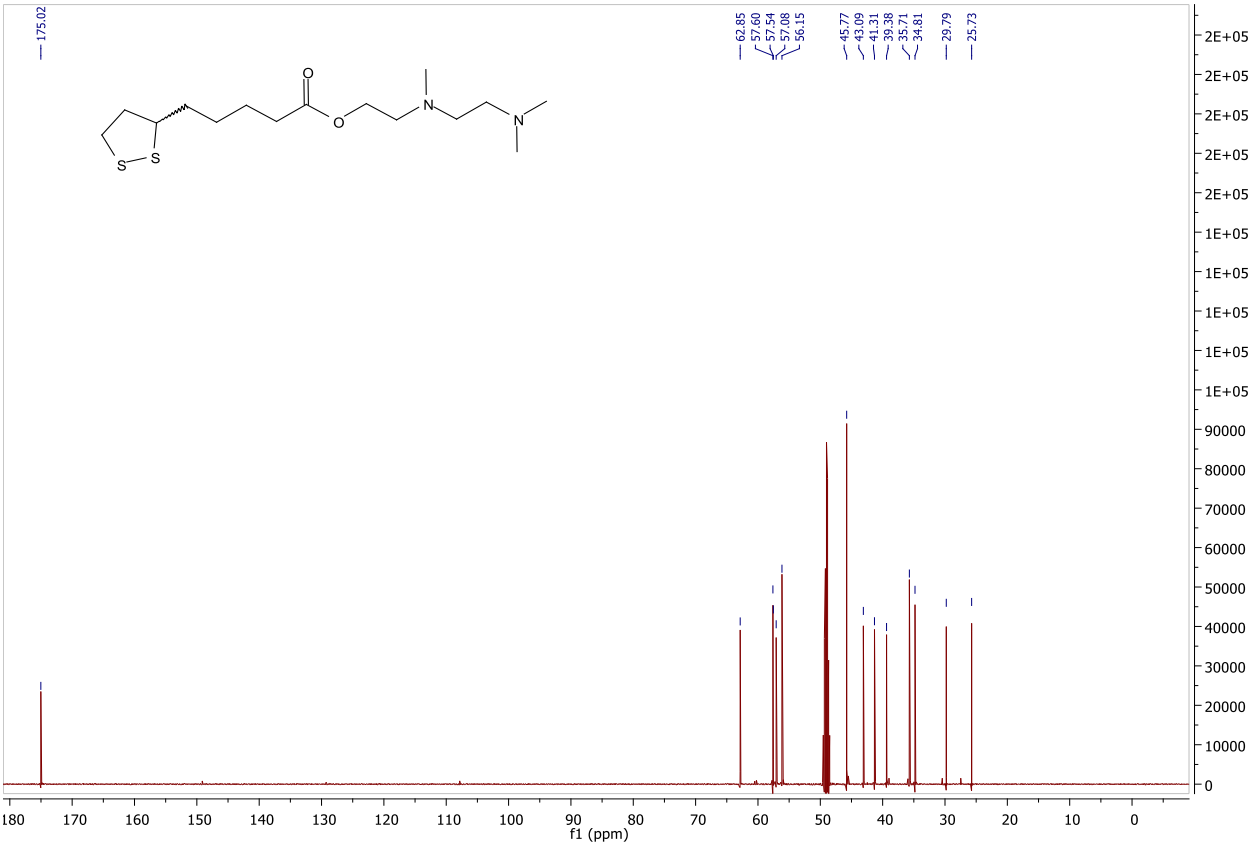
175.02
62.85
57.60
57.54
57.08
56.15
45.77
43.09
41.31
39.38
35.71
34.81
29.79
25.73
O
N
N
S
S
f1 (ppm)

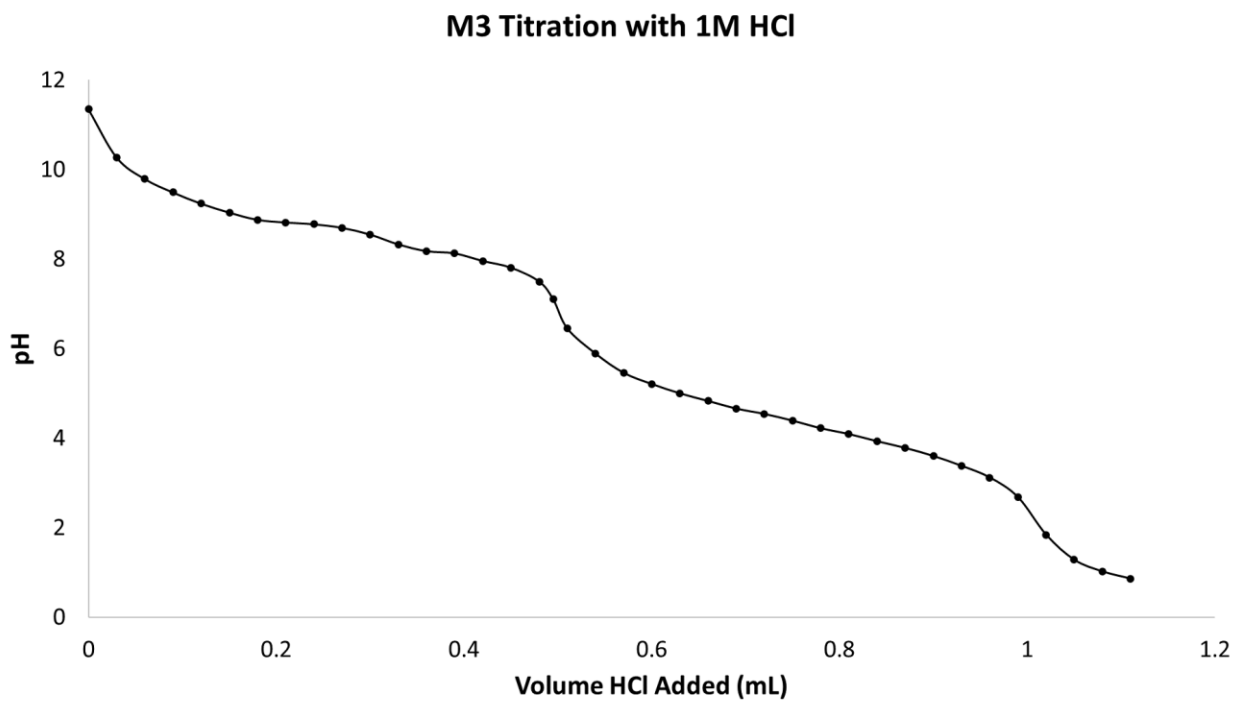
M3 Titration with 1M HCl
12
10
8
6
4
2
0
pH
0
0.2
0.4
0.6
0.8
1
1.2
Volume HCl Added (mL)

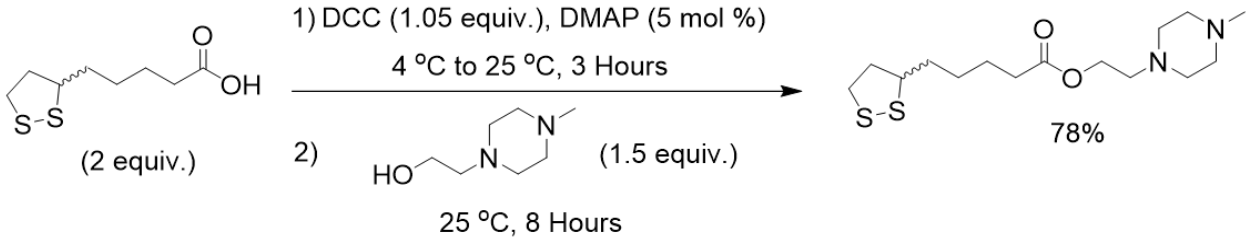

Scheme S4.4 Synthesis of **M4.**

M4 Yield: 1.26 grams, 78%

^{1}H NMR (CD_3OD, 500 MHz): δ(ppm)= 4.24-4.20 (t, *J*= 5.5 Hz, 2H), 3.62-3.54 (quint, *J*= 6.5 Hz, 1H), 3.22-3.06 (m, 2H), 2.80-2.30 (broad, 8H), 2.69-2.64 (t, *J*= 6.0 Hz, 2H), 2.50-2.43 (sext, *J*= 5.5 Hz, 1H), 2.38-2.34 (t, *J*= 7.5 Hz, 2H), 2.29-2.27 (s, 3H), 1.95-185 (sext, *J*= 6.5 Hz, 1H), 1.80-1.58 (m, 4H), 1.54-1.42 (m, 2H); ^{13}C NMR (CD_3OD, 500 MHz): δ(ppm)= 174.98, 62.39, 57.59, 57.55, 55.62, 53.85, 46.00, 41.31, 39.36, 35.71, 34.80, 29.78, 25.75; ESI-MS: $C_{15}H_{28}N_2O_2S_2$ [M+H$^+$], Calculated 333.16, Found: 332.7; The ESI-MS, ^{1}H and ^{13}C NMR spectra, and pH titration curve of **M4** are attached below:

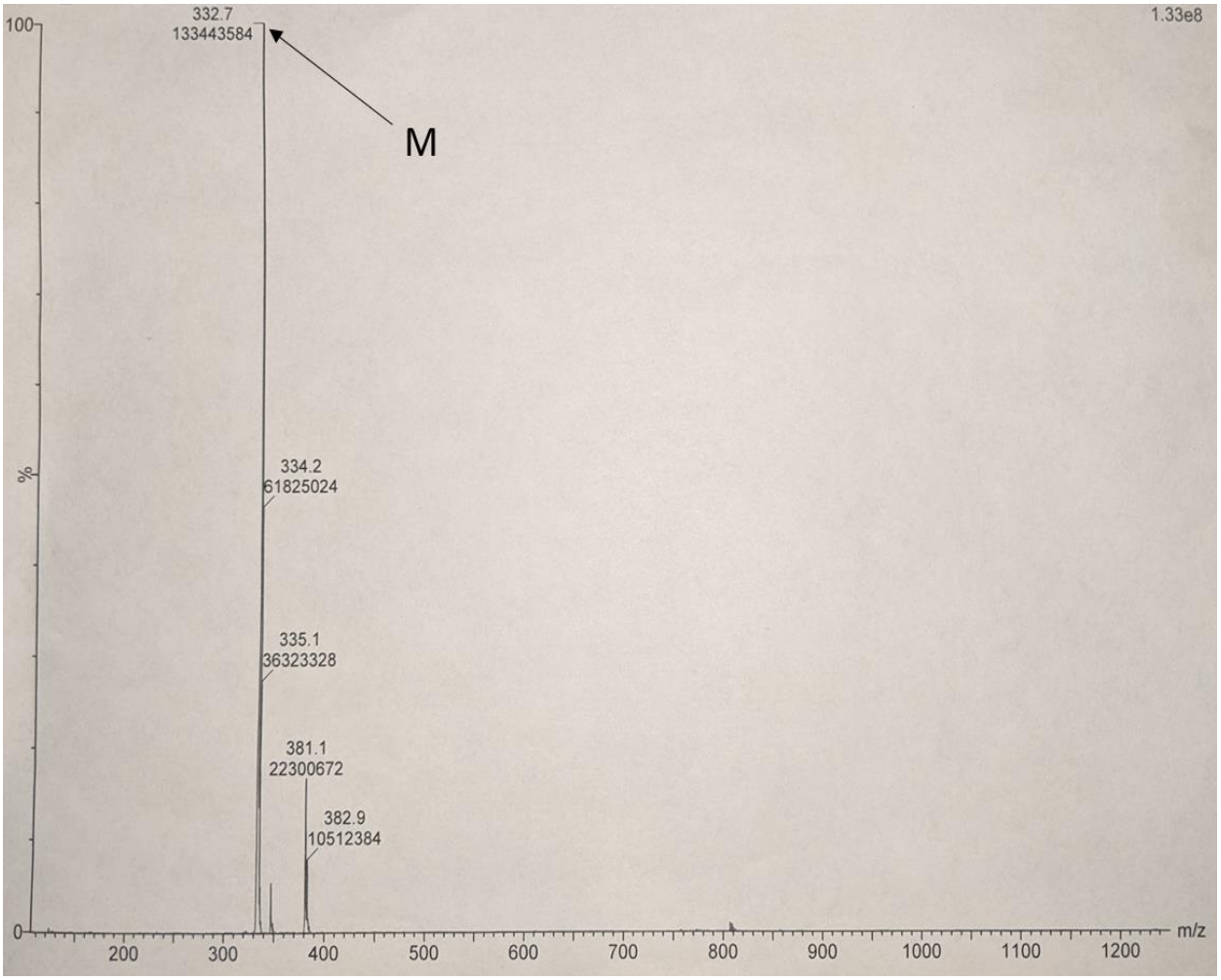

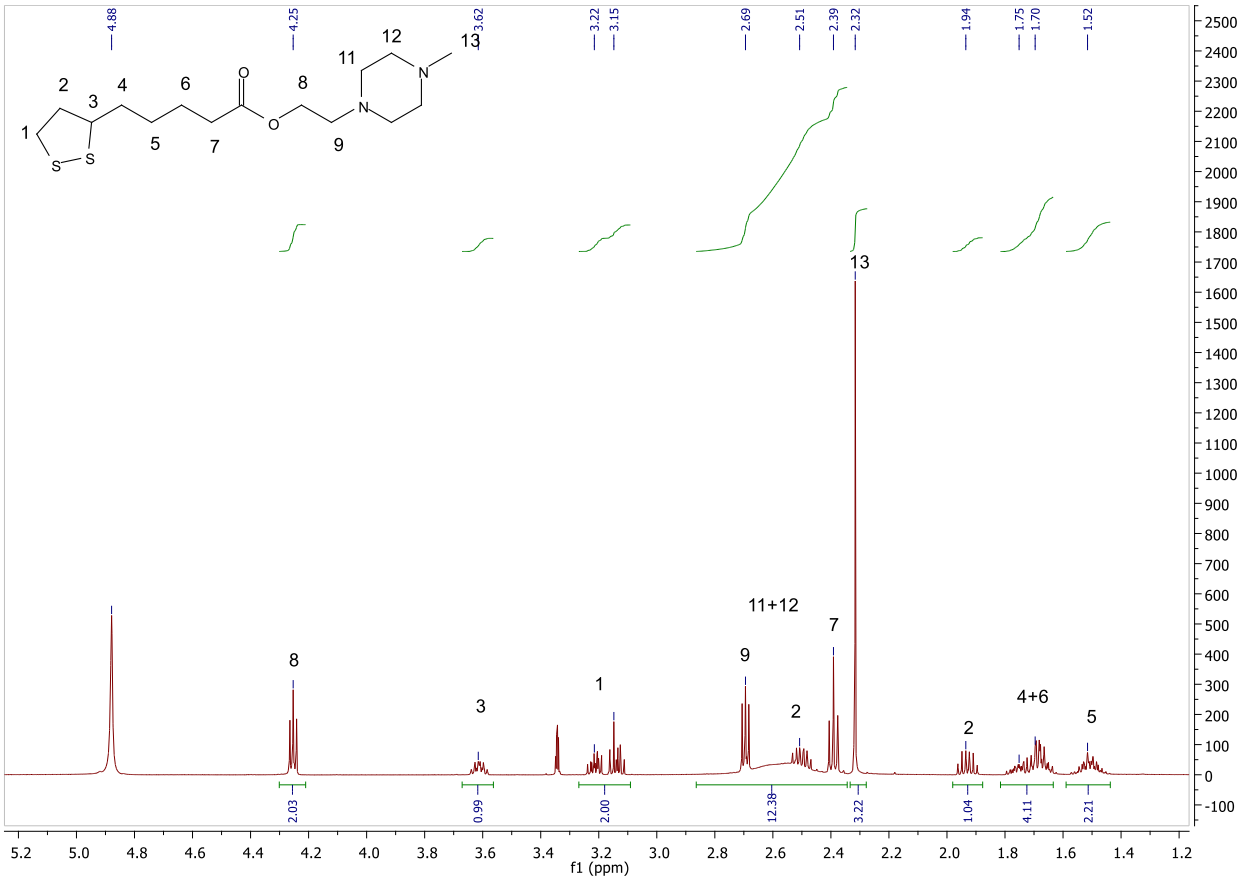
4.88
4.25
3.62
3.22
3.15
2.69
2.51
2.39
2.32
1.94
1.75
1.70
1.52
1
2
3
4
5
6
7
8
9
11
12
13
S
S
O
O
N
N
8
3
1
9
11+12
2
7
13
2
4+6
5
2.03
0.99
2.00
12.38
3.22
1.04
4.11
2.21
f1 (ppm)

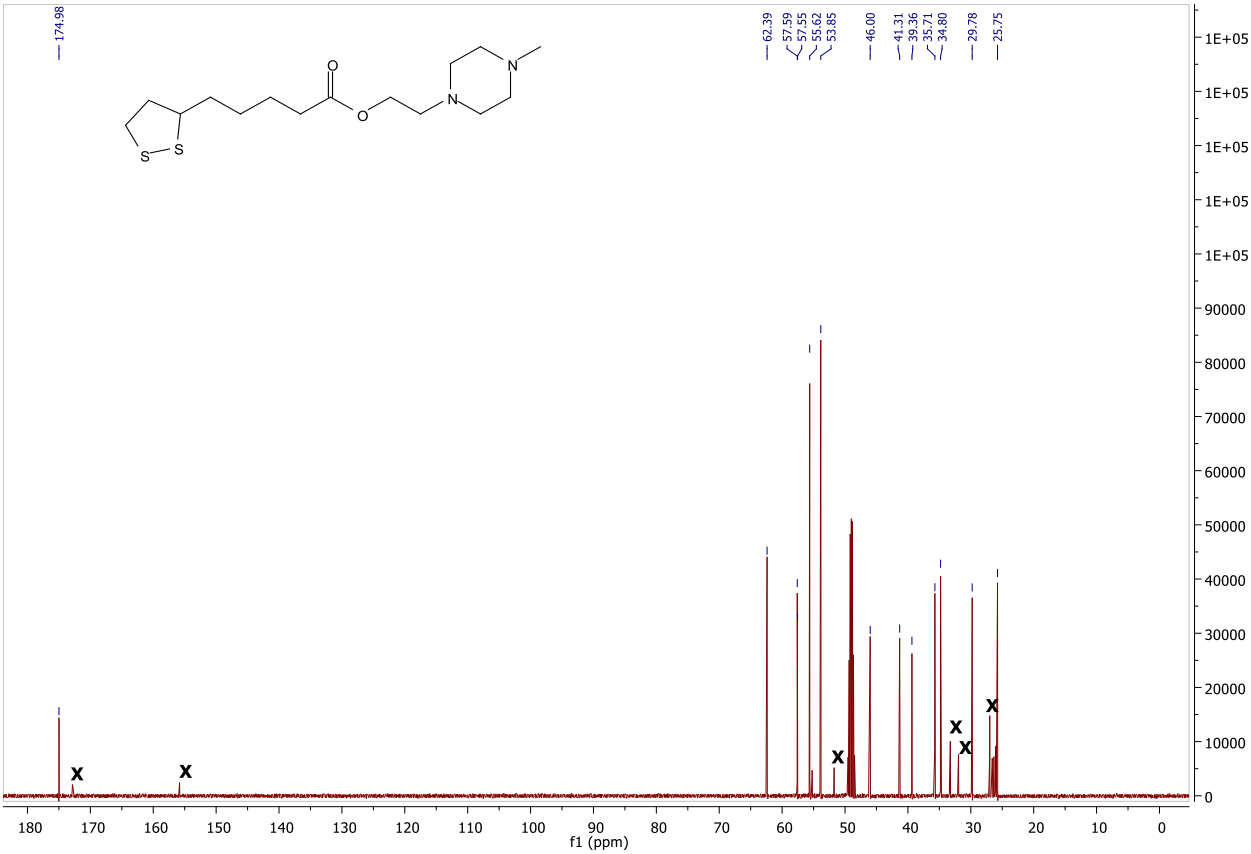
174.98
62.39
57.59
57.55
55.62
53.85
46.00
41.31
39.36
35.71
34.80
29.78
25.75
S
S
O
O
N
N
X
X
X
X
X
X
f1 (ppm)

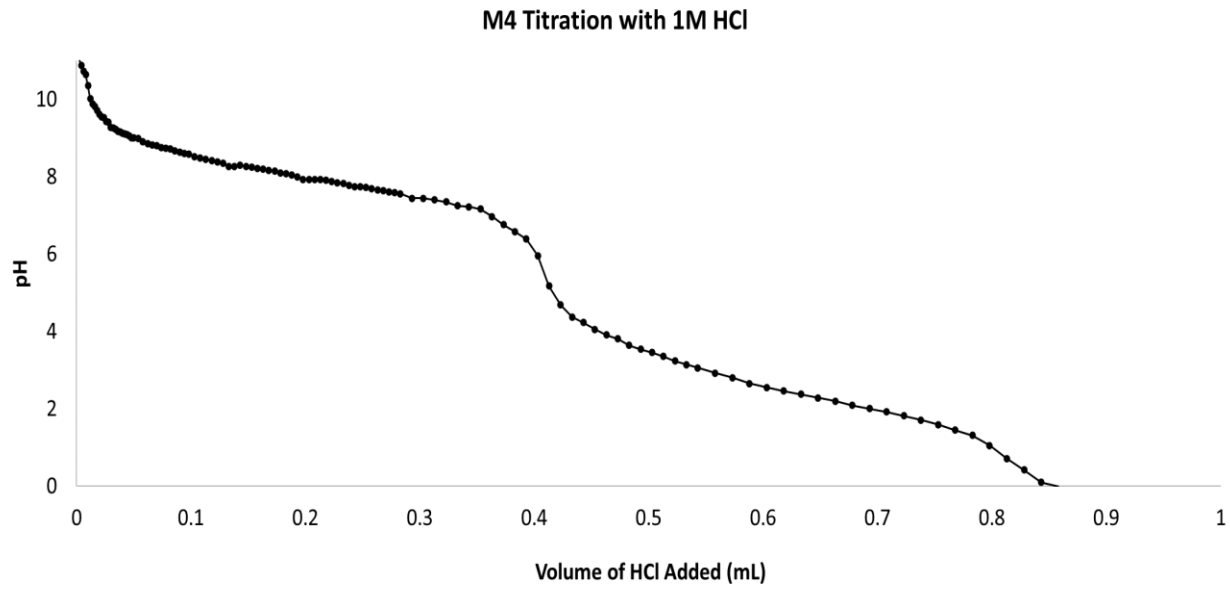
M4 Titration with 1M HCl
pH
10
8
6
4
2
0
0
0.1
0.2
0.3
0.4
0.5
0.6
0.7
0.8
0.9
1
Volume of HCl Added (mL)